THE JOURNAL OF

PHYSICAL CHEMISTRY

(Registered in U. S. Patent Office)

CONTENTS

AN ELECTROCHEMICAL STUDY OF HYDROGEN PRODUCING REACTIONS CATALYZED BY GOLD AND GOLD–PALLADIUM CATHODES

BY SIGMUND SCHULDINER AND JAMES P. HOARE

Naval Research Laboratory, Washington, D. C.

Received July 25, 1956

The hydrogen overvoltage of gold, β-phase-palladium–hydrogen, and gold–palladium alloys of Au/Pd atomic ratios 0.24, 0.43, 0.88 and 2.70 were determined. It was found that the rate-controlling step for the hydrogen producing reaction on β-phase-palladium–hydrogen alloy, and gold–palladium alloys up to a Au/Pd ratio of 0.6 was the electrochemical desorption; beyond this ratio and for pure gold the rate-controlling step was the combination of hydrogen atoms. The effect of successive additions of the alloying gold on the decrease in catalytic activity of palladium was large up to the 0.6 Au/Pd atomic ratio, but for higher ratios the successive addition of gold produced a much smaller decrease in the catalytic activity. Pure gold was shown to be an acceptable hydrogen electrode.

Introduction

A recent study[1] of the β-phase-palladium–hydrogen system in acid solutions showed that the catalytic activity for the hydrogen producing reaction on cathodic polarization was higher than the catalytic activity for the hydrogen producing reaction on α-phase-palladium.[2] This indicated that when the positive holes in the d-bands of palladium were filled with electrons from hydrogen atoms, the catalytic activity of the palladium surface was increased. A series of gold–palladium alloys were used to determine the effect on hydrogen overvoltage and catalytic behavior by the replacement of hydrogen with gold in the palladium lattice.

Alloying palladium to approximately a Au/Pd atomic ratio of 0.6 was shown by Vogt[3] and others to lower the paramagnetic susceptibility of the palladium to zero. These authors conclude that this is a result of the filling of the positive holes in the d-bands of the palladium with electrons from gold atoms. When gold is alloyed with palladium, it forms solid solutions in which the components are completely miscible in all proportions.[4] Up to a Au/Pd ratio of 0.6, an equivalent number of protons

in β-phase-palladium–hydrogen alloys are replaced with gold ions. Gold added above this amount cannot contribute electrons to a d-band.

Experimental

A series of gold–palladium alloys of the following atomic percentages of gold were made: 19.3, 29.8, 46.9 and 73.0. This gave a series of alloys for which the Au/Pd atomic ratios were: 0.24, 0.43, 0.88 and 2.70, respectively. In addition, electrodes of pure gold (99.97%) and the β-phase-palladium–hydrogen alloy were investigated. All measurements were made in electrolytically purified 2 N sulfuric acid solutions stirred vigorously with purified hydrogen. The experimental techniques and the Teflon cell used for overvoltage measurements were the same as previously described.[1,5] Small beads of the metals varying in size from 0.125 to 0.150 cm. in diameter were used as the working electrodes. Each bead was electrolytically cleaned by anodic polarization at 40 ma. for 200 seconds followed by cathodic polarization at the same current and for the same length of time. As done in the previous work, pure palladium and gold–palladium electrodes were converted to the β-phase-palladium–hydrogen alloy and to the analogous gold–palladium–hydrogen alloys, respectively, by this cathodic polarization. By this technique all the cathodes studied were ones in which the positive holes in the d-bands of the palladium were completely filled with electrons from either hydrogen or gold atoms or both. Interrupter measurements[6] were used to confirm electrode cleanliness and to determine solution iR drop for all determinations. The solution temperature was 29 ± 1°. It is to be noted that all overvoltage measurements were determined against a Pt/H₂ electrode in the same solution.

Results and Discussion

The hydrogen overvoltage of the Au/Pd series, pure gold, and the β-phase-Pd–H alloy are shown

(1) J. P. Hoare and S. Schuldiner, *J. Electrochem. Soc.*, **102**, 485 (1955).

(2) J. P. Hoare and S. Schuldiner, *ibid.*, in press.

(3) (a) E. Vogt, *Z. Metallkunde*, **27**, 40 (1935); (b) N. F. Mott and H. Jones, "Properties of Metals and Alloys," Oxford University Press, London, 1936, pp. 190–200; (c) A. Couper and D. D. Eley, *Disc. Faraday Soc.*, **8**, 172 (1950).

(4) C. J. Smithells, "Metals Reference Book," Vol. 1, Butterworth Scientific Publ., London, 1955, p. 334.

(5) S. Schuldiner, *J. Electrochem. Soc.*, **101**, 426 (1954).

(6) S. Schuldiner, *ibid.*, **99**, 488 (1952).
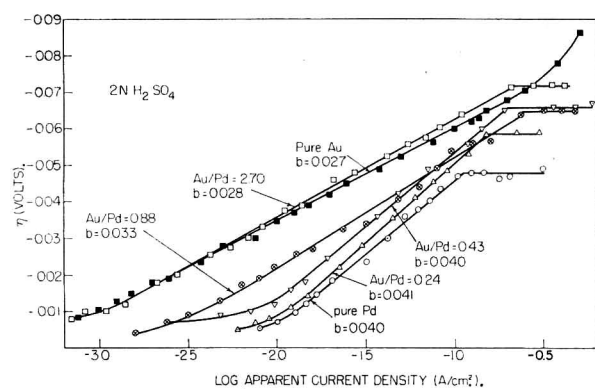
Fig. 1.—Hydrogen overvoltage on Pd–Au.
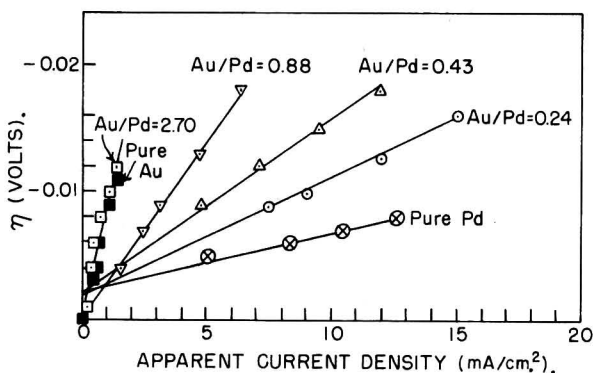
Fig. 2.—Hydrogen overvoltage in the range in which η is linearly dependent on current density.
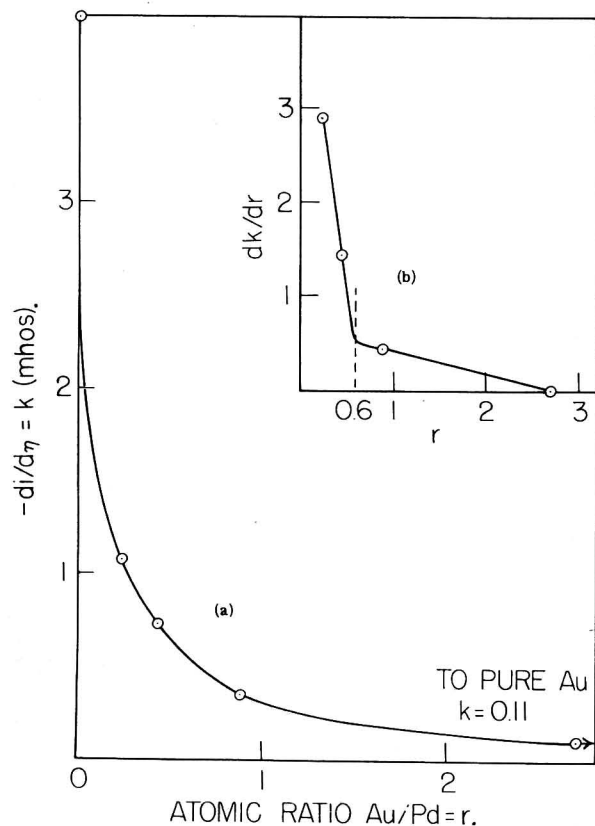
Fig. 3.—(a) Effect of Au/Pd atomic ratio on the rate constant of the over-all hydrogen producing reaction in the range in which η is linearly dependent on current density. (b) Change in the rate constant with increasing Au/Pd atomic ratio vs. Au/Pd atomic ratio.

in Fig. 1. From these results it can be seen that the shapes of the overvoltage curves for the β-phase-Pd–H alloy and the (Au + H)–Pd alloys of Au/Pd atomic ratios of 0.24 and 0.43 were the same. There was a small increase in the Tafel "a" value as the gold percentage increased and the value of overvoltage at which the overvoltage became virtually independent of current density also increased. The Tafel "b" values of 0.04 for each of these curves indicated that the rate-controlling step was the electrochemical desorption of an adsorbed hydrogen atom by combination with a hydrogen ion in the double layer and an electron from the metal on an electrode surface sparsely covered with atomic hydrogen.[7]

The pure gold and Au/Pd = 2.7 alloy, on the other hand, gave Tafel "b" slopes of 0.03. This indicated that the rate-controlling step was the combination of pairs of adsorbed hydrogen atoms on the surface of these metals. Also for pure gold there was no flattening off of the overvoltage curve to give a region in which the overvoltage, η, was virtually independent of the current density, i. However, for the Au/Pd = 2.7 alloy such a region was found. This showed that for even this alloy there is a marked influence of the palladium component in this region.

The polarization behavior of the Au/Pd = 0.88 alloy was intermediate between the low and high gold content electrodes. Taking into consideration the electron configuration of the (Au + H)–Pd alloys, one may expect a sharp change in the electrochemical behavior of these alloys at an atomic ratio greater than 0.6, since at that atomic ratio all the protons in the β-phase-Pd–H alloy are replaced with gold ions and an excess of gold beyond this critical ratio will go into solution without contributing electrons to a d-band. It must also be remembered that hydrogen in the atomic state can be dissolved electrolytically in palladium in which the d-bands are filled.[8]

The results in Fig. 1 show that when the atomic ratio of the Au/Pd alloys did exceed 0.6, then the electrochemical behavior of the alloys did change markedly. For the highest gold content alloy the behavior, with the exception of the region in which the overvoltage was virtually independent of i, was similar to that of pure gold. For the Au/Pd = 0.88 alloy the behavior was intermediate to that of the Au/Pd alloys with atomic ratios below 0.6 and to that of the high gold alloy. Evidently, this was because the electrode was in substance a mixture of the Au–Pd analog of the β-phase-Pd–H alloy plus gold and hydrogen atoms in solid solution with palladium.

The rate constants for the over-all hydrogen producing reaction on these electrodes in the overvoltage region where η is a linear function of i may be expressed as $-(di/d\eta)$.[1,5,9] Linear plots of η vs. i in the low current density range are shown in Fig. 2. Here it can be seen that as the hydrogen ions in the β-phase of the Pd–H alloy are replaced with gold

(7) R. Parsons, *Trans. Faraday Soc.*, **47**, 1332 (1951).

(8) S. Schuldiner and J. P. Hoare, *J. Electrochem. Soc.*, **103**, 178 (1956).

(9) P. Dolin, B. Ershler and A. Frumkin, *Acta Physicochim. URSS*, **13**, 779 (1940).

ions the rate constant decreases. After the d-bands in the palladium are completely filled with electrons from gold rather than from hydrogen and after an excess of gold atoms are added, the rate constant continues to decrease, but at a much slower rate. The relationship between the rate constant $-(di/d\eta)$ and the atomic ratio Au/Pd is shown in Fig. 3a. The curve in Fig. 3b was prepared by determining geometrically the slope of the $-(di/d\eta)$ vs. Au/Pd atomic ratio curve in Fig. 3a at the points corresponding to those Au/Pd compositions used in the overvoltage measurements; and by plotting these slopes against the Au/Pd atomic ratio. This curve (Fig. 3b) which shows the change in rate constant with increasing atomic ratio vs. atomic ratio emphasizes the fact that beyond an atomic ratio of 0.6 there is a sharp decline in the change of the catalytic activity of the hydrogen producing reaction. In other words, when the positive holes in the palladium d-bands are partially filled with electrons from hydrogen atoms and the remaining holes are filled with electrons from gold atoms, the catalytic activity of the alloy is markedly decreased by increasing the ratio of gold ions to protons. However, once the positive holes in the palladium are completely filled with electrons from the gold atoms (0.6 atomic ratio) and the gold content is increased by adding gold atoms, the effect on the catalytic activity for the over-all hydrogen producing reaction owing to these added gold atoms is small.

In cases where palladium is a component of the electrode material, the overvoltage curves exhibited a plateau (see Fig. 1). This may be interpreted as meaning that hydrogen is dissolved as atomic hydrogen in the lattice of these alloys.[1,8] When the plateau is reached the alloy is saturated with atomic hydrogen and the rate constant for the hydrogen producing reaction becomes very large (see below). It will be observed that as the gold content was increased the plateau was reached at higher overvoltage values. It is suggested that this is the case because as the gold content is increased the electrochemical energy needed to saturate the lattice with hydrogen atoms is increased.

Couper and Eley[3c] showed that while there were positive holes in the d-band of palladium, the activation energy of the parahydrogen conversion was constant at 3.5 kcal./mole. The activation energy abruptly increased to 8.5 kcal./mole at the point where the d-band of palladium was completely filled with electrons from added gold. Experiments which involved the addition of electrons from hydrogen atoms rather than gold also showed a sharp increase in the activation energy when the d-band of the palladium was filled. These authors pointed out that the hydrogen atoms would be more strongly adsorbed on the surface of palladium with vacancies in its d-band than on a palladium surface in which the d-bands were filled.

It has been postulated by Horiuti and Polanyi[10] that if the slow discharge step is rate determining then the catalytic activity of the metal would increase with increasing heat of adsorption of atomic

hydrogen on the metal. Oikawa's[11] results for hydrogen overvoltage measurements on copper-nickel alloys, where his experiments indicate that the discharge step is rate determining, show that the overvoltage is increased as the positive holes in the d-band of nickel are filled with electrons from alloyed copper. These results indicate that, when the slow discharge step is rate controlling and when the hydrogen is more strongly bound to the metal, the overvoltage will be lower and the catalytic activity higher.

However, as shown above,[1,2] the situation for Pd is the reverse of that for Ni, with β-palladium having a higher catalytic activity than α-palladium. These results indicate that when the atomic combination step or the electrochemical desorption step at low atomic hydrogen surface coverage is rate-controlling, then, the more strongly the hydrogen atoms are adsorbed on the surface the slower is the rate of the reaction.

As hydrogen is added electrolytically to β-palladium the heat of adsorption of atomic hydrogen on the surface decreases and the rate of the combination step increases. When the palladium is effectively saturated with hydrogen (H/Pd $\sim$ 1), the valence bonds for Pd–H are completely saturated and therefore the heat of adsorption of atomic hydrogen on the palladium surface would drop to a low value. This discontinuity in the heat of adsorption vs. composition relationship would occur at the point at which the overvoltage becomes virtually independent of current density. Because of the low heat of adsorption of atomic hydrogen the combination step would be very fast, but the rate of the discharge step would become so slow that it effectively does not occur. This would imply that a new hydrogen-producing mechanism takes over in this region, most likely one which would be independent of the heat of adsorption of atomic hydrogen on palladium. This contention is supported by the experimental evidence, since the break in the overvoltage curve indicates that a new hydrogen-producing mechanism has taken over. A more detailed discussion of the kinetic mechanisms involved is contained in a recent paper.[12]

It can be concluded from the experiments with gold and palladium that the heat of adsorption of atomic hydrogen on gold is greater than on β-palladium. This follows from the decrease in the catalytic activity of the palladium–gold alloys as the Au/Pd atomic ratio increases.

As shown in Fig. 2, the open circuit potential of a Au/H$_2$ electrode against a Pt/H$_2$ electrode is zero volts. This means that a properly cleaned gold electrode makes an acceptable hydrogen electrode. The disadvantage of such a hydrogen electrode is the ease with which the gold surface is poisoned. The proper preparation for a Au/H$_2$ electrode is a strong anodic polarization followed by a strong cathodic polarization in a very pure acid solution stirred by a very pure hydrogen. If, as shown by Knorr,[13] the gold electrode is anodized in the same

(10) J. Horiuti and M. Polanyi, Acta Physicochim. USSR, **2**, 505 (1935).

(11) M. Oikawa, Bull. Chem. Soc. Japan, **28**, 626 (1955).

(12) S. Schuldiner and J. P. Hoare, presented at the International Colloquium on Reference Electrodes and Structure of the Double Layer, Paris, France, October, 1956.

solution in which it is cathodized, a black, finely-divided deposit of gold covers the electrode. A bright active gold electrode can be prepared by anodizing in acid solution outside of the cell, rinsing the electrode with conductivity water and finally

(13) C. A. Knorr, *Z. Elektrochem. Ber. Bunsenges. physik Chem.*, **59**, 647 (1955).

cathodizing in the electrolytic cell. The overvoltage measurements on a gold electrode shown in Fig. 1 are for a bright gold electrode. Measurements on a gold-black electrode showed an identical Tafel slope which means that the electrochemical kinetics of the hydrogen producing reaction are the same for bright gold and gold-black electrodes.

THE THERMO-OSMOSIS OF THE RARE GASES THROUGH A RUBBER MEMBRANE

By RICHARD J. BEARMAN[1]

Department of Chemistry and Chemical Engineering, Stanford University, Stanford, California

Received September 20, 1956

A theory of thermo-osmosis based on the thermodynamics of irreversible processes is developed. Results on the thermo-osmosis through a rubber membrane of the rare gases (with the exception of radon) and of carbon dioxide are presented and then interpreted. A discussion of various sources of experimental error also is given.

I. Introduction

Thermo-osmosis, the "diffusion of a fluid through a membrane under the influence of a temperature gradient,"[2] was discovered by Lippmann[3] in 1907, but the lack of a theory of irreversible processes prevented progress toward understanding the phenomenon. In 1926 Eastman[4] developed a highly intuitive theory in which he attempted to relate the flow of fluid through the membrane to a heat of passage, but the theory was very unsatisfactory. However, not long thereafter Onsager[5] in 1931 discovered the now famous reciprocal relations, which through the work of several theoreticians were made the basis of a more rigorous thermodynamics of irreversible processes. By 1952 the understanding of this thermodynamics had progressed to the extent that Denbigh and Raumann[2,6] were able to develop a workable theory of thermo-osmosis and interpret within the framework of that theory quantitative data obtained by them on the thermo-osmosis of gases through rubber. In order to provide still more data with which to test the thermodynamics of irreversible processes we decided to continue their work in a systematic fashion. For this reason we chose to study the thermo-osmosis of the noble gases through a rubber membrane.

In this paper we describe the results of our measurements, and also present a refined version of the theory evolved by Denbigh and Raumann.

II. Theoretical

A. Description of the System Used to Study

(1) Sterling Chemistry Laboratory, Yale University, New Haven, Conn. This paper is based on a dissertation submitted by the author to Stanford University in partial fulfillment of the requirements for the Ph.D. The dissertation itself is available on microfilm for $1.40 from University Microfilms, 313 N. First St., Ann Arbor, Mich. A preliminary report of this work has been published by R. J. Bearman and F. O. Koenig, *J. Am. Chem. Soc.*, **78**, 691 (1956).

(2) K. G. Denbigh and G. Raumann, *Proc. Roy. Soc. (London)*, **A210**, 377 (1952).

(3) G. Lippmann, *C. R. Acad. Sci. (Paris)*, **145**, 104 (1907).

(4) E. D. Eastman, *J. Am. Chem. Soc.*, **48**, 1482 (1926).

(5) L. Onsager, *Phys. Rev.*, **37**, 405 (1931); **38**, 2265 (1931).

(6) K. G. Denbigh and G. Raumann, *Proc. Roy. Soc. (London)*, **A210**, 518 (1952).

Thermo-osmosis.—The system is drawn in cross-section in Fig. 1. A and A' are heat reservoirs (at temperatures T_A and T_A') separated by the membrane assembly, which consists of two porous, thermally conducting, chemically inert, circularly cylindrical plates β and β' together with appropriate thermal insulation. The thin circular membrane γ of the same area a as the plates is supported by them. The symmetry is such that (i) the pressure is uniform throughout the membrane, (ii) the membrane is of uniform thickness l, and (iii) the gradients of all properties not constant throughout the membrane are perpendicular to the membrane. If we call the direction normal to the membrane the z-direction, then all physical properties defined at a point may be specified by giving the value of the z-coordinate ($z = 0$ is at the surface of the membrane in contact with β).

Containers α and α', each holding the same gas, are immersed in the baths A and A'. The gas in α has access to one side of the membrane through β; that in α' has access to the other side through β'. A, A', α, α' β, β' and γ remain constant in volume. α and α' are at the temperatures T_A and T_A'. The temperature in each plate varies continuously from the temperature of the reservoir in contact with that plate to the temperature of that outer surface of the membrane which touches the plate.

To study thermo-osmosis we first admit gas to α and α' and then observe the pressures in α and α' and also observe the temperatures at the surfaces of the membrane until a stationary state of no gas flow is reached.

B. Hypotheses of the Thermodynamics of Irreversible Processes. Applicability of Equilibrium Concepts and Relationships.

—The independent properties which determine the state at each point are the same as those properties which determine the state when the system is in equilibrium. The equation of state is the same as the equilibrium equation and the fundamental Gibbsian equation which relates the differential of energy to those of entropy, volume and number of moles is also valid in the non-equilibrium situation.

Energy Flow and Mass Flow.[7]—The energy flow J_U in the membrane is partially defined by the differential equation

$$\frac{\partial J_U}{\partial z} = -\frac{\partial u}{\partial t} \qquad (1)$$

where t is time and u is the energy per unit volume. To complete the definition we specify that J_U at $z = 0$ is

$$a(J_U)_0 \equiv \left[\frac{\partial w_\alpha}{\partial t} - \frac{\partial U_A}{\partial t}\right] - \frac{\partial U_{\alpha+\beta}}{\partial t} \qquad (2)$$

where U_A and $U_{\alpha+\beta}$ are the energies of A and $\alpha + \beta$. $\partial w_\alpha/\partial t$ is the rate at which work is done on α, and is zero when α is constant in volume.[8]

The mass flow of gas (component 1) J_1 may be defined in a similar fashion. It obeys the differential equation

$$\frac{\partial J_1}{\partial z} = -\frac{\partial c_1}{\partial t} \qquad (3)$$

where c_1 is the concentration of gas.

At each point fixed in the membrane the fundamental Gibbsian equation may be written

$$du = Tds + \mu_1 dc_1 \qquad (4)$$

where T is the absolute temperature, s is the entropy per unit volume, and μ_1 is the chemical potential of the gaseous component.

Using eq. 1, 3 and 4 it may be shown readily that

$$\frac{\partial s}{\partial t} = -\frac{\partial}{\partial z}\left(\frac{J_U - \mu_1 J_1}{T}\right) + \left[-\frac{J_U}{T}\frac{\partial T}{\partial z} - TJ_1\frac{\partial \mu_1/T}{\partial z}\right] \qquad (5)$$

As we shall see below, the form of eq. 5 is of great importance in the thermodynamics of irreversible processes.

The Phenomenological Relations and the Reciprocal Relation.—When $(1/T)(\partial T/\partial z)$ and $T\cdot[(\partial\mu_1/T)/\partial Z]$ are zero everywhere in the membrane the system is in equilibrium. When the gradients are not zero we assume that at each point in the membrane we may express the flows of matter and energy in a Taylor's series, neglecting terms higher than those of first order. Thus

$$J_1 = -TL_{11}\frac{\partial\mu_1/T}{\partial z} - \frac{L_{1U}}{T}\frac{\partial T}{\partial z}$$

$$J_U = -TL_{U1}\frac{\partial\mu_1/T}{\partial z} - \frac{L_{UU}}{T}\frac{\partial T}{\partial z} \qquad (6)$$

These equations are called "phenomenological relations"; the coefficients in the expansion (that is, the L's) are called "phenomenological coefficients"; and the functions $-T[(\partial\mu_1/T)/\partial Z]$ and $-(1/T)(\partial T/\partial Z)$ are called "forces," and are often denoted by the symbols X_1 and X_U. The phenomenological coefficients are functions of the local state but not of the gradients.

Now the fact that in experimental situations the flows often can be expressed as linear functions of

Fig. 1.

the forces is in itself of great importance. Of greater physical significance however is the validity of the reciprocal relation. To introduce it we shall first call attention to the form of eq. 5 which may be written

$$\frac{\partial s}{\partial t} = -\frac{\partial}{\partial z}J_s + \frac{J_1X_1 + J_UX_U}{T}$$

where J_s is an "entropy flow." Onsager[5] using statistical-mechanical arguments demonstrated that if the time derivative of the entropy per unit volume is split up into a divergence of an entropy flow and a source term written as in the above equation, then when the J's are expressed as linear functions of the X's the phenomenological coefficients obey the reciprocal relation

$$L_{1U} = L_{U1} \qquad (7)$$

This equality from the standpoint of a phenomenological theory is purely an assumption which must be verified by experimental means.[9]

The Assumption of Local Heterogeneous Equilibrium.—The chemical potential of the gas in the membrane at a surface is equal to the chemical potential of the free gas (which permeates the porous plate) at that surface.

C. Derivation of the Equation Valid in the Stationary State. The Approach to the Stationary State.—When $J_1 = 0$, by eq. 6

$$TL_{11}\frac{\partial\mu_1/T}{\partial z} = -\frac{L_{1U}}{T}\frac{\partial T}{\partial z} \qquad (8)$$

Integrating eq. 8 from $z = 0$ to $z = l$ gives

$$\left(\frac{\mu_1}{T}\right)_1 - \left(\frac{\mu_1}{T}\right)_0 = -\int_{T_0}^{T_1}\frac{L_{1U}}{T^2L_{11}}dT \qquad (9)$$

where T_0 and T_1 are the temperatures at 0 and l. From equilibrium thermodynamics we know that in the gas phase to a sufficient degree of approximation

$$\mu_1 = \mu_1{}^0(T) + RT\ln P \qquad (10)$$

where R is the gas constant and P is the pressure in the gas phase, and in the membrane phase at each point

$$\mu_1 = \mu_1{}^*(T, P_m) + RT\ln a_1(T, N_1, P_m) \qquad (11)$$

where a_1 is the activity of the gas, N_1 is the mole fraction of the gas, and P_m is the pressure in the membrane phase. Under the assumption of local heterogeneous equilibrium we may substitute eq. 10 into eq. 9. Adding and subtracting H_1^* yields

$$R\ln\frac{P_{\alpha'}}{P_\alpha} = -\int_{T_0}^{T_1}\left[\Delta H + \frac{L_{1U} - H_1^*L_{11}}{L_{11}}\right]\frac{dT}{T^2}$$

(7) Because we wish to indicate the operational aspects of the theory, we are presenting only as much as we require. In particular we have avoided the use of the generalized hydrodynamic equations (see J. G. Kirkwood and B. Crawford, Jr., THIS JOURNAL, **56**, 1048 (1952)) which have not been formulated as yet from the operational point of view.

(8) In this definition of energy flow we have neglected convective motion.

(9) Our account of what Onsager showed is oversimplified, and it cannot be said that a satisfactory proof of this reciprocal relation exists. To ascertain whether or not it is valid is one of the more important problems yet to be solved by the statistical mechanics of transport processes. On the phenomenological level, an experimental test of the reciprocal relation has yet to be carried out. We believe that it has not been emphasized sufficiently that the relevant evidence is still inconclusive.

where P_α and $P_{\alpha'}$ are the pressures of gas in α and α' (the porosity of the plates ensures that the pressure throughout β is the same as in α and likewise the pressure in β' is the same as in α')

$$H_1^* \equiv - T^2 \frac{\partial \mu_1^*/T}{\partial T}$$

and

$$\Delta H \equiv T^2 \frac{\partial(\mu_1^0 - \mu_1^*)/T}{\partial T}$$

ΔH is a differential heat of solution of the gas in the membrane. Applying the mean value theorem of the integral calculus we find that

$$R \ln \frac{P_{\alpha'}}{P_\alpha} = - \left(\Delta H + \frac{L_{1U} - H_1^* L_{11}}{L_{11}}\right)_\omega \left(\frac{1}{T_0} - \frac{1}{T_1}\right) \tag{12}$$

$(\Delta H + [(L_{1U} - H_1^* L_{11})/L_{11}])$ is evaluated at the values of T and N_1 which occur at a point ω in the membrane. We may write eq. 12

$$R \ln \frac{P_{\alpha'}}{P_\alpha} = - (\Delta H + Q_m^*)_\omega \left(\frac{1}{T_0} - \frac{1}{T_1}\right)$$
$$= - (Q^*)_\omega \left(\frac{1}{T_0} - \frac{1}{T_1}\right) \tag{13}$$

Q^* is called the heat of transfer.

From the derivation of eq. 13 we see that $(Q^*)_\omega$ depends in principle upon the temperature distribution, the concentration distribution of gas and the pressure P_m in the membrane. The limit of $(Q^*)_\omega$ (keeping the total amount of gas in the system fixed and P_m constant) as the temperature difference approaches zero is of importance. For

$Q^* (T, N_1, P_m) = \lim (Q^*)_\omega$
$= \Delta H(T, P_m) -$
$\dfrac{L_{1U}(T, N_1, P_m) - H_1^*(T, P_m)L_{11}(T, N_1, P_m)}{L_{11}(T, N_1, P_m)}$ (14)

where T and N_1 are now the uniform temperature and composition throughout the membrane. Thus extrapolation of thermo-osmosis data permits the evaluation of Q^* at definite values of the independent variables which determine it.

In order to simplify our notation and to agree with Denbigh and Raumann, we shall in our discussion below call the heat of transfer obtained by substituting experimental data into eq. 13 Q^*, although it is really $(Q^*)_\omega$ which is thereby determined.

The splitting of Q^* into two terms, ΔH and Q_m^*, is somewhat arbitrary, but this choice does have two important virtues. Firstly, it divides the total heat of transfer into a purely thermodynamic part and a part which depends on non-equilibrium quantities. Secondly, Denbigh and Raumann[2] have shown that if the activities of the gas at 0 and l in the membrane are equal for all temperature differences then Q_m^* is zero. Because these activities (which in the limit of zero concentration are the mole fractions) should not greatly differ, the extent of thermo-osmosis may be determined by the purely thermodynamic quantity ΔH.

The approach to the steady state involves a more approximate treatment than the steady state, for tractable equations are more difficult to obtain. However, no new matters of principle arise. In order to treat this case, Denbigh and Raumann

made the following additional assumptions: (i) J_1 is constant across the membrane. This cannot be true exactly if there is also local heterogeneous equilibrium. (ii) The temperatures at the membrane surfaces are constant in time. (iii) The temperature gradient in the membrane is constant. (iv) Q^* and L_{11} are constant across the membrane and in time. Under these assumptions they showed that

$$\ln \frac{x_\infty - x_0}{x_\infty - x_t} = kt \tag{15}$$

where

$$x \equiv \ln \frac{P_{\alpha'}}{P_\alpha} \tag{16}$$

(the subscript on x denotes the time at which it is evaluated) and

$$k \equiv \frac{4aPp}{nV_0 l} \tag{17}$$

where P is the mean gas pressure, nV_0 is the total volume of gas in the system at standard conditions, and p is a mean isothermal permeability of the membrane.

The equations which describe thermo-osmosis do not require the use of the reciprocal relation in their derivation, and consequently the study of thermo-osmosis alone affords no verification of the reciprocal relation.

D. The Calorimetric Interpretation of the Heat of Transfer.—In this section we shall consider the relationship of the reciprocal relation to thermo-osmosis and in so doing shall justify calling Q^* the heat of transfer.

When $T_\alpha = T_{\alpha'}$ the stationary state is one of equilibrium and therefore $P_\alpha = P_{\alpha'}$. Under these circumstances we may consider the slow transfer, by changing the volumes of α and α', of $-d(n_1)_\alpha$ moles of gas from α to α' while the system remains isothermal and the pressures remain equal. By eq. 2

$$a(J_U)_0 = \left[-P_\alpha \frac{\partial V_\alpha}{\partial t} - \frac{\partial U_A}{\partial t}\right] - \frac{\partial U_{\alpha+\beta}}{\partial t} \tag{18}$$

Also

$$\frac{\partial U_{\alpha+\beta}}{\partial t} = \bar{U}_\alpha \frac{d(n_1)_\alpha}{dt} \tag{19}$$

$$\frac{\partial V_{\alpha+\beta}}{\partial t} = \bar{V}_\alpha \frac{d(n_1)_\alpha}{dt} \tag{20}$$

where $\bar{U}_\alpha$ and $\bar{V}_\alpha$ are the molar energy and volume of gas. By eq. 6

$$(J_U)_0 = - L_{U1} \frac{\partial \mu_1}{\partial z}$$

and

$$a(J_1)_0 = - aL_{11} \frac{\partial \mu_1}{\partial z} = - \frac{d(n_1)_\alpha}{dt}$$

Therefore

$$(J_U)_0 = - \frac{L_{U1}}{aL_{11}} \frac{d(n_1)_\alpha}{dt} \tag{21}$$

Substituting eq. 19, 20 and 21 into eq. 18 yields

$$- \frac{\partial U_A}{\partial t} = \left(\bar{U}_\alpha + P_\alpha \bar{V}_\alpha - \frac{L_{U1}}{L_{11}}\right) \frac{d(n_1)_\alpha}{dt}$$

or

$$\frac{\partial q_{\alpha + \beta}}{\partial(n_1)_\alpha} = \left(\bar{H}_\alpha - \frac{L_{U1}}{L_{11}}\right) = \left(H_1^0 - \frac{L_{U1}}{L_{11}}\right) \quad (22)$$

where $q_{\alpha + \beta}$ is the heat given to $\alpha + \beta$ by the reservoir A and

$$\bar{H}_\alpha = H_1^0 \equiv - T^2 \frac{d\mu_1^0/T}{dT}$$

$\bar{H}_\alpha$ is the molar enthalpy of the gas. Substituting eq. 7, the reciprocal relation, into eq. 22 and using eq. 12, 13 and 14 we find that

$$\frac{\partial q_{\alpha + \beta}}{\partial(n_1)_\alpha} = - Q^* \quad (23)$$

Thus Q^* is the heat removed from the reservoir A (and taken in by A′) per mole of gas transferred from α to α' under these quasistatic conditions. This of course is the justification for calling Q^* the heat of transfer.

To summarize, our analysis has shown that neither the thermo-osmosis experiment nor the calorimetric experiment taken alone will suffice to test the reciprocal relation, but comparison of the results of the two experiments will provide such a test.

III. Experimental[10]

A. Apparatus.—Our apparatus was patterned after that of Denbigh and Raumann.[6]

The Membrane Assembly.—The membrane assembly, very similar to the assembly "B" of Denbigh and Raumann, was placed between two constant ($\pm 0.05°$) temperature baths separated by a Lucite partition. Aluminum housings, about $^3/_4$ in. thick, were shrunk on circular, porous bronze plates, which were $^1/_8$ in. thick and $1^3/_4$ in. in diameter, so as to squeeze them tightly. The housings fitted tightly into Lucite rings which when held together by screws caused raised rims on the aluminum housings to pinch the membrane and thereby form a sealed sandwich. The rings were then fitted into a larger Lucite ring which in turn fitted into the Lucite partition separating the baths.

To determine the temperature at each membrane surface, Denbigh and Raumann used two thermocouples in each bronze plate, and extrapolated the readings to the surface. We glued a single thermocouple (# 39 B&S constantan soldered to # 40 B&S copper) into a little notch on the face of each bronze plate, so that the thermocouple junction was flush with the membrane surface. This method of directly measuring the surface temperature should be no less accurate than the extrapolation procedure employed by Denbigh and Raumann.

Pressure Measurement.—So that all of the gas on each side of the membrane would be at a uniform temperature, we used manometers with capillary arms and reservoirs similar to one described by Gilmont.[11] These manometers were first calibrated and the reservoirs were then immersed in the constant temperature baths. The calibration enabled us to determine the pressure from a reading of the height of mercury in the capillary without simultaneously observing the height in the reservoir. A slight correction was made for the temperature dependence of the density of the mercury.

B. Materials.—In all of the experiments we used a single sample of a 0.01 in. thick natural rubber membrane which contained 2% sulfur.[12]

The carbon dioxide came from a cylinder and was passed through a Dry Ice trap in order to freeze out any water.

The rare gases came in sealed glass flasks and with the exception of neon were stated to be spectroscopically pure. The label on the flask of neon specified that it contained 760 mm. neon, 2 mm. argon, and $^1/_2$ mm. chlorine. The gas from this flask was passed through a liquid nitrogen trap to

(10) For further details the reader is referred to the dissertation mentioned in reference 1.

(11) R. Gilmont, *Anal. Chem.*, **20**, 474 (1948).

(12) The rubber membrane was kindly donated by Dr. G. E. P. Smith, Jr., of the Chemical and Physical Research Laboratories of the Firestone Tire and Rubber Company.
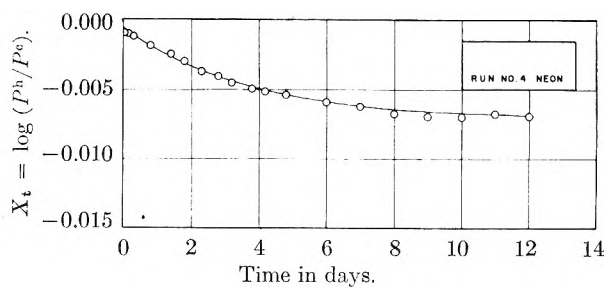
Fig. 2.
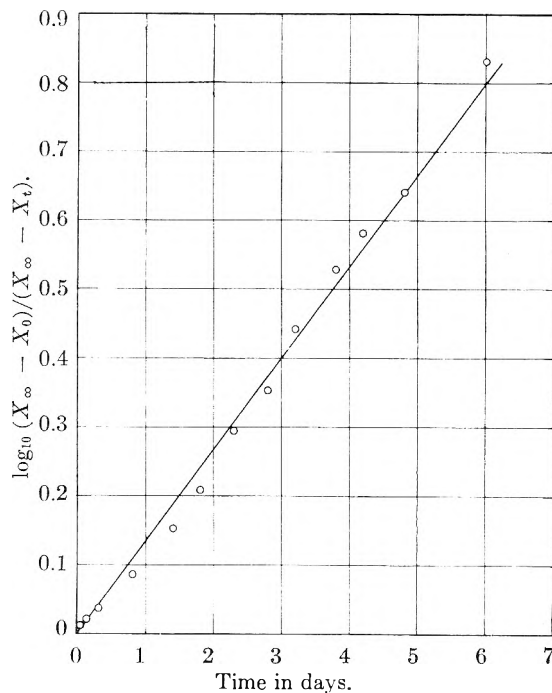
Fig. 3.

freeze out the chlorine. The other gases were not purified further.

C. Procedure.—1. The membrane assembly was placed between the temperature baths before the first run and was not altered or removed until the completion of the last run.

2. The temperature baths were set at temperatures of 18.3 and 44.3° (the exact temperature difference across the membrane itself depended on the gas dissolved in it, but was always near 4°).

3. To degas the membrane the system was evacuated to five microns and kept at that pressure overnight. Previous to the first run the membrane was degassed for several days.

4. The gas was admitted to the membrane assembly.

5. The height of the mercury level in the capillary tubing of each manometer was read through a cathetometer, and the temperature of each side of the membrane was measured with the thermocouples. Such measurements were taken until after the steady state had been attained.

IV. Results

The heats of transfer were calculated from the steady-state data by use of eq. 13, and the permeabilities were obtained graphically from the rate data with the aid of eq. 15, 16, and 17. Figures 2 and 3 illustrate the results of the neon run which happened to be the one of longest duration but was otherwise typical (in Fig. 2, P^h and P^c refer to the pressures on the hot and cold sides of the membrane). Table I lists the results of all of the runs together with comparable results from the literature.

TABLE I

Gas	Run	T mean, °C.	P, mean cm.	$Q^* \times 10^2$, cal./mole	p (pres. exp.) $\times 10^{-8}$, cm.²/sec.-atm.	p (lit.) $\times 10^{-8}$, cm.²/sec.-atm.
CO₂	1	33.0	46	− 9.8		
				−18.6[6]		
He	2	34.0	63	+11.2	33.7	33 (at 35°)[13]
	3	34.0	62	+11.4	53.4[a]	23 (at 25°)[13]
						17 (at 25°)[14]
Ne	4	34.5	45	+ 9.0	8.6	
A	5	34.5	62	− 0.6		
	6 + 7	34.5	55		22.0[b]	
	7[b]	34.5	55	+ 0.3		
Kr	8	34.5	65	− 1.7	48.4[a]	
Xe	9	34.5	40	− 3.2	73.5[a]	33 (at 25°)[14]

[a] These permeabilities are based on fewer data than our others. [b] Run 7 is run 6 resumed after a temporary failure of the temperature controls. The steady-state data obtained from run 7 combined with rate data from run 6 provided our value of p.

V. Errors and Uncertainties

Errors in the temperature measurement may arise from non-uniformity of temperature on a surface of the membrane, inequality of the temperature on the bronze with that on the membrane, and inaccurate recording of the surface temperature because of the existence of a temperature gradient in the thermocouple junction. It is possible in principle to eliminate the influence of these errors, as well as the influence of the temperature dependence of Q^*, on the calculation of the heat of transfer by the extrapolation of sufficient data to zero temperature difference. Unfortunately the difficulty in measuring the temperature difference accurately increases as the difference approaches zero, so that extrapolation may not be practicable. Some evidence that extrapolation may not be necessary was brought forth by Denbigh and Raumann[6] who found that in their apparatus the heat of transfer of carbon dioxide for temperature differences ranging from 9 to 16 degrees was, within the limits of reproducibility, independent of temperature difference. However, even if Q^* is in actuality independent of temperature difference, this result proves at best that the ratio of the measured temperature difference to the actual temperature difference was constant at the several temperature differences observed. Further study is therefore needed to determine whether or not extrapolation is desirable. The errors in the temperature measurement do not affect the value of the mean permeability obtained from the approximate theory which we used, because a knowledge of the temperature in the membrane is not required for the calculation.

The principal source of error in the pressure measurement arose from the capillary depression of the mercury in the arms of the manometers. We did not attempt to correct for this because we found by comparison of the manometers at equal pressures that the measured difference in the pressures (the error in which determined the error in the pressure ratio) was incorrect only by 0.05 cm. Because the continued degassing of the membrane during the course of a run was not great and was nearly equal on both sides of the membrane, it did not affect the pressure ratio appreciably.

Although we assumed that the pressure was uniform in the interior of the membrane, the nature of the squeezing was such that this probably was not the case. Because the membrane assembly was left undisturbed throughout all of the runs, the non-uniformity probably altered the absolute values more than the relative values. Inasmuch as most thermodynamic properties of condensed phases are rather insensitive to pressure, the phenomenological coefficients likewise may be insensitive, and therefore there is a good possibility that the pressure effect is in any event not great.

Since more approximations are made in relating theory to experiment, the measurement of the permeability is less accurate than that of the heat of transfer. By examination of the data we were able to test the validity of the assumptions that during a run the volume of the system is constant (the reason for this requirement is made clear in the derivation given by Denbigh and Raumann[2]) and the temperature difference across the membrane is also constant. We found that the changing mercury levels in the manometers altered the volumes (about 30 cc. on each side of the membrane) by at most 1% and that the temperature difference varied by at most one-half degree. All of the assumptions taken together imply that a plot of ln $(x_\infty - x_0)/(x_\infty - x_t)$ versus time is linear, and Fig. 3 shows that within the scatter of the points the plot is indeed a straight line. The formula for calculating p involves the thickness of the membrane as a multiplicative factor. Because the actual thickness of the rubber membrane in the assembly was unknown, we used the thickness 0.01 in. before squeezing, and hence the absolute values of the permeabilities are to a greater or lesser extent in error by a constant factor.

From Table I we see that our values of Q^* differed only by a few hundredths kilocalorie per mole in duplicate measurements, and this compared favorably with the reproducibility achieved by Denbigh and Raumann.[6] When we undertook this research we were not primarily interested in the permeability, and consequently were not careful to obtain duplicate rate determinations. The two runs with helium present the only information concerning the reproducibility of permeability measurements in our apparatus. Unfortunately the second run of the two contained fewer rate data than any of the other runs, so that comparison of the two probably gives only a lower limit to the reproducibility.

The solubilities of the gases in rubber are probably sufficiently small that the heats and permeabilities are virtually unaffected by changes in mean concentration of gas in the rubber over the (gas phase) pressure range studied. Provided that the other independent variables are held constant, this permits meaningful comparison of results for different gases obtained, as in our experiments, at various pressures not necessarily associated with the same mean concentration. Since our membrane was not disturbed from run to run except to degas and admit gas and since the temperature difference across the membrane and also the mean temperature were approximately

constant from run to run, we may compare as we do in Figs. 4 and 5 our results for the different gases. In fact, the comparative values of Q^* and p may be rather better quantitatively than the absolute values which possibly have been seriously affected by systematic errors.

VI. Discussion

The few previously published results are presented in Table I for comparison with the present data. Our value of Q^* for carbon dioxide (which we measured especially for the comparison) of -1.0 kcal. per mole compares not unfavorably with -1.9 kcal. per mole obtained by Denbigh and Raumann. The disagreement may arise from errors or from variability in the properties of rubber membranes. The value of p for helium of 34×10^{-8} cm.^{2} sec.$^{-1}$ atm.$^{-1}$ quantitatively agrees with 33×10^{-8} cm.^{2} sec.$^{-1}$ atm.$^{-1}$ found by van Amerongen,[13] but the very close agreement no doubt is to some extent accidental. The data of Norton[14] on helium and xenon at 25° qualitatively substantiate our results. In this case it is reasonable to suppose that the differences are due in part to temperature effects, and the value of the permeability to helium found by van Amerongen[13] at 25° lends support to this view.

The heats of solution of carbon dioxide and helium in rubber have been found to be -2.8 and $+1.8$ kcal. per mole by van Amerongen.[15] These values, which have the same sign as the heats of transfer and do not differ greatly from them, indicate that ΔH contributes in an important way to the total heat of transfer, $\Delta H + Q_m^*$. If we plot Q^* versus atomic weight in the case of the rare gases (Fig. 4), we discover that it is a monotonic function, and for argon, krypton and xenon the curve is almost linear. The difference in Q^* in going from neon to argon is much sharper than in going from helium to neon. A systematic study of the heats of solution of the rare gases in rubber has not been carried out. However, Lannung[16] evaluated the heats of solution of helium, neon and argon in various organic solvents, and a plot of his results shows not only monotonic behavior but also a greater difference in ΔH between neon and argon than helium and neon. This suggests that the differences in Q^* among the rare gases are determined by the differences in the heats of solution.

(13) G. J. van Amerongen, *J. Appl. Phys.*, **17**, 972 (1946).

(14) F. J. Norton, *J. Chem. Phys.*, **22**, 1145 (1954).

(15) G. J. van Amerongen, *J. Poly. Sci.*, **5**, 307 (1950).

(16) A. Lannung, *J. Am. Chem. Soc.*, **52**, 68 (1930). His u may be taken to be $-\Delta H$ for the purposes of our comparison.
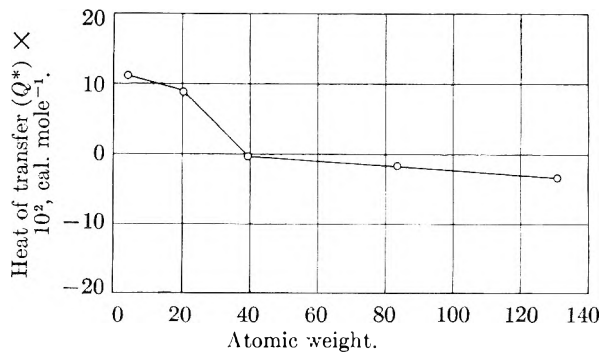
Fig. 4.
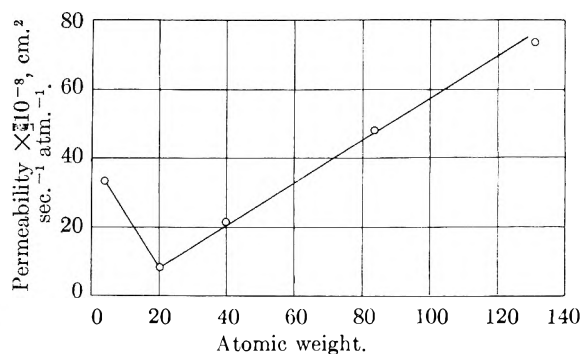
Fig. 5.

The permeability when plotted against atomic weight (Fig. 5) exhibits a minimum at neon, and is very nearly linear thereafter. The permeability p is equal to Ds where D is the diffusivity and s is the solubility.[17] It is reasonable to guess that D is a monotonic decreasing function of atomic weight, and solubility data obtained by Lannung[16] suggest that s is a monotonic increasing function. Thus p is the product of two functions monotonic in opposite senses, and so may possess a minimum. If D and s were monotonic in the same sense, the product could not exhibit an extremum. The linearity in the graph is very likely fortuitous.

(17) W. Jost, "Diffusion in Solids, Liquids, Gases," Academic Press, Inc., New York, N. Y., 1952.

AGING OF SILICA–ALUMINA CRACKING CATALYST. I. KINETICS OF STRUCTURAL CHANGES BY HEAT AND STEAM

By W. G. Schlaffer, C. Z. Morgan and J. N. Wilson

Shell Development Company, Emeryville, California

Received November 5, 1956

A systematic study has been made of the rate of change in the specific surface area and specific pore volume of silica-alumina cracking catalysts exposed to temperatures in the range 478–950° and steam partial pressures in the range 0–7 atmospheres. The decline in specific surface area is described accurately by an empirical equation of the form $-dS/dt = kS^n$ where S is the specific surface area, t is time, and n and k are constants at any given set of conditions. These constants vary smoothly with changing temperature and partial pressure of steam. The rate of change in specific pore volume is proportional to the rate of change of specific surface area at the highest temperatures, but decreases relative to the rate of change of specific surface area as the temperature decreases; changes in the partial pressure of steam at a given temperature have a small but definite effect on this relationship. The results are discussed in terms of a model for the structure of silica-alumina catalysts and of various possible mechanisms of material transport involved in the aging process.

Introduction

The decline in specific surface area of silica–alumina cracking catalyst during its use in the catalytic cracking process is a phenomenon of economic importance and technical interest. It is accompanied by a decline in specific pore volume and in catalytic activity. The most important factors controlling the rate of decline are temperature and partial pressure of steam.

Little information concerning the kinetics of this deactivation process is available in the literature. Some relations between the resulting changes in the physical properties of the gels have been reviewed by Ries.[1] His principal conclusions were the following.

(1) During aging at high temperatures (800–1000°) in high vacuum the distribution of pore radii (as defined by the Kelvin equation for the relative vapor pressure of liquids in cylindrical capillaries) remains almost unchanged, and the average pore radius (proportional to the ratio of specific pore volume to specific surface area) remains approximately constant.

(2) During aging at lower temperatures (500–600°) in the presence of steam the average pore radius increases considerably; the distribution of pore radii broadens and the median pore radius increases.

The work reported here was undertaken with two objectives.

(1) To obtain detailed knowledge of the kinetics of the process and of the dependence of the rate on the temperature and on the partial pressure of steam.

(2) If possible, to relate the changes in the gross physical properties of the system to the structure of the gel and to the mechanisms of material transport involved in the aging process.

Experimental

Catalyst.—The catalyst was a synthetic microspheroidal silica–alumina gel commercially manufactured by the American Cyanamid Company in 1951. It contained 12.4%w. Al_2O_3, 0.04%w. Fe_2O_3, 0.02%w. Na_2O and 0.3%w. sulfate based on catalyst weight after ignition to 1100°. After elutriation to remove particles less than 40 μ in diameter and calcination at 565° to remove the excess water, the catalyst had a specific surface area of 608 m.²/g. and a specific pore volume of 0.73 cc./g. All experiments were made with catalyst that had been pretreated in this way.

Elutriation.—Approximately one liter of catalyst was

placed in a Pyrex tube 90 cm. long, 9 cm. in diameter having a sintered frit close to the bottom to support the catalyst. Air, dried over drierite, was passed upward through the column of catalyst powder at a rate of 14 liters per minute for a period of 16 hours.

Calcination and Dry Air Aging.—The catalyst was calcined at 565° in the quartz tube and furnace shown in Fig. 1. The maximum charge of catalyst was 1000 cc. which, when fluidized by a stream of dry air (4 cc./min./g. catalyst), extended one-half of the length of the furnace. The temperature profile of the bed was maintained to ±2° by means of a Celectray controller. For calcination, the temperature was gradually raised to 200° at a rate of 2° per minute and then raised to 565° at a rate of 5° per minute. The time of calcination, 6 hours unless otherwise stated, was considered to start when the catalyst bed reached the temperature desired.

For high temperature aging in dry air the same apparatus was used. The calcined catalyst was brought to temperature at a rate of 5°/min. in a stream of dry air.

Aging in Steam at One Atmosphere.—For aging in one atmosphere steam pressure, water was fed to the bottom of the vertical quartz tube used for the calcinations; from there it is changed to steam and passed through the catalyst column. The water was maintained at a constant level by the arrangement of the inverted two liter graduate and leveling bulb (G) of Fig. 1 the drain of which was connected directly to the bottom of the catalyst tube. The drain and air vent of the leveling bulb were of 1 mm. capillary tubing. These restrictions prevented surging of the water. With this arrangement, the passage of water as steam through the catalyst powder could be held remarkably constant at 20 g. per hour.

Samples were withdrawn periodically by lowering a quartz thimble suspended by a platinum wire into the fluidized bed of catalyst.

Aging at Less Than One Atmosphere Steam.—For aging at less than one atmosphere steam pressure, the air humidifier (H) was attached to the bottom of the catalyst tube. The air was saturated with water to any desired level by controlling the temperature of the humidifier.

Aging at Greater Than One Atmosphere Steam.—The reactor tube consisted of an enamel lined stainless steel vessel which fitted into the Hevi-Duty furnace; it is shown in Fig. 2. The operation of the pressure steamer is self-evident from the figure. Samples were withdrawn via the decompression chamber (H) connected to a concentric tube leading to the catalyst bed.

For all agings the catalyst was heated to the nominal temperature at a rate of 5° per minute in a fluidizing stream of dry air at 4 cc./min./g. catalyst. After equilibration of the temperature, the air flow was discontinued and either water or humidified air was allowed to flow to the lower end of the catalyst tube by connecting the appropriate apparatus.

The zero time sample is that withdrawn when the catalyst had reached the temperature of the experiment, *i.e.*, just before the introduction of steam. Before a surface area or pore volume measurement each sample was dried at 500° for one hour in a stream of dry air. Values of surface areas and pore volumes refer to a gram of catalyst in the condition resulting from aging and drying with whatever water remains.

(1) H. E. Ries, Jr., *Advances in Catalysis*, IV, 87 (1952).

TABLE I

AGING OF SILICA–ALUMINA CATALYST AT VARIOUS TEMPERATURES IN THE PRESENCE OF STEAM

Temp., °C. →	478			576			576			576			576		
Steam pressure, atm. (abs.)	1			0.30			1			3			7		
Time, hr.	S, m.²/g.	V_p, cc./g.	$\bar{d}$, Å.	S, m.²/g.	V_p, cc./g.	$\bar{d}$, Å.	S, m.²/g.	V_p, cc./g.	$\bar{d}$, Å.	S, m.²/g.	V_p, cc./g.	$\bar{d}$, Å.	S, m.²/g.	V_p, cc./g.	$\bar{d}$, Å.
0	..	...	...	..	...	...	609	0.719	47.2	..	...	...	..	...	...
.1	..	...	...	587	0.732	49.9	599	.702	46.9	..	...	...	..	...	...
.2	..	...	...	602	...	...	565	.695	49.3	..	...	...	..	...	...
.3	..	...	...	578	.734	50.8	..	...	...	..	...	...	..	...	...
.4	..	...	...	586	.735	50.2	564	.698	49.5	..	...	...	..	...	...
.5	..	...	...	..	...	...	..	...	...	..	...	...	259	0.603	93.1
.6	..	...	...	569	.721	50.7	..	...	...	..	...	...	..	...	...
.7	..	...	...	..	...	...	523	.682	52.1	..	...	...	..	...	...
1.0	..	...	...	..	...	...	505	.678	53.7	..	...	...	230	.601	105
1.3	..	...	...	561	.704	50.2	..	...	...	..	...	...	..	...	...
1.8	..	...	...	555	.708	51.0	..	...	...	326	0.633	77.7	..	...	...
2.0	..	...	...	..	...	...	464	.675	58.2	..	...	...	201	.591	117
2.5	..	...	...	545	.699	51.3	..	...	...	..	...	...	..	...	...
3.5	..	...	...	531	.692	52.1	..	...	...	297	.617	83.1	..	...	...
4	537	0.700	52.1	..	...	...	418	.660	63.2	..	...	...	170	.586	138
10	..	...	...	488	.688	56.4	377	.642	68.1	..	...	...	..	...	...
14	..	...	...	478	.682	57.1	..	...	...	..	...	...	..	...	...
20	474	.690	58.2	471	.679	57.7	341	.634	74.4	216	.598	111	..	...	...
48	426	.684	64.2	435	.670	61.6	..	...	...	182	.597	131	..	...	...
92	..	...	...	..	...	...	276	.616	89.3	..	...	...	..	...	...
96	..	...	...	418	.657	62.9	..	...	...	168	.599	143	..	...	...
120	380	.675	71.0	405	.654	64.6	273	.612	89.7	162	.594	147	..	...	...
144	..	...	...	396	.653	66.0	261	.609	93.3	..	...	...	..	...	...
192	..	...	...	387	.647	66.8	..	...	...	152	...	...	..	...	...
196	360	.671	74.6	..	...	...	245	.608	99.3	..	...	...	..	...	...
216	..	...	...	..	...	...	..	...	...	147	.608	166	..	...	...
288	..	...	...	365	.644	70.6	..	...	...	..	...	...	..	...	...
360	335	.659	78.7	..	...	...	230	.600	104	..	...	...	..	...	...
456	..	...	...	357	.634	71.0	..	...	...	..	...	...	..	...	...
504	316	.661	83.8	..	...	...	219	.596	109	..	...	...	..	...	...
672	..	...	...	339	.631	74.5	..	...	...	..	...	...	..	...	...
696	..	...	...	..	...	...	214	.593	111	..	...	...	..	...	...
960	..	...	...	321	.626	78.0	..	...	...	..	...	...	..	...	...

Temp., °C. →	678			778			778			778			863		
Steam pressure, atm. abs.	1			0.11			0.3			1			1		
0	588	0.710	48.3	571	0.675	47.3	581	0.700	48.2	493	0.648	52.7	396	0.527	53.2
.1	..	...	...	511	.659	51.6	492	.636	51.7	395	.579	58.6	172	.303	70.5
.2	..	...	...	513	.655	51.1	449	.607	54.1	343	.534	62.3	131	.264	80.6
.3	..	...	...	505	.637	50.4	..	...	...	311	.516	65.7	117	.252	86.2
.4	..	...	...	494	.633	51.3	387	.570	58.9	289	.506	70.0	104	.241	92.7
.5	..	...	...	..	...	...	..	...	...	..	...	...	97	.231	94.8
.6	..	...	...	487	.620	50.9	..	...	...	267	.489	73.8	..	...	...
.7	..	...	...	..	...	...	369	.562	60.9	..	...	...	..	...	...
1.0	..	...	...	..	...	...	347	.527	60.7	..	...	...	..	...	...
1.3	..	...	...	453	.593	52.2	..	...	...	228	.461	80.9	..	...	...
1.8	..	...	...	423	.586	55.4	..	...	...	212	.450	84.9	..	...	...
2.0	..	...	...	..	...	...	315	.497	63.1	..	...	...	..	...	...
2.5	..	...	...	410	.576	56.2	..	...	...	192	.442	92.1	..	...	...
3.5	..	...	...	395	.568	57.5	..	...	...	177	.429	96.9	..	...	...
4	293	.585	79.9	..	...	...	273	.482	70.6	..	...	...	..	...	...
7	..	...	...	363	.533	58.8	..	...	...	146	.413	113	..	...	...
10	..	...	...	341	.520	61.0	233	.451	77.4	133	.402	121	..	...	...
14	..	...	...	326	.502	61.6	..	...	...	123	.397	129	..	...	...
20	224	.549	98.0	305	.492	64.5	197	.426	86.5	111	.390	141	..	...	...
48	..	...	...	258	.446	69.1	167	.400	95.8	..	...	...	..	...	...
92	171	.527	123	..	...	...	..	...	...	..	...	...	..	...	...
96	..	...	...	225	.417	74.1	..	...	...	..	...	...	..	...	...
120	165	.522	127	217	.406	74.8	142	.379	107	..	...	...	..	...	...
144	..	...	...	209	.401	76.7	136	.376	111	..	...	...	..	...	...
192	..	...	...	191	.393	82.3	126	.374	119	..	...	...	..	...	...
196	152	.515	136	..	...	...	..	...	...	..	...	...	..	...	...
216	..	...	...	..	...	...	124	.373	120	..	...	...	..	...	...
288	..	...	...	174	.380	87.4	114	.363	127	..	...	...	..	...	...
360	135	.506	150	..	...	...	111	.355	126	..	...	...	..	...	...
384	..	...	...	163	.369	90.6	..	...	...	..	...	...	..	...	...
456	..	...	...	159	.364	91.6	104	.352	135	..	...	...	..	...	...
480	..	...	...	..	...	...	104	.357	137	..	...	...	..	...	...
504	125	.501	160	..	...	...	..	...	...	..	...	...	..	...	...
552	..	...	...	152	.368	96.8	..	...	...	..	...	...	..	...	...
696	117	.494	169	..	...	...	..	...	...	..	...	...	..	...	...
864	112	.483	173	..	...	...	..	...	...	..	...	...	..	...	...
984	107	.484	181	..	...	...	..	...	...	..	...	...	..	...	...
1320	95	.464	197	..	...	...	..	...	...	..	...	...	..	...	...

TABLE II
AGING OF SILICA–ALUMINA CATALYST IN A STREAM OF DRY AIR

| Temp., °C. Time, hr.	785 S, m.²/g.	785 V_p, cc./g.	785 $\bar{d}$, Å.	847 S, m.²/g.	847 V_p, cc./g.	847 $\bar{d}$, Å.	900 S, m.²/g.	900 V_p, cc./g.	900 $\bar{d}$, Å.	940 S, m.²/g.	940 V_p, cc./g.	940 $\bar{d}$, Å.	950 S, m.²/g.	950 V_p, cc./g.	950 $\bar{d}$, Å.
0	494	C.639	51.7	484	0.598	49.4	384	0.495	51.5	..	...	...	139	0.205	59.0
.2	486	.628	51.7	..	...	...	..	...	...	..	...	...	..	...	...
.3	475	.631	53.1	..	...	...	..	...	...	180	0.266	59.1	..	...	...
.5	470	.623	53.0	436	.564	51.7	..	...	...	169	.262	62.0	111	.167	60.2
.7	477	.619	51.9	..	...	...	..	...	...	165	.256	62.1	..	...	...
1.0	465	.622	53.5	441, 451	.560	50.2	317	.395	49.8	159	.249	62.6	104	.148	56.9
1.5	..	...	...	446	.552	49.5	305	.378	49.6	154	.232	60.3	97	.137	56.5
2	468	.614	52.5	405, 408	.544	53.5	292, 310	.378	50.3	143	.225	62.9	92	.125	54.3
3	460	.611	53.1	406, 437	.547	53.9	295	.388	53.6	133	.223	67.1	87	.115	52.9
4	..	...	...	..	...	...	282	.364	51.6	119	.191	64.2	82	.112	54.6
5	467	.608	52.1	410, 419	.534	53.5	282	.380	53.9	114	.183	64.2	..	...	...
6	..	...	...	..	...	...	280	.345	49.3	110	.174	63.3	..	...	...
7	457	.601	52.6	..	...	...	269	.341	50.7	103	.154	60.0	72	.094	52.2
24	431	.593	55.0	402, 405	.511	50.7	..	...	...	..	...	...	..	...	...
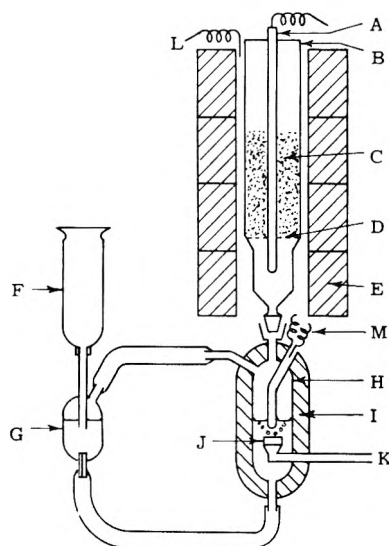
Fig. 1.—Apparatus for aging in steam at less than one atmosphere pressure: A, removable well for recording thermocouples; B, quartz tube, 80 cm. long, 7 cm. diameter; C, gel charge; D, slotted quartz plate with Refrasil cloth and platinum; E, model M-3024S Hevi-Duty furnace; F, water reservoir, 2-liter graduate; G, water leveling bulb; H, heating tape; I, asbestos insulation of air humidifier; J, sintered glass frit; K, air inlet; L, controlling thermocouples to celectray; M, controlling and indicating thermocouples.

Specific pore volumes were determined by the method of Benesi, Bonnar and Lee[2] but using n-heptane and dibutyl phthalate instead of carbon tetrachloride and cetane. Specific surface areas were measured by the BET method with nitrogen.

For brevity, specific surface area (m.²/g.) and specific pore volume (cc./g.) will be referred to hereafter simply as surface area and pore volume, respectively.

Results and Conclusions

Decline of Surface Area.—The data for agings at 478, 576, 678, 778 and 863° in one atmosphere of steam, at 576° and 0.3, 3 and 7 atmospheres of steam, at 778° in 0.11 and 0.3 atmosphere of steam and at 785, 847, 900, 940 and 950° in a stream of dry air are recorded in Tables I and II. When the log surface area is plotted *versus* log time, as shown in Fig. 3, almost straight lines are obtained. In most cases there is a perceptible downward curvature, which, in the case of the agings in steam, becomes progressively less marked at higher temperatures.

(2) H. A. Benesi, R. U. Bonnar and C. F. Lee, *Anal. Chem.*, **27**, 1963 (1955).

It is quite evident that both temperature and steam pressure exert powerful influences on the decline of surface area. This is shown clearly in Table III, by the half-life, $t_{1/2}$, defined as the time necessary to reduce the surface area to 304 m.²/g.

TABLE III
HALF LIFE OF SURFACE AREA UNDER VARIOUS AGING CONDITIONS

t, °C.	Aging conditions atm. (abs) steam	$t_{1/2}$, hr.
478	1	740
576	0.3	3000
576	1	60
576	3	3.2
576	7	0.2
678	1	4
778	0.11	21
778	0.3	2.3
778	1	0.37
785	Dry air	10^{11}
847	Dry air	10^6
863	1	0.02
900	Dry air	2
940	Dry air	<0.01
950	Dry air	<0.01

Self-steaming.—Loss of surface area at high temperatures in a stream of dry air occurs extremely rapidly at first and then much more slowly. The initial loss, which incidentally is the major loss in these experiments, occurs in less than 0.1 of an hour. Indeed, most of the loss occurs even before the catalyst reaches the nominal temperature of aging, that is, during time taken to heat the catalyst from 565° to the desired aging temperature.

The initial part of the heat aging is complicated by the phenomenon of self-steaming. The catalyst contains 2% water after calcination at 565° for 6 hours in a stream of dry air. During the subsequent heating period to temperatures in excess of 565°, much of this water is unavoidably released from the catalyst. Since the steam pressure in the vicinity of the catalyst surface can be momentarily high, some steam aging occurs. Most of the self-steaming occurs at the lower temperatures because less and less water is released per degree rise in temperature as the temperature is increased. At an air rate of 4 cc. (STP)/min./g. of catalyst, a partial

pressure of steam as high as 0.06 atmosphere could have existed in the effluent air. This is high enough at temperatures upwards of 600° to cause some steam aging. At the higher temperatures (900° and above), very little additional water is released and any further aging becomes more nearly "thermal."

In order to assess the importance of self-steaming, the calcined catalyst was heated very slowly (ca. 1°/min.) from 565–950°. This gave more time for water removal before a high temperature was reached. Samples were taken at 847, 900 and 950°. An appreciable self-steaming in the earlier experiments is shown by the fact that the surface area at a given temperature was higher with slow heating (in spite of the longer time) as can be seen below in Table IV.

<center>Table IV</center>

<center>Surface Areas After Heating in Dry Air</center>

Temp. attained, °C.	Rapid heating (5°/min.)			Slow heating (1°/min.)		
	Surface area, m.²/g.	Pore vol., cc./g.	Pore diameter, Å.	Surface area, m.²/g.	Pore vol., cc./g.	Pore diameter, Å.
847	484	0.598	49.4	536	0.665	49.6
900	384	.495	51.5	455	.595	52.3
950	139	.205	59.0	263	.320	48.7

Heating experiments in a high vacuum (<5 μ pressure) on the same catalyst were performed by Roper.[3] Here the steam evolved is pumped away as rapidly as it is formed and self-steaming should be very small indeed. The results showed that even during the slow heating in a stream of dry air considerable self-steaming occurred. For example at 950° the surface area for slow heating was 263 m.²/g. and that for the vacuum heating was 430 m.²/g.

The foregoing results show that catalysts heated in dry air were not aged by a purely thermal process, but were partially aged by steam before reaching the nominal aging temperature. Indeed, it is expected that aging by self-steaming continued for some time at the nominal temperature. The influence of steam, however, would diminish rapidly with time as a consequence of the rapidly diminishing evolution of water.

Since the steam originates on the catalyst surface, whether in a stream of extremely dry air or in the highest vacuum, there will always be a finite residence time of the freed water in the catalyst particle. It becomes apparent, then, that a purely thermal aging of a catalyst cannot be attained but merely approached.

Empirical Equation for Decline of Surface Area. —The decline rate of surface area under all conditions studied can be expressed by the empirical equation

$$-\frac{dS}{dt} = kS^n \tag{1}$$

where S is the specific surface area, t is time, and k and n are constants. In an expression of this type, k represents the reaction rate constant and n the order of the reaction.

Integration of this equation with the condition that $S = S_0$ at zero time gives

(3) E. E. Roper, Shell Development Company, unpublished work.
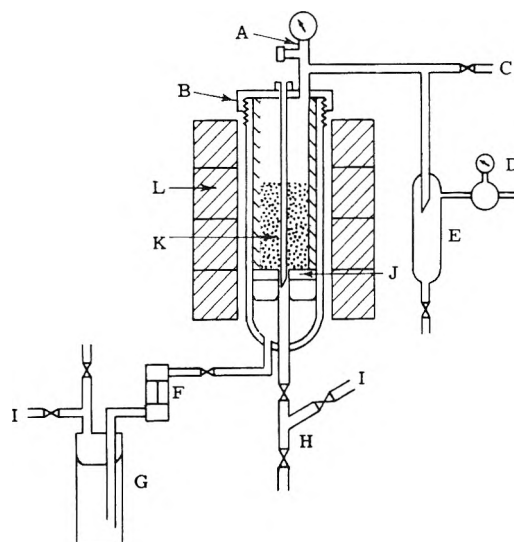
Fig. 2.—Apparatus for aging in steam at greater than one atmosphere: A, pressure gage and bursting disk; B, enamel-lined stainless steel vessel with concentric thermowell; C, helium for constant gas bleed through regulator; D, grove pressure regulator; E, liquid–vapor separator; F, rotameter for water feed; G, pressured water; H, decompression chamber for withdrawing samples; I, high pressure helium; J, perforated plate and Refrasil cloth; K, gel charge; L, Hevi-Duty furnace (Model 3024S).
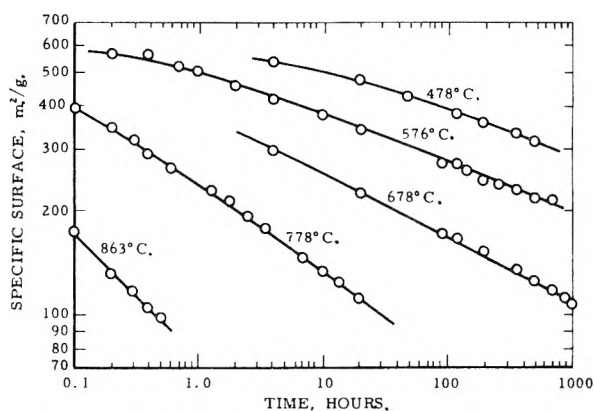
Fig. 3.—Effect of temperature upon aging silica–alumina in one atmosphere steam.

$$(S_0/S)^{n-1} = k(n - 1)S_0^{n-1}t + 1 \tag{2}$$

which may be rearranged to

$$\log S = \log S_0 - \frac{1}{n-1}\log k(n - 1)S_0^{n-1} - \frac{1}{n-1}\log \left(t + \frac{S_0^{1-n}}{k(n - 1)} \right) \tag{3}$$

or

$$\log S = -\frac{1}{n-1}\log k(n - 1) - \frac{1}{n-1}\log (t + B) \tag{4}$$

Because of the fact that some aging occurs by self-steaming while the sample is being brought to temperature in a stream of dry air, the surface area at the start of the isothermal aging period is smaller than S_0. This may be formally taken into account by increasing the aging time under isothermal conditions by an unknown amount Δt, so that the addi-
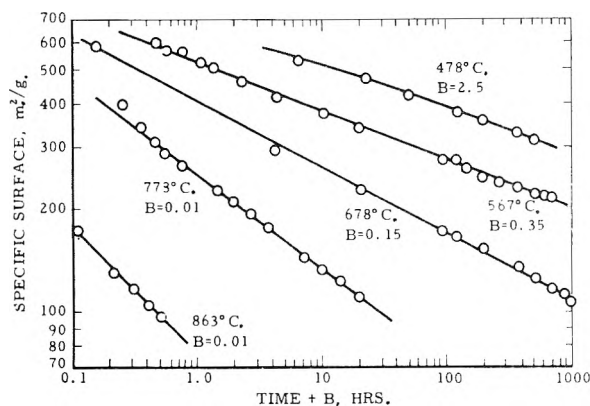
Fig. 4.—Aging of silica–alumina catalyst in one atmosphere steam at various temperatures.

tive constant B in equation[4] becomes

$$B = \Delta t + S_0^{1-n}/k(n - 1) \qquad (5)$$

By adjusting the value of B so that a plot of log S versus log $(t + B)$ is linear, n can be determined from the slope and k from the value of log S where $t + B$ is unity on the time scale.

The small scatter of points about the straight lines for the agings in one atmosphere steam at various temperatures (Fig. 4) shows the excellent agreement with equation 4 and hence with equation 1. The value of n at one atmosphere steam pressure decreases regularly from 9.1 at 478° to 3.8 at 863°. The changing value of n, which may be termed the "order" of the reaction, suggests that the mechanism for the loss of surface area may be changing with temperature.

TABLE V
Aging of Silica-Alumina Catalyst in One Atmosphere Steam Pressure

According to the expression $- \dfrac{dS}{dt} = kS^n$

t, °C.	n	k (m.²/g.)$^{(1-n)}$(hr.)$^{-1}$	B
478	9.1	1.5×10^{-24}	2.5
576	8.2	3.7×10^{-21}	0.35
678	6.3	3.6×10^{-16}	.15
778	4.7	3.2×10^{-10}	.15
863	3.8	2.0×10^{-6}	.01

Steam pressure also influences the value of n as shown in Table VI.

It has been pointed out to us by Hughes[5] of these laboratories that the range covered by the values of k is very considerably decreased if equation 1 is written in the form

$$- \frac{1}{S_0} \frac{dS}{dt} = k'(S/S_0)^n \qquad (6)$$

This formulation also has the advantage that the rate constant k' has the dimensions of reciprocal

TABLE VI
Steam Aging of Silica-Alumina Catalyst

According to the Expression $- \dfrac{dS}{dt} = kS^n$

| t, °C.	Steam pressure, atm. abs.	n	k (m.²/g.)$^{(1-n)}$ (hr.)$^{-1}$	B
576	0.3	11.4	4.5×10^{-31}	2.0
	1	8.2	3.7×10^{-21}	0.35
	3	6.9	1.4×10^{-16}	0
	7	4.6	7.6×10^{-10}	0.5
778	0.11	6.0	3.5×10^{-15}	1.3
	0.30	5.7	1.4×10^{-13}	0.5
	1	4.7	3.2×10^{-10}	0.15

time.[6] The value of k' can be obtained from k by multiplication by S_0^{n-1}. The value of S_0 to be chosen is subject to some uncertainty; it has been chosen as the actual initial surface area of the sample, about 600 m.²/g.

Values of k' derived from Table VI are shown in Table VII, together with values of the ratio k'/p^2 where p is the partial pressure of steam. At 576° this ratio is nearly constant; the deviant value at 7 atm. would be brought into agreement with the rest by a change in the value of n from 4.6 to 4.7. This change in n would not exceed the experimental uncertainty. At 778°, however, the value of k' has a dependence on p that is intermediate between the first and second powers.

Application of equation 6 to the data of Table V yields values of k' which obey an Arrhenius equation such that for all the data up to a temperature of 778°

$$\log k' = 6.18 - 5.64 \times 10^3/T$$

TABLE VII
Rate Constants Derived from Equation

$$- \frac{1}{S_0} \frac{ds}{dt} = k'(S/S_0)^n$$

t, °C.	Steam pressure, atm. abs.	n	k' (m.²/g.)$^{-1}$	k'/p^2 (m.²/g.)$^{-1}$ (atm.)$^{-2}$
576	0.3	11.4	0.0316	0.35
	1.0	8.2	0.37	.37
	3.0	6.9	3.36	.37
	7.0	4.6	7.6	.16
778	0.11	6.0	0.269	22
	0.30	5.7	1.53	17
	1.0	4.7	6.1	6.1

The point at 863° deviates from this relation by more than the experimental error. This relation corresponds to an activation energy of 26.8 kcal./mole and a value of 1.5×10^6 hr.$^{-1}$ for k'_0. In view of the changing apparent "order" of the process and the fact that $k'(n - 1)$ is essentially the rate of change of $(S_0/S)^{n-1}$, the significance of this activation energy is not clear. Nevertheless, the relation is still useful for purposes of extrapolation or interpolation.

The dependence of n on temperature at constant steam pressure is shown in Fig. 5. The substantial

(4) It should be noted that an empirical equation of the form of equation 4, a linear relation between log S and log $(t + B)$, has been used in the petroleum industry for many years for describing catalyst deactivation. As early as 1948, it was applied by E. Gordon and R. P. Trainer at the Houston Research Laboratory of Shell Oil Company.

(5) R. R. Hughes, private communication, March, 1956.

(6) An obvious alternative to equation 6 is $-d \log S/dt = k(S/S_0)^n$. This leads to the integrated form log $(S_0/S) = 1/n$ log $nk + 1/n$ log $(t + 1/nk)$, whereas (6) leads to log $S_0/S = 1/(n - 1)$ log $(n - 1)k + 1/(n - 1)$ log $(t + 1/(n - 1)k)$. Both equations, therefore, appear to be equally satisfactory for an empirical description of the aging process.

variations suggest that the mechanism of material transport, or the competition among various mechanisms, may be affected by both temperature and partial pressure of water vapor.

If equation 5 is applied to the aging curves obtained at high temperatures in dry air, very high values of n are obtained especially at the lower of these temperatures. For instance, at 847° the n value appears to be about 35. These high values are probably without any real physical significance and as such do not describe thermal aging in the absence of water vapor. Since the deactivation comprises two consecutive reactions, initially one of high rate (self-steaming), followed by one of low rate, the apparent value of n necessarily would be high. Of primary interest are the constants for the second reaction, i.e., the more nearly thermal one. If the latter portions (after one hour) of the aging curves are fitted to the equation much more reasonable values are obtained. The large values of B necessary to give a straight line are consistent with the existence of the initial fast reaction of self-steaming. The value of B is essentially the time necessary under the conditions prevailing during the latter, or thermal, part of the aging to account for the relatively large loss of surface area caused by self-steaming.

The surface area data for 785 and 847° showed too much scatter for the small decline of surface area after one hour to give any reliable estimate of the constants. It can only be said that it is possible that the values of n are similar to those at the higher temperatures, but the rate constants, k, are lower. The constants at 900, 940 and 950° from data after one hour are recorded in Table VIII.

TABLE VIII
CONSTANTS FOR HEAT DEACTIVATION

t, °C.	n	$\dfrac{k}{(\mathrm{m.^2/g.})^{(1-n)}}$ $(\mathrm{hr.})^{-1}$	B
900	4.0	9.6×10^{-10}	9.0
940	3.5	4.6×10^{-7}	2.2
950	4.9	2.3×10^{-9}	1.0

In the temperature range studied for aging in dry air there seems to be no trend of n with temperature. The data summarized in Table VIII could be fitted, for example, with a uniform value of $n = 4.0$. Because of the large probable error involved a more definite statement cannot be made. Even after one hour the aging may still be influenced by some self-steaming so that if anything the real values of n are even lower. The n values for heat aging were somewhat higher than those anticipated by extrapolation of the curve for steam aging to the same temperatures. The rate constants, k, however, are 10^7 less than for steam aging at similar temperatures. This, of course, shows the powerful accelerating effect of steam for the decline of surface area.

Decline of Pore Volume and Enlargement of the Pores.—Aging by both heat and steam also causes the disappearance of pore volume. The collapse of the pore volume occurs at a rate dependent on the temperature and the presence of steam and is seemingly not related to the surface area decline. The relative rates of surface area
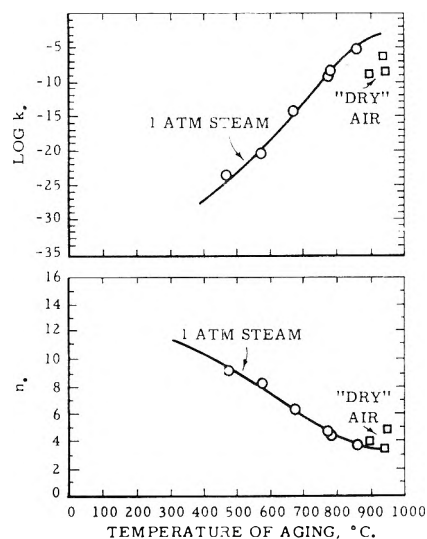

Fig. 5.—Constants for the aging of silica–alumina.

and pore volume disappearance are such in the presence of steam that there is an effective increase in the average "diameter" of the micropores.[7] The rate of increase of average pore diameter is strongly influenced by temperature in the presence of steam. The increase is greatest at the lowest temperatures and becomes progressively less as the temperature is increased. This is seen easily in Fig. 6 where the surface area is plotted versus the pore volume for the various agings. Any straight line through the origin is a line of constant pore diameter. The diagonal line between fresh catalyst and the origin, then, is the line of the pore diameter of the fresh catalyst (48A). The pore diameters become progressively larger as the points depart to the right and downward of this diagonal. It is worthy of note that for aging in steam the least change of pore volume for a given change in surface area occurs at the lowest temperature.

Aging by heat alone in a stream of dry air causes only a small enlargement of the micropores (Fig. 7). Although the points are very close to the diagonal there is a small, but nevertheless real, systematic deviation from the diagonal. It should be noted that the line for the steam deactivation at 863°, when drawn back to the fresh catalyst, passes through the points for thermal deactivation (absence of steam) at 847°, a temperature which is relatively close to 863° (compare Fig. 6 and 7). A similar situation exists for steam at 778° and dry air at

(7) Pore diameters are calculated from the formula $\bar{d} = 4 \times 10^4 V_\mathrm{p}/S$, where $\bar{d}$ is in Å. if V_p is in cc./g. and S is in m.²/g. This formula is valid for cylindrical pores open at both ends. In view of recent more exact knowledge about catalyst structure, however, it should be recognized that $4 \times 10^4 V_\mathrm{p}/S$ is not a true pore diameter. A silica–alumina gel is not a solid permeated by cylindrical pores, but rather is an aggregate of small spheres. If r is the sphere radius, F the fraction void, and ρ the solid density of an individual sphere, then

$$S_\mathrm{s} = 3 \times 10^4/\rho r, \text{ for } r \text{ in Å.}$$
$$V_\mathrm{p} = F/(1 - F)\rho$$
$$4 \times 10^4 V_\mathrm{p}/S = 4Fr/3(1 - F)$$

Thus surface area is determined by size of the ultimate spheres, pore volume by packing, and the apparent pore diameter by a combination of the two. The packing may be expressed in terms of the fraction void, or in terms of the number of spheres, N, touching a given sphere. The apparent pore diameter is still a convenient way of stating the ratio of V_p to S and it will be used to some extent for correlation.
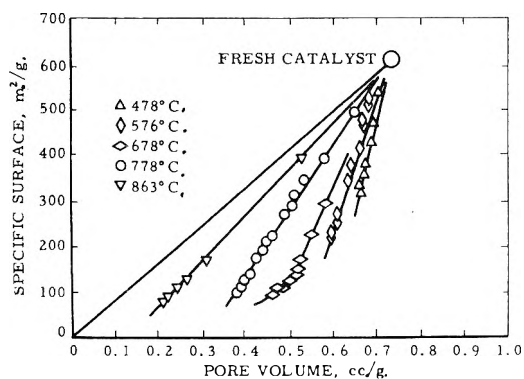
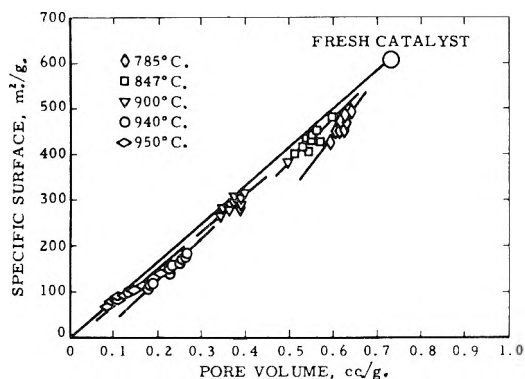Fig. 6.—Surface area–pore volume relationship upon aging of silica–alumina in one atmosphere of steam.

Fig. 7.—Surface area–pore volume relationship upon aging of silica–alumina in a stream of dry air.

785°. This strongly suggests that the pore volume–surface area relationship during aging of a catalyst is a function of the temperature only and that the primary effect of steam is to accelerate the change of physical properties along the path determined by the temperature. This implies no fundamental difference between heat aging and steam aging at high temperatures.

Work of others is not in agreement with the concept that temperature alone determines the change in average pore diameter of a catalyst. Van Nordstrand, et al.,[8] observed the same pore diameter for silica gel aged in a high vacuum at various temperatures ranging from 600–1040°. However, their data for silica–alumina cracking catalyst suggest a small increase of pore diameter at the lower temperatures. At higher temperatures, however, the pore diameter is again the same as for the fresh catalyst. The deviation from constant pore diameter is probably not real and may be experimental error. Roper[9] observed no increase of pore diameter during high vacuum deactivation of high alumina catalysts at temperatures between 875 and 970°.

In our experiments the pore diameter of catalyst aged by "heat" in a stream of dry air was always higher than that of the fresh catalyst. The increase was relatively greater at the lower temperatures. It is possible that the small enlargement is the result of self-steaming by the water released from the catalyst during the aging, and that no increase in

pore diameter would occur under truly anhydrous conditions. Some self-steaming has already been shown to have occurred. However, the same enlargement of pore diameter occurs during the slow heating that gives more nearly pure thermal aging. Thus, the small increase of pore diameter at the lower temperatures followed by a decrease at the higher temperatures may be real. As mentioned earlier, Van Nordstrand made a similar observation. This coincidence, although possibly fortuitous, leads one to suspect that the widely accepted constancy of pore diameter during thermal deactivation is only approximate.

Experiments at 576 and 778° at various pressures of steam show a small but definite effect of steam pressure on the changes in pore diameter. As the steam pressure is lowered from 1 to 0.3 to 0.11 atm. at 778° the pore diameter increases less rapidly with decreasing surface area. This same effect is present although not as apparent at 576° and 7, 3, 1 and 0.3 atmospheres steam pressure. These data imply that perhaps at zero steam pressure (dry heat) the pore diameter would be the same as for the fresh catalyst.

Thus, to summarize, *the apparent diameter of the pores at a given surface area during aging is a function both of the temperature and the steam pressure.* The effect of more than traces of steam, however, is of minor importance. This is clearly shown in Fig. 8 which shows the effect of steam pressure on dV_p/dS at various temperatures. Above one atmosphere steam, there is little if any additional influence on the enlargement of pores; but, below one atmosphere, the pressure of steam becomes increasingly more important. Figure 9 shows the dependency of dV_p/dS on the temperature of aging.

Speculations Concerning Mechanism.—It has often been suggested in the past that inorganic gels consist of a loosely packed aggregate of small particles.[10] Direct evidence to support this view has been obtained recently by electron microscopy[11,12] of cracking catalysts and of silica gels. A reasonable model for the structure of cracking catalyst is thus an assembly of small, dense, roughly spherical particles in a rather open or loose random packing. Spheres will be the preferred shape since these materials are non-crystalline. The surface area of the structure will be determined by the radius of the particles; for a surface area of 600 m.²/g. this radius is 23 Å. The pore volume is the sum of the volumes of the irregular spaces between the particles.

Such a structure will be thermodynamically unstable because of its high surface free energy. The surface free energy for silica–alumina cracking catalyst is estimated to be of the order of 400 ergs/cm.² at room temperature. Consequently, when the surface area decreases from 600 to 100 m.²/g., the system should become more stable by about 50 cal./g. The lowest energy regions in the system are the regions of contact between the elementary particles,

(8) R. A. Nordstrand, W. E. Kreger and H. E. Ries, Jr., This Journal, 55, 621 (1951).

(9) E. E. Roper Shell Development Company, unpublished data.

(10) A. von Buzagh, "Colloid Systems," The Technical Press, Ltd., London, 1937; P. C. Carman, Trans. Faraday Soc., 36, 964 (1940).

(11) K. D. Ashley and W. B. Innes, Ind. Eng. Chem., 44, 2857 (1952).

(12) C. R. Adams and H. H. Voge, This Journal, 61, 722 1957.

since these are the regions of smallest (concave) radius of curvature. The first result of any transport of solid material in the system should therefore be the formation of fillets between the particles by the deposition of material in the regions of contact. The possible loss of surface area by fillet formation alone is quite limited and can account for only a small part of the observed aging process. For instance, the surface area lost by the formation of a fillet between two equal spheres would be less than 3% of the original surface of the two isolated spheres; if four fillets were formed per particle the surface area of a fresh catalyst would decline from 600 m.²/g. to only 560 m.²/g. Nevertheless, the process of fillet formation is believed to be important since it provides the necessary bridges between the particles for subsequent material transport by surface migration, volume diffusion, or viscous flow and contributes also to the mechanical strength of the aggregate.

The second result should be the disappearance of the smallest particles in the system and the growth of larger ones. This may occur either by the growth of the larger particles already present at the expense of the smaller ones, or by the coalescence of several small particles to form a larger one. Which of these processes predominates will be determined by the nature of the transport processes involved. The possible processes for material transport are surface migration, volume diffusion, vapor-phase transport, and viscous flow.

The kinetic analysis of Kuczynski,[13] who studied the growth of fillets between small spherical metal particles and a plane surface of the same metal, has been generalized by Herring,[14] who showed by fairly general arguments that at a given temperature and with a given mechanism for material transport the time required for the average particle size in an aggregate to increase by a constant factor should vary as (r_0^p) where r_0 is a measure of the initial average diameter of the particles in the aggregate. This was demonstrated only for the case where all the aggregates considered have the same packing and distribution of particle sizes and shapes, so that they differ only in the magnitude of r_0. The power p was shown to depend on the mechanism of material transport and to have the following values: for surface migration, $p = 4$; for volume diffusion, $p = 3$; for vapor phase transport, $p = 2$; for viscous (Newtonian) flow, $p = 1$. These conclusions are consistent with our empirical finding that $-dS/dt = kS^n$ but the values of n found empirically in our experiments are considerably larger than the values predicted by Herring's analysis. It is shown readily that the relation between the exponent n of our empirical rate equation and the exponent p of Herring's analysis is $n = p + 1$ for a given process of material transport. Thus the largest value of n predicted by Herring's analysis is 5.

We have reason to believe that the larger values

(13) G. C. Kuczynski, *J. Metals,* **1**, 169 (1949).

(14) C. Herring, "Structure and Properties of Solid Surfaces," edited by R. Gower and C. S. Smith, University of Chicago Press, 1953, p. 56; "Progress in Metal Physics," Vol. 4, edited by B. Chalmers, Interscience Publishers, New York, N. Y., 1953; *J. Appl. Phys.,* **21**, 301 (1950).
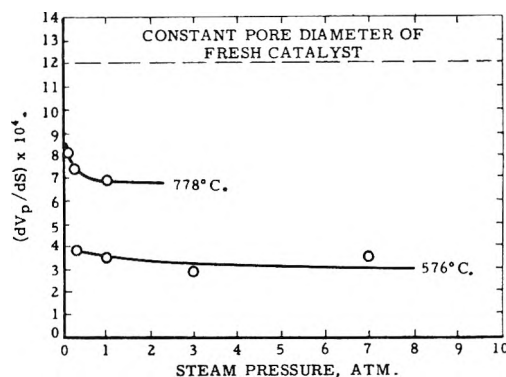
Fig. 8.—Influence of steam partial pressure on the relative change of pore volume and surface area.
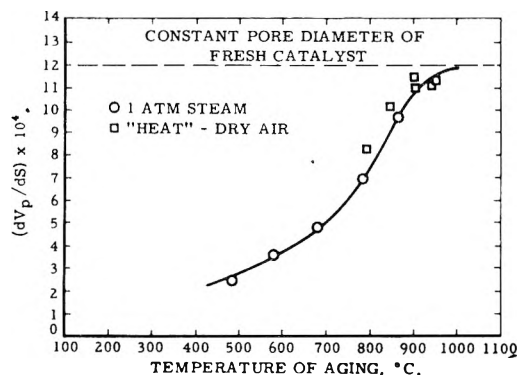
Fig. 9.—Influence of temperature on the relative change of pore volume and surface area.

of n observed at the lower temperatures in the presence of steam can be accounted for by a vapor phase transport process involving the formation of volatile species like $Si(OH)_4$. It has been pointed out to us by C. R. Adams of these laboratories that the dependence of the rate on the partial pressure of steam at the lower temperatures is also consistent with such a mechanism. At higher temperatures the lower values of n are consistent, in the light of Herring's analysis, with the predominance of processes such as surface migration and volume diffusion. Such a change in the relative importance of the various mechanisms of material transport with changing temperature would be expected *a priori* since the different mechanisms should have different activation energies.

The ratio dS/dV_p (loss of surface area to loss of pore volume) also depends on the mechanism of transport. If the aging occurs only by surface migration or vapor phase transport, the geometric centers of the surviving elementary particles tend to remain in the same relative positions in the aggregate, so that the pore volume remains constant while the surface area decreases. This, of course, implies an increase in the calculated pore diameter. The occurrence of volume migration processes such as volume diffusion or plastic flow, on the other hand, will permit the geometric centers to approach each other; the whole aggregate will shrink and the pore volume will decrease. These effects will be reflected in a lower rate of increase of the pore diameter, or a lower value of dS/dV_p. The curve shown in Fig. 9 indicates that the importance of volume transport processes increases steadily

relative to that of surface transport processes (surface migration and vapor-phase transport) as the temperature of aging increases.

Aging at the highest temperatures results in very little change in the pore diameter. This observation is consistent with a nearly complete predominance of volume transport processes over surface processes, with the result that a kind of local fusion or coalescence destroys both surface area and pore volume simultaneously and in constant proportion. The occurrence of such a process is strongly indicated by the observations of Adams.[12] As is shown in Fig. 6, the aging process approaches this course more and more closely as the temperature of aging increases.

Steam has a strong accelerating effect on the aging process at all temperatures. The relatively small dependence of dV_p/dS on the partial pressure of steam (Fig. 8) suggests that both volume transport processes and surface transport processes are accelerated to nearly the same extent by steam, presumably by a process of hydrolytic attack on the silicon–oxygen or aluminum–oxygen bonds in the gel network.

AGING OF SILICA–ALUMINA CRACKING CATALYST. II. ELECTRON MICROSCOPE STUDIES

By C. R. Adams and H. H. Voge

Shell Development Company, Emeryville, California

Received November 5, 1956

The physical structure of an unaged silica–alumina gel consists of coherent aggregates of dense, smooth, spherical particles, about 45 Å. in diameter, with a relatively narrow distribution of particle sizes. The specific surface area is the geometrical surface area of these particles and the pore structure is the void structure resulting from the packing together of these particles. Aging in the presence of steam at low temperatures (below about 800°) results in an increase in the ultimate particle diameter, with a widening of the distribution. The decrease in surface area is quantitatively accounted for by this increase in size. Aging at high temperatures is characterized by a complete collapse of microscopic regions of the gel, the remaining regions having essentially the same physical structure as that of the fresh gel. This high temperature sintering is strongly accelerated by the presence of steam.

Introduction

The fine structure of inorganic gels has been the subject of intensive investigation and discussion for many years. The interest in, and importance of, these gels is due, in part, to those properties which result from this structure: namely, pore structure, surface area and the subsequently important surface chemical activity. It is the purpose of this paper to present the results of a high magnification electron microscope study of the structure of a silica-base gel and the structural changes produced in this gel by treatments with steam and high temperatures. A systematic study of the changes in pore volume and surface area of this gel, as a function of temperature, steam pressure and time, has been reported by Schlaffer, Morgan and Wilson.[1]

Experimental

The gel used in these studies was a sample of a commercial powdered cracking catalyst manufactured by the American Cyanamid Company by the hydrolysis of an aluminum salt in the presence of a silica hydrogel. The powder was in the form of microspheres about 60 μ in diameter, obtained by spray-drying the composited hydrogel. This gel contained 12.4% Al_2O_3, had a surface area of 608 m.²/g., and a pore volume of 0.73 cc./g. The experimental techniques of deactivation are given in detail by Schlaffer, Morgan and Wilson.[1]

Serious experimental problems are posed in an electron microscope study of such a gel, inasmuch as the diameters of the ultimate particles are about 30–50 Å., a range requiring high resolution and magnification. The greatest single problem was that of specimen contamination in the electron beam.[2–5] This deposition of amorphous matter was so great (often as high as 5–6 Å. per minute) at the higher beam intensities necessary for high magnification exposures that the utmost haste had to be employed to obtain a true picture. Exposures were usually made within 15–20 seconds after beam illumination, and many pictures of each sample were taken to ensure accurate representation of the true structure. Another major problem was the instability of the support film. Nitrocellulose films were used in most cases. These films have a tendency to stretch and move for a few seconds after beam illumination but, because of the contamination problem, it was impossible to wait until the film became completely stabilized. Evaporated silicon monoxide films were used in some instances, but the advantage of the greater stability of this film was offset by the great tendency to charge up in the electron beam. Evaporated carbon films[6] have been found in later work to be very superior supports.

Samples were usually lightly ground by hand for a few seconds in a small mortar and either suspended in water or mounted dry by dusting onto the support film. Measurements on specimens prepared by both techniques indicated that the suspension in water and subsequent drying had no effect upon the physical structure of the gel. This is in agreement with other studies[7] on aggregated, calcined $BeO–In_2O_3$ gels which have shown that aqueous suspension and subsequent evaporation to dryness had no effect upon the pore size distribution within the aggregate.

Electronic manifications of 20,000× were obtained in an RCA EMU-2C microscope, with optical enlargements of the resulting negatives employed to obtain prints at a total magnification of 200,000×. The particle size distributions were obtained from the photographic prints by direct meas-

(1) W. G. Schlaffer, C. Z. Morgan and J. N. Wilson, This Journal, **61**, 714 (1957).

(2) R. L. Stewart, *Phys. Rev.*, **45**, 488 (1934).

(3) J. H. L. Watson, *J. Appl. Phys.*, **18**, 153 (1947).

(4) J. Hillier, *ibid.*, **19**, 226 (1948).

(5) A. E. Ennos, *Brit. J. Appl. Phys.*, **5**, 27 (1954).

(6) D. E. Bradley, *ibid.*, **5**, 65 (1954).

(7) C. R. Adams and W. O. Milligan, This Journal, **58**, 219 (1954).

urement. Measurements of different specimens of each sample showed the distribution of sizes in different aggregates to be the same within the accuracy of the measurements. For instance, measurements of three different pictures of the fresh gel yielded number-average diameters of 45.3, 45.7 and 44.1 Å., counting 596, 561 and 778 particles, respectively, with similar agreement in the shape of the distribution. Most of the distributions given here represent a count of 1000–2000 particles for each sample. Such a large count was necessary to obtain a reliable value for the surface-area-average diameter, a quantity very sensitive to small fluctuations in the large particle tail of the distribution function. Continuous curves were obtained from the histograms by plotting on arithmetic probability paper. Although the distributions were not exactly Gaussian, the curvature was usually slight, so that a smooth curve could be easily drawn.

Results and Conclusions

Structure of the Fresh Gel.—An electron micrograph (200,000X) of the fresh gel (after calcination at 565° for 6 hours) is shown in Fig. 1a. The ultimate particle size distribution is given in Fig. 2. The ultimate particles have a rather narrow distribution of sizes with a number-average diameter of 44.7 Å. and a surface-area-average diameter of 50.7 Å. Number-average diameter is defined as $\Sigma n_i d_i / \Sigma n_i$, and surface-area-average diameter as $d_{EM} = \Sigma n_i d_i^3 / \Sigma n_i d_i^2$. Then $S_{EM} = 6 \times 10^4 / \rho d_{EM}$ where S_{EM} is in m.²/g. if d_{EM} is in Å. Using a skeletal density of 2.308 g./cc. as determined by Schlaffer,[8] an electron microscope surface area (S_{EM}) of 513 m.²/g. was obtained. This is in reasonable agreement with a surface area (S_{Ads}) of 608 m.²/g. as determined by BET nitrogen adsorption. The diameter ($d_{Ads} = 6 \times 10^4 / \rho S_{Ads}$) of a smooth sphere having this surface area and the density quoted would be 42.8 A. Although the deviation of 18% between the two values for the surface area is probably within the absolute experimental error of the two measurements, a contamination layer of only 3.9 Å. would account for all the discrepancy. It is apparent that the structure observed in the electron microscope is the true ultimate physical structure of the gel.

The physical structure of the fresh gel may thus be described as an assembly of spherical particles, having a roughness factor (here defined as S_{Ads}/S_{EM}) of essentially unity, about 45 Å. in diameter, and packed rather loosely together into arbitrarily shaped primary aggregates. The term primary aggregate is used here to denote those aggregates which appear to have no lower state of subdivision above the ultimate particle size level. The size of these primary aggregates could not be judged with precision, but appeared to extend over a wide range (0.05 to > 3 μ). Furthermore, there appeared to be an endless hierarchy of higher aggregation.[9] It is postulated that the primary aggregates are formed during the aging of the sol. The secondary aggregate structure is at least partially built up when the gel sets. This secondary (and higher order) aggregation is certainly strengthened and built up further during the drying of the gel. The effect of lightly grinding the dried powder is to break up this higher order aggregation and would not be expected to affect the much stronger primary aggregate structure.

It is apparent from Fig. 1a that the pore structure of this gel is merely due to the interstices between the ultimate particles and results from the mode of packing of these particles. Although the size of these interstices agrees approximately with the size of a hypothetical cylindrical "pore" computed from gas desorption measurements,[7] the concept of straight cylindrical pores or parallel plates should never be taken literally. Although these two models are the most accessible mathematically, the real pore structure of a gel of this type is a very complicated interconnected maze of void space.

Aging by Steam at Low Temperatures.—Schlaffer, Morgan and Wilson[1] and Ries[10] have shown that deactivation (i.e., loss of surface area) of silica-base gels appears to occur in different ways. Deactivation in steam at rather low temperatures results in an increase of "pore" size. Ashley and Innes[11] examined fresh and steamed silica–alumina catalyst with the electron microscope and found that the particle size increased upon steaming, corresponding to the decrease in surface area.

An electron micrograph is given in Fig. 1b of the silica–alumina gel after steaming for 504 hours at 476° and one atmosphere steam pressure, with a resulting adsorption surface area of 316 m.²/g. This steamed gel resembles the fresh gel very closely in appearance except that the ultimate particle size has increased. The material consists of discrete, individual spheres loosely packed together into aggregates very similar in size and shape to those of the fresh gel. The particle size distribution given in Fig. 2 is quite uniform with a number-average diameter of 64.5 Å. and a surface-area-average diameter of 77.1 Å. This size corresponds to an electron microscope surface area of 342 m.²/g. The nitrogen surface area corresponds to smooth spheres of 83.4 Å. in diameter, or a roughness factor of 0.92. An electron micrograph is given in Fig. 1c of the gel after one atmosphere steaming at 678° for 1320 hours, with an adsorption area of 95 m.²/g. This material has a slightly different appearance in that no isolated, individual particles were observed. The particles appear to be firmly bound in the aggregates, although surface area calculations show that most of the area of the ultimate particles is still accessible. The aggregates are roughly the same size and shape as the aggregates of the fresh gel. The distribution of ultimate particle sizes given in Fig. 2 has a number-average diameter of 214 Å. and a surface-area-average diameter of 262 Å. This corresponds to an electron microscope surface area of 100 m.²/g., in excellent agreement with adsorption measurements of 95 m.²/g.

The observation was made above that the aggregates appeared similar at various stages of steaming. This observation allows an explanation for

(8) W. G. Schlaffer, unpublished data.

(9) Ideas on the clustering of ultimate particles of gels into primary aggregates and of the further aggregation into roughly isometric secondary aggregates were proposed independently here by J. N. Wilson in 1953.

(10) H. E. Ries, Jr., "Advances in Catalysis," Vol. IV, Academic Press, New York, N. Y., 1952, p. 87, and earlier papers cited there.

(11) K. D. Ashley and W. B. Innes, Ind. Eng. Chem., 44, 2857 (1952).
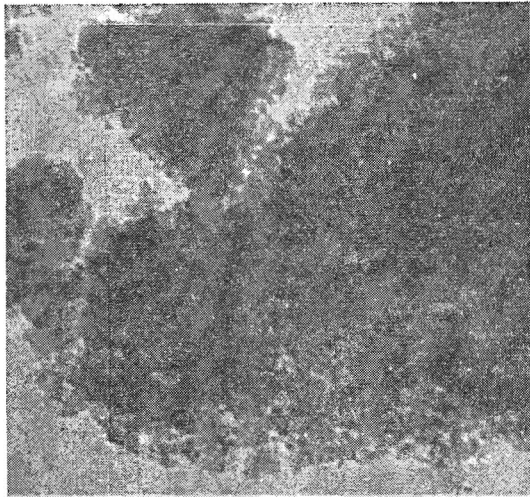
a) Fresh Gel, 608 m²/g.
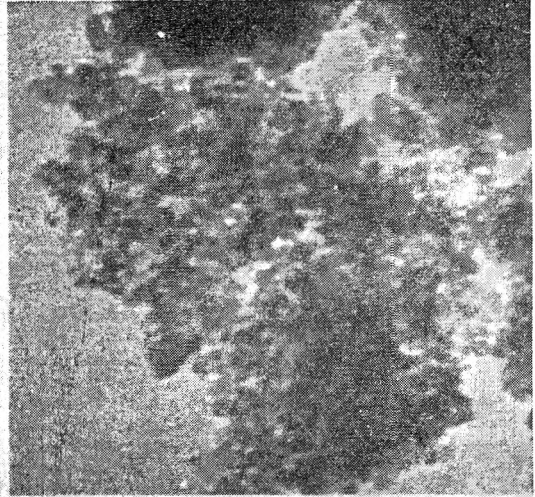
b) Deactivated by Steam to 316 m²/g. at 478°C.
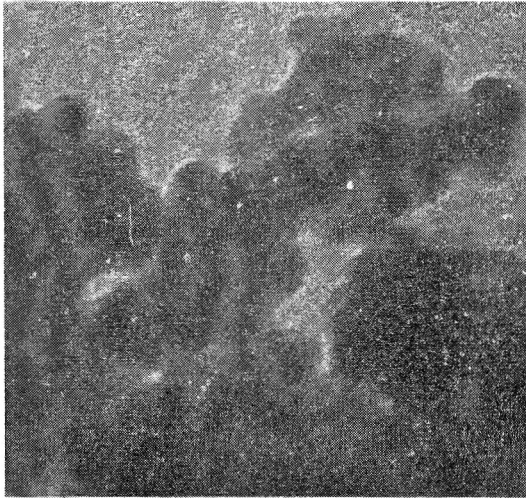
c) Deactivated by Steam to 95 m²/g. at 678°C.
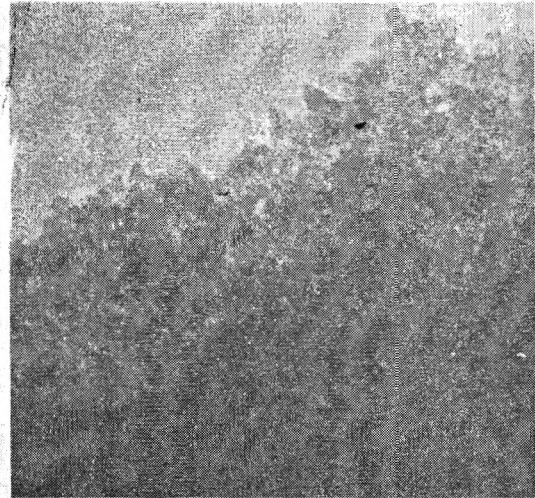
d) Heated in Air to 269 m²/g. at 900°C.
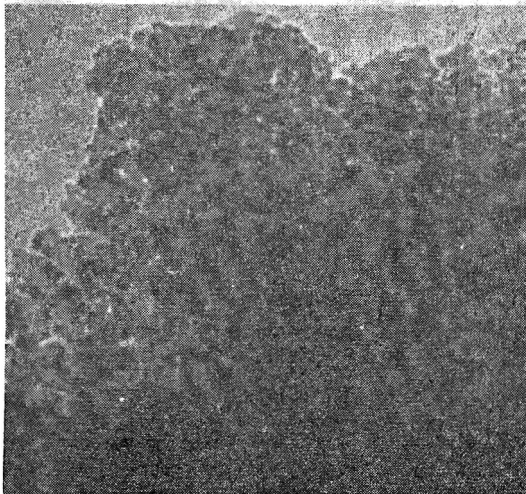
e) Heated in Air to 100 m²/g. at 940°C.

0.1 μ

25 50 100 200 400
Diameter, A.

Fig. 1.—Electron micrographs of silica–alumina gel; magnification: 200,000 diameters.

the relatively constant pore volume and increasing pore diameter observed over the course of low temperature steam deactivation. It is postulated that the aggregates retain their approximate shape and size during the process of steaming. This is strongly demanded by the appearance of the aggregates of the sample steamed to 95 m.^{2}/g., where the ultimate particles are obviously strongly bound into the aggregates, yet the irregular shape of the ultimate aggregates clearly shows that they could not be fragments broken off mechanically from a large homogeneous mass. Arguments will be advanced below to indicate that only two mechanisms are possible for low temperature steam deactivation: surface migration or vapor phase transport. Either mechanism will require that essentially all material transport occur within the aggregate. Since, by either mechanism, transport of matter to or from a given ultimate particle will be incoherent with respect to transport to and from all particles at least two particle diameters away, and since each aggregate contains a very large number of ultimate particles, the size and shape of the aggregate would be expected to remain essentially unchanged.

The above results clearly show the effect of steam deactivation at low temperatures upon silica–alumina gel: namely, the regular growth of individual spheres of the solid, at the expense of the smaller particles. Thus the larger particles are constantly growing larger and the smaller ones are constantly getting smaller and disappearing. This would result in size distributions spreading out toward the larger sizes, as steam deactivation proceeded, and yet still having one side of the distribution extend into the small particle range. These are exactly the facts observed here and displayed in Fig. 2. The concept of collapse, sintering or amalgamation of two or more particles is not consistent with the observations of (a) round particles having (b) a roughness factor of essentially unity, (c) individually observable particles, (d) broadening distributions as deactivation continues, (e), the presence of an appreciable number of small particles even after prolonged aging, and (f) the continuous, smooth increase of the average particle size with steaming. The consistently spherical shape of the particles indicates that surface tension forces are prominent in such growth. Only two mechanisms of growth are consistent with all the above observations: surface migration or molecular diffusion in the gaseous state. In either case surface tension forces would become important and the presence of steam would be expected to accelerate the growth. It should be pointed out that this type of deactivation does not result from movement of silica from the surface of wider capillaries to fill in the smaller capillaries or pores, as has been suggested elsewhere.[12]

Aging at High Temperatures.—A second method of deactivating silica-base gels consists of heating the gel at high temperatures. This type of destruction of surface area is characterized by a constancy of pore size and pore size distribution,[1,10,13] result-

(12) R. K. Iler, "The Colloid Chemistry of Silica and Silicates," Cornell University Press, Ithaca, N. Y., 1955, p. 270.

(13) W. O. Milligan and H. H. Rachford, Jr., THIS JOURNAL, **51**, 333 (1947).
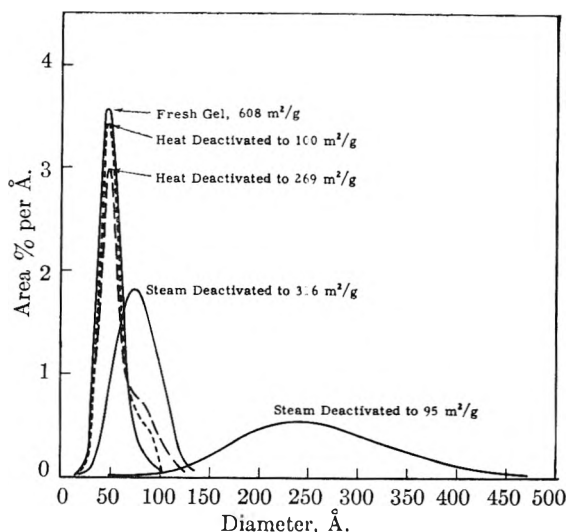
Fig. 2.—Ultimate particle size distributions of fresh, steamed and heat deactivated gel.

ing from an equivalent amount of pore volume destroyed when the surface area decreases. An electron micrograph is given in Fig. 1d of the silica–alumina gel heated in a stream of dry air for 7 hours at 900°. The resulting nitrogen surface area was 269 m.^{2}/g. The secondary aggregate structure of this high temperature deactivated sample is distinctively different from that of the fresh or steamed samples. The secondary aggregates of this sample are considerably larger, usually several microns in size. The aggregates are regularly shaped, having a shard-like appearance, with frequent fracture edges present in the ground material. In contrast to the low temperature steam deactivated samples, the ultimate particles of this heat deactivated sample have not changed in size from that of the fresh gel, as shown in Fig. 2. An electron micrograph is given in Fig. 1e of the gel heated in air for 7 hours at 940°, with a resulting surface area of 100 m.^{2}/g. The aggregate appearance of this sample is quite similar to that of the sample heated at 900°. The ultimate particle size distributions, given in Fig. 2, are unchanged from that of the fresh gel, with the exception of slight shoulders on the larger particle side. It is postulated that these shoulders are due to only a few particles fused together.

It has been shown by Schlaffer, Morgan and Wilson[1] that the deactivations in "dry air" were influenced at least in part by steam generated at the high temperatures from the water originally combined in the gel. Electron micrographs were, therefore, also obtained of a sample of fresh gel which had been calcined *in vacuo* at 1012° for 1.7 hours by E. E. Roper. This material had a surface area of 104 m.^{2}/g. The aggregate appearance of this sample was identical with that of the gel heated in "dry air." The ultimate particle size distribution, given in Fig. 3, is the same as that of the fresh gel, again with the exception of a slight increase in the number of larger particles. Thus conclusions drawn about the mechanism of deactivation of the samples heated in air will apply equally well to deactivation *in vacuo*. It appears that the presence
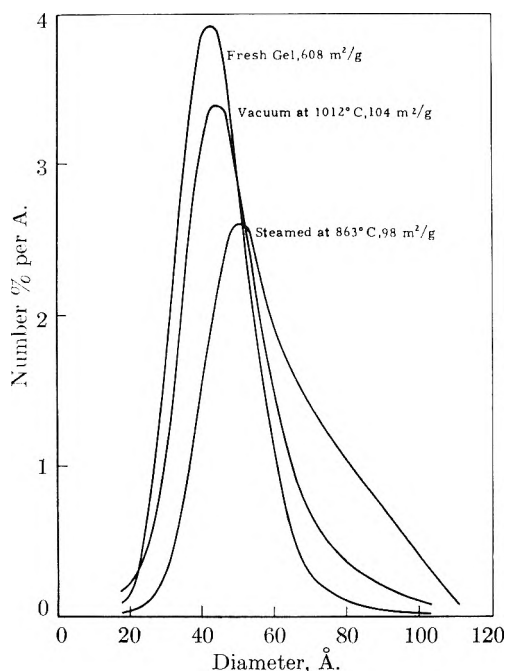
Fig. 3.—Ultimate particle size distributions of fresh gel, after vacuum calcination at 1012°, and after steaming at 863°.

Fig. 4.—Photomicrograph of heat deactivated particle of gel dyed with methyl red, approx. 1000×.

of steam at high temperatures merely accelerates the mechanism that occurs when the gel is heated *in vacuo*. An examination of a sample deactivated to 98 m.²/g. by 0.5 hour at 863° in one atmosphere of steam has shown that this accelerating effect of steam can be very marked. Heating in "dry air" at this temperature and for this length of time would have reduced the area to only about 400 m.²/g.,

while vacuum calcination would scarcely have changed the area at all from the original value of 608 m.²/g. The ultimate particle size distribution for the sample steamed at 863° is given in Fig. 3. Although there appears to be some (about 20%) increase in ultimate particle size, due to the low temperature steam mechanism, it is apparent that the major mechanism is that of high temperature deactivation. The average particle size would have increased to above 200 Å. if the decrease of area had been due solely to the low temperature steaming mechanism.

The mechanism of high temperature deactivation appears to be that of heterogeneous sintering, resulting in local collapses of structure which spread through the mass in a process similar to fusion. This conclusion is based upon (a) the linear decrease of pore volume with respect to surface area, and the constancy of (b) average pore size, (c) pore size distribution, (d) average ultimate particle size, and (e) ultimate particle size distribution for heat-deactivated silica-base gels. Although this evidence is somewhat indirect in that the data describe the properties of the uncollapsed regions, it is possible to get direct information about the collapsed regions. This has been done by dying samples of heat-deactivated gels with a benzene solution of methyl red. It has been shown[14] that the methyl red forms a monolayer on the surface, so that particles having appreciable internal surface area will be dark red, while particles having no internal surface will be clear. A photomicrograph of a particle of gel, heat-deactivated to 100 m.²/g., is shown in Fig. 4. The dark regions of the particle shown in Fig. 4 are regions having a high internal surface area while the clear regions have essentially no internal area. It should be mentioned that dyed particles of the fresh gel appear uniformly dark. Furthermore, skeletal density measurements of the heat-deactivated gels indicated no occluded voids so that the clear regions visible in Fig. 4 represent solid, fused masses, rather than glazing. The number of clear particles visible in the light microscope is not great enough (only about 5%) to account for all of the deactivation. A majority of the fused domains must therefore be below the resolution of the light microscope. This is understandable in terms of the aggregate structure discussed above. The extent of these fused domains would be expected to be limited to the primary aggregates, until essentially all of the ultimate particles had fused together.

The mechanism given here for thermal sintering of silica-base gels is not new. Van Nordstrand, Kreger and Ries[15] arrived at the same conclusion on the basis of pore size measurements. However, Ries[10] in a later review of the structure and sintering properties of cracking catalysts, attempted to disprove this mechanism by showing that physically separated shell and core portions of a heat-deactivated catalyst bead had the same surface area as that of the whole bead. However, since the domains of fusion are limited by the size of the very small pri-

(14) I. Shapiro and I. M. Kolthoff, *J. Am. Chem. Soc.*, **72**, 776 (1950).

(15) R. A. Van Nordstrand, W. E. Kreger and H. E. Ries, Jr., THIS JOURNAL, **55**, 621 (1951).

mary aggregates, and since the state of aggregation was probably consistent throughout the bead, one would not expect to find any variation in surface area for various macroscopically large regions of the bead.

ON THE STRUCTURE OF THE RHENIDE ION[1]

BY J. W. COBBLE

Contribution from the Department of Chemistry, Purdue University, Lafayette, Indiana

Received November 10, 1956

The thermodynamic factors controlling the stability of the rhenide ion have been examined. The conclusion is reached that rhenide exists in aqueous solution as an oxygenated complex, and that solid rhenides must be "hydrated" to be stable. Other ions of this general type are also examined.

Introduction

It is not generally recognized that data are available in literature which help to elucidate the structure of the rhenide ion.[2] That this ion exists seems no longer subject to question. It has been confirmed by a number of investigators,[3-6] including this author; further, recent reports have appeared on the preparation of solid potassium,[7] lithium[8] and thallous rhenides.[7] The former two solid rhenides appear to be stable (as hydrates), characterized mainly by great ease of oxidation. Further, aqueous solutions of rhenide ion appear to reduce hydrogen ion slowly. It is the purpose of this communication to demonstrate that the aqueous rhenide ion is almost certainly not a simple halogen-like ion, but some type of an oxygenated complex.

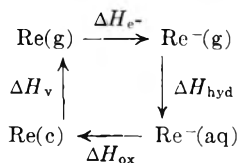**The Thermodynamics of Aqueous Rhenide.—** Consider the thermodynamic cycle in Fig. 1

Fig. 1.—Cycle for the aqueous rhenide ion.

In this figure the assumption is made initially that the structure of the aqueous ion is simple, *i.e.*, Re^-. A careful examination of the four ΔH values, for which the cycle must close, is necessary.

A. The Heat of Vaporization of Rhenium (ΔH_v). —The heat of vaporization of rhenium has been estimated by Brewer[9] to be 189 kcal. at 25°. Recently Sherwood, *et al.*,[10] have measured the vapor

pressure of rhenium metal and have reported $\Delta H^0{}_0$ as 187 ± 1 kcal. Corrected[11] to 25° this becomes 183 $\pm$ 2 kcal. very close to Brewer's original estimate of 189 kcal. There is no evidence either way for the existence of dimeric or polymeric gaseous rhenium species. However, the closeness of the estimated and experimental heats of vaporization leads one to believe that these species, if present, are a minor constituent and have not greatly affected the value for ΔH_v.

B. The Heat of Oxidation of $Re^-(aq)$ (ΔH_{ox}). —A close estimate of the heat of oxidation of aqueous rhenide comes from the chemical observation that aqueous rhenide solutions oxidize hydrogen ion moderately fast. This property is common to other aqueous ions whose oxidation–reduction potentials are around 0.4 volt (the practical oxidation stability limit of unit activity H^+ in aqueous solutions) for the reaction: M(reduced) = M (oxidized) + e^-. Thus Latimer[12] gives E^0 for Re^- = Re(c) + e^- as 0.4 volt. This estimate is almost certainly accurate to a few tenths of a volt, and is independent of the structure of the aqueous species. However, following our previous assumption that the structure is $Re^-(aq)$, a value of ΔH can be estimated from the E^0 of 0.4 volt as follows: the entropy of Re(c) has been determined as 8.89 e.u.[13]; the entropy of $Re^-(aq)$ can be estimated to be 28 $\pm$ 5 e.u.[14] if the ionic radius is taken as approximately[15] 2.3 $\pm$ 0.3 Å. ΔS^0 then becomes -3 $\pm$ 5 e.u. for the reaction

$$Re^-(aq) + H^+(aq) = Re(c) + \tfrac{1}{2}H_2(g) \quad (1)$$
$$E^0 = +0.4 \pm 0.2 \text{ v.}$$
$$\Delta F^0 = -9 \pm 5 \text{ kcal.}$$

(1) This research was supported by the United States Air Force Office of Scientific Research of the Air Research and Development Command under contract No. AF 18(600)-1525.

(2) G. E. F. Lundell and H. B. Knowles, *J. Research Natl. Bur. Standards*, **18**, 629 (1937).

(3) O. Tomicek and F. Tomicek, *Collection Czech. Chem. Communs.*, **11**, 626 (1939).

(4) J. J. Lingane, *J. Am. Chem. Soc.*, **64**, 2182 (1942).

(5) E. K. Maun and N. Davidson, *ibid.*, **72**, 3509 (1950).

(6) C. L. Rulfs and P. J. Elving, *ibid.*, **73**, 3287 (1951).

(7) J. B. Bravo, E. Griswold and J. Kleinberg, *ibid.*, **58**, 18 (1954).

(8) A. V. Grosse, *Z. Naturforsch.*, **8b**, 533 (1953).

(9) L. Brewer, "Chemistry and Metallurgy of Miscellaneous Materials: Thermodynamics," National Nuclear Energy Series, Vol. IV-19B, edited by L. L. Quill, McGraw-Hill Book Co., New York, N. Y., 1950, p. 26.

(10) E. M. Sherwood, D. M. Rosenbaum, J. M. Blocker, Jr., and I. E. Campbell, *J. Electrochem. Soc.*, **102**, 650 (1955).

(11) Using $H_0 - H_{298}$ data for Re(g) from reference 9, and from reference 13 for Re(c).

(12) W. M. Latimer, "Oxidation-Potentials," Prentice–Hall, Inc., New York, N. Y., 1952, pp. 12, 243.

(13) Wm. T. Smith, Jr., G. D. Oliver and J. W. Cobble, *J. Am. Chem. Soc.*, **75**, 5785 (1953).

(14) R. E. Powell and W. M. Latimer, *J. Chem. Phys.*, **19**, 1139 (1951).

(15) The ionic radius of Re^- is estimated by a comparison of the covalent and ionic radii of the halogens. The difference between the covalent and univalent radii of Cl, Br and I is 0.82, 0.84 and 0.88 Å., respectively. It is plausible that the difference between the covalent radius of Re and Re^- will also be 0.88 Å. The covalent radius of Re would appear to be almost the same as the observed metallic radius of 1.37 Å. Thus the radius of Re^- is 2.3 Å., which should be accurate to at least 0.3 Å. Radii were taken from L. Pauling, "Nature of the Chemical Bond," Cornell University Press, Ithaca, N. Y., 1945.

$$\Delta S^0 = -3 + 5 \text{ e.u.}$$
$$\Delta H^0 = -10 \pm 7 \text{ kcal.}$$

Either this reaction or its abbreviated form, $Re^- = Re + e^-$, constitutes the heat of oxidation of rhenide.

C. The Heat of Hydration of Rhenide (ΔH_{hyd}). —The heat of hydration of a halide-like univalent ion can be obtained either by extrapolation of the known heats for the halide ions as a function of ionic size, or by use of the Born expression as modified by Latimer[16] to obtain the free energy and then the heat of hydration employing the proper entropy values. Thus from the previous estimate of the entropy of aqueous rhenide, 28 ± 5 e.u., combined with the entropy of gaseous rhenide,[17] a ΔS^0 of hydration can be obtained of −14 ± 5 e.u.[18] This ΔS_{hyd} value can then be combined with the ΔF_{hyd} from the Latimer–Born expression to obtain a ΔH_{hyd}. By the first halide method, ΔH_{hyd} is estimated to be −66 ± 9 kcal.; by the Latimer–Born method, −73 ± 9 kcal. Both values are based upon the choice of an ionic radius as given above of 2.3 ± 0.3 Å., and the estimated errors are assigned wholly on this basis. The value of −73 ± 9 kcal. will be adopted.

D. The Electron Affinity of Rhenium (ΔH_e).— The most difficult quantity to estimate is the electron affinity of gaseous rhenium. Qualitatively, the affinity will almost certainly be less than that of fluorine atoms, −83.5 ± 2 kcal. mole^{-1}.[19] An admittedly poor extrapolation through a isoelectronic series (O_s^+, Ir^{++}, Pt^{+++}) leads to a value of ∼−63 kcal., which may be compared to the heaviest halogen atom, iodine, of −74.6 ± 1.5 kcal. Such extrapolations usually underestimate the affinity. In any event, the electron affinity will be less than −83.5 and probably greater than −65. The lower value will be used for illustrative purposes.

With these values, it is now possible to complete the cycle (Table I).

TABLE I

Born cycle for rhenide	ΔH, kcal.	
$Re(c) = Re(g)$	+183	± 5
$Re(g) + e^-(g) = Re^-(g)$	−65	± 10
$Re^-(g) = Re^-(aq)$	−73	± 9
$H^+(aq) + Re^-(aq) = Re(c) + \frac{1}{2}H_2(g)$	−10	± 7
$\frac{1}{2}H_2(g) = H^+(aq) + e^-(g)$	105.6^a	
	141	± 31

^{a} This quantity comes from any attempt to list single ion thermodynamic values; in any closed cycle calculations its absolute magnitude has been predetermined by assignment of the hydration energies. Brewer (ref. 9, p. 157) lists 103.9 kcal.; the above value is based upon a slightly different set of hydration energies. Its absolute value in no way affects the over-all numerical result of the cycle.

It can be seen that the cycle fails to "close" to the extent of 141 kcal. It is the high sublimation energy of rhenium metal which discriminates

(16) W. M. Latimer, *J. Chem. Phys.*, **23**, 90 (1955).

(17) For the entropy of gaseous rhenide, the Sackur–Tetrode value of 26.00 + 3/2 *R* ln *M* or 42 e.u. is used. This assumes no electronic contributions to the entropy.

(18) This value also neglects a small additional entropy term due to a change of standard states.

(19) H. O. Pritchard. *Chem. Revs.*, **52**, 529 (1953).

highly against rhenide. The only obvious value to change is the electron affinity of rhenium; to close the cycle would require ΔH_e^- of −206 ± 31 kcal., the minimum value of which is over twice as large as for fluorine. That this situation is improbable is clear from the nature of the species involved.

The most obvious conclusion from this analysis is that the structure of rhenide is not halogen like, *i.e.*, Re^-. If the ion were combined with oxygen and hydrogen such as can be represented by a formula of the type[20] $H_8ReO_4^-$, then our analysis would no longer be valid. For example, another term would have to be included in ΔH_{hyd}; it appears that the hydration energy could remain about the same, but a heat of reaction (and perhaps ionization) would have to be included. Other oxygenated species, such as H_2ReO^-, $H_4ReO_2^-$, $H_3ReO_2^=$ would not seem to be favored because of the required tetra-coördination apparently needed to stabilize the species. This will be discussed further under solid rhenides.

Solid Rhenides.—The discovery of solid rhenides[21] has provided further information on the stability of the rhenide ion. The most significant fact is that the only stable rhenides prepared to date appear to be hydrates.[22] Possibly the only anhydrous rhenide observed is formed upon the addition of thallous ion to a rhenide solution which results in a white precipitate that rapidly decomposes.[7,8]

Qualitatively, the non-existence of an anhydrous rhenide and the low reactivity of the element toward active metals only confirms the previous conclusions of a low electron affinity for rhenium. A more detailed analysis can be made in terms of a crystal energy calculation for a hypothetical solid anhydrous rhenide. Since a monovalent rhenide probably would crystallize in either a sodium chloride or cesium chloride structure, for which almost identical Madelung constants of 1.748 or 1.763 would be valid, the crystal energies for some rhenides can be calculated (Table II) from the equation

$$V^0 = \frac{-329.7A}{r_{12}}[1 - 1/n] \qquad (2)$$

In this expression, r_{12} is equal to the sum of the ionic radii of rhenide (2.3 Å.) and the metallic ion in question; the repulsion term, n, for rhenide is assumed to be ∼12.

A calculation can now be made on the stability of a solid anhydrous rhenide, *e.g.*, TlRe (Table III).

It is thus obvious that solid anhydrous rhenides (if ionic) are not stable. For minimal stability, the electron affinity of rhenium would again have to be greater than −200 kcal. in agreement with our

(20) The formula is written in this manner to distinguish from normal hydration, $Re(H_2O)_4^-$. The energy of normal hydration has already been included in the ΔH_{hyd} term. A highly stable oxygenated compound is required.

(21) E. Griswold, J. Kleinberg and J. B. Bravo, *Science*, **115**, 375 (1952).

(22) There has been one report of a direct interaction of an alkali metal (K) with rhenium metal (ref. 8). We have not been able to duplicate this result in our laboratory, nor have others (E. Scott, private communication). It should be noted that fusion of rhenium metal with an active metal followed by solution in water and observance of rhenide ion does not, in itself, prove that there was a direct interaction in the solid state, since the reduction of Re could conceivably take place in an aqueous suspension.

TABLE II

HYPOTHETICAL CRYSTAL ENERGIES FOR
SOME SOLID RHENIDES

Rhenide	r_{12}, Å.	$-V^0,b$ kcal. mole^{-1}
LiRe^a	3.27	163 ± 16
NaRe^a	3.30	157 ± 16
KRe	3.63	144 ± 14
TlRe	3.80	134 ± 13

^{a} In these crystals, $r_+/r_- \gg 0.414$, and the interatomic distances are fixed by anion–anion repulsion. ^{b} The calculation will not be greatly affected whatever the crystal structure, since the Madelung constant per valence bond for all known crystal types does not vary more than about 20% (D. H. Templeton, *J. Chem. Phys.*, **21**, 2097 (1953)).

TABLE III

Born cycle for thallous rhenide^a	ΔH, kcal./mole	
Tl(c) = Tl(g)	44.5	
Tl(g) = Tl$^+$(g) + e$^-$(g)	142.3	
Re(c) = Re(g)	183	± 2
e$^-$(g) + Re(g) = Re$^-$(g)	− 65	± 10
Tl$^+$(g) + Re$^-$(g) = TlRe(c)	−134	± 13
Tl(c) + Re(c) = TlRe(c)	171	± 28

^{a} Auxiliary data from "Selected Values of Chemical Thermodynamic Properties," U.S. Bureau of Standards, 1949.

previous conclusions. The situation is also similar for other solid rhenides. It is apparent that the observation of *a bona fide* solid anhydrous rhenide would require a rather serious revision of our thinking concerning reactivity as well as electronic structure.[23]

Hydrated Solid Rhenides.—The hydrated solid species appears to be stable not because of any simple hydration phenomena but because the four water molecules observed for potassium rhenide *are built into and are an integral part of* the rhenide ion. The $5d^2 6s^2 6p^4$ (dsp^2) electronic structure proposed[24] for this ion appears to agree with the

(23) The possibility should be examined that the rhenide ion does not contain a −1 oxidation state of rhenium at all, but is, rather, a hydride ReH$^-$, similar to the borohydrides. Analytical data available to date would not alone rule out this species. Further, by oxidation the H$^-$ would be oxidized to hydrogen, and Re to ReO$_4^-$, and the requirement of eight equivalents per mole of "rhenide" would be satisfied. Thermodynamic arguments are more difficult to make in this case but the very high electrode potential estimated for the hydride ion of 2.25 volts (ref. 12, p. 36), as well as the fact that none of the simple, metallic hydrides are stable in contact with water would tend to rule out this possibility.

(24) L. Pauling, *Chem. Eng. News*, **25**, 2970 (1947).

magnetic observation of a very low paramagnetism.[7] It would appear that the requirements for this type of ion to exist would be a central atom capable of forming covalent bonds, with a proper electronic structure required for a high orbital stabilization. In addition, it is doubtful whether the central ion could accept more than one electron to get into a favorable electronic structure since this would almost certainly be discriminated against in a large, unfavorable second electron affinity. Thus W(H$_2$O)$_4^-$ would not be a likely prospect. However, Ta(H$_2$O)$_8^-$ (d^{2}sp^3) might be stable. It is also possible that a simple halide-like ion might exist in some non-aqueous solvents which are more stable toward reduction such as ammonia. Further, there is no reason to suspect that the *gaseous* mono or even di negative ions could not be observed.[25]

The Technetide Ion.—Another possibility exists for a rhenide-like ion in the closely similar element technetium. Here the question would appear to be whether the covalent nature of technetium is similar enough to rhenium to form the Tc(H$_2$O)$_4^-$ species, since the other thermodynamic properties of the two elements are similar.[26] However, attempts by this author in 1952 to prepare an aqueous solution of rhenide by reduction of TcO$_4^-$ in a Jones reductor (which was successful for a similar reduction of ReO$_4^-$) did not give a solution of the required reducing power.

Conclusion

Arguments have been presented for suggesting that the structure of the aqueous rhenide ion is not simple, but consists rather of some type of oxygenated complex such as H$_8$ReO$_4^-$. The instability of a hypothetical simple Re$^-$ ion is based essentially upon a high sublimation energy for rhenium metal which cannot be compensated for by a reasonable electron affinity. Necessary stabilization of a −1 oxidation state apparently rises from a fortunate circumstance of covalent character and electronic structure in an oxygenated species. Predictions for certain other halide-like ions are given.

(25) To this list should be added such species as reported for the carbonyls: Re(CO)$_5^-$, Mn(CO)$_5^-$, Co(CO)$_4^-$, Cr(CO)$_5^-$, Fe(CO)$_4^-$, etc. At present the discussion must be limited to simple ions or hydration complexes; there are no quantitative thermochemical data on those carbonyl species apparently stable in aqueous media.

(26) As a matter of fact ΔH_v is estimated (ref. 9) to be some 50 kcal. less for Tc which would tend to favor the existence of technetide.

THERMODYNAMIC PROPERTIES OF SELECTED METHYLBENZENES FROM 0 TO 1000°K.

By S. H. Hastings and D. E. Nicholson

Humble Oil and Refining Company, Technical and Research Divisions, Baytown, Texas

Values of the heat capacity, the heat content function, the free energy function, the entropy, heat of formation and free energy of formation have been calculated at selected temperatures, from 0 to 1000°K. for eight methylbenzenes in the ideal gas state. All of the methylbenzenes for which vibrational assignments had not been made previously were included: namely, 1,2,3-trimethylbenzene, 1,2,4-trimethylbenzene, and three tetramethylbenzenes, pentamethylbenzene and hexamethylbenzene. Minor changes were made in the assignments for 1,2-dimethylbenzene published previously by Pitzer and Scott. The potential barrier associated with the hindered rotation of the *ortho*-methyl group in 1,2,4-trimethylbenzene was found to be 1400 cal./mole on the basis of frequency assignments and the experimental entropy. Employing this *ortho*-barrier for the methyl groups in the 1- and 3-positions in 1,2,3-trimethylbenzene, a barrier of 3200 cal./mole was found for the central methyl group. Comparison of the tetramethylbenzene isomerization equilibrium measured experimentally with that calculated from results of the statistical calculations shows good agreement.

Introduction

The thermodynamic properties of benzene and the C_7-, C_8- and C_9-methylbenzenes in the ideal gas state have been published by Taylor, *et al.*[1] The object of the present investigation was to establish reliable values of the heat capacity, the heat content function, the free energy function, and quantities derived from these for the tetra-, penta- and hexamethylbenzenes. Recently Kilpatrick and co-workers[2,3] have determined entropies from low temperature heat capacity and other data for the 1,2,3- and 1,2,4-trimethylbenzenes. The availability of the entropy data permits a more precise assignment of the potential barriers associated with restricted rotation of the methyl groups for these molecules than has heretofore been possible.

Spectral Data.—Although infrared and Raman spectra for a number of the compounds studied were available from the literature,[4-6] it was necessary to provide additional data. The near infrared spectra of pentamethylbenzene and hexamethylbenzene and the 15 to 35μ infrared spectra of the eight hydrocarbons were determined in this Laboratory. Purities of the hydrocarbons were as follows: 1,2-dimethylbenzene, 99.93% (mole); 1,2,3-trimethylbenzene, 99.98%; 1,2,4-trimethylbenzene, 99.67%; 1,2,3,4-tetramethylbenzene, 99.92%; 1,2,3,5-tetramethylbenzene, 99.92%; 1,2,4,5-tetramethylbenzene, 99.86%; pentamethylbenzene, 95.8%; hexamethylbenzene, 95%. All of the hydrocarbons were API standards with the exception of penta- and hexamethylbenzenes, which were Eastman white label grade used without further purification. Spectral data in the 15–35 μ region were obtained with a Perkin–Elmer Model 112-C infrared spectrometer having cesium bromide optics.

Equilibrium Measurements.—Isomerization equilibria among the methylbenzenes were established to compare with the equilibria calculated from free energies of formation. At 300°K. aluminum bromide and aluminum chloride, promoted with the corresponding hydrogen halides, were used as isomerization–disproportionation catalysts. The starting materials were 1,2,4-trimethylbenzene (95 mole %) (200 g.) and the anhydrous powdered aluminum halide (15–45 g.) in one series of experiments. Reaction times varied from 10–72 hours with the equilibrium vessels being provided with continuous stirring. In the second and third series of runs 5–20 mole % solutions of 1,2,4,5-tetramethylbenzene in benzene and 1,2,3,4-tetramethylbenzene (99.8% purity) were chosen as starting materials to establish the tetramethylbenzene equilibria. At 700°K. equilibria were established using a flow reactor having a volume of 150 ml. filled with an alumina–silica catalyst (SiO_2, 85.6%; Al_2O_3, 12.9%; H_2O, 1.5%) having a surface area of 303 m.²/g. The products from a given run were recirculated to the reaction zone at least three times to ensure that equilibrium had been attained. Hydrocarbon starting materials in the experiments at 700°K. were 1,2,4-trimethylbenzene, a solution of 1,2,4,5-tetramethylbenzene in benzene, and an equimolar mixture of 1,2,3,5- and 1,2,4,5-tetramethylbenzenes. It was assumed that equilibrium had been reached when no change in isomer concentration could be detected as contact time increased by a twofold factor.

Analysis of Products.—Reaction products from the isomerization–disproportionation experiments were analyzed, without the need for prior distillation, by a combination of infrared and mass spectrometric techniques. Penta- and hexamethyl benzene concentrations were determined from mass spectral patterns and the individual C_6–C_{10} benzenes by infrared spectrometric analysis. Thus total aromatic concentrations for a given molecular weight value were obtained by two independent means. The infrared procedure provides corrections for deviations from Beer's law and utilizes a thick cell to minimize the effects of wave length shifts of the absorption bands.[7]

Discussion

Vibrational Assignments.—All of the methyl-

(1) W. J. Taylor, D. D. Wagman, M. G. Williams, K. S. Pitzer and F. D. Rossini, *J. Research Natl. Bur. Standards*, **37**, 95 (1946).

(2) R. D. Taylor, B. H. Johnson and J. E. Kilpatrick, *J. Chem. Phys.*, **23**, 1225 (1955).

(3) W. E. Putnam and J. E. Kilpatrick, unpublished data.

(4) American Petroleum Institute Research Project 44 at the Carnegie Institute of Technology, Catalogs of Infrared and Raman Spectral Data.

(5) K. W. F. Kohlrausch and A. Pongratz, *Monatsh*, **64**, 361, 374 (1934).

(6) K. W. F. Kohlrausch and A. Pongratz, *Sitzb. Akad. Wiss. Wien.*, **143**, 275, 288, 358 (1934).

(7) R. B. Williams, S. H. Hastings and J. A. Anderson, Jr., *Anal. Chem.*, **24**, 1911 (1952).

TABLE I

FREQUENCY ASSIGNMENT FOR COMPOUNDS OF V_h AND C_{2v} SYMMETRY

Symmetry class V_h	C_{2v}	Freq. no.	Benzene	1,2,4,5-Tetra-methylbenzene	Penta-methylbenzene	1,2,3,5-Tetra-methylbenzene	1,2,3-Tri-methylbenzene
					Frequency in cm.$^{-1}$		
A_{1g}		1	993	508	568	573	654
		2	3062	1262	3050	3050	3046
		6a	606	430	484	330	514
		7a	3048	3033	786	1212	1240
		8a	1595	1620	1572	1614	1589
	A_1	9a	1178	346	353	1142	1163
		12	1010	582	682	736	654
B_{1u}		13	3060	1383	1371	1380	1377
		18a	1035	230	223	232	228
		19a	1485	1368	1450	1482	1386
		20a	3080	3050	1012	1293	3046
		3	1298	1202	892	1214	1220
B_{2g}		6b	606	346	340	551	509
		7b	3048	735	796	938	990
		8b	1595	1560	1572	1608	1553
		9b	1178	790	526	329	1191
	B_1	14	1693	1451	1450	1488	1653
		15	1170	844	307	232	306
B_{3u}		18b	1035	260	263	275	269
		19b	1485	1368	1346	1376	1377
		20b	3080	1280	1270	3050	3046
B_{1g}		10a	850	346	350	275	269
	A_2	16a	400	146	150	456	484
A_{1u}		17a	985	446	446	883	810
		4	685	690	326	330	709
B_{3g}		5	1016	867	526	512	938
	B_2	10b	850	260	712	705	269
B_{2u}		11	671	170	176	232	228
		16b	400	446	153	165	458
		17b	985	780	679	456	488

benzenes for which vibrational assignments have not been made previously were included in the present investigation: namely, 1,2,3-trimethylbenzene, 1,2,4-trimethylbenzene, the three tetramethylbenzenes, pentamethylbenzene and hexamethylbenzene. 1,2-Dimethylbenzene also was included since some changes in the published assignments were made. In making the frequency assignments extensive use was made of the Teller–Redlich product rule analog in the manner outlined by Pitzer and Scott.[8] This procedure was essential for a number of reasons, including lack of polarization data for the available Raman spectra and an indication that certain thermodynamically-important low-frequency Raman bands were not observed. For the methylbenzenes there are thirty ring-frequencies; in addition, the hydrogens of each methyl group contribute nine degrees of freedom. Eight of these degrees of freedom will be vibrational modes and one will be the internal rotation of the methyl group against the remainder of the molecule. The methyl group vibrations are identified by Pitzer and Scott as follows: M_1, one symmetrical stretching mode (2950 cm.$^{-1}$); M_2, two unsymmetrical stretching modes (2950 cm.$^{-1}$); M_3, one symmetrical bending mode (1380 cm.$^{-1}$); M_4, two unsymmetrical bending modes (1450 cm.$^{-1}$); M_5, two wagging modes (1050 cm.$^{-1}$). The frequencies of these vibrations do not vary greatly among the various methylbenzenes and

since they make comparatively small contributions to the thermodynamic properties, the average values cited above were employed, except for the wagging modes.

Tables I–III give the symmetry classes, vibrational modes, and frequency assignments for all of the methylbenzenes studied. The number system in the tables is that of Wilson.[9] It is possible to calculate approximate values of τ for methyl substitution. For the methyl ring stretching modes the value of τ is the square root of the ratio of the mass of the hydrogen atom to the mass of the methyl group, viz., $(1/15)^{1/2} = 0.258$. Similarly, the τ-value for each methyl bending mode is the ratio of the moment of inertia of a hydrogen atom referred to the benzene ring to the moment of inertia of the methyl group with respect to the point of attachment ($= 0.171$). There will be one methyl–ring stretching and two methyl–ring bending modes (in-plane and out-of-plane) for each methyl group. In order to determine the class into which a given methyl–ring vibration frequency will fall (with its attendant τ-value) one simply applies the covering operations of the appropriate point group to the symmetry of the vibration in question. It should be realized that within a symmetry class frequency assignments can be permuted to some extent among the various observed bands without affecting the values of τ calculated from the product rule. From the selec-

(8) K. S. Pitzer and D. W. Scott, J. Am. Chem. Soc., 65, 803 (1943).

(9) E. B. Wilson, Phys. Rev., 45, 706 (1934).

TABLE II

FREQUENCY ASSIGNMENTS FOR COMPOUNDS OF C*$_{2v}$ AND C$_s$ SYMMETRY

Symmetry class C$_{2v}$* / C$_s$	Freq. no.	Benzene	1,2-Di-methyl-benzene	1,2,3,4-Tetra-methyl-benzene	1,2,4-Tri-methyl-benzene
	1	993	733	650	744
	2	3062	3062	1255	1239
	6a	606	582	325	474
	7a	3048	1223	1255	1239
	8a	1595	1584	1586	1615
A$_1$	9a	1178	1185	1165	1150
	14	1693	1680	1455	1680
	15	1170	1156	240	928
	18b	1035	180	270	285
	19b	1485	1550	1380	1377
A′ 20b		3080	3080	3050	3038
	3	1298	1287	1255	1212
	6b	606	583	550	541
	7b	3048	1275	1280	3038
	8b	1595	1606	1606	1571
	9b	1178	1145	320	321
B$_1$	12	1010	740	550	557
	13	3060	3046	1380	3038
	18a	1035	256	240	285
	19a	1485	1585	1375	1377
	20a	3080	3080	3080	1239
	4	685	685	325	541
	5	1016	862	470	704
A$_2$	10b	850	256	270	285
	16a	400	436	440	160
A″ 17a		985	823	817	806
	10a	850	823	804	748
B$_2$	11	671	256	240	240
	16b	400	405	155	439
	17b	985	862	485	874

TABLE III

FREQUENCY ASSIGNMENT FOR HEXAMETHYLBENZENE

Point Group D$_{6h}$

Symmetry class	Mode	Benzene	Hexamethyl-benzene
A$_{1g}$	1	993	553
	2	3062	1385
A$_{2g}$	3	1298	508
	R$_z$	$\sqrt{I}$ = 17.06	40.0
B$_{2g}$	4	685	313
	5	1016	378
E$_{1g}$	10	849	343
	R$_x$	$\sqrt{I}$ = 12.02	28.2
	R$_y$	$\sqrt{I}$ = 12.02	28.2
E$_{2g}$	6	606	343
	7	3047	783
	8	1596	1568
	9	1178	367
A$_{2u}$	11	671	171
	T$_z$	$\sqrt{M}$ = 8.84	12.73
B$_{1u}$	12	1011	553
	13	3046	1385
B$_{2u}$	14	1693	1462
	15	1170	229
E$_{1u}$	18	1035	229 ⎫
	19	1485	1060 ⎬
	20	3080	1272 ⎭
	T$_x$	8.84	12.73
	T$_y$	8.84	12.73
E$_{2u}$	16	400	155
	17	985	450

tion rules[10] it is found that there should be two fundamentals for 1,2,4,5-tetramethylbenzene (Point Group D$_{2h}$) which are inactive in both the infrared and Raman spectra. Hexamethylbenzene (D$_{6h}$) has nine inactive fundamental frequencies, as does benzene; the high degree of symmetry, however, greatly facilitates application of the product rule analog because the increased number of symmetry classes results in fewer vibration modes falling in a given class. The least certain of the assignments is probably that for 1,2,4-trimethylbenzene, the low symmetry of which does not permit as detailed an analysis of the vibrational spectrum as was possible for the other compounds. Agreement between the theoretical and calculated τ-values is within 1% for all compounds studied.

An additional check on the vibrational assignments is afforded by application of the vibrational sum rule as formulated by Bernstein.[11,12] Strict application of this sum rule requires that parameters be evaluated which take into account differences in the sum of frequencies (over-all, in-plane and out-of-plane) for position isomers. This leads to absurd results and indicates that the data are not sufficiently accurate to evaluate these

(10) G. Herzberg. "Infrared and Raman Spectra," D. Van Nostrand Co., Inc., New York, N. Y., 1945.

(11) H. J. Bernstein, J. Chem. Phys., 20, 263 (1952).

(12) Private communication.

differences (which are apparently small). If one assumes that there is no difference then it is possible to evaluate an average effect of methyl substitution on the various frequency sums. The out-of-plane sums show very good agreement and indicate that the assignments are reasonably certain. The over-all and in-plane sums show a higher variation on a wave number basis; however, on a percentage basis the agreement is even better.

Another useful check on the vibrational assignments is provided by the fact that certain frequencies are relatively unaffected by methyl substitution. Examination of Fig. 6 of reference 8 shows that in vibrational modes 7b, 9a, 10a, 17a and 20b the groups located on the vertical axis (in the plane of the drawing) are motionless during the vibration and hence should not affect the frequency appreciably. In modes 6b and 18a only a slight motion of these groups is indicated, so that here also the frequencies should be relatively unaffected by methyl substitution. Vibrations 7b and 20b apparently are misassigned by Pitzer and Scott for 1,3,5-trimethylbenzene, but since these fall in the same symmetry class the product rule is unaffected.

The vibrational contributions to the thermodynamic properties were programmed on an IBM Model 650 computer. Some of the regularities in the contributions to the heat capacity at 500°K. for the methylbenzenes are shown in Fig. 1. There appears to be a constant increment for each successive methyl group and the variation among position isomers is of the order of one cal./deg. mole.

Because of the uncertainties in the frequency assignments average values of the vibrational contributions were used for each set of isomers. This method of calculation amounts to an assumption that the vibrational contributions of isomers are identical. A further justification for employing average values for the vibrational contributions is that slightly better agreement in the experimental and calculated tetramethylbenzene isomerization equilibria at both 300 and 700°K. was obtained when using the average values.

Moments of Inertia and Barriers to Internal Rotation.—Carbon–carbon bond lengths in the planar benzene ring were taken as 1.39 Å. and carbon–carbon bond lengths between the methyl groups and the benzene ring were selected to be 1.54 Å. Bond lengths between the hydrogen and carbon atoms in the methyl groups and joining the benzene ring were 1.09 and 1.08 Å., respectively. Tetrahedral angles in the methyl groups were assumed in preparing coördinate tables. The symmetry numbers for over-all and internal rotation and the principal moments of inertia, for those compounds not previously reported,[1] are given in Table IV. The reduced moments of inertia for the restricted rotation calculations were computed from equations 1b and 1e in the paper by Pitzer and Gwinn.[13] A value of 5.48×10^{-40} g. cm.^{2} was used for the reduced moments of inertia of all the methyl groups in the tetra-, penta- and hexamethylbenzenes.

TABLE IV

MOLECULAR PARAMETERS

Compound	Symmetry no.	Principal moments of inertia, g. cm.$^2 \times 10^{39}$		
		I_x	I_y	I_z
1,2,3,4-Tetramethylbenzene	162	69.92	41.91	109.75
1,2,3,5-Tetramethylbenzene	162	67.67	48.64	114.20
1,2,4,5-Tetramethylbenzene	324	35.12	80.54	116.43
Pentamethylbenzene	486	59.49	81.07	137.91
Hexamethylbenzene	8748	79.70	80.54	160.03

Cosine functions of the type $V(\phi) = \frac{1}{2} V_0(1 - \cos n\phi)$ were assumed to describe the internal rotation of the methyl groups. The barriers for *ortho* and central methyl groups ($n = 3$) were calculated from the entropy data of Kilpatrick, *et al.*,[2,3] for 1,2,4- and 1,2,3-trimethylbenzenes. On the basis of the vibrational assignments and the entropy data, barriers for the *ortho* and central methyl groups are 1400 and 3200 cal./mole, respectively. The barrier for an isolated methyl group, as in methylbenzene or 1,4-dimethylbenzene was assigned a value of 750 cal./mole as had been selected previously.[1] Using the vibrational assignments in this study, the *ortho* barrier in 1,2-dimethylbenzene was computed as 1800 cal./mole from entropy data. It is quite possible that in certain cases, *e.g.*, for hexamethylbenzene, due to an interlocking effect the six barriers should be greater than 3200 cal./mole for each methyl group. Experimental entropy data for 1,2,3,4- and penta- and hexamethyl-
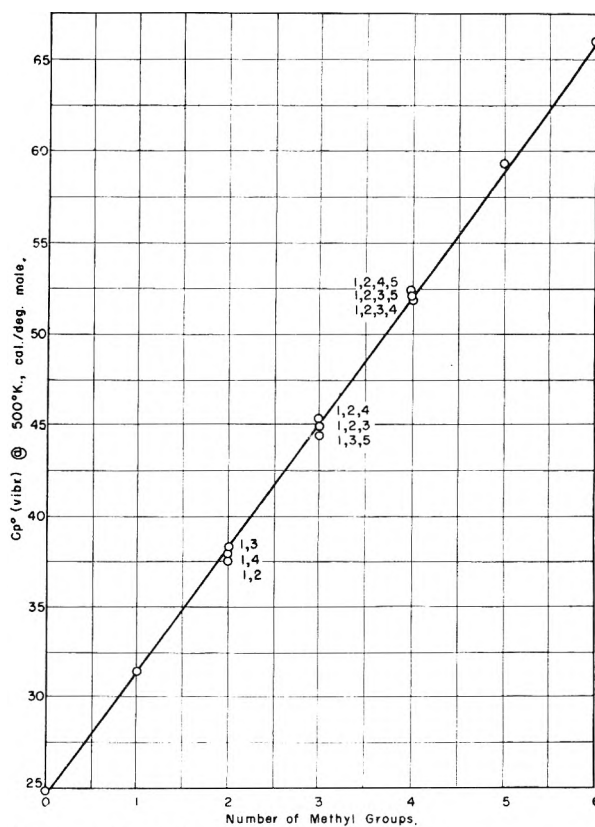
Fig. 1.—Effect of methyl substitution on heat capacity of benzene (vibrational).

benzene would, of course, be required before an answer to this question is possible. It is interesting to note, however, that in the isomerization-disproportionation experiments at 700°K. the reaction products contained about 2.0% (wt.) pentamethylbenzene and 0.1% hexamethylbenzene. The calculated concentrations were 6.5% and 0.3% penta- and hexamethylbenzene, respectively. Increasing the rotational barrier height would lower the calculated equilibrium concentrations of these components and give better agreement between theory and experiment, provided all the discrepancy can be attributed to an error in barrier assignment.

Thermodynamic Functions.—From the vibrational assignments, the moments and reduced moments of inertia, and the barriers to internal rotation described above, values of the thermodynamic functions $(H° - H°_0)/T$, $(F° - H°_0)/T$, $S°$, $C°_p$, at selected temperatures from 0 to 1000°K. were computed. The atomic weights of hydrogen and carbon were taken as 1.0080 and 12.010, respectively. Values of other natural constants were: Planck's constant, 6.624×10^{-27} erg. sec.; gas constant, 1.9863 cal./deg./mole; 1 calorie = 4.1833 international joules. The harmonic-oscillator rigid-rotor equations were used and it was assumed that the internal rotors could be treated independently. These thermodynamic quantities are presented in Table V.

Thermodynamic data for graphite and hydrogen given by Wagman, *et al.*,[14] were used for the cal-

(13) K. S. Pitzer and W. D. Gwinn, *J. Chem. Phys.*, **10**, 428 (1942).

(14) D. D. Wagman, J. E. Kilpatrick, W. J. Taylor, K. S. Pitzer and F. D. Rossini, *J. Research Natl. Bur. Standards*, **34**, 143 (1945).

TABLE V

THERMODYNAMIC VALUES FOR EIGHT METHYLBENZENES

Temp., °K.	1,2-Dimethyl-benzene	1,2,3-Trimethyl-benzene	1,2,4-Trimethyl-benzene	1,2,3,4-Tetramethyl-benzene	1,2,3,5-Tetramethyl-benzene	1,2,4,5-Tetramethyl-benzene	Penta-methyl-benzene	Hexa-methyl-benzene
			$(H° - H_0°)/T$ (cal./deg. mole)					
298.16	18.83	22.26	22.05	26.22	26.01	26.72	29.40	32.91
300	18.91	22.35	22.14	26.33	26.12	26.83	29.52	33.04
400	23.32	27.44	27.08	32.42	32.07	32.61	36.64	41.28
500	27.67	32.54	31.94	38.43	37.90	38.23	43.60	49.37
600	31.82	37.33	36.73	43.93	43.34	43.53	49.89	56.48
700	35.66	41.81	41.19	49.03	48.41	48.54	55.68	62.92
800	39.21	45.93	45.30	53.71	53.08	53.13	60.95	68.81
900	42.50	49.72	49.10	57.98	57.36	57.38	65.75	74.10
1000	45.50	53.21	52.60	61.92	61.31	61.30	70.17	78.99
			$-(F° - H_0°)/T$ (cal./deg. mole)					
298.16	65.51	69.53	72.49	73.33	74.98	73.31	76.69	75.21
300	65.62	69.66	72.62	73.48	75.13	73.46	76.86	75.41
400	71.67	76.80	79.72	81.92	83.48	82.00	86.37	86.09
500	77.35	83.49	86.25	89.82	91.27	89.89	95.31	96.22
600	82.74	89.85	92.51	97.33	98.68	97.35	103.85	105.87
700	87.97	95.99	98.50	104.59	105.80	104.40	112.14	115.44
800	92.98	101.79	104.27	111.33	112.51	111.20	119.74	123.84
900	97.76	107.43	109.84	117.91	119.01	117.72	127.21	132.39
1000	102.40	112.83	115.17	124.20	125.24	123.93	134.34	140.33
			$C_p°$ (cal./deg. mole)					
298.16	31.93	37.74	36.81	45.31	44.39	44.58	51.74	59.42
300	32.10	37.82	36.99	45.50	44.57	44.77	51.99	59.73
400	40.99	48.01	46.96	56.81	55.76	55.50	65.00	74.18
500	48.98	57.25	56.26	67.01	66.03	65.62	76.43	86.65
600	55.84	65.16	64.29	75.68	74.81	74.38	86.08	97.13
700	61.61	71.87	71.12	83.13	82.39	81.97	94.27	105.97
800	66.50	77.56	76.93	89.42	88.79	88.41	101.29	113.51
900	70.68	82.42	81.87	94.82	94.27	93.94	107.20	119.99
1000	74.24	86.58	86.10	99.47	99.01	98.71	112.33	125.55
			$S°$ (cal./deg. mole)					
298.16	84.34	91.79	94.54	99.55	100.99	100.03	106.09	108.12
300	84.53	92.01	94.76	99.81	101.25	100.29	106.38	108.45
400	94.99	104.24	106.80	114.34	115.55	114.61	123.01	127.37
500	105.02	116.03	118.19	128.25	129.17	128.12	138.91	145.59
600	114.56	127.18	129.24	141.26	142.02	140.88	153.74	162.35
700	123.63	137.80	139.69	153.62	154.21	152.94	167.82	178.36
800	132.19	147.72	149.57	165.04	165.59	164.33	180.69	192.65
900	140.26	157.15	158.94	175.89	176.37	175.10	192.96	206.49
1000	147.90	166.04	167.77	186.12	186.55	185.23	204.51	219.32
			$H_f°$ (kcal./mole)					
0	+11.057	+5.480	+4.503	-1.155	-1.782	-2.104	-7.608	-13.839
298.16	+4.540	-2.290	-3.330	-10.020	-10.710	-10.820	-17.800	-25.260
300	+4.505	-2.332	-3.372	-10.064	-10.754	-10.863	-17.852	-25.319
400	+2.709	-4.453	-5.574	-12.332	-13.097	-13.203	-20.329	-27.937
500	+1.178	-6.214	-7.491	-14.155	-15.047	-15.204	-22.273	-29.870
600	-0.079	-7.677	-9.014	-15.678	-16.659	-16.867	-23.883	-31.485
700	-1.115	-8.884	-10.251	-16.875	-17.936	-18.168	-25.126	-32.743
800	-1.916	-9.735	-11.216	-17.766	-18.897	-19.179	-25.946	-33.608
900	-2.488	-10.385	-11.920	-18.403	-19.588	-19.892	-26.680	-34.214
1000	-2.869	-10.776	-12.363	-18.742	-19.979	-20.311	-26.985	-34.436
			$F_f°$ (kcal./mole)					
298.16	29.173	29.828	27.968	29.496	28.377	28.553	29.447	33.909
300	29.324	30.029	28.164	29.745	28.623	28.802	29.802	34.258
400	37.873	41.114	38.995	43.357	42.106	42.376	46.024	53.583
500	46.842	52.740	50.383	57.490	56.138	56.506	62.842	73.483
600	56.177	64.676	62.103	71.961	70.524	71.000	80.004	93.751
700	65.545	76.803	74.069	86.604	85.130	85.788	97.315	114.012
800	75.097	89.136	86.175	101.525	99.954	100.680	115.008	134.935
900	84.794	101.537	98.391	116.484	114.867	115.706	132.675	155.578
1000	94.517	114.020	110.703	131.525	129.858	130.846	150.442	176.503

culations. The heats of formation of gaseous penta- and hexamethylbenzene have not been reported.[15] These heats of formation for gaseous $C_{11}H_{16}$ and $C_{12}H_{16}$ were estimated to have values -17.79 and -25.26 kcal./mole, respectively, at $298.16°K$. The derived quantities $\Delta H_f°$ and $\Delta F_f°$ as a function of temperature are shown in Table V.

TABLE VI

COMPARISON OF CALCULATED AND EXPERIMENTAL ISOMERIZATION EQUILIBRIA AMONG THE TRI- AND TETRAMETHYLBENZENES

Component, mole %	Temp., °K. → 300 Exptl.	Calcd.	700 Exptl.	Calcd.
1,2,3-Trimethylbenzene	..	3	9	9
1,2,4-Trimethylbenzene	..	59	65	68
1,3,5-Trimethylbenzene	..	38	26	23
1,2,3,4-Tetramethylbenzene	8	8	22	18
1,2,3,5-Tetramethylbenzene	47	53	45	50
1,2,4,5-Tetramethylbenzene	45	39	33	32

(15) E. J. Prosen, W. H. Johnson and F. D. Rossini, J. Research Natl. Bur. Standards, 36, 455 (1946).

Isomerization Equilibria.—Data from the isomerization experiments are given in Table VI at 300 and 700°K. and are compared with the concentrations calculated using the free energies of formation from the present investigation. The agreement is believed to be within the limits imposed by probable errors in product analyses and assumptions in the statistical calculations.

Acknowledgments.—The authors are glad to acknowledge helpful discussions with Professors F. A. Matsen and J. O. Hirschfelder during the course of this work. A communication from Dr. H. J. Bernstein with regard to his sum rule was instrumental in effecting an improvement in the assignment for 1,2,4-trimethylbenzene. Raman spectral date of 1,2,3,4-tetramethylbenzene were determined by Dr. Boyd E. Hudson of the Esso Research and Engineering Company. In addition, Mr. B. M. Holleman performed most of the equilibrium measurements and Messrs. J. Dzilsky and T. Hines obtained the analytical results.

THE ELECTROPHORETIC MOBILITY OF DECYL-, DODECYL- AND TETRADECYLAMINE HYDROCHLORIDE MICELLES

By H. W. Hoyer and A. Greenfield

Chemistry Department, Hunter College, New York 21, New York

Received November 17, 1956

The electrophoretic mobilities of the decyl-, dodecyl- and tetradecylamine hydrochloride micelles were studied as functions of their concentrations in aqueous solutions. In addition the effect of ionic strength and temperature upon micelle mobility was studied for the dodecylamine hydrochloride micelle. Measurements on dodecylamine hydrochloride at temperatures of 18, 25 and 35° give values of the mobilities of 3.74, 4.43 and 5.56 × 10⁻⁴ cm.² per volt-sec. at the critical concentration. The determination of the mobilities of the decyl- and tetradecylamine hydrochloride micelles at 25° gave values of 3.62 and 5.75 × 10⁻⁴ cm.² per volt-sec. at the critical concentrations. The micelle mobilities are more dependent upon the ionic strength of the solution than upon the nature of the organic monomer ion.

Introduction

Within the past few years considerable progress has been made toward elucidating the nature of the particles existing in solution of colloidal electrolytes. McBain[1] was one of the first to recognize that these particles were formed by the association of simple molecules and/or ions into complex ions of colloidal dimensions. In recent years Debye and others[2-4] have applied light scattering techniques to the determination of the molecular sizes of these colloidal electrolytes or micelles. For dodecylamine hydrochloride Debye found that the molecular weight at the critical concentration for the formation of micelles varies from 12,300 in pure water to 31,400 in a 0.045 M sodium chloride solution.

Little work has been directed toward elucidating the charge on these micelles. Van Rysselberghe[5] has attempted to analyze the available conductivity and diffusion data for lauryl sulfonic acid and has obtained values for the charge on the micelle varying from -1 in dilute solutions to -89 in

0.6 molar solutions. Brady and Salley[6] were able to estimate the percentage of the sodium ions which remained bound to the micelles of Aerosol OT and Aerosol MA by using a radioactive tracer technique but could not obtain an absolute value for the charge on the micelles. Hoyer and Mysels[7] have suggested a micelle tagging technique based upon the preferential solubility of water insoluble dyes in the micelle. This technique was applied by Hoyer, Mysels and Stigter[8] to the determination of the electrophoretic mobility of the potassium laurate and sodium lauryl sulfate micelle and by Stigter and Mysels[9] to the determination of the mobility of the micelle of sodium lauryl sulfate in solutions of different ionic strengths. The last two authors interpreted their results in terms of Booth's theory[10] of the electrophoresis of colloidal particles and arrived at a value of 23 for the charge on the sodium lauryl sulfate micelle at its critical concentration.

The present paper is concerned with the electrophoretic mobility of some aliphatic amine hydrochloride micelles, specifically those of decyl-,

(1) J. McBain, J. Chem. Soc., 101, 2042 (1912); 105, 417 (1914); 113, 825 (1918).
(2) P. Debye, This Journal, 50, 1 (1949).
(3) P. Debye, Ann. N. Y. Acad. Sci., 51, 575 (1945).
(4) J. N. Phillips and K. J. Mysels, This Journal, 59, 325 (1955).
(5) P. Van Rysselberghe, ibid., 43, 1048 (1939).

(6) A. P. Brady and D. J. Salley, J. Am. Chem. Soc., 70, 914 (1948).
(7) H. W. Hoyer and K. J. Mysels, This Journal, 54, 966 (1950).
(8) H. W. Hoyer, K. J. Mysels and D. Stigter, ibid., 58, 385 (1954).
(9) D. Stigter and K. J. Mysels, ibid., 59, 45 (1955).
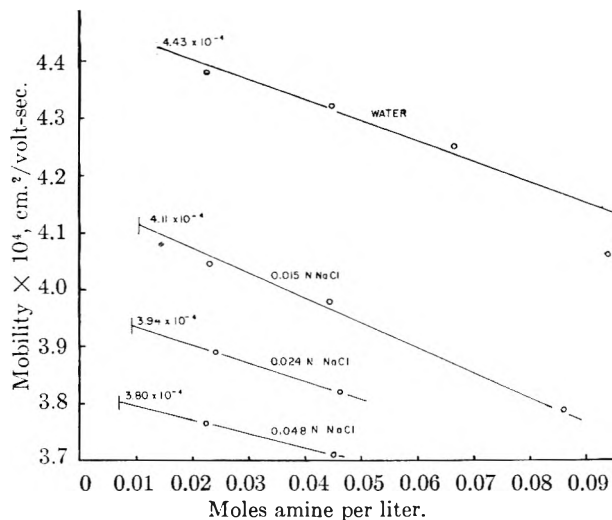(10) F. Booth, Proc. Roy. Soc. (London), A203, 514 (1950).

Fig. 1.—Electrophoretic mobility at 25° of dodecylamine micelle in H₂O and NaCl solutions.
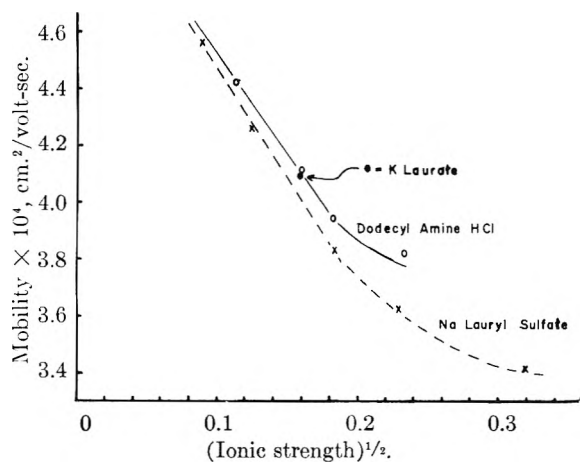

Fig. 2.—Effect of ionic strength at the critical concentration upon the mobilities of the micelles of dodecylamine HCl and sodium lauryl sulfate.
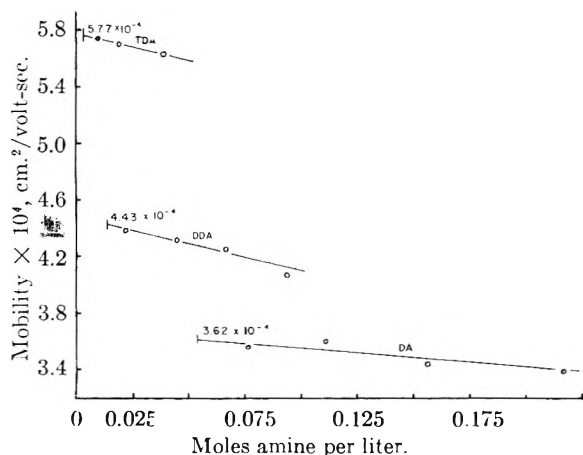

Fig. 3.—Mobilities of decyl-(DA), dodecyl-(DDA) and tetradecylamine hydrochloride at 25°.

dodecyl- and tetradecylamines. The effect of ionic strength and temperature upon the mobility of the dodecylamine micelle was studied as was the effect of monomer molecular weight upon micelle mobility.

Experimental

The open tube method of measuring electrophoretic mobilities which was used in these investigations has been described previously.[8] The only modification introduced consisted of using the recently described hydrogen ion coulometer[11] as a convenient and precise method for determining the coulombs passed through the system during each determination.

Sudan IV was used as the solubilized dye. The commercial sample (C.I. No. 258 from National Aniline) was purified by dissolving in acetone and precipitating from solution with water. The amines were commercial samples and were fractionated in a one meter vacuum jacketed column before being used.

Critical micelle concentrations (CMC) were determined by the conductivity method for the solutions of the different amines in pure water and are described in a separate note.[12] Our value of 0.0138 mole per liter for dodecylamine at 25° is slightly larger than the value of 0.0131 determined by a dye titration method by Corrin and Harkins.[13] This discrepancy produces a negligible difference in the extrapolated mobility of the micelle at the CMC because of the slight slope of the mobility *versus* concentrations curves. The equation of Corrin and Harkins connecting CMC with salt concentration was used to determine the critical concentration for the solutions of dodecylamine hydrochloride in sodium chloride solutions.

Results

Effect of Ionic Strength.—The effect of monomer concentrations and of sodium chloride concentration upon the mobility of the dodecylamine micelle at 25.0° is shown in Fig. 1. The short vertical line to the left of the plots indicates the critical micelle concentration of the particular solution. The number above each line gives the mobility of the micelle in each particular solution at the CMC for that solution. Both for the dodecylamine hydrochloride micelle and for the sodium lauryl sulfate micelle studied earlier by Stigter and Mysels[9] the mobility decreases as the normality of the sodium chloride in the solution is increased.

The essential similarity in the mobility of the micelles of these two substances, one a cationic, the other an anionic, detergent is shown in Fig. 2 where the micelle mobility at the critical micelle concentration is plotted as a function of the square root of the total salt concentration existing at the critical concentration. Included is the one point for the potassium laurate micelle determined in the earlier work of Hoyer, Stigter and Mysels.[8] The data reveal a marked lack of influence of structure upon micelle mobility. All three substances show essentially the same mobility *versus* concentration behavior. At the highest ionic strength for which the dodecylamine mobility was measured a deviation of only 4% exists between it and the mobility of the sodium lauryl sulfate micelle.

Effect of Molecular Weight of Monomer upon Micelle Mobility.—The effect of monomer hydrocarbon chain length upon the electrophoretic mobility of the micelle at 25° was studied with decyl-, dodecyl- and tetradecylamine hydrochlorides. The solution containing 0.0415 mole of tetradecylamine per liter apparently was supersaturated at 25° and the electrophoresis apparatus contained a slight precipitate at the end of each

(11) H. W. Hoyer, This Journal, **60**, 372 (1956).

(12) H. W. Hoyer and A. Greenfield, *ibid.*, **61**, 818 (1957).

(13) M. L. Corrin and W. D. Harkins, *J. Am. Chem. Soc.*, **69**, 683 (1947).

determination. Three separate runs with this solution gave an average value of 5.63×10^{-4} cm.^{2}/volt-sec. with an average deviation of $\pm 1.0\%$. This average value is included along with the other mobilities for the tetradecyl-, dodecyl- and decyl-amine hydrochloride micelles in Fig. 3.

The apparently considerable difference in the mobilities of these three substances is due largely to the differences in the ionic strengths of the solutions. This is shown in Fig. 4 in which the logarithm of the micelle mobility, μ, is plotted against the logarithm of the total salt concentration at the critical micelle concentration. The data may be expressed by the equation

$$\log \mu = -0.146 \log (C + C_0) - 3.617 \qquad (1)$$

where C is the added sodium chloride concentration and C_0 is the critical micelle concentration, both being expressed in moles per liter.

Effect of Temperature on Micelle Mobility.—Figure 5 illustrates the effect of temperature upon the mobility of the dodecylamine hydrochloride micelle. The mobilities at the critical micelle concentration are compared in Table I with the fluidity of water at the same temperature, taking the values at 25° as unity. The close agreement between these values shows that there is little change in micelle structure in the temperature range of 18 to 35° or that, if there is any change, mobility measurements cannot detect it. The mobility-temperature data may be expressed in the more common form for equivalent ionic conductance

$$l_t = l_{25}[1 + a(t - 25)] \qquad (2)$$

TABLE I

Temp., °C.	Fluidity ratio	Mobility ratio
18	0.846	0.845
25	1.000	1.000
35	1.237	1.256

where l_t now represents the micelle conductance at the critical micelle concentration, t the temperature in degrees centigrade, c the temperature coefficient which has the average value of 0.024 and l_{25} is the equivalent micelle conductance at 25° and at the critical micelle concentration. The numerical value of l_{25} is 42.75 cm.^{2} per ohm-equivalent.

Discussion

The similarity in micelle mobility which is demonstrated by Figs. 2 and 4 is remarkable. In Fig. 2 the micelles of dodecylamine hydrochloride, sodium lauryl sulfate and potassium laurate are shown to have essentially the same mobility in solutions of the same ionic strengths. All three substances possess different polar groups but have a twelve carbon chain in common. Debye[3] has outlined a theory of micelle structure which supposes a disk shaped micelle stabilized by a balance between short-ranged van der Waals forces of the hydrocarbon chains and long-ranged electrostatic forces of the polar heads. The data of Fig. 2 would appear to support some such theory. When substances with the same hydrocarbon chain length,
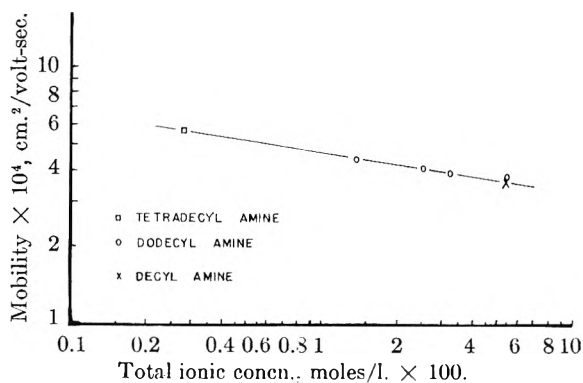

Fig. 4.—The dependence of micelle mobility upon the total salt concentration.
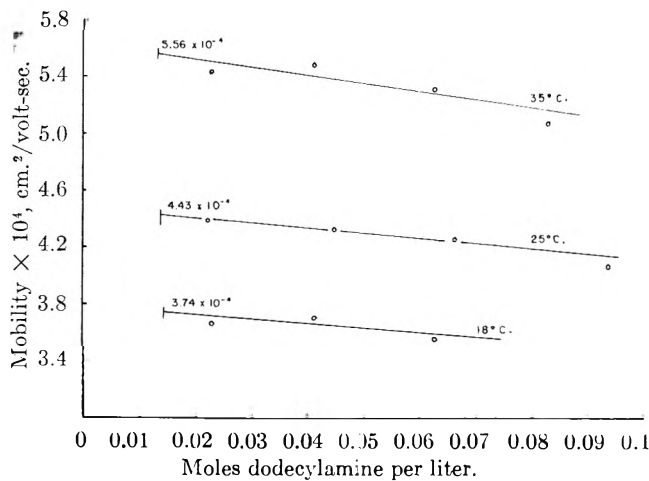
Fig. 5.—Effect of temperature upon the mobility of the dodecylamine HCl micelle.

and therefore similar van der Waal forces, are studied in solutions of equal ionic strength the electrostatic forces are also equal as is shown by the marked similarity of the electrophoretic mobilities.

Figure 4 demonstrates that, at least to a first approximation, the micelle mobilities for the aliphatic amines are independent of the molecular weight of the monomer and only affected by the total sodium ion concentration existing in equilibrium with the micelle. That this is only a first approximation is suggested by the points for the dodecylamine hydrochloride micelle which seem to lie on a line with a slightly different slope.

Attention should also be drawn to the magnitude of the slope of the mobility vs. square root of the ionic strength plot of Fig. 2. Stigter and Mysels[9] have calculated a charge of 23 units for the sodium lauryl sulfate micelle at its critical concentration yet the slope in this figure, as calculated from Onsager's equation[14] is somewhat less than that of a doubly charged ion. While some deviation from Onsager's equation can be expected in the concentration range studied, a deviation of 1200% from the predicted value implies the existence of a fundamental difficulty in the direct application of the theoretical principles to the experimental data.

Instead of regarding the micelle as a uniformly charged multivalent ion there is an alternate con-

(14) See, e.g., D. A. MacInnes, "The Principles of Electrochemistry," Reinhold Publishing Corp., New York, N. Y., 1939, Chapter 18.

cept which might correct this difficulty. On the surface of the micelle in a more or less regular arrangement must be located the various ionized groups of the micelle. For the three substances plotted in Fig. 2 these will be singly ionized groups, either amino, sulfate or carboxyl groups. If these groups are sufficiently far apart the ion atmospheres of each group will be uninfluenced by those of neighboring groups. The micelle will then be surrounded by ion atmosphere "clouds" centered over each ionized group. Each "cloud" will be essentially similar to the ion atmosphere surrounding a singly charged ion. If the ionized groups are not sufficiently far apart then the ion atmospheres will overlap and the resulting atmosphere around the micelle will resemble that of a singly, doubly or triply, etc., charged ion or some fraction thereof depending upon the distance between the groups and the extent of overlapping. This overlapping of ionic atmospheres will also vary with the ionic strength of the solution and will only be complete when the atmosphere of each group embraces the entire micelle.

When complete overlapping occurs, i.e., in a dilute enough solution, the slope of the mobility-square root of ionic strength plot will be determined by the total charge on the micelle. For the sodium lauryl sulfate micelle with a radius of about 21 Å. this will occur at an ionic strength of approximately 0.002. Since the lowest concentration plotted in Fig. 2 is only 0.008 the observed slope cannot be the limiting one. At this concentration the "radius" of the ion-atmosphere is approximately 33 Å., just about double the average separation of 23 charges equally distributed on the surface of a sphere of radius 21 Å.

# THE PROPERTIES OF FLAMES SUPPORTED BY CHAIN-BRANCHING REACTIONS[1]

By J. Calvin Giddings and Joseph O. Hirschfelder

*The University of Wisconsin Naval Research Laboratory, Madison, Wisconsin*

Received November 21, 1956

Numerical calculations have been completed on flames supported by a Semenoff type (chain branching with first order chain breaking step) sequence of reactions: $A \rightarrow 2B$, $B \rightarrow C$, $A + B \rightarrow 2B + C$ (FOB). This sequence is peculiar in that, according to the steady-state approximation, there is an explosion point at which both the radical concentration and reaction rate go to infinity. Whether or not the explosion point is reached in a particular flame depends upon the assumed reaction rates. The Klein method was used to solve the flame equations for five cases. The deviation of the actual concentration of the free radical (B) from the pseudo stationary concentration (B)* is measured by ϵ where $(B) = (1 + \epsilon)(B)^*$. A procedure is given for making a preliminary estimation of ϵ in the reaction zone which is found to be very accurate. This estimation of ϵ was useful in selecting the flame parameters since the Klein method of integration does not converge if ϵ is greater than around 0.4. The examples were chosen so as to show both the effect of nearness to the explosion point and the effect of variations in the coefficient of diffusion of the free radical. Since ϵ becomes large near the explosion point, the values of ϵ considered here are somewhat larger than for any of the flame systems previously considered. We find, as before,[2] that in contrast to the diffusional theories of flame propagation, the flame velocity decreases as the coefficient of diffusion of the free radical is increased.

In a recent paper[2] the authors outlined two chemical reaction schemes of sufficient simplicity to make feasible the mathematical treatment of flames supported by chain branching reactions. Each reaction scheme is designed to illustrate a different aspect of actual chain branching flames (for which the combustion of H_2 and O_2 serves as an example). A second-order reaction is given the chain-breaking role in one reaction scheme (SOB)

$$2B \longrightarrow A \qquad (SOB) \qquad (1)$$
$$A + B \longrightarrow 2B + C$$
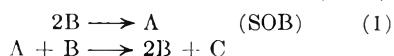
while for the Semenoff scheme, a first-order chain-breaking (FOB) step terminates the chain

$$A \xrightarrow{k_1} 2B$$
$$B \xrightarrow{k_2} C \qquad (FOB) \qquad (2)$$
$$A + B \xrightarrow{k_3} 2B + C$$
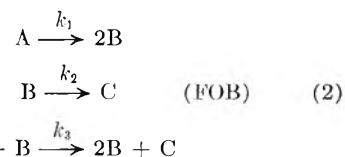
In the particular example of hydrogen combustion, a first-order chain-breaking step of importance is $H + O_2 \rightarrow HO_2$ (inactive). Chain termination, however, cannot proceed solely by this mechanism, since second-order radical recombinations will occur wherever the radical concentration is finite. The most characteristic feature of a (FOB) reaction sequence is the existence of an explosion limit at the point that the rate of branching, $k_3(A)(B)$, equals the chain-breaking rate, $k_2(B)$. At this point the steady-state radical concentration goes to infinity (see equation 4). Exactly at this point, the ubiquitous recombinations are most important, since their number increases

as the square (second-order) of radical concentration. Thus with the necessary inclusion of second-order processes at high concentrations, the steady state radical concentration can become very large (modified explosion point), but not approach infinity (explosion point).

In inventing simple reaction schemes which mimic the properties of actual kinetic schemes, two cases arise. In the first case, first-order chain-breaking steps are not important, and the steady-state radical concentration shows no abrupt changes with conditions. This case, the (SOB) scheme, is treated extensively elsewhere.

In the second case, first-order chain-breaking steps are important. These lead to rapid changes in the steady-state radical concentration at the modified explosion point. This same effect can be accomplished in (FOB) scheme by adjusting the kinetic parameters such that the explosion point is not quite reached. The properties of flames with underlying kinetics of this type are examined in this paper.

The explosion limit can be considered in the light of the quasi-equilibrium (steady-state) approximation. From the set of reactions (2), we find K_B, the net rate of production of the radical, B.

$$K_B = d(B)/dt = 2k_1(A) - k_2(B) + k_3(A)(B) \quad (3)$$

Equating this to zero, we get the quasi-equilibrium concentration.

$$(B)^* = \frac{2k_1(A)}{k_2 - k_3(A)} \quad (4)$$

The rate of reaction is proportional to the radical concentration

$$K_C = [k_2 + k_3(A)](B) \quad (5)$$

It is convenient to introduce the parameter

$$S = k_3(A)/k_2$$

Then S describes the nearness to explosion. The explosion point is defined as the condition under which $S = 1$. At the explosion point $(B)^*$ becomes infinite and K_C becomes very large.

It is clear that the flame problem becomes unusually complicated near the explosion point. The steady-state radical concentration ceases to exist, so we do not have a reasonable first approximation for this quantity. Also, a term just of the form of (4) appears in the equations, making them untractable near the explosion point. By properly adjusting the kinetic parameters, we approach but do not reach the explosion point, as suggested above.

The study of the quasi-equilibrium approximation to radical concentrations has been found to be one of the most important aspects of flame theory,[3,4] both from a mathematical and from a physical point of view. This approximation does not yield exact concentration profiles, but it is often quite close over most of the temperature range. The

difference between the quasi-equilibrium concentration $(B)^*$, and the actual value (B), is given in terms of ϵ, where $(B) = (B)^* (1 + \epsilon)$. It is found necessary, in flame calculations, to have a reasonable input for the (B) profile. When ϵ is small,[3] $(B)^*$ is that input. When ϵ is not small, there is no close approximation available. Aside from the input problem, one also finds great difficulty in bringing the equations to convergence when ϵ is large in the reaction zone. Such has been the case for the AB^2C flame,[5,6] for which final results have not yet been obtained. The HBr flame is no doubt complicated by this effect.[7] In the present calculations, we find for the cases where ϵ approaches the value $-\frac{1}{2}$ in the reaction zone, the equations diverge. Work in this Laboratory is now directed toward finding the solution to the flame equations even where the quasi-equilibrium approximation is poor and ϵ is large.

The first problem then is to make a rough estimate of ϵ_m. In a recent paper,[4] an approximate equation was given which very simply describes ϵ_m, the value of ϵ at the point of maximum radical concentration. We have

$$\epsilon_m = -\frac{(D_{ab} + D_{bc})t_B}{2D_{ac}t_A} \quad (6)$$

where D_{ab}, D_{ac} and D_{bc} are the binary diffusion coefficients, t_B and t_A are the respective radical and reactant relaxation times defined by[4]

$$t_B = \frac{(B)^*\epsilon}{-K_B} = \frac{1}{k_2 - k_3(A)}$$

$$t_A = \frac{(A)}{-K_A} = \frac{1}{k_1 + k_3(B)^*} \quad (7)$$

where K_A is the rate of production of reactant molecules assuming the steady-state reaction rate. All quantities on the right of equations 6 and 7 are evaluated at T_m, the temperature of maximum radical concentration, $(B)^*_{max}$. In estimating (A) at T_m we suppose that (A) varies linearly with the temperature. This assumption is not very good but it does not lead to a large error in t_B. Thus

$$\epsilon_m = -\left(\frac{D_{ab} + D_{bc}}{2D_{ac}}\right)\left(\frac{k_1}{k_2}\right)\left(\frac{1 + S_m}{1 - S_m}\right)^2 \quad (8)$$

There are a considerable number of ways of considering the deviations of (B) from its pseudo-stationary values, $(B)^*$, and each approach leads to a slightly different relation for ϵ_m. Thus eq. 6 is not strictly unique but it can be expected to give values of ϵ_m which are close to the correct value. This accuracy has been demonstrated by comparing the values of ϵ_m as calculated by eq. 6 with the values obtained by accurate point-to-point numerical integrations of the flame equations first for the ABC flame, then for the SOB flame, and presently for the FOB flame. The excellent results obtained for the FOB flame are given in Table VI.

From preliminary estimates of ϵ_m, we were able to select a set of interesting numerical examples which come fairly close to the explosion limits.

(3) By this, we mean that ϵ is small in the reaction zone. Whenever diffusion is considered, the cold boundary value of ϵ is many orders of magnitude greater than unity. The flame equations are not sensitive to the value of ϵ in this region as compared to its value in the hotter region.

(4) J. C. Giddings, University of Wisconsin Naval Research Laboratory Report, Squid-6, June, 1956.

(5) G. Klein, University of Wisconsin Naval Research Laboratory Report, Squid-4, August 1955; *Proc. Roy. Soc. (London)*, in press (1957).

(6) T. F. Schatzki, University of Wisconsin Naval Research Laboratory Report CM-853, September, 1955.

(7) J. O. Hirschfelder and E. S. Campbell, unpublished results.

Table I
Flame Calculations for FOB Flame, Case I
The flame velocity, $v_f = 110.81$ cm./sec.

T	g	x_A	$g_B = 2G_B$	x_B	x_B*		S
3000	0	0	0	0	0	0	0
2900	0.02798	0.01834	0.04767	0.01125	0.00953	0.18128	0.06580
2800	.05129	.04085	.06494	.01876	.01794	.04587	.13775
2700	.07114	.06694	.06399	.02343	.02462	− .04841	.21117
2600	.08798	.09618	.05185	.02573	.02920	− .11894	.28243
2500	.10209	.12822	.03419	.02611	.03146	− .16998	.34849
2400	.11354	.16267	.01468	.02490	.03134	− .20546	.40658
2300	.12246	.19922	− .00245	.02268	.02900	− .21779	.45452
2200	.12894	.23744	− .01595	.01974	.02486	− .20595	.49047
2100	.13304	.27693	− .02448	.01650	.01963	− .15920	.51307
2000	.13487	.31730	− .02841	.01321	.01418	− .06821	.52150
1900	.13452	.35820	− .02822	.01013	.00932	.08744	.51571
1800	.13218	.39935	− .02520	.00741	.00554	.33679	.49636
1700	.12804	.44052	− .02048	.00515	.00298	.72886	.46452
1600	.12234	.48157	− .01530	.00339	.00144	1.3501	.42205
1500	.11535	.52241	− .01048	.00209	.00062	2.3658	.37130
1400	.10734	.56303	− .00657	.00120	.00024	4.1052	.31491
1300	.09858	.60347	− .00375	.00064	.00008	7.3323	.25605
1200	.08930	.64379	− .00193	.00031	.00002	13.927	.19786
1100	.07968	.68410	− .00089	.00014	0	29.486	.14363
1000	.06987	.72450	− .00036	.00005	0	66.136	.09629
900	.05995	.76517	− .00013	.00002	0	238.91	.05815
800	.04998	.80637	− .00004	.00001	0	1133.0	.03048
700	.04000	.84875	− .00001	0	0	9680.8	.01306
600	.03	.89408	0	0	0	100000	.00416
500	.02	.94938	0	0	0	20142000	.00082
400	.01	1.0665	0	0	0	26534000000	.00007
300	0	1	0	0	0	∞	0

Table II
Flame Calculations for FOB Flame, Case II
The flame velocity, $v_f = 112.73$ cm./sec.

T	g	x_A	$g_B = 2G_B$	x_B	x_B*		S
3000	0	0	0	0	0	0	0
2900	0.02872	0.02081	0.03908	0.01256	0.01091	0.15096	0.07465
2800	.05375	.04488	.05641	.02116	.02003	.05657	.15134
2700	.07547	.07204	.05883	.02649	.02705	− .02066	.22725
2600	.09405	.10196	.05147	.02904	.03171	− .08418	.29941
2500	.10958	.13440	.03881	.02933	.03385	− .13370	.36528
2400	.12205	.16901	.02387	.02771	.03345	− .17173	.42242
2300	.13153	.20555	.01020	.02489	.03074	− .19014	.46896
2200	.13811	.24365	− .00097	.02124	.02617	− .18827	.50330
2100	.14188	.28293	− .00845	.01728	.02052	− .15797	.52419
2000	.14299	.32301	− .01241	.01334	.01472	− .09376	.53089
1900	.14165	.36357	− .01322	.00975	.00961	.04466	.52344
1800	.13812	.40431	− .01189	.00670	.00568	.17943	.50253
1700	.13273	.44502	− .00936	.00430	.00304	.41635	.46927
1600	.12582	.48558	− .00657	.00256	.00146	.75022	.42556
1500	.11777	.52592	− .00410	.00140	.00063	1.2217	.37380
1400	.10890	.56607	− .00227	.00069	.00024	1.9042	.31661
1300	.09951	.60608	− .00111	.00031	.00008	2.9586	.25715
1200	.08980	.64603	− .00047	.00012	.00002	4.7325	.19855
1100	.07993	.68602	− .00017	.00004	0	8.1562	.14404
1000	.06998	.72614	− .00005	.00001	0	14.301	.09651
900	.05999	.76655	− .00001	0	0	39.435	.05826
800	.05	.80752	0	0	0	137.62	.03052
700	.04	.84967	0	0	0	844.46	.01308
600	.03	.89476	0	0	0	12758	.00416
500	.02	.94974	0	0	0	869480	.00083
400	.01	1.0667	0	0	0	798480000	.00007
300	0	1	0	0	0	∞	0

TABLE III

FLAME CALCULATIONS FOR FOB FLAME, CASE III

The flame velocity, v_f = 195.09 cm./sec.

	g	x_A	$g_B = 2G_B$	x_B	x_B*	ϵ	S
3000	0	0	0	0	0	0	0
2900	0.01592	0.02640	0.00210	0.00061	0.00060	0.01373	0.15153
2800	.03287	.05385	.00387	.00117	.00115	.01505	.29054
2700	.05064	.08294	.00532	.00168	.00166	.01456	.41863
2600	.06881	.11339	.00621	.00213	.00211	.00752	.53277
2500	.08674	.14520	.00612	.00248	.00252	− .01473	.63142
2400	.10350	.17821	.00483	.00268	.00284	− .05419	.71267
2300	.11824	.21267	.00237	.00269	.00302	− .10950	.77633
2200	.13009	.24849	− .00068	.00249	.00297	− .16098	.82127
2100	.13839	.28552	− .00340	.00212	.00257	− .17468	.84638
2000	.14284	.32358	− .00505	.00165	.00186	− .11337	.85092
1900	.14350	.36242	− .00533	.00116	.00111	.04784	.83486
1800	.14077	.40183	− .00451	.00073	.00056	.30913	.79911
1700	.13530	.44158	− .00316	.00041	.00025	.63673	.74503
1600	.12785	.48153	− .00186	.00020	.00010	.97839	.67522
1500	.11913	.52158	− .00093	.00009	.00004	1.2802	.59314
1400	.10969	.56170	− .00039	.00003	.00001	1.5236	.50266
1300	.09991	.60188	− .00014	.00001	0	1.7279	.40859
1200	.08999	.64214	− .00004	0	0	1.9523	.31577
1100	.08001	.68250	− .00001	0	0	2.3077	.22928
1000	.07001	.72305	0	0	0	2.6199	.15375
900	.06001	.76390	0	0	0	4.7990	.09289
800	.05001	.80532	0	0	0	10.283	.04870
700	.04001	.84791	0	0	0	36.424	.02335
600	.03001	.89345	0	0	0	301.56	.00664
500	.02001	.94887	0	0	0	10912	.00132
400	.01001	1.0662	0	0	0	5306200	.00012
300	0	1	0	0	0	∞	0

TABLE IV

FLAME CALCULATIONS FOR FOB FLAME, CASE IV

The flame velocity, v_f = 235.09 cm./sec.

T	g	x_A	$g_B = 2G_B$	x_B	x_B*	ϵ	S
3000	0	0	0	0	0	0	0
2900	0.01249	0.02543	0.00188	0.00060	0.00059	0.01506	0.16419
2800	.02614	.05184	.00363	.00117	.00115	.01929	.31462
2700	.04098	.07981	.00538	.00174	.00169	.02579	.45321
2600	.05692	.10918	.00707	.00232	.00225	.02942	.57711
2500	.07359	.13996	.00811	.00287	.00284	.01004	.68471
2400	.09020	.17200	.00782	.00331	.00348	− .04782	.77381
2300	.10573	.20568	.00560	.00354	.00421	− .15949	.84467
2200	.11904	.24096	.00185	.00346	.00494	− .29885	.89593
2100	.12919	.27772	− .00222	.00311	.00519	− .40109	.92617
2000	.13563	.31576	− .00534	.00255	.00410	− .37801	.93415
1900	.13823	.35480	− .00676	.00190	.00222	− .14384	.91947
1800	.13722	.39455	− .00647	.00128	.00094	.35740	.88271
1700	.13313	.43476	− .00503	.00076	.00036	1.1215	.82521
1600	.12665	.47521	− .00325	.00040	.00013	2.0787	.74966
1500	.11854	.51578	− .00177	.00019	.00005	3.1112	.65987
1400	.10943	.55641	− .00081	.00007	.00001	4.1327	.56017
1300	.09981	.59708	− .00031	.00003	0	5.1436	.45600
1200	.08994	.63782	− .00010	.00001	0	6.2927	.35285
1100	.07999	.67867	− .00003	0	0	8.9834	.25649
1000	.07	.71969	− .00001	0	0	10.982	.17217
900	.06	.76102	0	0	0	19.197	.10410
800	.05	.80292	0	0	0	45.393	.05462
700	.04	.84599	0	0	0	183.25	.02344
600	.03	.89202	0	0	0	1785	.00746
500	.02	.94792	0	0	0	77244	.00148
400	.01	1.0659	0	0	0	44989000	.00013
300	0	1	0	0	0	∞	0

Table V

Flame Calculations for FOB Flame, Case V

The flame velocity, v_f = 238.67 cm./sec.

T	g	x_A	$g_B = 2G_B$	x_B	x_B*		S
3000	0	0	0	0	0	0	0
2900	0.01223	0.02547	0.00150	0.00060	0.00059	0.01195	0.16445
2800	.02559	.05192	.00286	.00117	.00115	.01472	.31514
2700	.04010	.07994	.00417	.00173	.00170	.01942	.45396
2600	.05574	.10937	.00549	.00232	.00226	.02572	.57811
2500	.07238	.14021	.00662	.00292	.00285	.02231	.68593
2400	.08953	.17227	.00711	.00347	.00350	− .00828	.77503
2300	.10622	.20596	.00621	.00384	.00424	− .09449	.84582
2200	.12100	.24129	.00368	.00358	.00501	− .23068	.89716
2100	.13244	.27816	.00043	.00346	.00531	− .34876	.92764
2000	.13958	.31635	− .00225	.00275	.00422	− .34712	.93589
1900	.14214	.35554	− .00351	.00194	.00228	− .15061	.92139
1800	.14048	.39541	− .00336	.00119	.00096	.23917	.88464
1700	.13545	.43566	− .00241	.00063	.00036	.72791	.82692
1600	.12807	.47609	− .00137	.00029	.00013	1.1774	.75104
1500	.11928	.51660	− .00063	.00011	.00005	1.4800	.66091
1400	.10976	.55715	− .00024	.00004	.00001	1.6212	.56091
1300	.09993	.59775	− .00008	.00001	0	1.6550	.45651
1200	.08998	.63842	− .00002	0	0	1.6689	.35318
1100	.08	.67920	0	0	0	1.7630	.25669
1000	.07	.72016	0	0	0	1.7687	.17228
900	.06	.76142	0	0	0	2.9877	.10416
800	.05	.80325	0	0	0	5.7940	.05464
700	.04	.84626	0	0	0	18.321	.02345
600	.03	.89221	0	0	0	132.11	.00746
500	.02	.94805	0	0	0	4080.6	.00148
400	.01	1.0659	0	0	0	1685900	.00013
300	0	1	0	0	0	∞	0

Because of the difficulty of carrying out the integrations for large values of ϵ, it was not possible to approach the explosion limits much closer.

In all of the numerical examples we took the pressure to be one atmosphere; the ambient temperature T_0 = 300°K.; the flame temperature T_∞ = 3000°K.; the molecular weight of A to be m_A = 20; the specific heat at constant pressure per mole (assuming that the specific heat per mole is the same for A as for B as for C species) C_p = 3.7037R where R is the gas constant, R = 1.98718 cal./mole deg.; the enthalpy released by the chemical reactions per mole of A is $m_A(H_A − H_C)$ = 10,000R; the enthalpy per mole of B is given by $m_B(H_B − H_C)$ = 10,000R; the coefficient of thermal conductivity is taken to be λ = 0.001$(T/T_\infty)^{1/2}$ cal./cm. sec. deg.; and the chemical rate constants are

$k_1 = 5 \times 10^8 (T/T_\infty)^{1/2} \exp(−40,000/RT)$, sec.$^{-1}$
$k_2 = 5 \times 10^8 (T/T_\infty)^{1/2} A_2$, sec.$^{-1}$
$k_3 = 5 \times 10^8 (T/T_\infty)^{1/2} \exp(−10,000/RT) A_3$,
$\qquad\qquad\qquad\qquad$ cm.^{3}/mole sec.

Here A_2 and A_3 are constants which are assigned various numerical values. The diffusion coefficients appear through the ratios of the Prandtl to the Schmidt numbers, $\delta_{ij} = D_{ij} n C_p/\lambda$ where n is the number of moles per cm.^{3}. The five examples for which calculations were made are[8]

Case I
$\delta_{AC} = \delta_{AB} = \delta_{BC} = 1$, $A_2 = 0.004$, $A_3 = 20,000$

Case II
$\delta_{AC} = 1$, $\delta_{AB} = \delta_{BC} = 1/2$, $A_2 = 0.004$, $A_3 = 20,000$

Case III
$\delta_{AB} = \delta_{AC} = \delta_{BC} = 1$, $A_2 = 0.100$, $A_3 = 800,000$

Case IV
$\delta_{AC} = \delta_{AB} = \delta_{BC} = 1$, $A_2 = 0.100$, $A_3 = 900,000$

Case V
$\delta_{AC} = 1$, $\delta_{AB} = \delta_{BC} = 1/2$, $A_2 = 0.100$, $A_3 = 900,000$

If we assume that these two cases have an x_A profile close to that for case I, we can calculate the values of ϵ_m from equation 8. For the first of these, we have $\epsilon_m \sim 0.4$, and for the second, $\epsilon_m \sim 0.5$. This again indicates the caution that must be used in applying conventional methods of calculation to those problems for which the steady-state approximation is poor.

We used Klein's method[9] of successive approximations of an integral equation to obtain solutions to the flame equations. The equations and procedure are so similar to those explained in great detail in connection with the SOB flame[2] that it is not necessary to repeat them here. As in the SOB flame, it is convenient to introduce a reduced temperature, τ = $10^{-4}T$, and a reduced distance ξ such that d$\xi = (MC_p/m_A \lambda)$ dz. Then the quantity g = dτ/dξ plays an important role in the flame equations. The mole fractions of A and of B are, respectively, x_A and x_B and the pseudo-stationary

(8) The following cases were tried but the solutions failed to converge
$\qquad \delta_{AC} = \delta_{AB} = \delta_{BC} = 1$, $A_2 = 0.004$, $A_3 = 30,000$
$\qquad \delta_{AC} = 1$, $\delta_{AB} = \delta_{BC} = 2$, $A_2 = 0.004$, $A_3 = 20,000$

(9) G. Klein, University of Wisconsin Naval Research Laboratory Report, Squid-1, February, 1955; *Proc. Roy. Soc. (London)*, in press (1957).

state mole fraction of B is x_B*. The fraction of the mass rate of flow which is contributed by B is G_B and $2G_B$ is Klein's variable, g_B. The calculations were made using the University of Wisconsin Numerical Analysis Laboratory IBM 650 Magnetic Drum Calculating Machine. The results are given in Tables I, II, III, IV and V.

The general properties of the profiles are the same here as for other flames calculated at this Laboratory. The introduction of an explosion point causes some changes. The free radical concentration becomes sharply peaked as we approach the explosion condition. Thus, the diffusion of radicals becomes important, and is responsible for the sizable values of ϵ_m. This also causes a sharp peak in the over-all reaction rate.

We have again investigated the effect of a changing radical diffusion coefficient upon flame velocity. The results given here help substantiate the conclusions of reference 1. Thus the diffusion of radicals, in contradiction to the so-called diffusion theories, has greater effect in depleting the supply in the reaction zone than it does in increasing the supply in the cold zone. This is shown by comparing case I with II, and case IV with V. In each comparison, the flame velocity is decreased by about 2% when the diffusion of the radical is doubled. In the only other calculation of this kind,[2] the flame velocity was found to decrease by only 0.3%. This is for the chain-branching SOB flame. The larger effect for the present calculations no doubt is due to the fact that depletion from the reaction zone is more important where ϵ_m is large. In either case, however, a decrease is found while the diffusion theories call for a substantial increase.

In Fig. 1, ϵ is presented as a function of temperature for the five cases. The general features of these curves can be understood qualitatively. Thus in that part of the graph where ϵ is negative (the reaction zone), the width of the valley is greatest for those cases that S is smallest (I, II), becomes smaller for intermediate S (III), and is very narrow for the cases where S approaches unity (IV, V). This results since, as the explosion limit is closely approached, there is a sudden jump in S, which causes an equally sudden jump in ϵ, equation 8. For those cases that the explosion limit is not closely approached, S is small and x_B* has no more than the usual slow change with temperature.

The comparison between ϵ_m as obtained by the approximate relaxation-time method and the ϵ_m resulting from our calculations, is given in Table VI. This agreement is quite satisfactory.

Table VI

Comparison of Estimated and Calculated ϵ_m for FOB Flame

Case	ϵ_m (from eq. 8)	ϵ_m (from numerical integrations)
I	0.25	0.17
II	.14	.11
III	.056	.11
IV	.12	.16
V	.075	.16
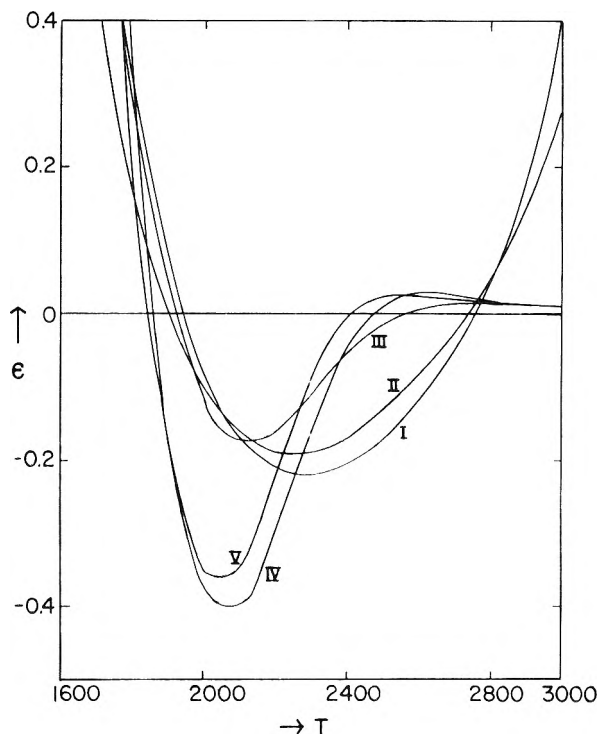
Fig. 1.—The variation of ϵ with temperature in the FOB flame for the five cases considered.

Looking at Tables I, II, III, IV and V, it will be noticed that in the hot portion of the flame ϵ is much higher for cases I and II, than for III, IV and V. This again can be explained on the basis of equation 8. Although equation 8 was derived for the point of maximum radical concentration, we expect from physical considerations that the equation will hold qualitatively wherever ϵ is small. Thus

$$\epsilon = -\left(\frac{D_{AB} + D_{BC}}{2D_{AC}}\right)\left(\frac{k_1}{k_2}\right)\left(\frac{1 + S}{1 - S}\right)^2 \qquad (9)$$

Using equation 9, we get the comparison between the estimated and calculated values of ϵ at the temperature $T = 2900°K$., as shown in Table VII.

Table VII

Comparison of Estimated and Calculated Values of ϵ for FOB Flame at $T = 2900°K$.

Case	ϵ (estimated from eq. 9)	ϵ (calcd. by numerical integration)
I	0.30	0.18
II	.15	.15
III	.016	.014
IV	.016	.015
V	.008	.012

Such good agreement might not be found at all times, but at least the results indicate that conditions near the hot boundary can be both predicted and explained by means of the relaxation-time model that led to equation 8.

PHASE RELATIONS IN THE SYSTEM BaCl₂–BaTiO₃

BY D. E. RASE AND RUSTUM ROY

Contribution No. 56-34, College of Mineral Industries, The Pennsylvania State University, University Park, Penn.

The phase relations in the system $BaCl_2$–$BaTiO_3$ were investigated using thermal curve, strip-furnace and quench techniques. The system is a simple eutectic-type with limited solid solubility near the barium titanate end-member. The eutectic appears at 938° and about 2.5 mole % $BaTiO_3$ where cubic barium chloride, cubic barium titanate solid solution and liquid coexist. The solid solution of cubic barium chloride in cubic barium titanate raises the cubic-hexagonal transition temperature of barium titanate from 1460 to about 1535°.

Introduction

During the past few years, these laboratories have conducted an extensive program concerning the stability relations of titanate systems with particular emphasis on the perovskite-type structures. One of the primary objectives has been to obtain fundamental phase equilibrium data subserving the preparation of large single crystals of barium titanate.

The first attempts to grow crystals of this unique oxide phase included halide–oxide melts in which barium chloride was used as the fluxing agent. The literature is not entirely clear as to the final results of this application. Some confusion exists concerning the polymorphic form of barium titanate which can be grown from various barium chloride–barium titanate melts. This confusion and the continued interest in the application of barium chloride as a fluxing agent prompted an investigation of the phase relations in the system $BaCl_2$–$BaTiO_3$.

Review of Literature.—The work of Wood[1] and Blattner, Kanzig and Merz[2] implies that the hexagonal modification of barium titanate may be obtained at low temperatures when $BaCl_2$, K_2CO_3 and Na_2CO_3 are employed as fluxes. Using a nitrogen atmosphere, Matthias[3] obtained hexagonal, monoclinic and cubic crystals from a $BaCl_2$–$BaCO_3$–TiO_2 melt. These crystals were highly discolored which Matthias attributed to platinum impurity originating from the crucibles containing the melt. The discoloration could be partially removed by heating at 200°.

Using a similar mixture without controlled atmosphere, Blattner, Matthias and Merz[4] were unable to obtain the hexagonal crystals of barium titanate. Instead they observed a pseudocubic phase which approximate chemical analysis indicated was $Ba_2Ti_3O_8$.

Limited phase relations in the system $BaCl_2$–$BaTiO_3$ have been reported by Belyaev and Sholokhovich[5] as part of their investigation of the ternary system $BaTiO_3$–$BaCl_2$–$BaCO_3$. The data are limited to the area containing more than 85 mole % $BaCl_2$. They indicated a eutectic at about 2 mole % $BaTiO_3$ and 900°. From their diagram it appears that the cubic form of barium titanate is the

stable phase in equilibrium with liquid and monoclinic barium chloride at the eutectic temperature.

The barium chloride end-member exists in two stable polymorphic forms above room temperature. The low temperature polymorph is monoclinic and transforms at 925° to a cubic (high temperature) form.[6] It has been shown by Kelley[7] to melt congruently at 960°.

The Curie temperature (*ca.* 120°) of barium titanate is associated with a tetragonal-cubic phase change which has been extensively studied and reported throughout the literature. The cubic phase has been shown to be stable to about 1460° by Rase and Roy[8] and DeVries and Roy.[9] Above 1460° the stable modification is hexagonal and it melts congruently at 1618°.

Experimental

Data were obtained from mixtures prepared from dried barium chloride and barium titanate and/or barium carbonate and rutile. Weighed amounts of constituents were mixed under absolute alcohol, dried and heat treated in platinum crucibles at temperatures below that of the solidus. All compositions were intermittently heat treated and ground for at least 48 hours or until they appeared homogeneous by microscopic observations. Weight loss determinations indicated loss of $BaCl_2$ by volatilization was not appreciable at sintering temperatures.

The "non-quenching" nature of all compositions in the system restricted the use of the quench technique[10] especially in defining liquidus temperatures. However, using binocular and petrographic methods to detect melting and quench growth, the method yielded useful data though somewhat less accurate than normally obtained for systems capable of being "quenched" to glasses. These data have been particularly useful in confirming values obtained by thermal analysis.

The majority of data reported here was obtained using differential thermal analysis and strip-furnace[11] methods. The limitations imposed by both these methods (interpretation of DTA patterns and determination of strip-furnace temperatures) and the volatility of the barium chloride component necessarily reduce the accuracy. The latter was especially critical for compositions containing only small amounts of barium chloride since slight losses in these resulted in an appreciable percentage loss.

Since the differential thermal technique was used almost exclusively to define the solidus (eutectic) temperature, loss of $BaCl_2$ would be expected to have no effect on the accuracy of these data. The system is essentially a simple eutectic-type and the solidus temperature is the same over a considerable range of composition. Loss of barium chloride there-

(1) E. A. Wood, *J. Chem. Phys.*, **19**, 976 (1951).

(2) H. Blattner, W. Kanzig and W. Merz, *Helv. Phys. Acta*, **22**, 35 (1949).

(3) B. T. Matthias, *Phys. Rev.*, **73**, 808 (1948).

(4) H. Blattner, B. T. Matthias and W. J. Merz, *Helv. Phys. Acta*, **20**, 225 (1947).

(5) I. N. Belyaev and M. L. Sholokhovich, *Dok. Akad. Nauk, USSR*, **77**, 51 (1951) (in Russian).

(6) "International Critical Tables of Numerical Data, Physics, Chemistry and Technology," 7 Vols. plus index, McGraw-Hill Book Co., New York, N. Y., 1926-33, Vol. 1, p. 147; vol. 4, p. 7.

(7) K. K. Kelley, U. S. Bur. Mines Bull. No. 393 (1936).

(8) (a) D. E. Rase and R. Roy, *J. Am. Ceram. Soc.*, **38**, 102 (1955); **38**, 389 (1955).

(9) R. C. DeVries and R. Roy, *ibid.*, **38**, 142 (1955).

(10) E. S. Shepherd, G. A. Rankin and F. E. Wright, *Am. J. Sci.*, **28**, 293 (1909).

(11) (a) H. Roberts and G. W. Morey, *Rev. Sci. Inst.*, **1**, 576 (1930); (b) M. L. Keith and R. Roy, *Am. Sci.*, **39**, 1 (1954).

TABLE I

SUMMARY OF DATA FOR THE SYSTEM BaCl$_2$–BaTiO$_3$

A. Thermal Analyses

| Composition, mole % | | M.p., °C. | Temp. (°C.) of heat effects | | | Others, some unassigned |
BaCl$_2$	BaTiO$_3$		BaCl$_2$ transition	Eutectic	Liquidus	
100.0	0.0	964	925			
97.0	3.0		928	?	946	838—unexplained
95.0	5.0		926	934	957	
92.5	7.5		923	942		836—unexplained
90.0	10.0		924	940	1100^a	835—unexplained
75.0	25.0		924	?	1325^a	
60.0	40.0		926	937	1604^a	850—unexplained
50.0	50.0		929	?	1610^a	
40.0	60.0		930	950 (?)	1617^a	875—unexplained 909—unexplained
25.0	75.0		1050	975^b	1619^a	868—unexplained 918—exsolution dome
20.0	80.0			1000^b		920—exsolution dome
15.0	85.0			1020^b	1615^a	910—exsolution dome
10.0	90.0			1570^b	1615^a	870—unexplained
0.0	100.0		1618			

B. Quenching Data

| Composition, mole % | | Temp., °C. | Time (hr.) | Phases present at room temp.^{c} | Remarks |
BaCl$_2$	BaTiO$_3$				
90.0	10.0	920	$^1/_4$	BaCl$_2$ + Tet. BT	No melting
		935	$^1/_4$	BaCl$_2$ + Tet. BT	No melting
		945	$^1/_4$	BaCl$_2$ + Tet. BT	Melting
50.0	50.0	920	$^1/_4$	BaCl$_2$ + Tet. BT	No melting
		935	$^1/_4$	BaCl$_2$ + Tet. BT	No melting
		945	$^1/_4$	BaCl$_2$ + Tet. BT	Melting
15.0	85.0	1528	$^1/_2$	Tet. BT	Melting
		1539	$^1/_2$	Hex. BT	
10.0	90.0	1519	$^1/_2$	Tet. BT	Melting
		1528	$^1/_2$	Tet. BT	
		1539	$^1/_2$	Hex. BT	
5.0	95.0	1507	$^1/_2$	Tet. BT	
		1519	$^1/_2$	Tet. + Hex. BT	
		1528	$^1/_2$	Hex. BT	
		1539	$^1/_2$	Hex. BT	Melting

^{a} Liquidus temperatures determined on strip furnace. ^{b} Temperature of first appearance of liquid (strip furnace). ^{c} Abbreviations: Tet. BT = tetragonal BaTiO$_3$ (cubic above 120°); Hex. BT = hexagonal BaTiO$_3$.

fore affects the *magnitude* of the heat effect and *not* the temperature at which it occurs. In the case of liquidus data, however, any volatile loss must necessarily affect the accuracy (*vide infra*). Liquid and solid compositions within the system showed no reaction with platinum and/or platinum-rhodium alloy. These materials, therefore, were used exclusively to contain the samples.

Wherever necessary, phases were identified by petrographic and X-ray techniques.

Results and Discussion

A summary of the thermal analysis and quench data is presented in Table I.

The melting temperature of barium chloride was determined as 964 ± 3° using both differential thermal and heating curve techniques. A large thermal effect corresponding to the monoclinic-cubic transition in barium chloride was observed at 925 ± 3°. Both these determinations are in agreement with those reported in the literature. No other heat effects were evident for C.P. grade barium chloride.

The phase diagram for the system BaCl$_2$–BaTiO$_3$, drawn from the data summarized in Table I, is illustrated in Fig. 1. It is essentially a simple eutectic-type system with some proposed limited solid solution at the barium titanate end. The eutectic appears at about 2.5 mole % BaTiO$_3$ and 938 ± 5°. From the eutectic composition and temperature, the liquidus rises sharply toward the BaTiO$_3$ end-member. For compositions containing more than 40% BaTiO$_3$, the data indicate that the liquidus is essentially flat, rising only slightly to the melting point of barium titanate.

Since these liquidus data were obtained using the strip-furnace and only very small amounts of sample, it is probable that the liquidus temperatures in this area are erroneously high. Therefore, even though the data obtained were reproducible, the results are represented by a "dashed-line" only. The boiling point of barium chloride is reported as 1560° and, although the addition of barium titanate undoubtedly raises it, the vapor pressure of the chloride at these temperatures is most likely quite appreciable. It follows that any volatilization of the chloride in the small sample utilized in the strip furnace determinations is an important factor. The loss effectively results in a composition much richer in BaTiO$_3$ and therefore the liquidus temperature approaches that of pure barium titanate
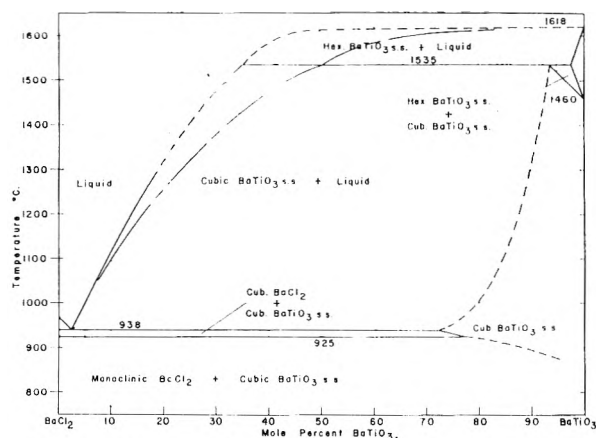
Fig. 1.—Phase equilibrium diagram for the system BaCl₂–BaTiO₃. Two alternative liquidus curves are presented, the upper one representing the curve drawn on the basis of actual observations, while the lower one is a curve which is regarded as more probable in view of the experimental difficulties with volatilization (see text).

(1618°). In the absence of volatilization, one would expect a liquidus curve more like that represented by the "dash-dot" line in Fig. 1. No effort has been made to determine the change in composition as a function of volatilization and the latter curve should be considered only as a possible liquidus in the absence of volatilization.

On heating, compositions containing less than 70 mole % BaTiO₃ all gave evidence of at least two distinct endothermic heat effects, one corresponding to the transition temperature of barium chloride and the other about 13° higher. Generally, their magnitude decreased as the composition became richer in barium titanate. It was not always possible to determine the temperature associated with the higher of these two thermal effects because it was almost always partially masked by the other. Binocular observation of quenches from temperatures just above that of the second thermal effect all indicated that at least partial melting had occurred, thus establishing it as the solidus reaction.

The data obtained for the portion of the system containing more than 75% BaTiO₃ are not as unambiguous. The temperature interval between the barium chloride transition and the eutectic gradually increased as the composition approached that of the titanate. The divergence of these temperatures can best be explained on the basis of a limited solid solution in the cubic form of barium titanate. The broken line shown in the diagram is a representation of such a solid solution *proposed* to account for the data. Such an explanation is consistent with the data regarding the effect of barium chloride on the cubic-hexagonal transition temperature of barium titanate (*vide infra*).

Besides the unexplained thermal effects mentioned later, only one other could be detected for mixtures containing more than 85% BaTiO₃. For these compositions, the temperature associated with the endothermic reaction was appreciably lower than that of the eutectic 938°, and even below the barium chloride transition. The lowering became progressively more evident with an increase in BaTiO₃ concentration. The heat effects, therefore, have been attributed to phase changes in-

volving the BaCl₂ in BaTiO₃ solid solution. Although the magnitude of the thermal effects in this region was small and made interpretation of the DTA patterns more difficult, the effect of composition on this reaction temperature was conclusive.

The Cubic-hexagonal Transition of BaTiO₃.—Small additions of barium chloride appear to raise the cubic-hexagonal transition temperature of barium titanate in a manner similar to that observed for TiO₂ and SiO₂. Quench data for compositions containing 85, 90 and 95% BaTiO₃ are summarized in Table I and indicate the transition temperature is raised to about 1535°. It was found that mixtures containing less than 5 mole % BaCl₂ gave unreliable results. In the latter case the same composition repeatedly quenched from the same temperature would indicate partial or complete conversion to the hexagonal form part of the time and no conversion at other times. Since data from these mixtures were not reproducible, they have not been included in the table. The inconsistent results have been attributed to a differential volatilization of BaCl₂—thus in some runs, where the loss was low, the mixture remained approximately "on composition" and would not, for example, indicate any conversion, while in a similar run where the loss was greater (composition more nearly that of BaTiO₃) complete or partial conversion might be observed. The same reasons may be used to argue that the data reported for the 85, 90 and 95% mixtures are similarly in error. However, these data were at least consistent and reproducible especially in indicating the lowest temperature at which the cubic barium titanate transformed to the hexagonal form.

For the reasons outlined above, the limits of solid solution indicated in Fig. 1 must only be regarded as approximations. Even an indication of solid solution in the system is a most unexpected result. No defect solid solutions of AX₂ compounds in an A₂X₃ structure are known. However, even though the liquidus data may be "explained" by assumptions regarding volatilization, no similar argument can be used about the solidus data.

From the invariant point where cubic solid solution, hexagonal solid solution and liquid are shown in equilibrium the solubility curve of cubic solid solution descends steeply. The extent of solid solution increases gradually to conform with the solidus observations in the 80, 85 and 90% mixtures. However, below the solidus, the same observations require that the extent of solid solution decrease rapidly with temperature so that below the transition temperature of BaCl₂ the limit of solubility is very small. This may be correlated with the fact that the monoclinic form of barium chloride is the stable polymorph at these temperatures.

The data indicating solid solution in this system are not as conclusive as in the case of systems BaO–TiO₂ and BaTiO₃–SiO₂,[8] but the proposed solid solution appears to be the best and simplest explanation of the data. The limits of solubility could be considerably less than indicated by the data since no correction has been made for volatility.

Unexplained Thermal Effects.—It was noted that DTA patterns obtained for some mixtures

during a cooling cycle often showed, in addition to the exothermic reactions associated with the transition and eutectic, one or more additional exothermic heat effects not apparent during the heating cycle. The additional reactions always occurred at temperatures somewhat lower than that of the barium chloride transition. They did not occur at the same temperature for all compositions nor were they reproducible for any one composition. Generally, however, they did occur at higher temperatures for compositions richer in barium titanate.

Investigation showed that these exothermic reactions occurred only when the thermal history of the sample included treatment above initial melting temperatures. However, they never were observed when the sample contained only barium chloride. Exploratory quench work designed to "freeze in" the phase present above and below the reaction temperature was entirely unsuccessful. X-Ray and optical examination indicated only the presence of the barium chloride and barium titanate phases.

The reaction or phase changes responsible for the additional thermal effects have not been defined and no attempt has been made to include them in subsolidus phase relationships. A combination of quenching and X-ray techniques has not been successful in solving the problem; however, two possible explanations may be offered without attempting to expand upon them: (1) the formation of a compound of barium not in the system BaCl$_2$–BaTiO$_3$, for example, an oxy-chloride or even a peroxide of barium, and (2) the delayed exsolution of the solid solution stable at higher temperatures.

The second of these would appear to be more likely, especially since the heat effects are exothermic and are observed only in samples after they have been heated above the temperature at which liquid first appears as a stable phase. One might expect that it would be possible to supercool that portion of material consisting of the "primary phase" while the solid solution crystallized from the eutectic liquid would exsolve quite readily due to its small crystalline size and intimate contact. Furthermore, a corresponding endothermic reaction is not observed even when a sample exhibiting the exothermic effect on cooling is reheated up to the solidus temperature.

ENZYME MODELS. IV. KINETICS OF THE CATALYZED DECARBOXYLATION OF BENZOYLFORMIC ACID

By Abraham S. Endler[1] and Ernest I. Becker[2]

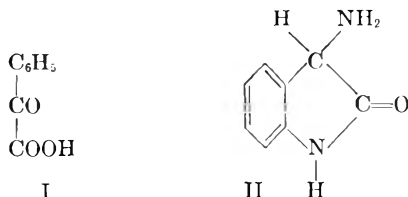*Contribution from the Chemical Laboratories of the Polytechnic Institute of Brooklyn, Brooklyn, N. Y.*

The rate of decarboxylation of benzoylformic acid in phenol solution, catalyzed by 3-aminoöxindole, α-phenylglycine and related compounds was studied. The range of temperature was 50 to 100°. α-Phenylglycine is ca. 1/15 as effective as 3-aminoöxindole and 3-methyl-3-aminoöxindole is ineffective. The energy and entropy of activation with 3-aminoöxindole are 18.5 ± 1.5 kcal./mole and −13 ± 4 cal./mole deg., resp. These data require a prototropic rearrangement in a Schiff base intermediate and make feasible an open-chain transition state as well as the cyclic one proposed earlier.

Introduction

The decarboxylation of benzoylformic acid (I) catalyzed by compounds such as 3-aminoöxindole (II) has been considered to be analogous to the decarboxylation of α-ketoacids as catalyzed by natural carboxylases.[3,4]
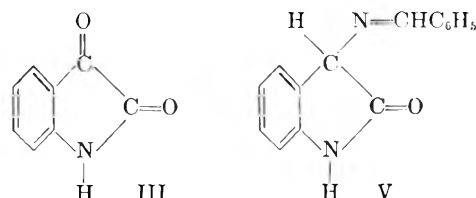
It has been shown that primary amines in general are catalysts for decarboxylation of I.[3] α-Amino-acids are generally more effective than simple amines, and lactams of α-aminoacids, such as II, are considerable more effective. Later work showed that II could be replaced as catalyst by the Schiff base formed by reaction of isatin (III) with benzylamine (IV).[4] It was proposed that this Schiff base had undergone a prototropic rearrangement, and actually possessed the structure V, which would also be obtained by reaction of II with benzaldehyde. This was substantiated in the previous paper in this series.[5]

Coupling these observations with the proposal of Langenbeck that the active intermediate in catalysis of the decarboxylation was the Schiff base of I with II, the following mechanism was suggested

II NH₂ + C₆H₅ C=O COOH —H₂O⟶ VI

↓ Rearrangement

V ←—CO₂— VII
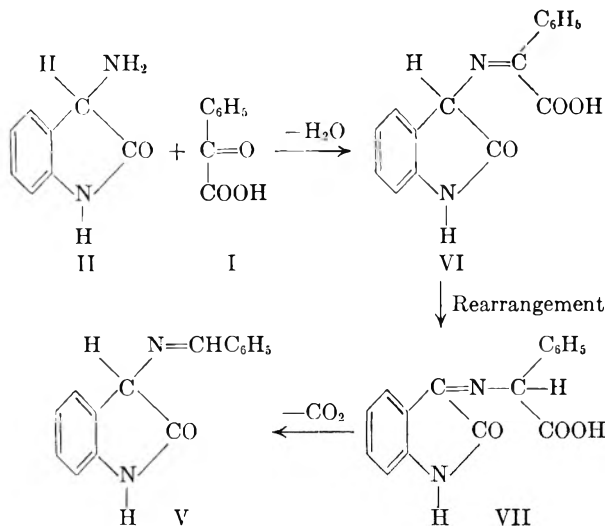
3-Benzylideneaminoöxindole (V), the product of this sequence of reactions, then could react with further benzoylformic acid substrate to liberate benzaldehyde and re-form the Schiff base VI.

The purpose of this work was to test the requirement of a protropic rearrangement of the Schiff base intermediate, and to determine the energy and entropy of activation of the rate-determining step of the decarboxylation, using different catalysts.

Compounds selected for kinetic study to provide information on these aims were: 3-methyl-3-aminoöxindole (VIII), α-phenylglycine (IX), methyl α-phenylglycinate, benzylamine and 1-methyl-3-aminoöxindole.

VIII
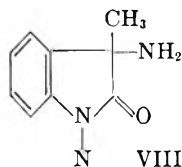
Experimental

Materials.—Phenol was A.R. grade, stored in a desiccator over phosphorus pentoxide. Benzoylformic acid, m.p. 65–66°, was prepared by acid hydrolysis of benzoyl cyanide.[6] Potassium benzoylformate was crystallized from methanol after neutralizing methanolic potassium hydroxide with a slight excess of benzoylformic acid. 3-Aminoöxindole hydrochloride was prepared by hydrogenation of β-isatoxime in aqueous-alcoholic hydrochloric acid, slightly modifying a published procedure.[7] α-Phenylglycine hydrochloride was prepared by alkaline hydrolysis of 5-phenylhydantoin[8,9] followed by conversion to the hydrochloride, which was recrystallized from alcohol. The carbon dioxide used was "bone dry" grade, reported to be 99.9% pure. (No effect was found in replicate experiments in which 99.0% gas was used.)

Procedure.—The reaction was conducted in phenol

(6) T. S. Oakwood and C. A. Weisgerber, in "Organic Syntheses," Coll. Vol. III, edited by A. H. Blatt, John Wiley and Sons, Inc., New York, N. Y., 1955, p. 114.

(7) F. J. DiCarlo and H. J. Lindwall, *J. Am. Chem. Soc.*, **67**, 199 (1945).

(8) H. T. Bucherer and W. Steiner, *J. prakt. Chem.*, [2] **140**, 291 (1934).

(9) H. T. Bucherer and V. A. Lieb, *ibid.*, [2] **141**, 5(1934).

solution. The usual reaction mixture contained approximately 5 g. of phenol, 0.5 g. of benzoylformic acid and 0.1 g. of potassium benzoylformate, each weighed into the reaction flask with a precision of 1 mg. The quantity of catalyst was of the order of 1 to 20 mg., and was weighed to 0.01 mg. precision.

All the components of the reaction mixture except the catalyst were placed in a 50-ml. flask, fitted with a rubber stopper. About 2 g. of carborundum chips was added to promote agitation when the flask was shaken. The catalyst, together with some phenol solvent, was placed in a wide-mouthed glass cup, fused to a glass rod which extended through the flask stopper *via* a gas-tight rubber sleeve. A gas inlet tube and an outlet tube also extended through the stopper.

The flask was immersed up to the neck in an oil-bath, and clamped to a shaker mechanism which provided a 5-mm. throw at 600 cycles per min. The bath temperature was thermostatically controlled to ±0.01°, and was measured by an NBS-calibrated thermometer using emergent stem correction. The flask outlet tube was connected to a water-jacketed gas cooler, consisting of 1.5 meters of stainless steel tubing, 1 mm. i.d., and thence to a jacketed gas buret. Mercury was used as the confining fluid, avoiding solubility corrections for carbon dioxide.

For each experiment, the flask and stopper were assembled with the catalyst cup held out of contact with the benzoylformic acid–phenol mixture. A stream of carbon dioxide, at a rate of 40–50 ml./min., was used to sweep the air out of the reaction flask for 20–30 min., by-passing the gas buret. Then, reducing the gas flow to half-rate, the flask was immersed in the oil-bath, and the flow continued for 5 min. as the reaction mixture melted. The gas flow was then cut off, and the three-way stopcock of the gas buret adjusted to connect the buret to the reaction flask. A period of up to 2 hr. was allowed for the flask to reach thermal equilibrium, and for the reaction mixture to become saturated with carbon dioxide. When the buret reading was steady for 20 min., the reaction was started by pushing the catalyst cup to the bottom of the flask and breaking it away from the glass rod, starting the shaking mechanism at once.

Pressure inside the system was maintained within a few millimeters of atmospheric by use of a leveling bulb. When taking a reading, the estimated error in bringing the gas to atmospheric pressure was estimated as 0.5 mm. Atmospheric pressure was measured periodically during the experiments, using a mercury barometer.

Gas buret readings could be taken every 30 sec. if desired. Timing was done by means of an accurate watch with a sweep-second hand held next to the buret as the reading was taken. The error of timing was ±1 sec. Errors in reading the buret were estimated to be ±0.05 ml., except when the rate of gas evolution was greater than 2 ml./min., when the error became about ±0.10 ml.

Errors due to lack of thermal equilibrium, and to possible un-catalyzed decomposition of benzoylformic acid substrate were checked in several runs where inactive materials were used as catalysts, and where no catalyst was used. The variation in the gas buret reading over a 30 min. period was ±0.2 ml., less than 1% of the volume of gas usually collected in a 30-minute period. There usually was a volume change of up to ±1.0 ml. in the first minute of reaction probably due to unsaturation or supersaturation of the solvent with carbon dioxide. Therefore in using the data the first minute was normally discounted. In the runs over 80° this effect was not noticeable.

In the experiments above 80°, it was suspected that volatilization of the benzoylformic acid would allow part of it to react with the catalyst in the cup before the cup was immersed in the reaction mixture. Such reaction would cause partial inactivation of catalyst. It was found that the addition of an excess of anhydrous, non-oxidizing strong acid (*p*-toluenesulfonic) to the catalyst-phenol mixture prevented such reaction completely, and when such a mixture was added to the customary benzoylformic acid–potassium benzoylformate mixture, the strong acid was neutralized and had no effect on the reaction rate. This procedure was followed in about half the runs above 80°, without noticeable difference in initial rates.

Results

Rate experiments were performed at five tem-

peratures, in the range 50 to 100°, as indicated in Table I. Carbon dioxide evolution, calculated as moles per mole of catalyst initially present, was plotted *vs.* time. Typical results are shown on Figs. 1 and 2.

TABLE I

RATE OF CATALYTIC DECARBOXYLATION OF BENZOYLFORMIC ACID

Catalyst	Temp., °C.	Rate constant, k_2 (min.$^{-1}$)	No. of expts.
3-Aminoöxindole hydrochloride	49.86	0.53 ± 0.03	16
	70.07	3.1 ± .2	16
	79.97	5.9 ± .4	10
	90.33	14.2 ± 1.0	6
	100.19	22.5 ± 2.8	6
1-Methyl-3-aminoöxindole	70.07	1.2 ± 0.2	1
3-Methyl-3-aminoöxindole	70.07	0.000	1
	79.97	0.000	2
	100.19	0.04[a]	2
α-Phenylglycine hydrochloride	79.97	0.33 ± 0.04	2
	90.33	0.80 ± .04	2
	100.19	1.43 ± .15	2
Methyl α-phenylglycinate hydrochloride	70.07	0.002	2
Benzylamine hydrochloride	70.07	0.000	1
	100.19	0.06[a]	2

[a] Based on maximum rate, reached after 40 min. reaction time.

Little or no induction period was found in the experiments with catalysts II and IX. Inspection of Fig. 1 indicates that at 70° maximum rate was reached in less than 5 min., while at 50° less than 10 min. was required. Figure 2 indicates no observable induction period at 90°.

The slopes of the gas evolution curves were determined by the chord method, and plotted *vs.* time. Extrapolation to zero time was used for the determination of the initial rate. It was found that a plot of the square root of the reciprocal of the rate usually gave close to a straight line result. This function usually was employed for the extrapolation.

The initial rate of reaction, expressed as moles of carbon dioxide per mole of catalyst per minute, was found to be invariant with concentration of benzoylformic acid in the range 0.3–0.8 molal, provided that the mole ratio of benzoylformic acid to 3-aminoöxindole catalyst was greater than *ca.* 30:1. With less active catalysts, like IX, a somewhat lower ratio could be employed without affecting the initial rate. Results from sixteen runs at 50° are plotted on Fig. 3, illustrating that the variation in rate found was random, with a standard error of about 6% and not correlated with the substrate concentration.

The effect of variation in the concentration of potassium benzoylformate in the standard reaction mixture was estimated in several runs, with results shown on Fig. 4, in which the initial rate is plotted *vs.* the mole ratio of potassium salt to catalyst. The rate rises from a non-zero value at zero concentration of potassium benzoylformate to a maximum at a ratio of about 10:1 remaining unaffected at higher ratios.
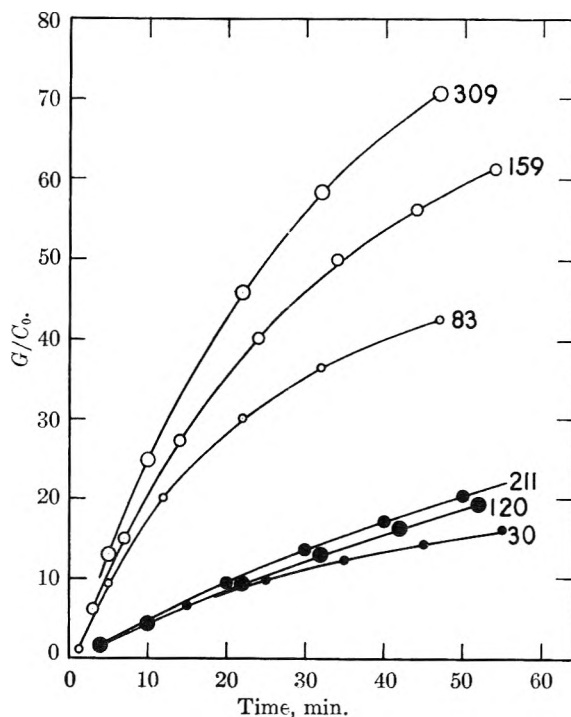

Fig. 1.—Typical experimental results at 49.86° (solid circles) and at 70.07° (open circles), showing carbon dioxide evolution, G/C_0, in moles/mole of catalyst, *vs.* time. The number on each curve gives the initial benzoylformic acid: catalyst mole ratio. 3-Aminoöxindole (II) hydrochloride catalysis.
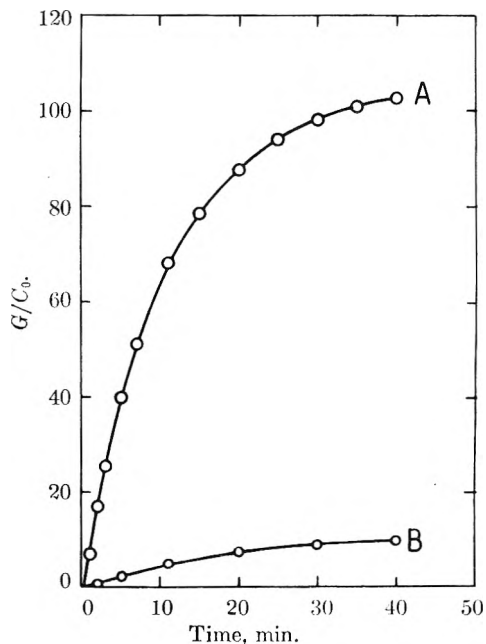

Fig. 2.—Typical experimental results. Carbon dioxide evolution, in moles/mole of catalyst, *vs.* time at 90.33°: curve A, 3-aminoöxindole (II) hydrochloride $S_0/C_0 = 256$; curve B, α-phenylglycine (IX) hydrochloride $S_0/C_0 = 30$.

Kinetic Treatment

The kinetic analysis proposed here is a modification of that proposed by Schachat, *et al.*[4] The basic outline of reaction steps is the same as that employed by Langenbeck.[3]
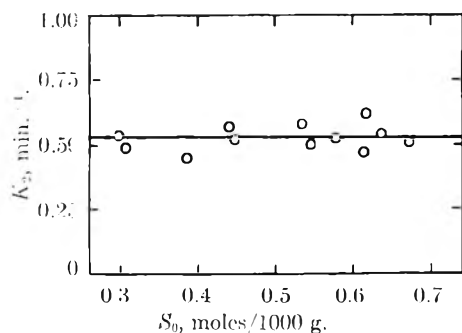
Fig. 3.—Calculated rate constant, k_2, at 49.86°, plotted vs. initial substrate molal concentration. 3-Aminoöxindole (II) hydrochloride catalysis.
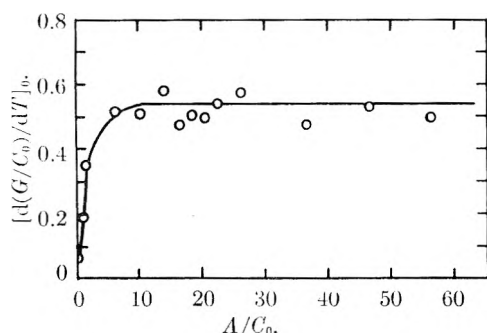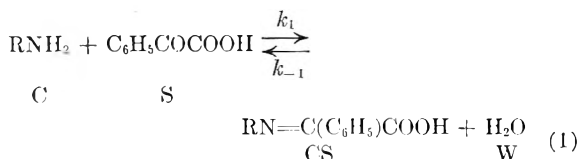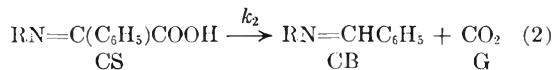

Fig. 4.—Initial reaction rate plotted vs. initial mole ratio of potassium benzoylformate to catalyst hydrochloride. 3-Aminoöxindole (II) hydrochloride catalysis at 49.86°.

Initiation reaction:

$$RNH_2 + C_6H_5COCOOH \underset{k_{-1}}{\overset{k_1}{\rightleftarrows}}$$
$$C \qquad S$$
$$RN{=}C(C_6H_5)COOH + H_2O \quad (1)$$
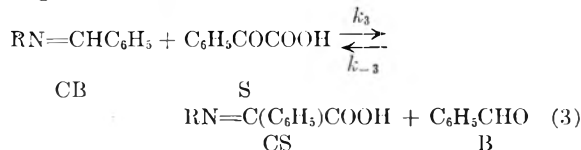$$CS \qquad\qquad W$$

Although reversible, examination of the data indicates that this reaction can be considered to be at least 95% complete in five minutes at 70°.

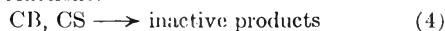Decarboxylation reaction:

$$RN{=}C(C_6H_5)COOH \overset{k_2}{\longrightarrow} RN{=}CHC_6H_5 + CO_2 \quad (2)$$
$$CS \qquad\qquad CB \qquad\quad G$$

Regeneration reaction:

$$RN{=}CHC_6H_5 + C_6H_5COCOOH \underset{k_{-3}}{\overset{k_3}{\rightleftarrows}}$$
$$CB \qquad\qquad S$$
$$RN{=}C(C_6H_5)COOH + C_6H_5CHO \quad (3)$$
$$CS \qquad\qquad\qquad B$$

Termination reactions:

$$CB, CS \longrightarrow \text{inactive products} \quad (4)$$

The nature of these reactions is not known. They are probably related to the reactions which produce violet-brown colored polymeric materials as side-products in the reaction of 3-aminoöxindole with benzaldehyde, and in the reaction of isatin with benzylamine.

Rate Equations.—If the concentration of catalyst active at time t is $[C_t]$, then

$$[C_t] = [CB] + [CS]$$

If the regeneration reaction equilibrium of eq. 3 is assumed to be rapid relative to eq. 2, we have

$$K_3 = \frac{k_3}{k_{-3}} = \frac{[CS][B]}{[CB][S]} \quad (5)$$

With the reaction conditions employed, and with 3-aminoöxindole catalysis, G was greater than 10 C_0 (C_0 = initial moles of catalyst) within five minutes. Then

$$[B] \doteq [G] + [B_0]$$
$$[S] \doteq [S_0] - [G]$$

Substituting and solving for $[CS]$ there is obtained

$$[CS] = \frac{k_3[C_t]}{\dfrac{[G] + [B_0]}{[S_0] - [G]} + K_3} \quad (6)$$

The rate of evolution of carbon dioxide then is

$$\frac{d[G]}{dt} = k_2[CS] = \frac{k_2 K_3[C_t]}{\dfrac{[G] + [B_0]}{[S_0] - [G]} + K_3} \quad (7)$$

To include the effect of inactivation of catalyst, the equation is divided by $[C_0]$, letting the fraction $[C_t]/[C_0] = F$

$$\frac{d[G]/[C_0]}{dt} = \frac{k_2 K_3 F}{\dfrac{[G] + [B_0]}{[S_0] - [G]} + K_3} \quad (8)$$

where $[G]/[C_0]$ is the moles of carbon dioxide evolved per mole of catalyst initially present.

Inverting to produce a linear function

$$\frac{F}{\dfrac{d[G]/[C_0]}{dt}} = \frac{1}{k_2} + \frac{[G] + [B_0]}{[S_0] - [G]}\bigg/ k_2 K_3$$

This equation is made more workable by calling

$$1\bigg/\left[d\frac{[G]}{[C_0]}\bigg/dt\right] = I; \text{ and } \frac{[G] + [B_0]}{[S_0] - [G]} = R$$
$$FI = 1/k_2 + R/k_2 K_3 \quad (9a)$$

If the function F, which depends on the inactivation reaction, were known, a plot of FI vs. R should give a straight line. Unfortunately no assumed first- or second-order termination step gave a function which provided such a straight line plot with the data obtained in this work.

It will be noticed that at zero time, $F = 1$, and $R = B_0/S_0$. When no benzaldehyde is initially present, $R_0 = 0$, and $I_0 = 1/k_2$. Thus, we infer that the initial rate in min.$^{-1}$ is equal to the first-order rate constant for the decarboxylation of the Schiff base intermediate.

The equations assume that reaction 2 is rate determining. We note that if reaction 3 were the slow step, the over-all reaction rate would depend on k_3, and would be only slightly affected by initial addition of benzaldehyde. This was found not to be the case.

This kinetic analysis indicates that the initial reaction rate should be first order in catalyst and zero order in substrate, provided that the substrate-catalyst mole ratio is high enough to validate the approximations used. This is similar to the usual kinetic analysis of enzyme reactions, based on the Michaelis-Menten equation.[10-12]

(10) L. Michaelis and M. L. Menten, *Biochem. Z.*, **49**, 333 (1913).

(11) G. E. Briggs and J. B. S. Haldane, *Biochem. J.*, **19**, 338 (1925).

(12) H. Lineweaver and D. Burk, *J. Am. Chem. Soc.*, **56**, 658 (1934).

Discussion

Effect of Added Benzaldehyde.—If benzaldehyde is initially present in the reaction mixture, eq. 9a becomes

$$I_0 = 1/k_2 + R_0/k_2K_3 \qquad (10)$$

The data from experiments performed with varying quantities of benzaldehyde added to the substrate solution are shown on Fig. 5. Despite some scatter of the data, the trend is consistent with eq. 10. From these results it is estimated that $K_3 = 0.25$ at $50°$ and 0.5 at $70°$. Thus in competition for catalyst between substrate (benzoylformic acid) and product (benzaldehyde), the product is favored in this case.

Effect of Water.—Assuming that water affects the over-all reaction by its influence on the initial formation of the Schiff base by reaction 1, the equilibrium constant governing this reaction may be written

$$K_w = \frac{[CS]\,[W]}{[C]\,[S]}$$

The fraction of catalyst initially converted to the Schiff base intermediate then is given by

$$\frac{[CS]}{[CS] + [C]} = \frac{K_w}{K_w + \dfrac{[W]}{[S_0]}} \qquad (11)$$

The effect of varying concentration of water on the initial decarboxylation rate will be given by an equation similar to (10)

$$I_0 = 1/k_2 + [[W]/[S_0]]/k_2K_w \qquad (12)$$

Data from experiments at $70°$ with added water are shown on Fig. 6. These indicate that $K_{w70°} = 0.5 \pm 0.1$. At a C_0/S_0 ratio of $1:50$, this would mean that 96% of the catalyst was converted to Schiff base.

The fact that the graph calculated from the initial rates of over-all reaction follows the linear equation 12 moderately well lends support to the assumption made in the kinetic analysis that the initiation step, reaction 1, is rapid relative to the decarboxylation step. This must be true since, if the *forward* step in reaction 1 were rate determining, the addition of water, which can affect only the *back* reaction, would not affect the initial rate.

Effect of Hydroquinone and Benzoin.—Duplicate experiments were run at $70°$ with each of these additives in the reaction mixture at a mole ratio to catalyst of over 25:1. No effect on the rate was found, since the initial rate in these cases was found to fall within the range of variation from the mean rate shown by the experiments without these additives.

The lack of effect by hydroquinone indicates that a free radical mechanism is not involved in this catalytic process. The lack of effect by benzoin confirms a previous report[4] and contradicts a catalyst inactivation mechanism suggested by Langenbeck.[3]

Effect of Potassium Benzoylformate.—The fact that a considerable molar excess of this salt over catalyst is required for maximum reaction rate, as shown on Fig. 4 may be explained if only the non-protonated form of the amine catalyst can react to form the Schiff base intermediate as ex-
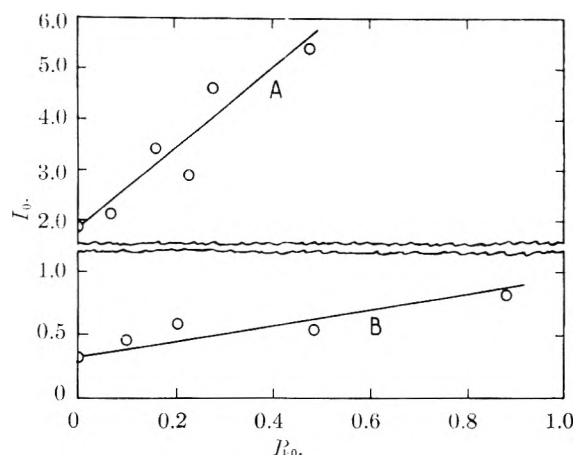

Fig. 5.—Effect of added benzaldehyde on rate. Reciprocal of initial rate *vs.* initial benzaldehyde:benzoylformic acid mole ratio, for catalysis by 3-aminooxindole (II) hydrochloride. Graph A, 49.86°; graph B, 70.07°.
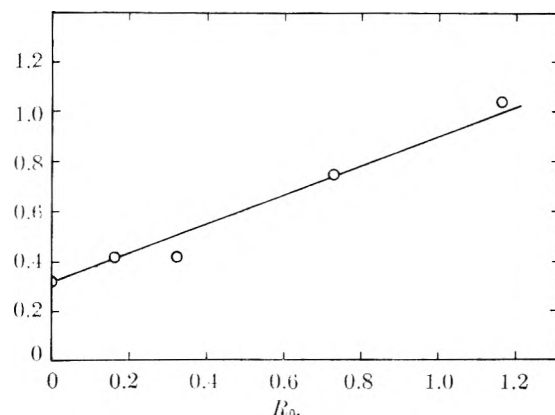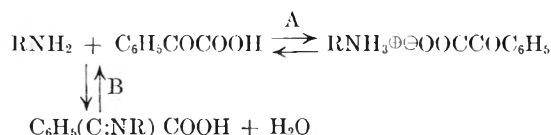

Fig. 6.—Effect of added water on rate. Reciprocal of initial rate *vs.* water:benzoylformic acid mole ratio, for catalysis by 3-aminooxindole (II) hydrochloride at 70.07°.

pected. The amine catalyst can react with benzoylformic acid in two ways

$$RNH_2 + C_6H_5COCOOH \underset{\xleftarrow{}}{\overset{A}{\rightleftharpoons}} RNH_3^{\oplus\ominus}OOCCOC_6H_5$$

$$\Big\downarrow\Big\uparrow B$$

$$C_6H_5(C\!:\!NR)\,COOH + H_2O$$

The addition of potassium benzoylformate increases the concentration of the benzoylformate anion, and drives the equilibrium of reaction path A to the left, increasing the proportion of non-protonated amine. When enough excess benzoylformate anion is present, reaction A is almost totally driven to the left, and the catalyst amine is free to react almost completely by reaction B. Further excess of the benzoylformate anion can then produce no further effect.

The fact that excess of strong acid completely prevents catalysis by II is in accordance with the above assumptions.

Energy and Entropy of Activation.—Assuming that the decarboxylation rate is determined by a single slow step (reaction 2 of the kinetic treatment) an Arrhenius plot of $\log_e k_2$ *vs.* $1/T$ was used to calculate the activation energy of the reaction. The transition state theory was employed to calculate

the entropy of activation.[13] The results are shown on Table II. The uncertainty in the determination of the entropy of activation for α-phenylglycine catalysis is unfortunately too great for comparison with 3-aminoöxindole.

TABLE II

| Catalyst	Energy of activation, kcal./mole	Entropy of activation, cal./mole deg.
3-Aminoöxindole hydrochloride	18.5 ± 1.5	-13 ± 4
α-Phenylglycine hydrochloride	19.5 ± 2.5	-14 ± 10

Mechanism of the Catalysis: The Role of Prototropic Rearrangement.—The proposed requirement of prototropic rearrangement in catalysis by II and similar compounds is strongly supported by the fact that VIII, in which a methyl group has replaced the labile hydrogen atom at the 3-position of II, is inactive as a catalyst.

The amino-acid catalyst, IX, was about 1/15 as effective as II. The Schiff base formed by reaction of IX with I need not undergo prototropic rearrangement in order to catalyze the decarboxylation of I.
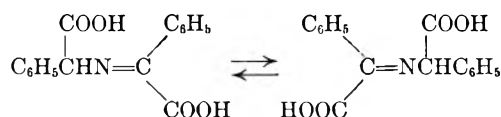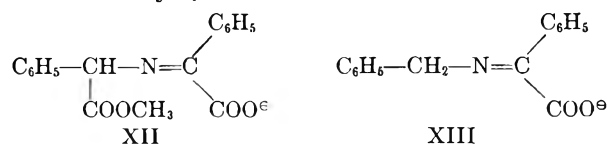

Due to the symmetry of the molecule, such a rearrangement would produce no structural change. It is also evident that benzylamine, produced by decarboxylation of IX, cannot be the true catalyst, since it is much less effective than is IX itself.

The mechanism suggested by Baddar[14] for the Strecker degradation can be usefully incorporated into a reasonable mechanism, explaining catalysis by IX and by other amino-acids.
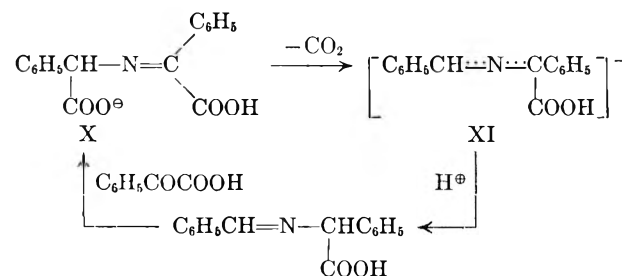

In this case prototropic rearrangement occurs *after* decarboxylation of the Schiff base intermediate. The loss of carbon dioxide from the carboxylate anion X is aided by the resonance-stabilization of the carbanion, XI. The fact that both methyl α-phenylglycinate and benzylamine are ineffective catalysts is in accord with this mechanism. The Schiff bases, XII and XIII, produced from these compounds cannot produce a stabilized carbanion by loss of carbon dioxide, since the single carboxylate group here is bonded to a doubly bonded carbon atom. In these cases, therefore, a prototropic shift

(13) A. A. Frost and R. G. Pearson, "Kinetics and Mechanism," John Wiley and Sons, Inc., New York, N. Y., 1953, p. 95 ff.

(14) F. G. Badda-, *J. Chem. Soc.*, 136 (1950); F. G. Baddar and Z. Iskander, *ibid.*, **203**, 209 (1954).

prior to decarboxylation is required, as with the lactam catalyst, II.

A similar mechanism, involving a resonance-stabilized carbanion intermediate, is now suggested to explain the ease of prototropic rearrangement shown by Schiff bases of II. Prototropic rearrangements in simpler systems have been shown to be base catalyzed.[15]
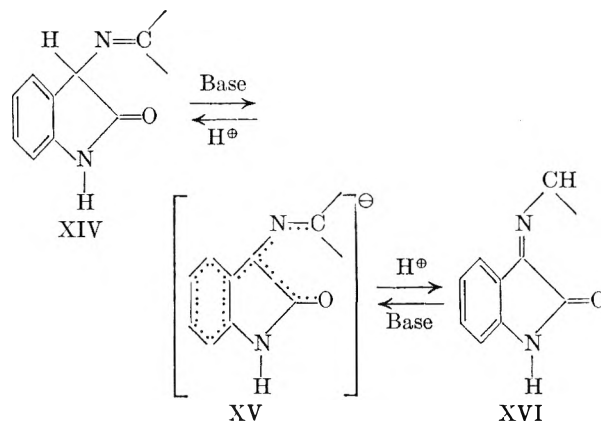
Attack by base at the 3-position of Schiff base, XIV, could produce the carbanion XV. The fused benzene ring, which is probably coplanar with the heterocyclic ring, can markedly assist resonance stabilization of XV. In contrast, a similar carbanion, XVII, derived from the Schiff base XII, would derive comparatively little stabilization from the benzene ring, since in this case the ring is not held in a coplanar configuration. This is proposed as the reason why IX methyl ester is not an effective decarboxylation catalyst. Similarly benzylamine
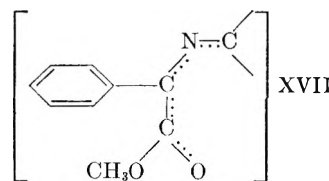
Schiff bases would not provide resonance-stabilization for a carbanion.

The entropy of activation for II hydrochloride does not have an unusually large negative value. The entropy of activation for IX hydrochloride is not sufficiently precise for comparison. As a result these data do not exclude either an open-chain transition state or the previously proposed cyclic transition state[4] for the mechanism of decarboxylation of the rearranged Schiff base intermediate.

(15) L. P. Hammett, "Physical Organic Chemistry," McGraw-Hill Book Co., New York, N. Y., 1940, pp. 247–249.

THE CRYSTAL STRUCTURE OF MONOCLINIC Sm₂O₃[1]

By Don T. Cromer

University of California, Los Alamos Scientific Laboratory, Los Alamos, New Mexico

Received December 3, 1956

In this paper the structure of the type "B" rare earth sesquioxide is reported. This form of Sm₂O₃ is monoclinic, probable space group C2/m with $a = 14.17_7$, $b = 3.63_3$, $c = 8.84_7$, all ± 0.01 Å., and $\beta = 99.96 \pm 0.03°$. There are six formula units per unit cell. There are layers of composition Sm₂O₃ at $y = 0$ and $y = 1/2$. Parallel to the xy-plane, layers of oxygen atoms alternate with layers of samarium atoms. Each samarium atom has seven oxygen neighbors at an average distance of about 2.46 Å.

Introduction

The rare earth sesquioxides have long been known to exist in three different crystalline forms. The "A" structure type is hexagonal and is observed in the rare earth oxides from La through Nd. The "C" type is cubic and is found in the rare earth oxides from Sm through Lu. A third form, called the "B" type, has been known to exist but its structure has heretofore been unknown. Goldschmidt, Ulrich and Barth[2] described type B as pseudotrigonal, orthorhombic or monoclinic.

Crystallographic data for single crystals of Sm₂O₃, type B, recently have been published by Douglass and Staritzky.[3] These crystals were prepared by Dr. I. R. Tannenbaum, of this Laboratory, by fusing Sm₂O₃ in an oxyacetylene flame at 3000 to 3500°. Douglass and Staritzky found this compound to be monoclinic, space group C2/m, C2 or Cm with $a = 14.17_7$, $b = 3.63_3$, $c = 8.84_7$, all ± 0.01 Å., and $\beta = 99.96 \pm 0.03°$. Their measured density is 7.68 g./cm.³ and the calculated density with six formula units per unit cell is 7.74 g./cm.³. After they had finished their work a single crystal fragment of the material was given to the author for a structure determination.

Experimental

The crystal used for intensity data was rather irregular in shape with approximate dimensions 0.15 × 0.15 × 0.08 mm. Weissenberg photographs about the b axis were taken with Mo K-α radiation. The b-axis was approximately parallel to one of the body diagonals of the fragment. It was immediately evident that the structure was a layer type with layers separated by $b/2$, because photographs of all of the even layers appeared to be identical and all of the odd layers were apparently identical. Geiger counter intensity data with Mo K-α radiation were obtained for the $h0l$ and $h2l$ layers within the range sin $_{Mo} \lesssim 0.7$. On the zero layer 285 reflections were observed out of approximately 395 investigated. The intensities were corrected for the Lp factors and converted to F_0 on a relative scale. No absorption corrections were made because of the irregular shape of the crystal.

The data were initially placed on an approximately absolute scale by application of Wilson's[4] method. The temperature factor obtained in this way was 0.12 × 10⁻¹⁶ cm.². It was later found that the scale factor was about 25% too low. The final average temperature factor for the samarium atoms was 0.24 × 10⁻¹⁶ cm.².

Determination of the Structure.—The diffraction symmetry offers a choice of three space groups: C2, Cm or C2/m. If the layering is perfect, the atoms must lie in the reflection plane of Cm or

C2/m. Space group Cm would then require that all atoms be in the twofold positions 2a. It seemed probable that such a simple compound would have more symmetry than this and the actual structure determination eliminated this space group.

The similarity of the even and odd k layers shows that the heavy atoms are certainly in layers separated by $b/2$. The choice between space groups C2 and C2/m then depends on whether the oxygen atoms are so slightly removed from the samarium layers that no detectable differences arise between the intensity distributions on the various even or odd layers.

The intensities of the $h2l$ layer were measured to provide as good evidence as possible that the oxygen atoms are on the same level as the samarium atoms. A sort of reliability index was computed and it was found that

$$\Sigma ||F(h0l)| - |F(h2l)||/\Sigma|F(h0l)| = 9.3\%$$

where the two layers were scaled so that $\Sigma|F(h0l)| = \Sigma|F(h2l)|$. This value is lower than the R finally obtained for the $h0l$ data, so that within the accuracy of the available data the structure is perfectly layered. The method used for scaling the the two layers did not take into account that the form factors decrease more rapidly on the zero layer than on the second layer as h and l increase. If the data had been converted to unitary structure factors, the agreement would no doubt be somewhat better.

In view of the above considerations the structure determination was pursued on the assumption that the space group is C2/m. There are therefore 3 kinds of samarium atoms and 4 kinds of oxygen atoms in positions $4i$ and one kind of oxygen atom in either $2a$ or $2b$.

A Patterson projection down the b-axis was computed on the Maniac. Approximate xz-coordinates for the samarium atoms were found without difficulty. The choice of y-coordinates of 0 or $1/2$ for these atoms was made by qualitative inspection of several of the $h1l$ intensities on a Weissenberg film. In order to get agreement with the $h1l$ intensities it was necessary to shift the original origin by $(-1/4, 0, -1/2)$.

These samarium coördinates were used to determine the phases of about two-thirds of the reflections and a Fourier projection was computed. This projection improved the samarium positions sufficiently to permit a second Fourier projection to be computed with nearly all terms included. This second Fourier is shown in Fig. 1.

(1) Work done under the auspices of the Atomic Energy Commission.

(2) V. M. Goldschmidt, F. Ulrich and T. Barth, *Skrifter Norske Videnskaps-Akad. Oslo, I, Mat.-Naturv. Kl.*, No. 5, 5 (1925).

(3) R. M. Douglass and E. Staritzky, *Anal. Chem.*, **28**, 552 (1956).

(4) A. J. C. Wilson, *Nature*, **150**, 152 (1942).

<div align="center">

Table I

Parameters in Sm_2O_3

</div>

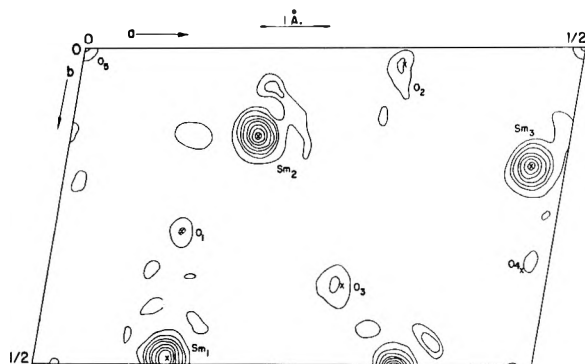| A tom	Derived from Fourier			Least-squares refinement		
	x	y	z	x	z	$B \times 10^{16}$, cm.^{2}
Sm_1	0.1340	$1/2$	0.4912	0.1349 ± 0.0005	0.4905 ± 0.0008	0.19 ± 0.08
Sm_2	.1900	$1/2$	.1376	.1897 ± .0005	.1380 ± .0008	.12 ± .08
Sm_3	.4676	$1/2$	.1860	.4663 ± .0005	.1881 ± .0009	.41 ± .10
O_1	.130	0	.290	.128 ± .003	.286 ± .005	.25 ± .52
O_2	.320	$1/2$	.020	.324 ± .003	.027 ± .005	.40 ± .49
O_3	.290	$1/2$	.370	.299 ± .003	.374 ± .005	.10 ± .60
O_4	.490	0	.340	.469 ± .003	.344 ± .005	.41 + .56
O_5	0	$1/2$	0	0	0	1.18 ± .10

Fig. 1.—Second Fourier projection of Sm_2O_3 down the b-axis. Contours are at equal arbitrary intervals except that the interval is five times as great around the samarium atoms as elsewhere. The crosses indicate the final atomic positions as derived from the least-squares refinement.
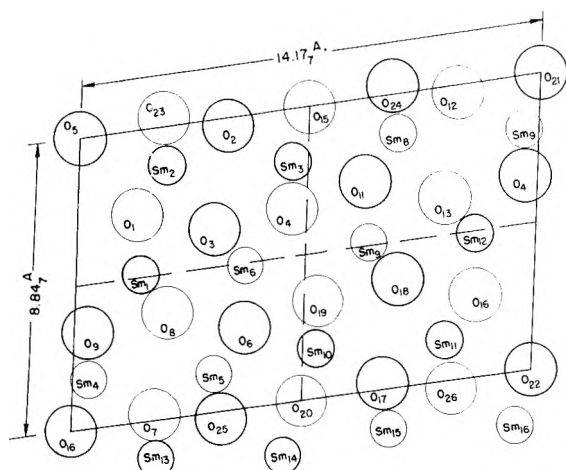

Fig. 2.—Projection of the Sm_2O_3 structure down the b-axis. The heavy circles are atoms at $y = 1/2$ and the light circles are atoms at $y = 0$.

In addition to the samarium peaks in Fig. 1 there are several small peaks which could be oxygen atoms. The twofold oxygen at the origin is clearly visible. There are six other peaks which could be considered as possible oxygen atoms. All the rest can be ruled out because they are too close to samarium atoms (all <1.8 Å.) or too close to a twofold axis. The peak below and to the left of the peak labeled O_1 is about 2.2 Å. from Sm_1 and the peak to the left of Sm_2 is 2.1 Å. from Sm_2, assuming in both cases that the y-coördinates differ by $1/2$. Both of these distances are rather short and probably unlikely. These two peaks were rejected in favor of the one shown as O_1 because the latter is

higher and more favorably located with respect to Sm_1 and Sm_2. The other peaks selected are indicated in Fig. 1.

The oxygen and samarium coördinates derived from the second Fourier were used as the starting point for a least-squares refinement. The y-coördinates of the oxygen atoms were chosen as 0 or $1/2$, whichever gave the more reasonable interatomic distances. The choice was quite obvious in all cases. These coördinates are given in Table I. Separate isotropic temperature factors were given to each crystallographically different atom. The problem was solved as a set of 3 × 3 equations for each atom, the cross-terms between different atoms being neglected. The temperature factor for the twofold oxygen and the scale factor were treated as one-dimensional equations. The Thomas–Fermi form factor was used for samarium after reduction by 1.2 electrons because of anomalous dispersion.[5] The McWeeney[6] form factor was used for oxygen. All reflections were given equal weight except for those with $F_{obsd} = 0$, which were omitted. All calculations were performed on the Maniac.

The final results are listed in Table III. The crosses in Fig. 2 indicate the final atomic positions from the least-squares refinement. The reliability index with the $F_{obsd} = 0$ terms omitted is 11.0%. The observed and calculated structure factors are given in Table II.[7]

Accuracy of the Structure.—The low value for the reliability index is rather surprising in view of the uncertainty in the data caused by absorption. The temperature factors for the atoms differ considerably. There is no structural reason why the thermal motions should be particularly different for the different atoms of the same species. Inspection of the standard deviations of the temperature factors shows that these differences are entirely without significance. It must be assumed that the inaccuracy of the data has had a considerable effect on the apparent thermal parameters. The least-squares method has done its best to bring the observed and calculated values into agreement and in so doing has produced unreal temperature factors. It must also be assumed that the atomic coördinates are likewise in error, although a physi-

(5) R. W. James, "The Optical Principles of the Diffraction of X-Rays," G. Bell and Sons, London, 1948, p. 608.

(6) R. McWeeney, Acta Cryst., 4, 513 (1951).

(7) Table II has been deposited as Document No. 5115 with the ADI, Library of Congress, Washington 25, D. C. A copy may be secured by citing the Document number and by remitting $1.25 for photoprints or $1.25 for 35 mm microfilm in advance by check payable to Chief, Photoduplicating Service, Library of Congress. A limited number of copies are available from the author.

cally satisfactory structure has certainly been obtained. Because of the uncertainty caused by absorption errors, which are rather more systematic than random, the standard deviations were arbitrarily assumed to be twice the value given by the usual formula

$$\sigma(\xi_i) = \left[\frac{\Sigma(\Delta F)^2}{(m - s)\Sigma(\partial F/\partial \xi_i)^2}\right]^{1/2}$$

where m is the number of observations and s is the number of variables. These doubled standard deviations are listed in Table I and were used in computing the standard deviations of the interatomic distances given in Table III.

Discussion of the Structure.—The structure in projection is shown in Fig. II. The various interatomic distances are given in Table III. The structure is a layer type with all atoms at $y = 0$ or $1/2$. Each of these layers has the composition Sm_2O_3. Parallel to the xy-plane somewhat corrugated sheets of oxygen atoms alternate with similarly corrugated sheets of samarium atoms. Each oxygen sheet is a distorted close-packed plane. The samarium atoms are arranged such that there are five rather than six samarium neighbors in their planes.

In the hexagonal R_2O_3 structure, each metal atom has seven oxygen neighbors. The RO_7 group is derived from an octahedron by adding a seventh oxygen atom along a threefold axis. In monoclinic Sm_2O_3, each samarium atom also has seven neighbors. The coördination about the Sm_3 atoms can formally be described as a distorted octahedron with a seventh oxygen atom along a "threefold" axis. This seventh oxygen atom, however, is almost too far away to be included in the primary coördination shell. The coördination about Sm_1 and Sm_2 is a distortion of the type found in the anions $NbF_7^=$ and $TaF_7^=$ with idealized symmetry 2mm.[8] Six oxygens form a trigonal prism and the seventh lies along a normal to a prism face.

The Sm–O distances vary from 2.25 to 3.12 Å., but the average distance from each of the samarium atoms to its seven neighbors is essentially the same, the average Sm–O distances being 2.45, 2.44 and 2.48 Å. for samarium atoms 1, 2 and 3, respectively. The Sm–O distance[9] in cubic Sm_2O_3 is 2.34 Å.

The minimum, maximum and average O–O distances in the coördination spheres about Sm_1, Sm_2 and Sm_3, respectively, are 2.74, 3.63, 3.13; 2.75, 3.63, 3.06; 2.56, 3.66 and 3.14 Å.

TABLE III

INTERATOMIC DISTANCES IN Sm₂O₃, TYPE B

The left-hand atom is crystallographically equivalent to the type indicated in the heading. The subscripts refer to Fig. 2. The standard deviations for Sm–O, O–O and Sm–Sm distances are ±0.06, ±0.08 and ±0.014 Å., respectively. In addition to the distances given below, each atom has two neighbors of its own kind at 3.63 Å., the length of the b-axis.

Samarium–oxygen distances

Samarium type 1		Samarium type 2		Samarium type 3	
Sm₆–O₃	2.29 (2)	Sm₅–O₆	2.49 (2)	Sm₁₀–O₁₉	2.28 (2)
Sm₆–O₄	2.56 (2)	Sm₅–O₂₅	2.32 (2)	Sm₁₀–O₂₀	2.57 (2)
Sm₆–O₄	2.25	Sm₅–O₉	2.38	Sm₁₀–O₁₇	2.26
Sm₆–O₈	2.71	Sm₅–O₇	2.29	Sm₁₀–O₆	2.31
Sm₆–O₁₉	2.49	Sm₅–O₂₀	2.76	Sm₁₀–O₁₈	3.12

Oxygen–oxygen distances

Oxygen type 1		Oxygen type 2		Oxygen type 3	
O₆–O₈	2.87 (2)	O₂₅–O₇	2.75 (2)	O₃–O₂	3.15
O₆–O₁₉	3.02 (2)	O₂₅–O₆	2.97	O₃–O₆	3.01
O₆–O₂₅	2.97	O₂₅–O₂₀	2.56 (2)	O₃–O₈	3.36 (2)
O₆–O₂₀	2.85 (2)	O₂–O₃	3.15	O₃–O₄	3.07 (2)
O₆–O₃	3.01	O₂–O₄	3.66 (2)	O₇–O₁	2.87 (2)

Oxygen type 4		Oxygen type 5	
O₄–O₂₀	3.07 (2)	O₂₀–O₁₇	3.16 (2)
O₄–O₁₉	2.74	O₁₆–O₄	3.16
O₄–O₁₁	3.02 (2)	O₂₀–O₂₅	2.56 (2)
O₄–O₁₆	3.16	O₂₀–O₁₇	2.56 (2)
O₄–O₂	3.66 (2)	O₂₀–O₆	2.85 (2)
		O₁₆–O₁₁	2.85 (2)

Samarium–samarium distances

Samarium type 1		Samarium type 2		Samarium type 3	
Sm₆–Sm₁	3.72 (2)	Sm₂–Sm₆	4.13 (2)	Sm₃–Sm₆	3.86 (2)
Sm₆–Sm₉	3.94	Sm₂–Sm₁	3.34	Sm₃–Sm₂	3.88
Sm₆–Sm₅	3.34	Sm₂–Sm₃	3.88	Sm₃–Sm₈	3.75 (2)
Sm₆–Sm₁₀	3.74 (2)	Sm₆–Sm₁₀	3.75 (2)	Sm₃–Sm₉	3.74 (2)
Sm₆–Sm₃	3.86 (2)	Sm₆–Sm₁₃	3.69 (2)	Sm₁₀–Sm₁₅	3.78 (2)
Sm₆–Sm₂	4.18 (2)	Sm₆–Sm₁₄	3.78 (2)	Sm₁₀–Sm₁₄	3.62

(8) J. L. Hoard, *J. Am. Chem. Soc.*, **61**, 1252 (1939).

(9) D. H. Templeton and C. H. Dauben, *ibid.*, **76**, 5237 (1954).

THE CATALYTIC PROPERTIES OF SUPPORTED SODIUM AND LITHIUM CATALYSTS

By Sterling E. Voltz

Houdry Process Corporation, Marcus Hook, Pa.

Received December 7, 1956

The catalytic properties of supported alkali metal catalysts for hydrogen–deuterium exchange and ethylene hydrogenation have been investigated. Sodium dispersed on dried alumina does not increase the activity of the alumina for hydrogen–deuterium exchange. However, hydriding the sodium–alumina greatly increases the exchange activity, the hydrided catalyst being active even at −195°. Sodium–silica catalysts are much less active than the corresponding sodium–alumina catalysts. Supported sodium and lithium catalysts are also active for ethylene hydrogenation even below room temperature; in this case, however, hydrogen treatments have relatively minor effects on the activities. The supported alkali metal catalysts are much more active than the bulk hydrides of sodium and lithium for both of these reactions. The major role of the support is probably to increase the effective area of the alkali metal. The results of this study suggest that the mechanisms of activation of hydrogen and ethylene on alkali metal hydrides are similar to those previously postulated for alkaline earth metal hydrides. The activations probably occur at metal sites at metal–metal hydride interfaces. The results obtained with the bulk hydrides suggest that hydrogen activation takes place more readily at lithium sites than at sodium sites, and the reverse situation is likely for ethylene activation.

Introduction

The recent development of the preparation of alkali metals dispersed on catalyst supports has made it easier to study the catalytic properties of these elements.[1] Only a few isolated references to the use of alkali metals dispersed over solids have been made previously.[1]

This investigation was concerned with the catalytic properties of supported sodium and lithium. In particular, the activities of these catalysts for hydrogen–deuterium exchange and ethylene hydrogenation have been studied.

The alkali metals and their hydrides have been used as reduction or hydrogenation catalysts.[2–6] They have also been used as catalysts for the alkylation of nitrogen compounds,[7,8] condensation reactions,[9–11] and polymerization.[12,13] The compounds used by most of these workers were limited to those which are readily metallated by the alkali metals. An exception is the use of cesium as a catalyst for the hydrogenation of ethylene.[14]

Investigations also have been made of the catalytic properties of the hydrides of other elements. In particular, the recent study of the catalytic activities of barium and calcium hydrides has been useful in correlating activities with other properties of these substances.[15]

(1) "High Surface Sodium," bulletin by U. S. Industrial Chemicals Co., New York. N. Y., 1953.

(2) F. W. Bergstrom and J. F. Carson. *J. Am. Chem. Soc.*, **63**, 2934 (1941).

(3) G. Egloff, U. S. 1,950,721 (1934); 1,954,477 (1934); 1,954,478 (1934); and 1,962,182 (1934).

(4) G. Hugel and co-workers, *Chimie et Industrie*, Special No. 128 (1929); *Can. Chem. Met.*, **13**, 5 (1929); *Bull. soc. chim.*, **49**, 1042 (1931); **51**, 639 (1932); *Ann. combustible liquides*, **6**, 1109 (1931); **7**, 59 (1932); U. S. 1,968,208 (1934).

(5) A. M. Muckenfuss, U. S. 1,958,012 (1934).

(6) O. Schmidt, *Z. physik. Chem.*, **A165**, 209 (1933).

(7) G. M. Whitman, U. S. 2,501,556 (1950).

(8) W. S. Fones, *J. Org. Chem.*, **14**, 1099 (1949).

(9) H. A. Bruson, U. S. 2,287,510 (1942).

(10) G. H. Daub and W. S. Johnson, *J. Am. Chem. Soc.*, **70**, 418 (1949); **72**, 501 (1950).

(11) N. Green and F. B. LaForge, *J. Am. Chem. Soc.*, **70**, 2287 (1948).

(12) A. Morton, unpublished results.

(13) K. Schirmacher and L. Van Zutphen, U. S. 1,838,234 (1931); Brit. 315,356 (1929).

(14) D. G. Hill and G. B. Kistiakowsky, *J. Am. Chem. Soc.*, **52**, 892 (1930).

(15) L. Wright and S. Weller, *ibid.*, **76**, 5302, 5305, 5948 (1954).

Experimental

The supported sodium and lithium catalysts were prepared by dispersing the molten metal over powdered alumina or silica which had been dried by evacuation at 500° for about 16 hours. In a typical preparation (sodium–alumina) the dried alumina and sodium were placed in a high vacuum reactor equipped with a magnetic stirrer. Transfers of materials to the reactor were made in a dry box in dry nitrogen. The reactor was heated slowly under evacuation while the solids were stirred. When the sodium melted, it dispersed over the alumina powder. The reactor was heated to about 150° and kept at this temperature (under evacuation and with stirring) for at least one-half hour. Small amounts of gaseous products were given off in some preparations when the molten alkali metal dispersed over the powder. In the preparation of lithium–alumina catalysts, the reactor was heated to about 250° because of the higher melting point of lithium (186°).

Bulk sodium and lithium hydrides were obtained from Metal Hydrides, Inc., Beverly, Mass.

Hydrogen–deuterium exchange reactions were carried out in a high vacuum apparatus equipped with an electromagnetic circulating pump. A static high vacuum system was used for ethylene hydrogenations. Catalysts were evacuated at 200° for two hours prior to being tested for activity. Equimolecular mixtures of hydrogen–deuterium or ethylene–hydrogen were charged to the catalysts at 600 mm. Gas samples were analyzed by mass spectrometry. The rate constants for hydrogen–deuterium exchange reactions were calculated from a first-order rate equation. In all ethylene hydrogenations, the rate constants were calculated from a second-order rate equation for equimolecular concentrations of the two reactants.

Results and Discussion

I. Properties of Supported Alkali Metal Catalysts.—Impregnation of a support with a molten alkali metal decreases the surface area. For example, the surface area of an alumina support decreased from 81 to 48 m.²/g. when 4 weight % sodium was dispersed on it. In the preparation of a sodium–silica catalyst, the surface area of the silica gel was decreased from 454 to 272 m.²/g. The sodium probably blocks some of the small pores of the supports. Similar results are observed with lithium. The average pore diameter of a silica gel is generally smaller than that of an alumina support. The most effective support for alkali metals would probably be a high area material which contains primarily large pores.

Supported alkali metal catalysts show large differences in their reactions with hydrogen. Sodium–alumina, sodium–silica and lithium–alumina all react with hydrogen at 300° but the rates of re-

action differ markedly. Sodium–alumina reacts very rapidly; all the hydrogen is sorbed within 20 minutes. In contrast, both sodium–silica and lithium–alumina react slowly with hydrogen for over a week.

II. Hydrogen–Deuterium Exchange.—The activity of a typical sodium–alumina (4 weight % sodium) catalyst for hydrogen–deuterium exchange is shown in Table I. The activity of alumina is about the same as that of sodium–alumina. An earlier study of this reaction over very pure alumina (ex aluminum isopropoxide) gave similar activity and temperature dependence.[16] The activity of the sodium–alumina catalyst is enormously increased by hydrogen treatment. The hydrided catalyst is active for hydrogen–deuterium exchange even at −195°; the other catalysts are inactive at this low temperature. The hydrogen taken up by the hydrided catalyst was equivalent to conversion of 13 weight % of sodium to sodium hydride. There is no evidence of deuterium exchange with catalyst hydrogen in the experiments.

Both sodium–silica and hydrided sodium–silica are less active for hydrogen–deuterium exchange than the corresponding sodium–alumina catalysts. The former are inactive at −78° and slightly active at 0° and higher.

TABLE I

Hydrogen–Deuterium Exchange Over Sodium–Alumina

Catalyst	Temp. of exchange (°C.)	Activity (min.$^{-1}$)[a]
Na–Al$_2$O$_3$[b]	−100	0.019
Na–Al$_2$O$_3$[b]	−123	0.0070
Na–Al$_2$O$_3$[b]	−195	Inactive
Hydride Na–Al$_2$O$_3$[c]	−195	0.0030
Al$_2$O$_3$[d]	−100	0.029
Al$_2$O$_3$[d]	−123	0.0074

[a] The quantities of hydrogen–deuterium charged were 2.4, 2.7 and 4.4 mmoles at −100, −123 and −195°, respectively. [b] 5 g. of sodium (4 weight %) dispersed on alumina (dried by evacuation overnight at 500°). [c] Na–Al$_2$O$_3$ was treated with hydrogen at 300°. [d] Evacuated at 500° for 16 hours.

Bulk sodium hydride is only slightly active for hydrogen–deuterium exchange (1.0% HD in 0.5 hour) at 100°. At this temperature there is no exchange between gaseous deuterium and catalyst hydrogen (hydride ions). At 125 and 150°, sodium hydride is very active for hydrogen–deuterium exchange and appreciable exchange occurs between gaseous deuterium and catalyst hydrogen.

Bulk lithium hydride is more active for hydrogen–deuterium exchange than sodium hydride. Typical data for a sample of lithium hydride are given in Table II. The atom per cent. deuterium in the gas phase remained constant during both of these runs, which means that no exchange occurs between gaseous deuterium and catalyst hydrogen under these conditions.

III. Ethylene Hydrogenation.—Sodium–alumina, lithium–alumina and sodium–silica are active for the hydrogenation of ethylene. Data for these catalysts are summarized in Table III. The difference in activities between sodium–alumina and

(16) S. G. Hindin and S. W. Weller, This Journal, **60**, 1501, 1506 (1956).

TABLE II

Hydrogen–Deuterium Exchange over Lithium Hydride[a]

Temp. (°C.)	HD (mole %)		
	5 min.	15 min.	30 min.
30	5.1	8.3	13.5
100	17.0	28.3	38.6

[a] 1.9 millimoles hydrogen–deuterium (at 600 mm.) charged to 3 g. lithium hydride.

hydrided sodium–alumina for ethylene hydrogenation is small compared to the difference observed for hydrogen–deuterium exchange. Sodium–alumina is more active than alumina for ethylene hydrogenation whereas they have similar activities for hydrogen–deuterium exchange. Sodium reacts readily with certain olefins and ethylene is probably more easily activated on sodium–alumina than alumina.

TABLE III

Ethylene Hydrogenation

Catalyst[a]	Activity[b] (mm.$^{-1}$ – min.$^{-1}$ × 10^4)	
Al$_2$O$_3$	..	0.0
Na–Al$_2$O$_3$	0.43	2.2
Hydrided Na–Al$_2$O$_3$[c]	1.2	2.9
Li–Al$_2$O$_3$	0.12	0.38
Hydrided Li–Al$_2$O$_3$[c]	0.73	1.6
SiO$_2$	..	0.03
Na–SiO$_2$	2.9	4.4
Hydrided Na–SiO$_2$[c]	..	0.30

[a] Catalysts were prepared by dispersing 1 g. alkali metal on 9 g. alumina or silica. [b] About 5 mmoles of an equimolecular mixture of ethylene and hydrogen (at 600 mm.) were charged to the reactor in each experiment. Duplicate runs were made in most instances; the above values represent the averages for these runs. [c] Treated with hydrogen at 300°.

Lithium–alumina is less active for ethylene hydrogenation than hydrided lithium–alumina; this is similar to the result observed with sodium–alumina. Sodium–silica is more active than sodium–alumina or lithium–alumina, but treatment with hydrogen decreases the activity of sodium–silica for ethylene hydrogenation, possibly because of pore blockage by sodium hydride. The activity of the silica gel base is negligible under these conditions.

The extents of hydriding for the three catalysts in Table III were 15, 11 and 10 weight % of the alkali metal for sodium–alumina, lithium–alumina and sodium–silica, respectively.

The activities of bulk sodium and lithium hydrides for ethylene hydrogenation are given in Table IV. The activity of the bulk sodium hydride is considerably less than sodium–alumina or hydrided sodium–alumina. From the kinetic data for sodium hydride between 100–200° the energy of activation is 8 kcal./mole. The energy of activation over lithium hydride is 17 kcal./mole which is double the value for sodium hydride. The energies of activation of the supported alkali metal catalysts listed in Table III are between 2–9 kcal./mole.

The slight activities (for ethylene hydrogenation) of some of these catalysts (such as sodium hydride) at high temperatures with no measurable

Temp. (°C.)	Activity (mm.$^{-1}$ − min.$^{-1}$ × 10^4)	
	NaH	LiH
30	Inactive[b]	..
100	0.85	0.02
150	4.2	..
200	8.6	2.5

3.5–3.9 mmoles of 1:1 mixture of ethylene and hydrogen
at 600 mm. were charged to 10 g. of hydride in each run.
[b] Pressure decreased only a few mm. in one hour.

activities at lower temperatures are consistent with
the results of Hill and Kistiakowsky[14] for cesium on
glass.

The bulk sodium hydride is more active than
bulk lithium hydride whereas the activities of
these catalysts are the reverse for hydrogen–deuterium exchange (see Table I). The decomposition
pressure of lithium hydride is much less than that
of sodium hydride. The pretreatment (evacuation
at 200°) used in this work should, therefore, result
in more surface defects in sodium hydride than
lithium hydride. The catalytic activities of the
two evacuated surfaces depend not only on the
number of defects, but are dependent on the energetics of the sites. The results obtained with
the bulk hydrides suggest that hydrogen activation
takes place more readily at lithium sites than at
sodium sites, and the reverse situation is likely for
ethylene activation. The rate controlling steps
in the two activations are probably different.

The supported alkali metal catalysts are more
active than the corresponding unsupported metals
or metal hydrides for both hydrogen–deuterium
exchange and ethylene hydrogenation. This is
probably the result of large differences in surface
areas. The major role of the support probably is to
increase the effective surface area of the alkali
metal. The sodium particle size on supported
sodium catalysts is reported to be about 0.5 to
1000 mμ, which is even smaller than in sodium dispersions.[1]

Weller and Wright[15] have proposed that the
activation of hydrogen and ethylene takes place on
calcium and barium hydrides at metal sites at
metal–metal hydride interfaces. This concept is
in agreement with many of the results obtained in
this study.

VACANCY DISTRIBUTION AND BONDING IN SOME OXIDES OF SPINEL STRUCTURE

BY K. P. SINHA AND A. P. B. SINHA

National Chemical Laboratory, Poona-8, India

The nature of the vacancy distribution in the defect spinel-type oxides γ-Fe$_2$O$_3$, γ-Mn$_2$O$_3$, γ-Cr$_2$O$_3$ and γ-Al$_2$O$_3$ has been considered in the light of the available magnetic and structural data. It is concluded that all vacancies lie in octahedral sites, their distribution being ordered in γ-Fe$_2$O$_3$, but random in the cases of the other oxides. The tetragonal symmetry of γ-Mn$_2$O$_3$ (and also of Mn$_3$O$_4$) which is attributed to dsp^2 square bonding of the cations in octahedral sites is stabilized by d^{2}sp irregular tetrahedral bonding in tetrahedral sites.

Introduction

In the three main spinel groups, namely, the aluminates (MeAl$_2$O$_4$), ferrites (MeFe$_2$O$_4$) and chromites (MeCr$_2$O$_4$), the classifying components are Al$_2$O$_3$, Fe$_2$O$_3$ and Cr$_2$O$_3$, respectively. It has been shown that components of rhombohedral structure, such as α-Al$_2$O$_3$, α-Fe$_2$O$_3$ and α-Cr$_2$O$_3$, must undergo transformation to the γ-form, a cubic defect spinel structure, before reacting in the solid state with the MeO components.[1] Recent work in this Laboratory leads to a similar conclusion in respect of the manganites (MeMn$_2$O$_4$). The γ-form of Mn$_2$O$_3$ has a pseudo-spinel structure and is related to Mn$_3$O$_4$ as γ-Fe$_2$O$_3$ is to Fe$_3$O$_4$. The distribution of cations and vacancies, and the nature of the interionic bondings in these oxides are of considerable interest but so far have not been elucidated fully.

The cubic close-packed arrangement of oxygen ions, located at 32-fold positions, forms the main framework of the spinel-type lattice, the cations being distributed among the 8-fold and 16-fold interstices.[2,3] Each unit cell of this arrangement has a framework of thirty-two O^{2-} ions with 64 tetrahedral interstices, each surrounded by four oxygen ions, and 32 octahedral interstices, each surrounded by six oxygen ions. In the ideal spinel lattice (space group Fd3m, O^7_h) only 24 of these sites (8 tetrahedral and 16 octahedral) are occupied by cations, with coördinates 8a:0 0 0, $^1/_4$ $^1/_4$ $^1/_4$, + f.c.c. and 16d: $^5/_8$ $^5/_8$ $^5/_8$, $^5/_8$ $^7/_8$ $^7/_8$, $^7/_8$ $^5/_8$ $^7/_8$, $^7/_8$ $^7/_8$ $^5/_8$, + f.c.c.

The Vacancy Distribution in γ-Fe$_2$O$_3$.—The crystal structure of γ-Fe$_2$O$_3$ is of the defect spinel type, i.e., with a number of vacant cation positions[4,5] since, out of the 24 cation sites occupied in an ideal spinel, such as Fe$_3$O$_4$, only twenty-one and one third per unit cell are occupied, the rest being vacant. Thus, the average unit-cell composition of γ-Fe$_2$O$_3$ may be written as Fe$_{21^1/_3}$□$_{2^2/_3}$O$_{32}$ where □ represents a vacant cation site.

(1) G. I. Finch and K. P. Sinha, *Proc. Roy. Soc. (London)*, **A239**, 145 (1957).

(2) T. W. F. Barth and E. Posnjak, *Z. Krist.*, **A82**, 325 (1932).

(3) E. J. W. Verwey and E. L. Heilmann, *J. Chem. Phys.*, **15**, 174 (1947).

(4) E. J. W. Verwey, *Z. Krist.*, **91**, 65 (1935).

(5) G. Hägg, *Z. physik. Chem.*, **B29**, 95 (1935).

The low electronic conductivity of γ-Fe_2O_3 rules out the presence of cations of differing valencies[6]; thus the iron is present only in the Fe^{3+} valence state. If a random distribution of cations were to exist, only those reflections should be present in X-ray diffraction patterns which are permissible in the case of a perfect spinel structure. However, the appearance of additional reflections such as 200, 210 300 (221), 310, 320, 321 and others forbidden in the case of the ideal spinel structure, points to the existence of a superstructure with a special distribution of vacancies in the available sites.[7,8]

There have been suggestions[6] that the vacancies in γ-Fe_2O_3 are mostly distributed among the octahedral interstices. The observed weakening of 111, 400, 222 reflections, which are sensitive to vacancy distribution, point to the same conclusion. Recent measurements of the average magnetic moment for γ-Fe_2O_3 by Henry and Boehm[9] do, indeed, indicate a preferential distribution of the iron ion vacancies in octahedral sites. Thus the formula unit can be written as $Fe[Fe_{5/3}\square_{1/3}]O_4$.

In view of the weak intensities of superstructure lines it is a formidable task to deduce uniquely the correct vacancy distribution. One can, at best, arrive at a tentative model consistent with most of the properties. The model suggested so far does not account for all the superstructure lines.[10] Recent work in this Laboratory, however, indicates a clustering of vacancies at octahedral sites around the cell center which may provide a suitable model for the presence of water of constitution and explain the appearance of the forbidden reflections.[11]

Spinel-type Oxides of Manganese.—The crystal structures of γ-Mn_2O_3 and Mn_3O_4 are of the pseudo-spinel type with tetragonal symmetry; in both, the axial ratio, i.e., $c/a = 1.16$ and a cation at a tetrahedral site is surrounded by four equidistant oxygen ions. However, unlike in the ideal cubic arrangement, the angular distribution does not correspond to that of a regular tetrahedron. All the six O–Mn–O angles are not equal to each other (109°28'), but two have the value 102°30' and the remaining four 113°34'. Similarly the octahedral metal ion is not surrounded by six equidistant oxygen ions but by four coplanar equidistant oxygen ions and the remaining two normal to this plane with a cation-oxygen distance greater by 16%.

Verwey and deBoer,[6] in their attempt to explain the deviation in the case of Mn_3O_4 from cubic symmetry, have suggested that the tendency of Mn^{4+} ions (placed at tetrahedral sites) toward a nonspherical field distribution may be responsible, while Goodenough and Loeb[12] have attributed the tetragonal symmetry distortion to coördinate covalent bond formation. For Mn_3O_4 the probable cat-

ion distribution is $Mn^{2+}[Mn_2^{3+}]O_4^{2-}$ in which the Mn^{2+} ions have all the d orbitals half filled and are supposed to form sp^3 empty hybrid orbitals. The tetragonal distortion is produced because of d^4 configuration of Mn^{3+} ions at octahedral positions and which can form square bonds. However, as pointed out above, the ions at tetrahedral positions do not form regular tetrahedrons, as far as the angles are concerned, which is not likely with sp^3 hybridization. Furthermore Goodenough and Loeb[12] have suggested that in γ-Mn_2O_3 all the vacancies are in tetrahedral sites; a conclusion which conflicts with the magnetic data. In what follows a generalized model of bonding, consistent with both magnetic and diffraction data, for Mn_3O_4 and γ-Mn_2O_3 is presented and which suggests the probable distribution of vacancies.

Moore, Ellis and Selwood[13] have measured the magnetic susceptibilities of all the oxides of manganese at temperatures 25, -80 and $-185°$. Using their data the effective magneton numbers, μ_{eff}, per manganese ion for Mn_3O_4 and γ-Mn_2O_3 were calculated from

$$\mu_{eff} = \sqrt{\frac{3k\chi_M(T + \theta)}{N_0\beta^2}} \qquad (1)$$

where χ_M is the molar susceptibility, k the Boltzmann constant, T the absolute temperature, θ the Weiss molecular field constant, N_0 Avogadro's number and β the Bohr magneton. The θ values for Mn_3O_4 and γ-Mn_2O_3 were ascertained by plotting the reciprocal susceptibility against temperature and extrapolating for θ to $1/\chi_M = 0$. Since the orbital magnetic moments are quenched for transition metal ions, the number n of unpaired electrons was calculated from

$$\mu_{eff} = \sqrt{n(n + 2)} \qquad (2)$$

The calculated data are set out in Table I. It is evident that the number of unpaired electrons in γ-Mn_2O_3 per formula unit, $Mn_{8/3}O_4$, is 8.64 or about 69.12 per spinel unit cell. This suggests that at least two electrons per formula unit are paired,

TABLE I

EFFECTIVE NUMBER OF UNPAIRED ELECTRONS PER
MANGANESE IONS IN γ-Mn_2O_3 AND Mn_3O_4

Substance	Structure	Curie-Weiss θ (°K.)	n(exptl.)
γ-Mn_2O_3	Defect pseudo-spinel	~150	3.24
Mn_3O_4	Pseudo-spinel	~160	3.02

TABLE II

UNIT CELL DIMENSIONS OF SOME MANGANITES

Substance	a in Å.	c in Å.	c/a
$CdMn_2O_4{}^a$	8.22	9.87	1.20
Mn_3O_4	8.15	9.44	1.16
γ-Mn_2O_3	8.15	9.44	1.16
$MgMn_2O_4{}^a$	8.07	9.28	1.15
$ZnMn_2O_4$	8.10	9.25	1.14

^{a} A. P. B. Sinha, N. R. Sanjana and A. B. Biswas, *Acta. Cryst.*, in press.

which affords a clue to the nature of the vacancy

(6) E. J. W. Verwey and J. H. deBoer, *Rec. trav. chim.*, **55**, 531 (1936).

(7) K. P. Sinha, Ph.D. Thesis, Poona University, 1956.

(8) L. C. F. Blackman, *J. Elect.*, **1**, 64 (1955).

(9) W. E. Henry and M. J. Boehm, *Phys. Rev.*, **101**, 1253 (1956).

(10) E. W. Gorter, *Philips Res. Rep.*, **9**, 295 (1954).

(11) Since this subject will be discussed in a future note, it is not considered in detail here.

(12) J. B. Goodenough and A. L. Loeb, *Phys. Rev.*, **98**, 391 (1955). For a list of hybridized orbitals see G. E. Kimball, *J. Chem. Phys.*, **8**, 188 (1940).

(13) T. E. Moore, M. Ellis and P. W. Selwood, *J. Am. Chem. Soc.*, **72**, 856 (1952).

distribution. No electronic configuration of cations and with vacancies at tetrahedral sites can possibly lead to theoretical spin values consistent with the observed magnetic value of 8.64 unpaired electrons per $Mn_{8/3}O_4$ molecule. If we picture the cation configuration at octahedral sites as Mn^{3+} [↑|↑|↑|↑| |] , at tetrahedral sites as Mn^{3+} [↑↓|↑|↑| |] and keep all the cation vacancies at octahedral sites, the number of unpaired electrons comes out to be $13^{1}/_{3} \times 4 + 8 \times 2 = 69.3$ per unit cell or 8.66 per formula unit. Thus, since this postulated arrangement is consistent with magnetic data, it may reasonably be concluded that there are no vacancies at tetrahedral sites, as has been suggested by Goodenough and Loeb[12] but that, on the contrary, these are distributed among the octahedral sites, the correct formula thus being $Mn^{3+}[Mn^{3+}_{5/3}\square_{1/3}]O_4^{2-}$. X-Ray data also support this conclusion and, since additional reflections are absent, there does not seem to be an ordered distribution of vacancies at octahedral sites. Furthermore, the ions at these sites maintain their coplanar square bond formation

Mn^{3+} [↑|↑|↑|↑|↑↓] [↑↓] [↑↓|↑↓] and, in addition, the ions at tetrahedral sites will by virtue of their changed electronic configuration give rise to a sort of irregular tetrahedral empty hybrid bond d^2sp depicted as Mn^{3+} [↑↓|↑|↑|↑↓|↑↓] [↑↓] [↑↓] . Since the tetrahedrons in γ-Mn_2O_3 are irregular this view may be regarded as more plausible than the assumption of sp^3 bonding.

For Mn_3O_4, Table I indicates that the number of unpaired electrons per molecule is about 9. If in $Mn^{2+}[Mn_2^{3+}]O_4^{2-}$ all the manganese ions had unpaired electrons, the total number would be 13. It follows that four electrons per molecule are paired. Since in view of the tetragonality of the structure, the Mn^{3+} ions at octahedral sites must take part in covalent square-bond formation, its electronic configuration should remain Mn^{3+} [↑|↑|↑|↑| |] . The pairing would therefore occur in Mn^{2+} at tetrahedral sites giving Mn^{2+} [↑↓|↑↓|↑| |] . The two empty d orbitals would again take part in the d^2sp tetrahedral empty hybrid bond formation. Thus it appears that the same coördinate covalent bonding mechanism is present in both γ-Mn_2O_3 and Mn_3O_4, i.e., dsp^2 square bonds at octahedral sites and d^2sp irregular tetrahedral bonds at tetrahedral sites. Furthermore, the tendency for empty d^2sp hybrid bond formation in these compounds seems to be so strong that some of the electrons of ions at tetrahedral sites get paired to give two empty d orbitals. Examples of such pairing of 3d electrons, in apparent violation of Hund's rule, are found in some nickel complexes having square bonds[14] and in antiferromagnetic superexchange coupling in some

rhombohedral sesquioxides.[15,16] Thus the crystal electric field also seems to influence this distribution of electrons over the 3d orbitals.

The ideal condition of bonding giving rise to tetragonal distortion seems to be attained when all the tetrahedral cations show d^2sp bonds and when octahedral cations enter into dsp^2 square type bonding. Both Mn_3O_4 and γ-Mn_2O_3 satisfy these conditions and have the axial ratio $c/a = 1.16$, which may be taken as a standard value. The axial ratios of some of the tetragonal manganites with normal spinel type structure are given in Table II. In the case of $CdMn_2O_4$ the axial ratio is $c/a = 1.20$. In virtue of the large size of the Cd^{2+} ion and its tendency to form tetrahedral covalent bonds, a larger contribution of the irregular bonds (presumably spd^2 in this case) is to be expected with a corresponding increase in the axial ratio. For others, where the tendency for the cations at tetrahedral sites to form d^2sp tetrahedral bond is less the c/a ratio decreases accordingly. The hypothesis of Goodenough and Loeb that the axial ratio is maximum when only the octahedral cations are covalently bound, and decreases with increasing amount of covalence at tetrahedral sites seems to be arbitrary and is at variance with the experimental values particularly for $CdMn_2O_4$.

γ-Cr_2O_3.—γ-Cr_2O_3 is an unstable phase of the normal α-Cr_2O_3 and is not found free in nature. Its existence was first reported in the dehydrated products of $CrOOH$[17]; no magnetic data are available. X-Ray data alone must therefore be relied on for assessing the vacancy distribution in this compound. The crystal structure of γ-Cr_2O_3 is cubic spinel type with $a = 8.36$ Å. There are no forbidden reflections in the diffraction patterns; thus it would appear that the vacancies are distributed randomly, either at octahedral or tetrahedral sites, or both. The intensities of some of the important reflections were calculated for these three distributions and compared with those observed by the above workers. The results are set out in Table III. The best fit between the observed and calculated values is for the case when all the vacancies are in octahedral positions. It is therefore concluded that, as in γ-Fe_2O_3 and γ-Mn_2O_3, the vacancies in γ-Cr_2O_3 are predominantly distributed among the octahedral sites. However, unlike γ-Fe_2O_3 and like γ-Mn_2O_3 there is no superstructure of vacancies and the distribution is random. Thus γ-Cr_2O_3 may be assigned the formula $Cr^{3+}[Cr^{3+}_{5/3}\square_{1/3}]O_4^{2-}$.

γ-Al_2O_3.—γ-Al_2O_3 is a cubic spinel with $a = 7.94$ Å. Various forms of aluminas obtained by dehydrating a variety of alumina hydrates at different temperatures have been reported in literature.[18] The differences in these aluminas noted by these authors may be due to the degree of dehydration and their order–disorder states with respect to the cation distribution. Even for γ-Al_2O_3 the reported

(14) K. S. Pitzer, "Quantum Chemistry," Prentice-Hall, New York, N. Y., 1953.

(15) Y. Y. Li, Phys. Rev., 102, 1015 (1956).

(16) D. Polder, Physica, 9, 709 (1942); J. Phys. Radium, 12, 174 (1951).

(17) A. W. Laubengayer and H. W. McCune, J. Am. Chem. Soc., 74, 2362 (1952).

(18) A. Stumpf et al., Ind. Eng. Chem., 42, 1398 (1950).

intensities depend much on the history of the preparation of the samples. The most reproducible form of γ-Al_2O_3, as judged by X-ray and electron diffraction, was obtained by oxidizing in air thin films of aluminum at about 800°.[7] Similar calculations as for γ-Cr_2O_3 were made for this case and the calculated intensity values are set out in Table IV together with the observed values.

Table III

Observed and Calculated Intensities for Various Distributions of Vacancies in γ-Cr_2O_3

γ-Cr_2O_3, $u = 0.383$, $a = 8.36$ Å.

hk	Vacancies in oct. sites	I, calcd. Vacancies in tet. sites	Vacancies randomly distributed	X-Ray intensity (visual impression)
111	4.7	36	11.7	Absent
220	33.8	17	27.7	W
311	100	100	100	VS
222	2.4	8.3	4.0	Absent
400	21.1	43.4	27.4	W
440	55.4	61	57	M

Table IV

Observed and Calculated Intensities for Various Distributions of Vacancies in γ-Al_2O_3

γ-Al_2O_3, $a = 7.94$ Å., $u = 0.383$

hkl	Vacancies in oct. sites	I, calcd. Vacancies in tet. sites	Vacancies randomly distributed	X-Ray intensity (visual impression)
111	10.6	45.2	19.4	Absent
220	38.8	17.7	31.9	M
311	108	98	105	VS
222	6.8	1.8	4.8	W
400	62.5	95.1	72.2	MS
331	0.5	1.5	0	Absent
422	16.1	7.1	12.6	W
440	100	100	100	VS

The absence of the 111 reflection is significant and almost rules out the possibility of vacancies in tetrahedral positions. There is a fair over-all agreement between the experimental intensities and those calculated on the assumption of the vacancies predominating at octahedral sites. This may indicate a random distribution of vacancies at octahedral positions. Certainly, the possibility of a statistical vacancy distribution both at octahedral and tetrahedral positions cannot be ruled out in the light of the existing data. However, in view of the known distribution in other defect spinels the tentative formula $Al^{3+}[Al^{3+}_{5/3}\square_{1/3}]O_4^{2-}$ may be assigned to γ-Al_2O_3.

Conclusion

X-Ray, electron diffraction and magnetic data for defect spinel type oxides indicate that the cation vacancies predominate among the octahedral positions. In γ-Fe_2O_3 there is an ordered distribution of the vacancies at octahedral sites probably around the cell center. In γ-Mn_2O_3, γ-Cr_2O_3 and γ-Al_2O_3 the vacancies are randomly distributed among the octahedral positions and an ordered superstructure of vacancies is apparently lacking in these oxides.

The tetragonal symmetry of γ-Mn_2O_3 and Mn_3O_4 is to be attributed to the ability of Mn^{3+} ions at octahedral sites to form dsp^2 empty hybrid square bonds with the overlapping oxygen orbitals, the tetragonal structure being further stabilized as a result of the formation by the Mn^{3+} and Mn^{2+} ions of d^2sp irregular tetrahedral bonds at tetrahedral positions. The ideal axial ratio of $c/a = 1.16$ seems to be attained when both these bonding mechanisms are operative.

HEAT CAPACITIES AT LOW TEMPERATURES, ENTROPY AND ENTHALPY INCREMENTS OF FOUR NICKEL–ZINC FERROSPINELS[1]

By Edgar F. Westrum, Jr., and D. M. Grimes

Contribution from the Departments of Chemistry and of Electrical Engineering of the University of Michigan, Ann Arbor, Michigan

Heat capacities from 5° to above 300°K. were determined on synthetic samples of $Ni_{1-x}Zn_xFe_2O_4$ with $x = 0.6, 0.7, 0.8$ and 0.9 to test a hypothesis of Yafet and Kittel concerning triangular transformations. The normal sigmoid dependence of heat capacity on temperature is modified by ferrimagnetic contributions, and an antiferromagnetic transformation near 10°K. becomes increasingly more pronounced with increasing zinc content. Thermodynamic functions have been evaluated from the data presented.

Spinel minerals are fairly common and include important ores. Synthetic ferrospinels (ferrites) possess interesting electromagnetic properties and are technologically significant components of high frequency electrical circuits. Despite these facts, thermal data extending to liquid helium temperatures (and thereby permitting a more accurate eval-

uation of the thermodynamic properties) are available probably only for zinc ferrite ($ZnFe_2O_4$).[2] Heat capacity data above 50°K. have, however, been published for more than twelve others,[3] and measurements on magnetite over the range 1.8 to 4.2°K. recently have been published.[4]

(1) Presented at the Ninth Annual Calorimetry Conference in Schenectady, New York, on September 18, 1954. This work was supported by the U. S. Army Signal Corps through the Engineering Research Institute of the University of Michigan.

(2) E. F. Westrum, Jr., and D. M. Grimes, *Phys. and Chem. of Solids*, in press.

(3) E. G. King, *J. Chem. Phys.*, **60**, 410 (1956). *Cf.* the references to other works contained therein.

(4) J. S. Kouvel, *Phys. Rev.*, **102**, 1489 (1956).

The gross magnetic properties of the ferrospinels have been explained by Néel[5] in terms of the parallel and antiparallel alignment of the magnetic moments of the ions on two sublattices. For instance, in nickel ferrite ($NiFe_2O_4$), the antiferromagnetic interaction between the moments of the two sublattices gives rise to ferrimagnetism at $0°$; however, in zinc ferrite ($ZnFe_2O_4$), the net spin of the zinc ion is zero and the iron atoms are paramagnetic at this temperature. Mixed nickel–zinc ferrites are ferrimagnetic with a magnetic moment increasing with nickel content over the range studied. For certain ratios of inter- to intra-sublattice interactions, it is anticipated by Yafet and Kittel[6] that the moments of two sub-sublattices composing one of the sublattices will be oriented neither parallel nor antiparallel with each other, but at some intermediate angle. The existence of such a triangular configuration would give rise to the possibility of transitions between triangular and ferrimagnetic or antiferromagnetic states and hence to singularities analogous to Curie and Néel points. Utilizing an experimental evaluation of the exchange interactions by Néel and Brochet[7] for mixed nickel–zinc ferrites ($Ni_{1-x}Zn_xFe_2O_4$), Yafet and Kittel[6] predicted the possible existence of such multiple transitions in mixed nickel–zinc ferrites with $x > 0.7$.

Such transitions should be detected readily at low temperatures by precise heat capacity determinations, for the discontinuities associated with the various types of transitions are well within the range of measurement of modern adiabatic, cryogenic calorimetry. The thermal method has the advantage of avoiding the spurious effects in magnetic measurements occasioned by ferromagnetic impurities. To test the theory of Yafet and Kittel, determination of the heat capacity of Ferramic E, a commercially available ferrite with x approximating 0.6, was first measured. Although no evidence of the anticipated spectrum of transformations was observed, the composition was indeed outside the range specified by Yafet and Kittel.[6] A ferrite of composition $x = 0.8$ was then fabricated and its heat capacity determined. An anomalously high heat capacity in the vicinity of $10°K$. provoked further measurements on additional samples over the range $0.6 \leq x \leq 1.0$. In conjunction with neutron diffraction data[3] it has been established that this anomaly arises as a consequence of the antiferromagnetic–paramagnetic transition in pure zinc ferrite.[2] Although resolution of the magnetic and lattice components of the heat capacity is not yet possible, the thermodynamic data are presented as a contribution to the thermodynamics of solid solutions.

Preparation and Purity of Samples.—Mixed nickel–zinc ferrites, the composition of which may be represented by the empirical formula $Ni_{1-x}Zn_xFe_2O_4$ with $x = 0.6, 0.7, 0.8$ and 0.9, were prepared by milling a slurry of weighed quantities of chemically pure oxides in a steel ball mill for six hours. After drying, the mixture was pressed into 50-g. slugs and fired at 1200° for four hours in air and the temperature then reduced 60°/hr. to about 400° in an oxygen atmosphere.

The slugs were fragmented in a hardened-steel "diamond mortar," annealed in an oxygen atmosphere and cooled at a rate of 60°/hr.

Because of the strong dependence of the heat capacity in the vicinity of $10°K$. upon composition as x approaches unity, especially great care was taken in the preparation technique to obtain a stoichiometric, homogeneous, noninverted sample of zinc ferrite. The details of the fabrication procedure utilized are described elsewhere.[2] Gravimetric chemical analyses for iron and zinc and spectrochemical analyses were made. Stannous chloride oxidation-reduction titrations were made to determine the ferrous iron content of the samples. X-Ray diffraction photographs were taken to establish the phase purity of the samples. The analytical data are presented in Table I.

TABLE I

PREPARATIVE AND ANALYTICAL DATA ON FERRITE SAMPLES

Sample $x =$	Annealing temp. (°C.)	Iron, % Detected	Theor.	Fe^{++}, %
$(0.6)^a$	...	46.9 ± 0.1		0.0 ± 0.1
.6	900	$46.8 \pm .1$	46.84	$.0 \pm .1$
.7	(1200)			$.1 \pm .1$
.8	1200	$46.7 \pm .1$	46.59	$.0 \pm .1$
.9	(1200)			$.0 \pm .1$
1.0^b	1100	$46.24 \pm .1$	46.33	$.0 \pm .1$

^{a} Ferramic E, General Ceramic and Steatite Corp. ^{b} Per cent. zinc found $= 27.2 \pm 0.1$ (theoretical, 27.12).

Cryogenic Technique.—The design and adiabatic method of operation of the Mark I cryostat[9] and calorimeters W-5[10] and W-9[11] have been described. A calorimeter was in turn loaded with sample, evacuated and 2 to 4 cm. of gaseous helium added at 25° to aid in the establishment of thermal equilibrium. Lubriseal stopcock grease was used on calorimeter W-5 for thermal contact between heater, thermometer and calorimeter for determinations on samples with $x = 0.6$ and 0.8 and on Ferramic E. Calorimeter W-9 with Apiezon T grease was employed for the balance of the runs to allow measurement to 350°K. Separate determinations of the heat capacity of the empty calorimeters were made with their respective conductivity greases. The following masses (*vacuo*) of samples were employed in the measurements: $x = 0.6$, 203.434 g.; $x = 0.7$, 164.515 g.; $x = 0.8$, 191.862 g.; $x = 0.9$, 180.265 g.

Temperatures were determined with a capsule-type platinum resistance thermometer (Laboratory Designation A-3) contained in a central well in the calorimeter. It was calibrated by the National Bureau of Standards from 10 to above 373°K. Below this temperature range a provisional scale was employed. It is considered that the thermometer reproduces the thermodynamic temperature scale within 0.1° from 4 to 10°K., within 0.03° from 10 to 90°K., and within 0.05° above 90°K. The ice point was taken as 273.16°K. Calibrated instruments were used in the determination of all the measured quantities including the timing of the energy input.

Heat Capacity Results.—The experimental heat capacity determinations for the four samples of ferrospinels synthesized in this Laboratory are presented in Table II in chronological sequence so that the temperature increments of the individual runs can be inferred from the adjacent mean temperatures. Corrections for curvature (occasioned by the finite temperature increments employed in the measurements) and for the slight differences in the amounts of helium and solder in the measurements on the empty and the full calorimeters have been applied. The data are presented in terms of the defined thermochemical calories of 4.1840 absolute joules and the formula (molal) weight in grams using 1953 International Atomic Weights.

Heat capacities below 50°K. are presented in Fig. 1. Figure 2 compares the heat capacities at higher temperatures with the smooth curve for zinc ferrite[2] in order to amplify the small differences between these curves. On both

(5) L. Néel, *Ann. phys.*, **3**, 137 (1948).

(6) Y. Yafet and C. Kittel, *Phys. Rev.*, **87**, 290 (1952).

(7) L. Néel and P. Brochet, *Compt. rend.*, **230**, 280 (1950).

(8) J. M. Hastings and L. M. Corliss, *Phys. Rev.*, **102**, 1460 (1956); *Rev. Mod. Phys.*, **25**, 114 (1953).

(9) E. F. Westrum, Jr., and A. F. Beale, Jr. (to be published).

(10) G. A. Burney and E. F. Westrum, Jr. (to be published).

(11) E. Greenberg and E. F. Westrum, Jr., *J. Am. Chem. Soc.*, **78**, 4526 (1956).

TABLE II
MOLAL HEAT CAPACITIES OF NICKEL ZINC FERROSPINELS
(in cal. degree⁻¹ g.-mole⁻¹)

$Ni_{0.4}Zn_{0.6}Fe_2O_4$ (mol. wt. = 238.404 g.)

T, °K.	C_p	T, °K.	C_p	T, °K.	C_p
Series I		219.59	29.73	10.00	0.2317
		228.65	30.01	11.11	.2569
63.23	6.324	237.58	31.41	12.38	.2950
69.11	7.354	246.56	32.19	13.77	.3415
75.83	8.556	255.62	32.91	15.27	.4018
83.16	9.900	264.65	33.62	16.86	.4653
91.49	11.418	273.70	34.30	18.52	.5393
90.54	11.255	282.71	34.92	20.28	.6274
98.30	12.613	291.70	35.52	22.17	.7363
106.78	14.100	300.83	36.09	24.37	.8862
115.28	15.589			26.80	1.073
123.12	16.933	Series II		29.37	1.304
130.70	18.189			32.14	1.591
138.60	19.456	4.50	0.068	35.29	1.956
147.06	20.77	4.87	.066	38.67	2.394
155.74	22.06	5.65	.085	42.16	2.879
164.52	23.30	4.75	.070	46.10	3.468
173.47	24.51	5.58	.082	50.74	4.204
182.58	25.65	5.49	.080	55.57	5.003
191.87	26.77	6.66	.105	60.34	5.818
201.18	27.83	7.87	.142	65.57	6.376
210.40	28.83	8.96	.184		

$Ni_{0.3}Zn_{0.7}Fe_2O_4$ (mol. wt. = 239.073 g.)

T, °K.	C_p	T, °K.	C_p	T, °K.	C_p
Series I		237.48	31.21	335.70	37.43
		247.58	32.07	345.83	37.84
35.79	2.522	257.62	32.86		
39.51	2.997	267.72	33.59		
48.00	4.276	277.94	34.29	Series III	
53.47	5.202	288.21	34.92		
58.77	6.093	298.73	35.55	5.71	0.142
64.43	7.079	309.38	36.16	6.58	.188
70.56	8.133	319.94	36.77	7.59	.300
77.46	9.330			8.56	.376
84.48	10.608	Series II		9.47	.444
91.47	11.826			10.33	.4923
99.32	13.162	173.08	24.45	11.30	.5186
107.50	14.567	182.60	25.62	12.41	.5713
115.56	15.917	192.25	26.75	13.65	.6353
123.76	17.273	201.97	27.81	15.10	.7055
132.32	18.646	211.82	28.84	16.75	.7946
140.88	19.962	221.95	29.81	18.55	.8878
149.47	21.25	232.37	30.76	20.42	1.0014
158.52	22.52	242.87	31.68	22.32	1.1307
168.10	23.82	253.32	32.51	24.43	1.2913
177.84	25.07	263.78	33.29	27.06	1.5209
187.66	26.25	274.26	34.02	30.05	1.8177
197.62	27.38	284.62	34.70	33.43	2.208
207.21	28.38	294.90	35.34	36.94	2.660
207.31	28.38	305.22	35.93	40.31	3.132
217.42	29.38	315.47	36.48	44.10	3.690
227.23	30.32	325.60	36.94	48.11	4.324

$Ni_{0.2}Zn_{0.8}Fe_2O_4$ (mol. wt. = 239.742 g.)

T, °K.	C_p	T, °K.	C_p	T, °K.	C_p
4.95	0.152	33.87	2.581	156.53	22.17
5.45	.154	37.27	3.023	165.21	23.31
5.94	.269	41.13	3.561	174.01	24.46
6.55	.438	45.42	4.196	182.75	25.48
7.49	.578	49.92	4.913	191.53	26.46
8.70	.721	54.87	5.728	200.38	27.42
9.91	.846	60.66	6.694	209.27	28.30
11.17	.8773	67.19	7.809	210.47	28.41
12.50	.9387	73.80	8.934	219.36	29.23
14.02	1.010	80.35	10.086	228.17	30.00
15.66	1.091	87.37	11.326	237.02	30.73
17.35	1.174	95.11	12.623	245.89	31.46
19.15	1.266	103.38	14.045	254.64	32.08
21.05	1.383	112.09	15.437	263.23	32.71
23.15	1.529	121.39	16.956	271.68	33.23
25.46	1.705	130.54	18.392	280.14	33.76
27.98	1.932	139.40	19.736	288.75	34.25
30.76	2.218	148.06	21.01	297.66	34.71

$Ni_{0.1}Zn_{0.9}Fe_2O_4$ (mol. wt. = 240.411 g.)

T, °K.	C_p	T, °K.	C_p	T, °K.	C_p
Series I		12.56	1.6665	94.52	12.191
		13.71	1.6839	101.80	13.372
6.22	0.330	15.33	1.6961	109.70	14.646
6.48	0.494	17.28	1.7102	118.99	16.123
7.08	0.688	19.34	1.7375	128.10	17.544
7.76	1.29	21.37	1.7923	136.30	18.770
8.54	1.53	23.49	1.8782	144.47	19.950
9.29	1.62	25.88	2.008	153.07	21.15
10.00	1.7283	28.31	2.175	162.33	22.37
11.32	1.6868	30.90	2.400	172.04	23.58
		33.91	2.706	181.55	24.70
Series II		37.40	3.111	190.90	25.73
		41.55	3.650	200.43	26.72
5.66	0.353	46.25	4.319	210.27	27.67
5.93	.543	51.44	5.109	220.43	28.59
6.27	.584	56.87	5.958	230.85	29.48
6.59	.647	61.98	6.800	241.44	30.32
6.98	.764	67.43	7.686	252.14	31.10
7.43	1.000	73.39	8.662	262.75	31.82
7.89	1.21	80.18	9.809	273.26	32.48
8.28	1.37	87.50	11.050	283.77	33.10
8.73	1.50	95.15	12.296	294.16	33.68
9.23	1.63			304.19	34.20
9.75	1.72	Series III		314.78	34.74
10.33	1.7323			324.97	35.15
10.90	1.6768	80.54	9.866	335.16	35.59
11.61	1.6651	87.37	11.023	345.44	35.98

plots the points indicated represent the individual determinations, and the heat capacities of Ferramic E and zinc ferrite[2] have been included for comparison. The significant features are: (1) the sharp antiferromagnetic–paramagnetic transition in zinc ferrite at about 9.7°K. which obviously persists in the mixed ferrospinels at approximately the same temperature, but decreases in intensity with increasing nickel content; and (2) the absence of other peaks or fluctuations in the curves. No singularities of the type predicted by Yafet and Kittel[6] were observed. The ferrimagnetic contributions to the thermal properties cannot at present be quantitatively resolved from those of the lattice.

Thermodynamic Functions.—The entropies and enthalpy increments computed by numerical quadrature from large scale plots of the heat capacity are provided at selected temperatures in Table III. Nuclear spin and isotope mixing contributions have not been included in the entropy. Extrapolation below about 5°K. was made with the Debye limiting law. The estimated probable error in the entropy increment is ±0.06 e.u. and that in the enthalpy increment is ±0.1%. More extensive tabulation of the temperature dependence of the thermodynamic functions of these four ferrites have been prepared.[12]
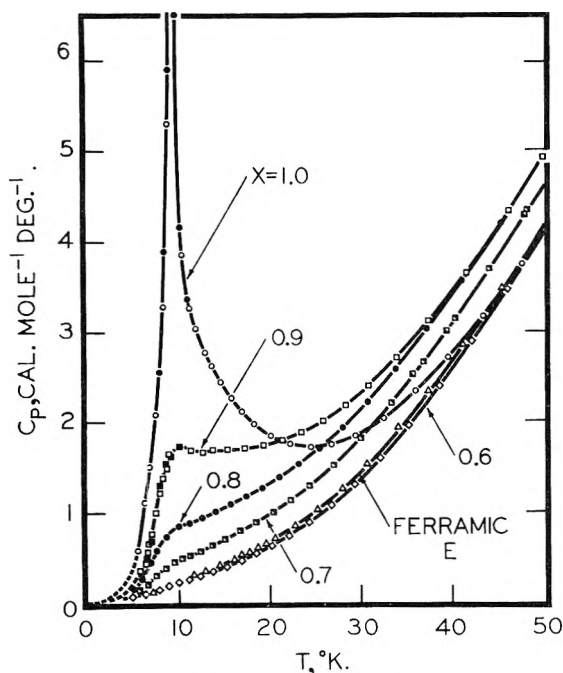
Fig. 1.—Molal heat capacity *vs.* temperature for six samples of $Ni_{1-x}Zn_xFe_2O_4$ compositions below 50°K.
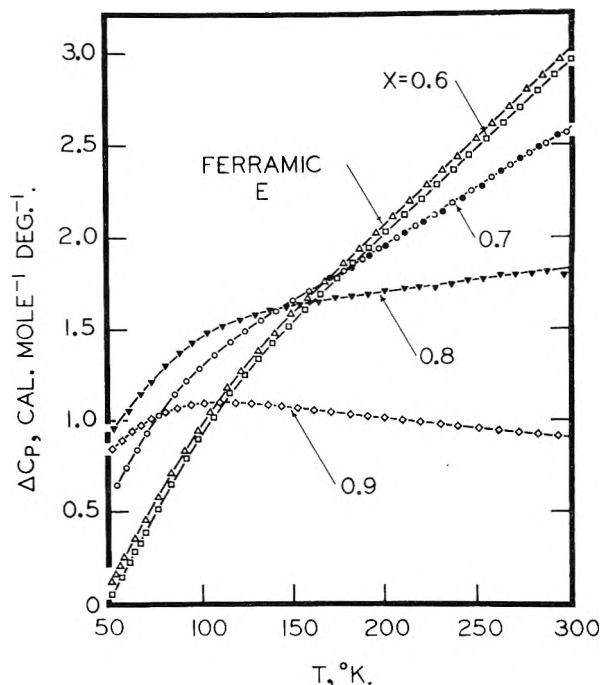

Fig. 2.—Deviation of the experimental molal heat capacity points of $Ni_{1-x}Zn_xFe_2O_4$ from the $ZnFe_2O_4$ smooth curve over the range 50 to 300°K. ($\Delta C_p = C_{pFerrospinel} - C_{pZnFe_2O_4}$).

If the nickel ions occupy B sites and zinc ions occupy A sites, then the configurational entropy resulting from mixing zinc and iron ions at random on the A sites is given by

$$S_A = -R \ln [x^x (1 - x)^{1-x}]$$

and the configurational entropy resulting from mixing zinc and iron ions at random on the B sites is given by

$$S_B = -R \ln [4^{-1}(1 - x)^{1-x}(1 + x)^{1+x}]$$

The sum of these two expressions represents an upper bound to the zero-point entropy and amounts to $0.72R$, $1.15R$, $1.46R$ and $1.67R$ for $x = 0.9, 0.8, 0.7$ and 0.6, respectively. The actual entropy at 0°K. will be less than the above due to the mutual ordering effects of the A and B sublattices by the electrical interactions between them.

Acknowledgment.—The authors express their appreciation to Prof. H. W. Welch, Jr., for his interest in this problem, to Clinton Jefferson and J. W. Kuiper for their preparation of the calorimetric samples and some of the analytical studies,

Table III
Molal Entropy and Enthalpy Increments of Nickel–Zinc Ferrospinels

T, °K.	$x = 0.6$	$x = 0.7$	$x = 0.8$	$x = 0.9$
	$S° - S_0^°$ (cal. deg.$^{-1}$ g.-mole^{-1})			
10	0.077	0.156	0.196	0.737
15	.197	.388	0.574	1.419
25	.507	.880	1.243	2.322
50	1.995	2.701	3.283	4.438
100	7.501	8.544	9.298	10.317
200	21.392	22.533	23.275	23.929
300	34.362	35.416	35.960	36.291
298.16	34.140	35.196	35.746	36.082
	$H° - H_0^°$ (cal. g.-mole^{-1})			
10	0.58	1.50	2.87	5.42
15	2.09	4.40	7.58	13.84
25	8.39	14.30	20.92	31.63
50	66.59	84.65	99.18	112.15
100	489.11	531.2	557.7	559.8
200	2579.0	2632.6	2655.3	2602.8
300	5806.5	5837.0	5809.0	5675.9
298.16	5740.3	5771.5	5745.0	5613.5

to George Grenier and John J. McBride for assistance with the heat capacity measurements and to Emilia R. Martin for the calculations.

POLAROGRAPHIC BEHAVIOR OF CHLORANILIC ACID[1]

By Joseph Weissbart[2a] and Pierre Van Rysselberghe[2b]

Department of Chemistry, University of Oregon, Eugene, Oregon

Received December 26, 1956

On the basis of several criteria of reversibility it is found that chloranilic acid behaves reversibly at the dropping mercury electrode. A plot of log $((i_d - i)/i)$ vs. potential gives the required value of 2 for the number of electrons involved in the electrode process. Cathodic, anodic and mixed anodic–cathodic waves exhibit practically the same half-wave potential at a given pH. The plot of the half-wave potential vs. pH consists of three linear segments connected by smooth curves. From the intersections of the linear segments the dissociation constants K_1 and K_2 are obtained for the chosen total ionic strength of 1.0. The diffusion current is found to be proportional to concentration over a 500-fold concentration range. The pH of the solution appears to have no effect on the diffusion current. By using the Ilkovic equation it is found that the average diffusion coefficient for the various reducible forms of chloranilic acid is 1.04×10^{-5} cm.^{2} sec.$^{-1}$

Introduction

The oxidation–reduction potential of chloranilic acid (2,5-dichloro-3,6-dihydroxy-p-benzoquinone) was first measured by Conant and Lutz.[3] They dissolved small amounts of the acid in buffered solutions, added enough reducing agent to convert approximately one-half of the acid to its reduced form and measured the corresponding potential of a noble metal electrode. Conant and Fieser[4] redetermined this potential in aqueous solutions and in 95 and 50% ethyl alcohol–water mixtures. Schwarzenbach and Suter[5] determined the empirical "redox potential" of chloranilic acid in buffered solutions at constant ionic strength and obtained the acid dissociation constants K_1 and K_2 on the basis of the change of this empirical "redox potential" with pH, a potentiometric titration with a reducing agent being carried out for each pH value.

Chloranilic acid solutions exposed to air are stable, the acid being then entirely in its oxidized red-colored form. Upon chemical reduction, by sodium hydrosulfite for example, the acid is decolorized but rapidly reverts to its oxidized form, unless care is taken to prevent contact with oxygen. Applying to chloranilic acid a spectrophotometric method for the determination of overlapping dissociation constants of dibasic acids (valid for K_1/K_2 smaller than 1000) Thamer and Voigt[6] obtained values of K_1 and K_2 in rather poor agreement with those reported by Schwarzenbach and Suter,[5] although the potentiometrically derived values of the latter authors were claimed to agree with parallel spectrophotometrically obtained results. Some uncertainty concerning the exact ionic strength used by the Swiss authors may account for part of the discrepancy (see Table I). The interest of Thamer and Voigt[6] in chloranilic acid was due to their previous investigations on zirconium chloranilate complexes.[7] For a similar reason (possibility of determining zirconium in solution by polarographic

measurement of the excess chloranilic acid after precipitation of zirconium chloranilate) and on account of the uncertainty as to the values of K_1 and K_2 we undertook the polarographic investigation reported here. Breyer[8] has observed the reduction of chloranilic acid at the dropping mercury cathode (d.-m.e.) in the range of 9×10^{-3} to 4×10^{-4} M, while Breyer and McPhillips[9] used chloranilic acid in the indirect determination of calcium based upon the wave heights of the remaining acid. They reported well-defined waves in the range 1×10^{-3} to 3.3×10^{-4} M.

Having recognized early in our work that the behavior of chloranilic acid at the d.m.e. was essentially reversible we were able to carry out a detailed examination of the variation of the half-wave potential with pH, to establish the corresponding values of pK_1 and pK_2, which are compared with previous values in Table I, and in addition to determine the concentration and pH ranges within which wave height and concentration are proportional to each other.

TABLE I
Comparison of Values of pK_1 and pK_2 for Chloranilic Acid at 25°

	Schwarzenbach and Suter[5]	Thamer and Voigt[6]	Present paper
pK_1	0.85	1.08	1.22
pK_2	3.18	2.42	3.01

Experimental

Apparatus.—All polarograms were taken with a Sargent Model XXI Recording Polarograph. In some phases of the work small Erlenmeyer electrolysis cells of the Heyrovsky type were used, while in other phases H cells of the Lingane–Laitinen type were used. In the former case a large mercury pool served as unpolarizable electrode, its potential being measured against a saturated KCl–calomel electrode. In the latter case either a S.C.E. or a saturated K_2SO_4–Hg_2-SO_4 electrode occupied one arm of the cell, the connection with the other arm containing a coarse sintered glass disc with an agar plug. The 6% agar solution was saturated with KCl or mixed with 4 M NH_4NO_3 in the case of runs with the sulfate electrode. The use of the sulfate electrode was necessary whenever polarographic waves were recorded on the positive side of the S.C.E. We found the sulfate electrode to be at all times, before and after the recording of polarograms, at +0.406 v. with respect to the S.C.E. The cells were immersed in a water thermostat kept at 25 ± 0.02°. The various capillaries used had an $m^{2/3}t^{1/6}$ product in the neighborhood of 1.6 mg.$^{2/3}$ sec.$^{-1/2}$ (see for instance Table III below).

Reagents.—All reagents used as supporting electrolytes or in the preparation of buffers were either of C.P. or analytical grade. Chloranilic acid was a practical grade (yellow

(1) From a thesis submitted by Joseph Weissbart to the Graduate School of the University of Oregon in partial fulfillment of the requirements for the Ph.D. degree, June 1956.

(2) (a) Westinghouse Research Laboratories, Pittsburgh, Pennsylvania. (b) Department of Chemistry, Stanford University, Stanford, California.

(3) J. B. Conant and R. E. Lutz, *J. Am. Chem. Soc.*, **46**, 1257 (1924).

(4) J. B. Conant and L. F. Fieser, *ibid.*, **46**, 1867 (1924).

(5) G. Schwarzenbach and H. Suter, *Helv. Chim. Acta*, **24**, 617 (1941).

(6) B. J. Thamer and A. I. Voigt, This Journal, **56**, 225 (1952).

(7) B. J. Thamer and A. I. Voigt, *J. Am. Chem. Soc.*, **73**, 3197 (1951).

(8) B. Breyer, *Australian J. Sci.*, **16**, 109 (1953).

(9) B. Breyer and J. McPhillips, *Analyst*, **78**, 666 (1953).

label) Eastman Kodak Co. product and was purified by the method of Thamer and Voigt.[6] The standard buffers either were bought from the Sargent Co. or prepared according to the recommendations of Lingane.[10] Table II below gives the composition of the buffers and the salts added to make up the constant ionic strength of 1.0 which we used in most of our work. The pH values were measured with a glass electrode–Beckman Model G pH-meter combination. Purified nitrogen was passed through the cells to remove dissolved oxygen.

Procedure.—The $E_{1/2}$ values were determined by interpolation between the initial and final potentials of the wave, these being measured by means of an external potentiometric circuit. The voltage scale was expanded to approximately 2.5 mv. per division on the recording paper. The $E_{1/2}$ values were reproducible within 1 mv., the required Ri correction being made in each case. In experiments carried out at a pH of or near 3.6 for the purpose of determining the diffusion current i_d gelatin in amounts varying from 0.01 to 0.05% had to be used to suppress a maximum in the waves. Residual current corrections were made in the i_d determinations and, on account of the slow decomposition of chloranilic acid occurring on standing, the i_d values were all obtained with freshly prepared solutions.

Results and Discussion

Reversible Behavior.—The reversibility of a polarographic oxidation–reduction reaction can be established by determining the $E_{1/2}$ values of cathodic, anodic and mixed anodic–cathodic waves observable in a given medium (with application of the proper Ri corrections) and verifying their coincidence. When half of the total concentration of the substance under study is in its oxidized form and the other half in its reduced form no Ri correction is necessary since i_d is then exactly, or close to zero. This method furnishes the most reliable criterion of reversibility. The corresponding equations have been given by Kolthoff and Lingane,[11] and by others.

Anodic waves were obtained after first reducing the chloranilic acid with an excess of sodium hydrosulfite. Mixed anodic–cathodic waves were obtained by adding enough sodium hydrosulfite exactly to decolorize the solution and exposing the solution to the oxygen of the air for different time intervals before taking the polarograms.

The $E_{1/2}$ values of cathodic, mixed anodic–cathodic and anodic waves of chloranilic acid were found to coincide. For a concentration of 1×10^{-3} M and a pH of 3.61, the $E_{1/2}$ value was found to be -0.098 ± 0.003 volt vs. S.C.E.

We can regard this test of reversibility as satisfactory. We also used the test based on a plot of $\log ((i_d - i)/i)$ against the potential of the d.m.e. The recording of the polarogram for 2×10^{-3} M chloranilic acid in a buffer of pH 4.71 was interrupted at nine points along the rising portion of the wave, the corresponding potential being measured with the external potentiometric circuit. The average current reading at each point was corrected for the residual current. An excellent linear plot was obtained with a slope corresponding to 1.97 ± 0.05 or 2 electrons for the reduction of one molecule of chloranilic acid, as expected.

The proportionality of the diffusion current to the square root of the corrected height of the mer-

cury column was rigorously verified in the case of 10^{-3} M chloranilic acid in 0.1 N H_2SO_4.

The variation of $E_{1/2}$ with pH was found to give the theoretically expected slopes in the various pH regions. This is discussed in the next section in connection with the determination of the acid dissociation constants.

Acid Dissociation Constants.—The determination of oxidation–reduction potentials as half-wave potentials of polarographic waves is particularly convenient in the case of a quinone system such as chloranilic acid. The usual assumption about the equality of the diffusion coefficients of oxidized and reduced forms has of course to be made and the activity coefficients, made practically constant through the use of a constant total ionic strength, are incorporated into the $E_{1/2}$ values. Let us represent chloranilic acid by the formula H_2Q. At the d.m.e. the reduction

$$H_2Q + 2H^+ + 2e^- \rightleftharpoons H_4Q \tag{1}$$

occurs. The dissociation of the very weak acid H_4Q is neglected, but H_2Q dissociates as

$$H_2Q \rightleftharpoons H^+ + HQ^- \tag{2}$$

$$HQ^- \rightleftharpoons H^+ + Q^{--} \tag{3}$$
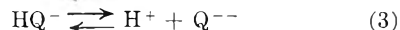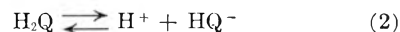
According to the treatment of Clark and Cohen,[12] representing by (Ox) the sum of the concentrations of the reducible species H_2Q, HQ^- and Q^{--}, and by (Red) the concentration of the oxidizable species H_4Q, the Nernst equation takes the form

$$E = E^0 + (RT/2F) \ln [(Ox)/(Red)] + (RT/2F) \ln (H^+)^4 - (RT/2F) \ln [(H^+)^2 + K_1(H^+) + K_1K_2] \tag{4}$$

At the half-wave (Ox) = (Red) and we have

$$E_{1/2} = E^0_{1/2} + (RT/2F) \ln (H^+)^4 - (RT/2F) \ln [(H^+)^2 + K_1(H^+) + K_1K_2] \tag{5}$$

in which K_1 and K_2 are the acid dissociation constants corresponding to equations 2 and 3.

Polarograms were taken for 10^{-3} M chloranilic acid in buffers in the pH range from 0.40 to 7.11, the total ionic strength being 1.0 in all cases. The $E_{1/2}$ values reported in Table II were found. When plotted against pH (Fig. 1) they are seen to align themselves along three linear segments and smooth connecting curves. Straight lines of slopes equal, respectively, to 0.059, 0.089 and 0.118 were drawn through the experimental points. The first two intersect at a pH of 1.22 equal to pK_1, while the last two intersect at a pH of 3.01 equal to pK_2. These values are reported in Table I.

Analytical Applications.—We found the diffusion current i_d of cathodic waves of chloranilic acid to be proportional to concentration over a 500-fold range extending from 5×10^{-3} to 1×10^{-5} M. The corresponding experiments were carried out in 0.1 N H_2SO_4 and in a buffer of pH 3.62. The results are reported in Table III. Different capillaries were used in the two series of measurements, the ratio $i_d/Cm^{2/3}t^{1/6}$ being found to be 4.05 in the case of the 0.1 N H_2SO_4 solutions and 4.03 in the case of the buffer of pH 3.62.

A possible effect of pH on the value of i_d for a given concentration of chloranilic acid was found to

(10) J. J. Lingane, "Electroanalytical Chemistry," Interscience Publishers, New York, N. Y., 1953.

(11) I. M. Kolthoff and J. J. Lingane, "Polarography," 2nd edition, Interscience Publishers, New York, N. Y., 1952.

(12) W. M. Clark and B. Cohen, U. S. Public Health Reports, **38**, 666 (1923).

TABLE II

VARIATION OF $E_{1/2}$ WITH pH FOR 10^{-3} M CHLORANILIC ACID
IN BUFFERS OF TOTAL IONIC STRENGTH 1.0

Composition	pH	$E_{1/2}$ vs. S.C.E., v.
H₂SO₄ + K₂SO₄	0.40	+0.160
H₂SO₄ + K₂SO₄	0.72	+ .145
H₂SO₄ + K₂SO₄	1.13	+ .123
H₂SO₄ + K₂SO₄	1.53	+ .095
Citric acid + Na₂HPO₄ + NaNO₃	2.07	+ .042
Citric acid + Na₂HPO₄ + NaNO₃	2.26	+ .024
Citric acid + Na₂HPO₄ + NaNO₃	2.50	+ .003
Acetic acid + NaAc + KCl	4.12	− .179
Acetic acid + NaAc	4.67	− .230
Citric acid + Na₂HPO₄ + K₂SO₄	5.12	− .293
Citric acid + Na₂HPO₄ + K₂SO₄	5.98	− .394
Na₂HPO₄ + NaH₂PO₄ + KCl	6.58	− .471
Na₂HPO₄ + NaH₂PO₄ + KCl	6.61	− .468
Na₂HPO₄ + NaH₂PO₄ + KCl	7.11	− .530

TABLE III

PROPORTIONALITY BETWEEN DIFFUSION CURRENT
AND CONCENTRATION

$C =$ $M \times 10^3$	$i_d,$ μa.	i_d/C	Deviation
In 0.1 N H₂SO₄, with $m^{2/3}t^{1/6}$ = 1.59 mg.$^{2/3}$ sec.$^{-1/2}$			
2.0	12.75	6.37	−0.08
1.0	6.43	6.43	− .02
0.10	0.645	6.45	.00
.02	.129	6.45	.00
.01	.066	6.55	+ .10
		Av. 6.45	±0.04
In citric acid + Na₂HPO₄ buffer of pH 3.62, with $m^{2/3}t^{1/6}$ = 1.68 mg.$^{2/3}$ sec.$^{-1/2}$			
5.0	32.80	6.75	−0.16
2.0	13.37	6.69	− .02
1.0	6.75	6.75	+ .04
0.5	0.342	6.84	+ .13
		Av. 6.71	±0.09

be non-existent, as is shown by the data of Table IV. On the basis of the Ilkovic equation we find that the average diffusion coefficient of the reducible
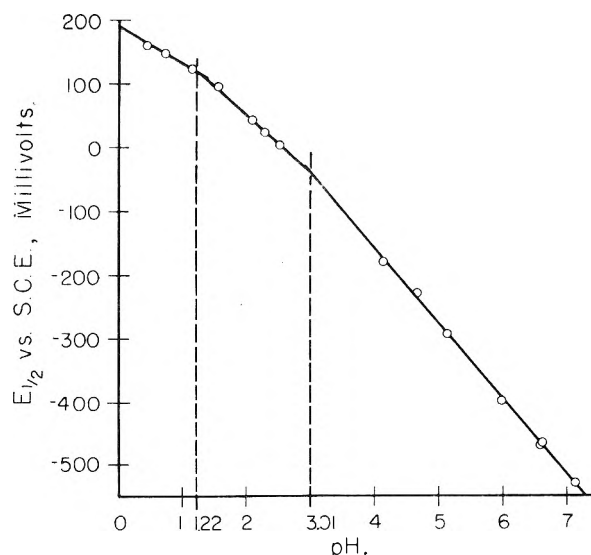

Fig. 1.—Variation of $E_{1/2}$ with pH for 0.001 M chloranilic acid in buffers of ionic strength of 1.0.

TABLE IV

CONSTANCY OF DIFFUSION CURRENT WITH pH FOR 10^{-3} M
CHLORANILIC ACID

pH	$i_d,$ mm.	pH	$i_d,$ mm.
4.32	106	2.44	110
3.89	107	1.82	110
3.48	109	1.70	106
3.30	107	1.23	106
2.88	109	0.91	110
		Av. 108 ± 1.6	

species H₂Q, HQ⁻ and Q⁻⁻ of chloranilic acid is 1.04×10^{-5} cm.² sec.⁻¹.

HIGH TEMPERATURE HEAT CONTENTS OF CALCIUM ORTHOSILICATE

By J. P. COUGHLIN AND C. J. O'BRIEN

Contribution from the Minerals Thermodynamics Experiment Station, Region II, Bureau of Mines, United States Department of the Interior, Berkeley, Cal.

High temperature heat content measurements were made involving four crystalline varieties of calcium orthosilicate. The entropies and heats of the $\beta \rightarrow \alpha'$, $\alpha' \rightarrow \alpha$, and $\gamma \rightarrow \alpha'$ transformations were evaluated. A table of smooth values of heat content and entropy increments above 298.15°K. and algebraic representations of the heat contents are included, for use in thermodynamic calculations.

Introduction.—There are four crystalline varieties of calcium orthosilicate (Ca₂SiO₄) according to the work of Bredig[1] and Trömel and Möller.[2] The designations α, α', β and γ, used by those authors, are adopted here. Two varieties are common at room temperature, β and γ. The β-form is

thermodynamically unstable throughout its temperature range of existence. It transforms at 970°K. into the α'-variety which itself is a metastable modification at this temperature. The γ-variety is the "dusting" form sometimes observed in the manufacture of Portland cement and during cooling of high lime-containing slags. It is the thermodynamically stable form to about 1120°K.

(1) M. A. Bredig. *J. Am. Ceram. Soc.*, **33**, 188 (1950).
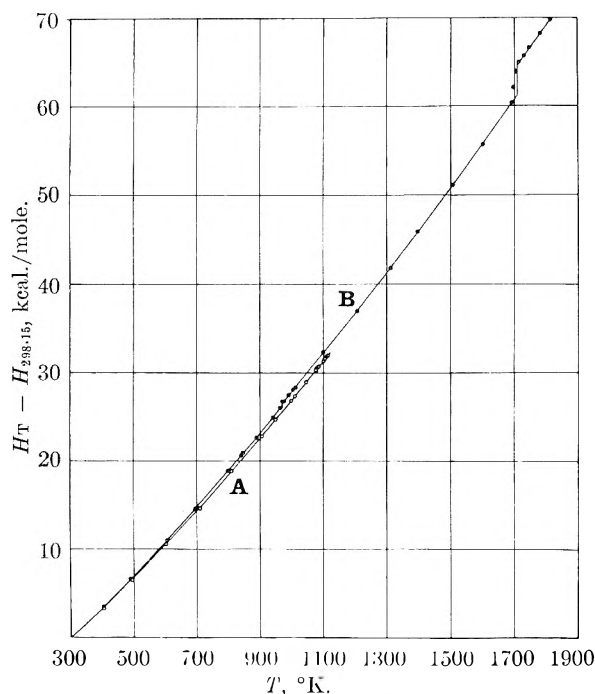(2) G. Trömel and H. Möller, *Fortsch. Mineral.*, **28**, 80 (1949).

Fig. 1.—Heat contents above 298.15°K.: A, $Ca_2SiO_4(\gamma)$; B, $Ca_2SiO_4(\beta,\alpha',\alpha)$.

where it transforms into α'. The α'-variety is thermodynamically stable between 1120 and 1710° K. where it, in turn, transforms into α. The α-variety is stable between 1710°K. and the melting point.

The energy relationships among these crystalline varieties have been known only qualitatively and it is the purpose of the present paper to supply some quantitative data. High temperature heat content measurements of the γ-variety have been conducted from 298 to 1113°K. Measurements starting with the β-variety at 298°K. were carried to 1816°K., data being obtained for the β-, α'- and α-varieties and for the transformations $\beta \rightarrow \alpha'$ and $\alpha' \rightarrow \alpha$. The only previous similar measurements of calcium orthosilicate are those of von Gronow and Schwiete[3] between 293 and 1573°K. Their measurements were made before the inter-relationships among the four varieties were completely unravelled and they leave much to be desired as to accuracy.

Materials.—The β-variety of calcium orthosilicate was part of the sample used by King[4] in heat of formation determinations and by Todd[5] in low temperature heat capacity measurements. The method of preparation, chemical analysis and X-ray diffraction are described by King.[4] The sample contained 64.47% calcium oxide, 34.68% silica, 0.32% aluminum and iron oxides, 0.14 magnesium oxide, and 0.02% water, as compared with the theoretical 65.11% calcium oxide and 34.89 silica.

The γ-variety was prepared from reagent-grade calcium carbonate and silica, using platinum containers. A stoichiometric mixture was made into a paste with water, dried at 1000°, heated 2 hours at 1440°, cooled to 1000° in 1 hour, transferred to a furnace at 500°, and allowed to cool slowly (overnight) to 350°. This process was repeated 4 times, with intervening grinding, mixing, analysis and adjustment of composition. The final product contained 34.88% silica, which is virtually the theoretical amount for pure

(3) H. E. von Gronow and H. E. Schwiete, Z. anorg. Chem., **216**, 185 (1933).

(4) E. G. King, J. Am. Chem. Soc., **73**, 656 (1951).

(5) S. S. Todd, ibid., **73**, 3277 (1951).

calcium orthosilicate. Its X-ray diffraction pattern agreed with that for the γ-variety in the ASTM catalog.

Measurements and Results.—The heat content measurements were conducted with previously described apparatus.[6] Sealed, platinum–rhodium capsules were used to contain the samples during the measurements. The heat contents of the empty capsules were determined in separate experiments. The results for calcium orthosilicate are expressed in defined calories (1 cal. = 4.1840 abs. joules) per mole, the molecular weight being 172.25, in accordance with the 1954–55 Report on Atomic Weights.[7] The measured heat contents are listed in Table I and plotted in Fig. 1.

TABLE I

HEAT CONTENTS OF CALCIUM ORTHOSILICATE ABOVE 298.15°K.

$T,°K.$	$H_T - H_{298.15}$, cal./mole	$T,°K.$	$H_T - H_{298.15}$, cal./mole	$T,°K.$	$H_T - H_{298.15}$, cal./mole
		$Ca_2SiO_4(\gamma)$ (mol. wt., 172.25)			
405.2	3,300	948.8	24,700	1079.4	30,490
494.4	6,470	999.1	26,830	1085.3	30,650
602.3	10,570	1008.6	27,280	1100.1	31,270
704.9	14,580	1045.4	28,900	1104.6	31,540
810.5	18,850	1050.8	29,220	1108.3	31,630
905.7	22,800	1075.2	30,270	1112.9	31,820
		Ca_2SiO_4 (β, α', α) (mol. wt., 172.25)			
406.0	3,540	974.1	26,720	1602.3	55,650
489.0	6,530	977.4	26,880	1690.6	60,410
604.9	10,990	990.4	27,430	1697.7	62,130[a]
694.2	14,580	1003.8	28,070	1706.7	63,880[a]
799.0	18,890	1012.3	28,410	1714.6	64,930
840.0	20,610	1099.1	32,260	1730.5	65,670
847.7	20,930	1206.0	36,910	1747.4	66,620
888.9	22,660	1312.2	41,800	1780.8	68,200
940.8	24,890	1397.3	45,850	1816.0	69,730
964.6	26,000	1506.8	51,100		

[a] Shows pretransition effect.

The heat content of the γ-variety follows a regular, reproducible course to about 1120°K., that is, to the temperature of transformation to α'. Reproducible values at higher temperatures could not be obtained because of the sluggishness of the $\alpha' \rightarrow \gamma$ transformation. The substance did not revert completely to the γ-form under the prevailing conditions, resulting in calorimetric end-products of variable crystallographic composition. This behavior is in line with the observations of Trömel and Möller.[2]

Measurements starting with the β-variety were highly reproducible over the entire temperature range from 298 to 1816°K. The $\beta \rightarrow \alpha'$ transformation was sharp and completely reversible under calorimetric conditions. The measurement at 964.6°K. showed no sign of any transformation effect, while that at 974.1°K. showed that complete transformation had occurred. The rounded temperature, 970°K., was adopted as the equilibrium $\beta \rightarrow \alpha'$ point. Likewise, the $\alpha' \rightarrow \alpha$ transformation was completely reversible under calorimetric conditions. Pretransition effects were noted in the measurements at 1697.7 and 1706.7°K., but the transformation was complete at 1714.6°K. The rounded value, 1710°K., was adopted as the equilibrium $\alpha' \rightarrow \alpha$ point.

(6) K. K. Kelley, B. F. Naylor and C. H. Shomate, U. S. Bur. Mines Tech. Paper 686 (1946).

(7) E. Wichers, J. Am. Chem. Soc., **78**, 3235 (1956).

Table II contains smooth values of the heat content and entropy increments above 298.15°K. Values in the columns headed "Ca₂SiO₄(γ)" are based upon the γ-variety as the reference state at 298.15°K. Those in the columns headed "Ca₂SiO₄(β,α',α)" are based upon the β-variety as the reference state at 298.15°K.

TABLE II

HEAT CONTENTS (CAL./MOLE) AND ENTROPY INCREMENTS (CAL./DEG. MOLE) ABOVE 298.15°K.

T, °K.	Ca₂SiO₄ (γ) $H_T - H_{298.15}$	Ca₂SiO₄ (γ) $S_T - S_{298.15}$	Ca₂SiO₄ (β, α', α) $H_T - H_{298.15}$	Ca₂SiO₄ (β, α', α) $S_T - S_{298.15}$
400	3,270	9.41	3,335	9.59
500	6,760	17.19	6,940	17.63
600	10,480	23.96	10,790	24.64
700	14,380	29.97	14,810	30.84
800	18,420	35.37	18,940	36.35
900	22,590	40.28	23,140	41.29
970	....	...	26,120(β)	44.48
970	....	...	26,560(α')	44.94
1000	26,890	44.81	27,860	46.26
1100	31,320	49.03	32,250	50.44
1120	32,220	49.84	33,140	51.24
1200			36,720	54.33
1300			41,290	57.99
1400			45,970	61.45
1500			50,780	64.77
1600			55,710	67.95
1700			60,780	71.03
1710			61,290(α')	71.33
1710			64,680(α)	73.31
1800			69,090	75.82

The heat content results in Table II are represented (to within the average deviations indicated below) by the equations

Ca₂SiO₄(γ)
$$H_T - H_{298.15} = 31.86T + 6.16 \times 10^{-3}T^2 + 4.64 \times 10^5 T^{-1} - 11,603$$
(0.2%, 298° – 1100°K.)

Ca₂SiO₄(β)
$$H_T - H_{298.15} = 34.87T + 4.87 \times 10^{-3}T^2 + 6.26 \times 10^5 T^{-1} - 12,929$$
(0.4%, 298° – 970°K.)

Ca₂SiO₄(α')
$$H_T - H_{298.15} = 32.16T + 5.51 \times 10^{-3}T^2 - 9,814$$
(0.1%, 970° – 1710°K.)

Ca₂SiO₄(α)
$$H_T = H_{298.15} = 49.00T - 19,110$$
(0.1%, 1710° – 1800°K.)

Discussion.—The heat and entropy of the β → α' transformation are, respectively, 440 cal./mole and 0.45 cal./deg. mole. Corresponding values for the α' → α transformation are 3,390 cal./mole and 1.98 cal./deg. mole. It is not possible from the present work alone to derive heat and entropy values for the γ → α' transformation, but such values are obtainable indirectly. This transformation was shown by the present work to occur near 1120°K., in agreement with the findings of Trömel and Möller.[2] Low temperature heat capacity data of King[8] fix the transformation entropy as 1.67 cal./deg. mole at 298.15°K. This value, in conjunction with entropy increments from Table II, yields 3.07 cal./deg. mole as the transformation entropy at 1120°K. The corresponding heat of transformation is 3,440 cal./mole. The entropies of these transformations appear to be qualitatively in line with the magnitudes of the structural changes.

(8) E. G. King, unpublished measurements of this Laboratory.

THE FORMATION OF OXIDE FILMS AND COPPER POWDER ON THE (111) FACE OF A COPPER SINGLE CRYSTAL DURING THE CATALYTIC REACTION OF HYDROGEN AND OXYGEN

BY ROBERT E. CUNNINGHAM AND F. W. YOUNG, JR.

Contribution of the Cobb Chemical Laboratory of the University of Virginia, Charlottesville, Va.

Received January 5, 1957

The catalytic reaction of hydrogen and oxygen was studied on the (111) face of a single crystal of copper in the temperature range of 325 to 425° with oxygen concentrations of 0 to 17 mole %. The surface was examined with elliptically polarized light during the reaction to detect the presence of any oxide films on the surface. Below an oxygen concentration of about 5% no oxide was found, but above 5% films of oxide up to 75 Å. thick were detected. The rates of the catalytic reaction on the (111) face also were measured. When no oxide was present on the surface, the rate was independent of oxygen concentration, but when oxide was present the rate increased with oxygen concentration. Also, when oxide was present, dendritic growths of copper powder formed at polishing imperfections on the surface over a period of several hours. This powder formation resulted in a considerable increase in reaction rate because of the increased surface area. Under conditions of reaction in which no oxide was present the powder slowly disappeared and apparently rejoined the single crystal lattice. As the powder disappeared the reaction rate decreased to its value before powder formation. The powder could not be removed by heating in hydrogen alone, even at 500°.

Introduction

Previous experiments in this Laboratory on the catalytic reaction of hydrogen and oxygen on a copper single crystal have shown the striking rearrangement of the surface to form facets.[1-5] When

the oxygen concentration was greater than about 5%, dendritic growths of copper powder up to sev-

(1) A. T. Gwathmey and A. F. Benton, *J. Chem. Phys.*, **8**, 569 (1940).

(2) H. Leidheiser, Jr., and A. T. Gwathmey, *J. Am. Chem. Soc.*, **70**, 1200 (1948).

(3) J. B. Wagner, Jr., and A. T. Gwathmey, *ibid.*, **76**, 390 (1954).

(4) R. E. Cunningham and A. T. Gwathmey, *ibid.*, **76**, 391 (1954).

(5) A. T. Gwathmey and R. E. Cunningham, *J. chim. phys.*, **51**, 497 (1954).
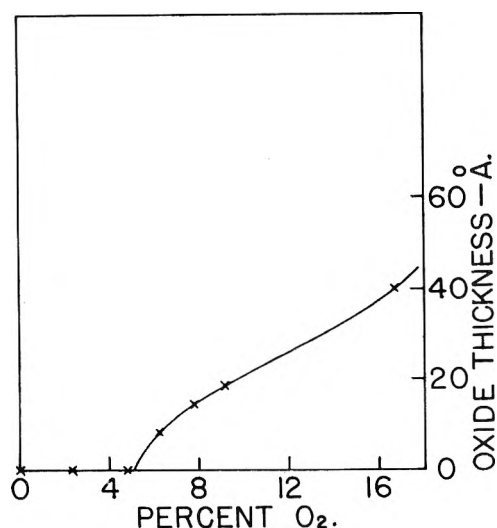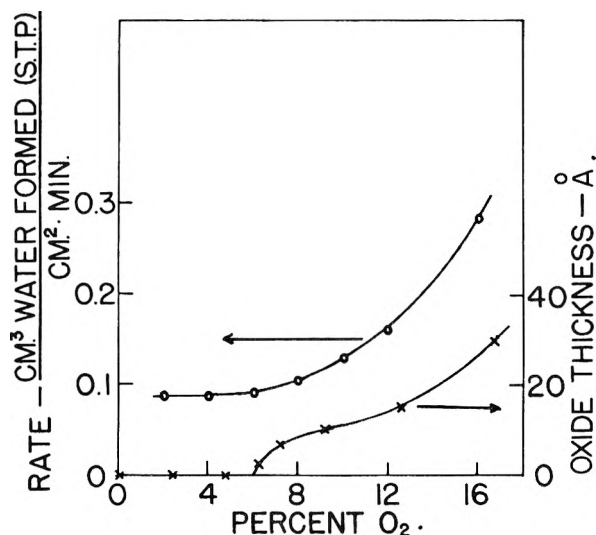
Fig. 1.—Reaction at 325°.

Fig. 2.—Reaction at 350°.

eral microns high also were formed on the surface. The crystallographic orientations of the facets and the rate of powder formation depended on the temperature, gas composition and crystal face. Thus when the experimental conditions were changed, the area and the surface structure of the catalyst were changed. The (111) face of copper was especially interesting since it did not rearrange or form powder over a wide range of conditions.

An important question concerning this reaction is whether copper oxide is present on the surface during reaction and, if so, what influence does it have on rearrangement, formation of powder and catalytic activity. Since the (111) face remains smooth, it is possible to examine this face with elliptically polarized light while the reaction is in progress in order to detect very thin oxide films.

This study is essentially concerned with the investigation of the oxide films and their relation to the catalytic properties of the surface.

Experimental Method

The apparatus previously used for studies of the oxidation of a single crystal[6] was modified so that mixtures of hydrogen

and oxygen could be passed through the reaction chamber. The copper crystal was prepared as described and annealed in hydrogen at 500° for one hour. The system was cooled to the reaction temperature, and the proper amount of oxygen was admitted to the gas stream to give the desired composition. The surface was examined with elliptically polarized light while the reaction proceeded until no further change in film thickness was observed. This technique of measuring cuprous oxide film has a precision of 2 Å. or less, so that less than a monolayer of oxide could be detected. The gas composition was then changed. After each set of measurements at a given temperature the crystal was exposed to pure hydrogen, and in every case the surface returned to its original condition, as indicated by elliptically polarized light. Between measurements at different temperatures the crystal was re-annealed in hydrogen at 500°.

The reaction rates on the plane face were determined using the apparatus and procedure previously described.[5] In the present case all rate measurements were made by determining the dew point of the gas leaving the reactor. Flow rates of 20–80 ml./min. were used, depending upon the temperature. Observation of the copper powder was made with an optical microscope.

At each temperature, at least two sets of observations were made of both film thickness and reaction rate.

Results

The thicknesses of the oxide films were measured at five temperatures from 325 to 425°. In every case with low oxygen concentration no oxide could be detected, but with oxygen concentrations greater than about 5 to 7%, films up to 75 Å. in thickness were found. These thicknesses were calculated from the measurements with polarized light by assuming that the film consisted of Cu_2O, and that it had essentially the same optical properties as Cu_2O formed by oxidizing copper in oxygen. The values for film thickness are given by the crosses in Figs. 1 to 5 according to the scale on the right. Except for Fig. 1 the reaction rates are also given in the same figures according to the scale on the left. It seems reasonable to assume that the oxide was Cu_2O in view of the relatively high temperatures and the large excess of hydrogen present in these experiments, but the films might not have exactly the same structure and composition as those formed by the oxidation of copper. Also, it was not possible to determine whether the films formed during the catalytic reaction were continuous or covered only part of the surface. Nevertheless, for the purposes of this study, which is concerned with the relationship of the oxide film to the catalytic properties of the surface, the thicknesses given should be sufficiently accurate.

At 400°, as shown in Fig. 4, and to a lesser extent at 375° and 425°, a maximum in the film thickness was obtained as the oxygen concentration was increased. This effect was reproducible.

In the measurement of film thickness the gas composition at the surface was not the same as that at the inlet, but this difference in composition was small except at 425°. The film thicknesses which are reported here did not change with time and could be approached from either higher or lower oxygen concentration, except at 425°. At this highest temperature the reaction rate was very fast and strongly dependent upon whether an oxide film was present. Thus the gas composition at the surface also depended on whether an oxide film was present. The oxygen concentration at the surface

(6) F. W. Young, Jr., J. V. Cathcart and A. T. Gwathmey, *Acta Met.*, **4**, 145 (1956).

at which oxide began to form at 425° was actually much lower than that shown, the concentration given being that of the inlet gas.

The study of reaction rates was complicated by the formation of copper powder on the surface. It was found that powder formed on the surface when the oxygen concentration was high enough to cause the formation of an oxide film. When the reaction was carried out under such conditions, the reaction rate increased continuously for a period of two or three hours because of powder formation and the consequent increase in surface area. The rate more than doubled during this period. The powder was observed to be associated with a few scratches and pits in the surface resulting from imperfect mechanical and electrolytic polishing. It was also found that, if the oxygen concentration was reduced to 4% so that no oxide film was present, the rate slowly decreased, requiring about three days to approach its initial value. At this time it was found that the copper powder had disappeared and the surface was smooth except for the scratches and pits mentioned above. No comparable amount of metal was found on the surfaces of the vessel, indicating that the copper atoms in the powder had rejoined the original lattice. The copper powder could not be made to disappear in the same period of time by heating in hydrogen alone, even at 500°.

If the reaction was allowed to proceed with oxide on the surface for only the short time required to make the measurements, rates were obtained before appreciable amounts of powder formed. Measurements could also be made over the entire oxygen concentration with powder on the surface. The results of both sets of rate measurements, with and without powder, at 400° are given by the circles in Fig. 4, the left hand ordinates giving the rate scale. The lower curve gives the rates with no powder on the surface and the upper curve gives the rates when there was powder on the surface. The vertical arrow upward at 8% oxygen indicates the rate during the formation of powder. The vertical arrow downward at 4% oxygen indicates the rate during the disappearance of powder. At the other temperatures powder would also form, but the rates were determined only for the powder free surfaces. The rates for the powder free surfaces are given by the circles in Figs. 2, 3 and 5. The rate at 325° was too slow to be measured conveniently. In these measurements the gas composition at the surface differed from that at the inlet, as in the measurement of film thickness. Since different reactors and flow rates were used for the film thickness and the rate measurements, the difference was not necessarily the same in both cases. This difference in composition, however, was small except at the highest temperature, and comparison of the rate with film thickness is significant at all but this temperature.

At 350 to 400°, as shown in Figs. 2 to 4, the rate was independent of oxygen concentration in the range where no oxide was present but increased with oxygen concentration when oxide was present. There was no abrupt change in the rate between these two oxygen concentration ranges.
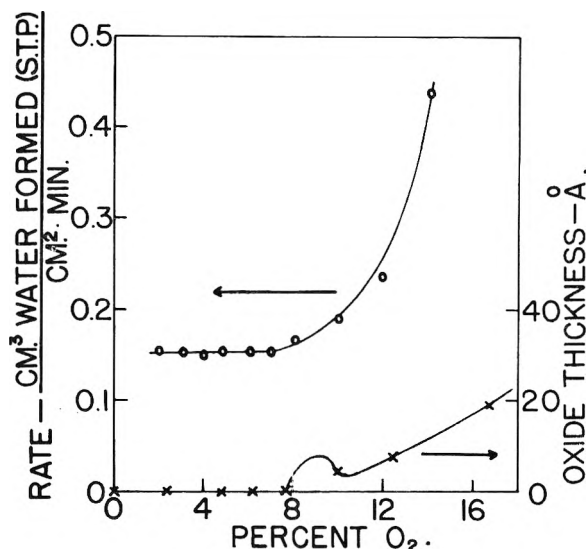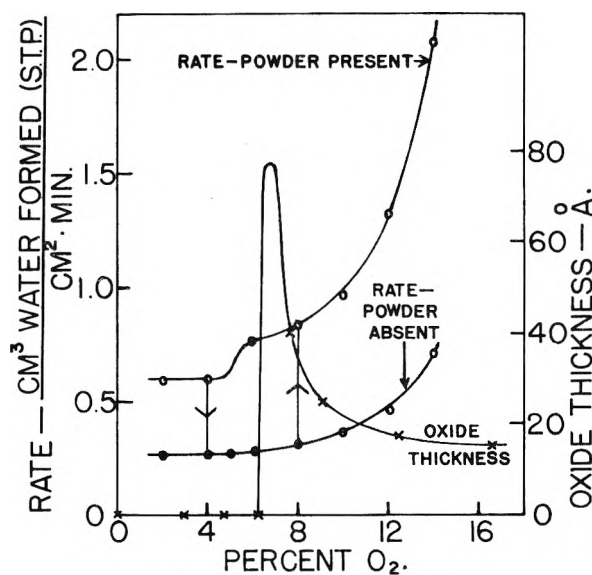

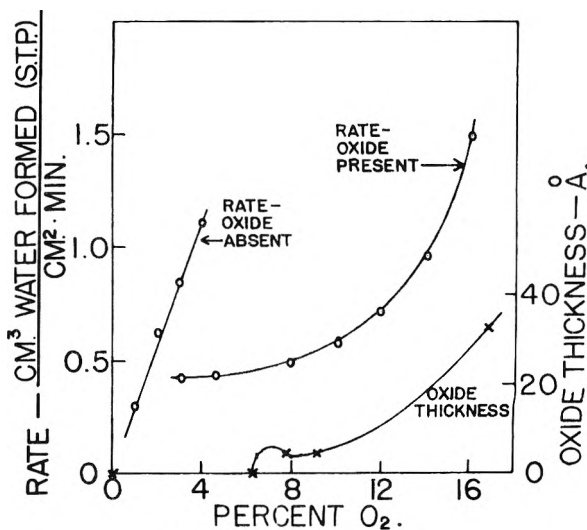
Fig. 3.—Reaction at 375°.

Fig. 4.—Reaction at 400°.

Fig. 5.—Reaction at 425°.

The results at 425° were different. As shown in Fig. 5, the rate in the absence of oxide corresponded to nearly complete conversion of the oxygen to water, but the rate was much less when oxide was present.

The most important features of these results are that an oxide film may or may not be present on the surface during the reaction depending on the temperature and the gas composition, that powder is formed when an oxide film is present and disappears when no oxide is present, and that the reaction kinetics change according to whether or not there is oxide on the surface. These factors will be discussed below.

Discussion

In the reaction of hydrogen and oxygen on copper previous investigators found that oxide was formed at low temperatures.[7] Experiments in this Laboratory have indicated that thick oxide films also formed very quickly at elevated temperatures if the oxygen concentration was high enough. In the range of temperature and gas composition used in the present study, however, no oxide could be seen on the surface with the unaided eye. Nevertheless, it was felt that it was important to determine whether a thin oxide film was present under these conditions. This study has shown that the catalytic reaction can occur with or without an oxide layer being present, and that the oxide affects the reaction and the formation of copper powder.

The reaction of hydrogen on copper can be discussed by considering one at a time three distinct ranges of conditions with respect to temperature and gas composition. First, the reaction can be carried out in the absence of oxide on the surface. The lower temperature limit of this range is indicated by previous investigators[7] to be about 200° and the upper limit is indicated by this study to be near 425°. The maximum oxygen concentration in this range for the (111) face is about 7% at 375°, and correspondingly less above or below this temperature. In at least a portion of this range the reaction rate is independent of the oxygen concentration.

With higher oxygen concentrations, there exists a second range of conditions in which the reaction occurred on a surface having a very thin layer of oxide. In this range the reaction rate increased with increasing oxygen concentration. It is somewhat surprising that at 350 to 400°, as shown in Figs. 2 to 4, the rates in this range formed continuous curves with those in the range where no oxide could be detected.

The formation of a thin oxide layer which does not continue to grow under a given set of conditions is difficult to understand in terms of equilibrium thermodynamics, but it is possible as a steady state of a non-equilibrium system. If the oxide layer formation is considered as a competitive process between oxidation and reduction, it is necessary that either the rate of oxidation decrease or the rate of reduction increase with increasing oxide thickness in order to obtain a state of constant oxide thickness. Otherwise the oxide thickness would continually in-

crease or the oxide would disappear completely, depending on whether the oxidation rate or the reduction rate was faster. One possible way for this to occur is with a surface only partly covered with oxide. If the uncovered copper surface then generated chemical species which enhanced oxidation or destroyed those involved in oxide reduction, a balance could be reached in which the surface was partly covered with oxide and the average oxide thickness would remain constant. The possible interaction of adjacent areas of the surface through the gas phase is indicated by the work of Mitchell and Marshall[8] who showed that the reaction of hydrogen with small amounts of oxygen on a platinum surface led to active hydrogen with a range of several cm.

With sufficient oxygen present a third range, that in which the oxide thickness continually increased, is indicated. The present study does not include this region.

In the growth of copper powder the important factors are the source of energy, the method of initiating growth and the means of transporting material. Previous studies in this Laboratory have indicated that the formation of powder depended on oxygen concentration. The present results show that this dependence involves the presence of oxide films. From the heat of formation of bulk cuprous oxide, it is estimated that the energy released by the formation of an oxide film, a few Ångström units in thickness, would exceed the difference between the surface energy of copper and the sum of the surface energy of cuprous oxide and the interfacial energy of copper–cuprous oxide. Thus in the presence of an oxide film, the total energy would be reduced by an increase in surface area, as by the formation of powder. The powder is presumed to be covered with oxide.

The formation of copper powder has been found to be associated with steps in the rearranging surface[3] and with other places where the crystal surface is growing. It has been suggested[5] that adsorbed gas and other material such as oxide on the surface might interfere with the regular growth of the crystal lattice as the surface rearranges, thus initiating powder formation. The (111) face itself does not rearrange, and it is significant that powder formation was associated with scratches and pits where the surface structure does change. In the case of spherical crystals where very smooth surfaces can be obtained, powder growth is not observed in the areas near the (111) poles.

The ease with which metal can move on the surface and the means of transport of material to the growing powder is indicated by the rearrangement of the surface which occurs during this reaction. In the absence of an oxide film, the surface energy of the metal provides a driving force for the disappearance of the powder. This disappearance of powder, however, is much slower than its formation. The energy involved is somewhat less than that provided for powder growth by a moderately thick oxide film (20–30 Å.), but it also appears that the ease of movement of metal atoms is reduced in the

(7) R. N. Pease and H. S. Taylor, *J. Am. Chem. Soc.*, **44**, 1637 (1922).

(8) A. E. Mitchell and A. L. Marshall, *J. Chem. Soc.*, **123**, 2448 (1923).

absence of the oxide. Since the powder was not changed appreciably by heating in hydrogen at 500° for three days, the movement of metal on the surface is certainly facilitated under the conditions of the catalytic reaction. The fact that a surface can either increase in area or be "catalytically sintered" with only a minor change in the operating conditions indicates that the formation of surface films can be very important in both the preparation and operation of some types of catalysts.

The rearrangement pattern on a spherical copper crystal also appears to be affected by an oxide film. At low oxygen concentrations, facets are developed parallel to the (110), (210), (311) and (111) faces. At higher oxygen concentrations, where oxide films are found on the (111) faces, the reflections indicate that (111) facets predominate. Since reaction rates vary markedly with crystal face, the conditions under which catalysis is carried out or the conditions of preparation can greatly affect the properties of a catalyst. The formation of surface films which stabilize facets parallel to certain crystal faces may be an important factor in determining catalytic properties.

This study has shown that oxide may or may not be present on the surface during the reaction of hydrogen and oxygen on copper, and that the presence of oxide affects the catalytic activity of the surface, the rearrangement of the surface, and the formation of copper powder. The problem of determining the nature of the surface layer on a catalyst during reaction is difficult since this layer is generally so thin that conventional methods cannot be used. The key to many problems in catalysis may be a better understanding of these thin films. It is felt that the technique of polarized light can be useful in the study of a wide variety of reactions.

THE HEAT CAPACITY OF SOLID DEUTERIUM BETWEEN 0.3 AND 13°K.[1,2]

BY O. D. GONZALEZ,[3] DAVID WHITE AND H. L. JOHNSTON

Cryogenic Laboratory, Department of Chemistry, The Ohio State University, Columbus 10, Ohio

The heat capacity of solid normal deuterium and solid mixtures containing 3, 14.5 and 18.5% para deuterium were measured from 1.3 to 13°K. in a Nernst-type calorimeter. Measurements of the heat capacity of normal deuterium were extended down to 0.3°K. using a calorimeter partially filled with ferric alum to cool the deuterium sample by adiabatic demagnetization. The heat capacity of solid deuterium for all ortho-para compositions except 3% para exhibits an anomaly beginning at approximately 10°K. In normal deuterium, the anomaly reached a maximum at approximately 1.3°K. The anomalous entropy for normal deuterium was found to be 0.60 ± 0.04 e.u. and the associated heat content 1.44 ± 0.08 cal. mole of n-D_2. The anomalous entropy is assumed to correspond to removal of the rotational degeneracy of the "frozen-in" state $J = 1$. It is shown that the anomaly in solid deuterium is not of the Schottky type, and it is suggested that the effect may be coöperative. The lack of the experimental data of a λ-type transition characteristic of coöperative phenomena may be due to the dilution effect of the ortho molecules in the solid system. Assuming that the $J = 1$ state is split into two substates $m = 0$ and $m = \pm 1$ by the crystalline field, the average energy difference between the two states has been estimated from the ΔH for the anomaly to be 6.5 cal. mole⁻¹.

Introduction

Like hydrogen, deuterium exists in two modifications, ortho and para, separately associated with the even and odd rotational levels. Since the transition probability between these states is very low, solidification of hydrogen or deuterium in the absence of a catalyst results in a mixture of molecules in both the $J = 0$ and the $J = 1$ states and therefore not in strict thermodynamic equilibrium. A Third Law check on both of these substances reveals that all of the entropy introduced by the $2J + 1$ degeneracy of the $J = 1$ state persists in the solids at the triple point.[4] For hydrogen the removal of this disorder has been observed as an anomaly in the heat capacity at liquid helium temperatures.[5] These measurements furthermore indicate that the ordering probably originates from the splitting of the degenerate $J = 1$ state by the crystalline field, and this has been confirmed by recent experiments using nuclear paramagnetic resonance absorption on solid hydrogen.[6]

Due to the different spin of the deuteron the molecular wave functions for deuterium possess different symmetry properties than for hydrogen, so that in the former the ortho form is associated with the even rotational levels, and the ortho–para ratio for the infinite temperature mixture becomes 2:1.[7] The heavier mass of deuterium increases the moment of inertia and the rotational magnetic moment, reduces the rotational spacing of the free molecules, but at the same time diminishes the

(1) Presented in part at the NBS Semicentennial Symposium on Low-Temperature Physics, Washington, D. C., March, 1951, and at the International Conference on Low Temperature Physics, Oxford, August 1951.

(2) This work was supported in part by the ONR under contract with The Ohio State University Research Foundation.

(3) Abridged from a dissertation submitted by O. D. G to the Graduate School, The Ohio State University, in partial fulfillment of the requirements for the degree of Ph.D.

(4) (a) W. F. Giauque, *J. Am. Chem. Soc.*, **52**, 4816 (1930); (b) K. Clusius and E. Z. Bartholome, *Z. physik. Chem.*, **B30**, 258 (1935); 277 (1954).

(5) (a) K. Mendelssohn, M. Ruhemann and F. Simon, *ibid.*, **B15**, 121 (1931); (b) R. W. Hill and B. W. A. Ricketson, *Phil. Mag.*, **45**, 277 (1954).

(6) (a) J. Hatton and B. V. Rollin, *Proc. Roy. Soc. (London)*, **A199**, 22 (1949); (b) F. Reif and E. M. Purcell, *Phys. Rev.*, **91**, 631 (1953).

(7) This mixture, which may be obtained at room temperature, is commonly called "normal," and this term is so used throughout this paper.

lattice zero point energy which should become a consideration at very low temperatures. Heat capacity data for deuterium at present exist only down to 10°K., and the relative importance of these differences to the ordering process has not been established. This investigation represents an attempt to measure the heat capacity of solid deuterium to temperatures sufficiently low to observe the complete anomaly and the corresponding entropy and heat content losses.

Apparatus

1. Calorimeters. a. Temperature Range above 1°K.—The investigation was divided into two phases corresponding to the temperature regions above and below 1°K. For the region above 1°K. an ordinary Nernst-type apparatus was employed. The calorimeter proper was a 35-cc. cylindrical copper container, 2.5 in. in length and 1 in. outer diameter with wall thickness 0.04 in., and was suspended by nylon threads inside of a cylindrical monel jacket. Six radial fins of 0.01 in. copper sheet were enclosed inside the calorimeter to improve thermal contact. Independent lengths of bare constantan and bare Pb-phosphor bronze wire were wound bifilarly around the calorimeter as heater and resistance thermometers. The wires were insulated electrically from the calorimeter walls by a bakelite coating and from each other by nylon thread. Several applications of General Electric 7031 adhesive were used to cement the wires to the walls. The eight current and potential leads (manganin) to the heater and thermometer were passed through a copper block in thermal contact at all times with the refrigerating bath, and through an additional small lead block situated very close to the calorimeter. Other features in this apparatus were similar to the one used below 1°K. and described in greater detail below.

The phosphor bronze wire[8] was a composite of 0.003 in. and 0.005 in. wire. Its resistance varied from 25 ohms at 4°K. to 1 ohm at 1.3°K. with its dR/dT varying likewise from 2.5 ohms/degree to 9.0 ohms/degree. With proper electrical arrangements it was possible to detect temperature changes of 0.0001° with this thermometer. The resistance of the constantan wire (No. 34 Driver-Harris "Advance") varied from 110 ohms at 16°K. to 108 ohms at 4°K., with a dR/dT average of approximately 0.1 ohm/degree within this region. A precision of 0.0005° was possible with this thermometer in the above temperature region.

b. Temperature Range below 1°K.—Temperatures below one degree were obtained by adiabatic demagnetization of ferric alum placed in thermal contact with a vessel containing the solid deuterium. The design adopted after several preliminary experiments is shown in Fig. 1.

Seventy-four grams of ferric alum (A) was compressed into a German silver can (D), 0.017 in. in wall thickness and about 4 in. long, and around copper-nickel cell (B) of 2.3-cc. volume and 0.006 in. in wall thickness into which deuterium was condensed. The powdered salt was compressed in the annular cylindrical space by means of a brass plunger operated by an ordinary hand press, the outside wall of the German silver container being protected during packing by a thick, close-fitting brass mold. The small concentric cell was similarly protected by a close-fitting steel rod. Measurement of the weight and volume of the packed salt indicated that 95% of the crystalline density was obtained on compres-

(8) Kindly prepared for us by Dr. R. I. Jaffe of the Battelle Memorial Institute.

sion. The lower exposed surface of the salt was varnished with many coatings of GE 7031 adhesive, and in order to retain the water of hydration of the salt, the vacuum chamber of the calorimeter was never evacuated above liquid nitrogen temperature.

A heater No. 32 manganin wire, double nylon insulated, wound bifilarly around the German silver container. The wire was evenly and closely wound to maintain the heating as uniform as possible and then varnished with many coats of GE 7031 varnish. The capillary (C) was of German silver, 0.020 in. i.d. and 0.010 in. wall thickness, and was coiled twice to increase its length. It was passed through a copper heater station (M) together with the electrical leads (L). There was also a small carbon resistor (not shown) in the heater station to indicate its temperature, and a manganin heater (H) was wound around the station and the capillary to permit evaporation of solid D_2 plugs. The can was suspended by nylon fishline threads (K). The vacuum jacket (F) was of brass and the pumping tube (G) of Monel.

A cylindrical cavity $1/4$ in. diameter and 1 in. long, with its axis parallel to the axis of the calorimeter was drilled in the packed salt. A small carbon resistor with electrical leads previously attached was inserted in this cavity and cemented to the salt by means of GE 7031 adhesive. The resistor, an ordinary commercial 30 ohm-un-insulated carbon resistor, was previously coated with bakelite. The resistor was very stable and gave a linear log R vs. log T plot between 1.2 and 4°K., to within experimental error. Some of the resistance values of this thermometer were 163.2 at 4.2°K., 286.2 ohms at 1.2°K. and 571.9 ohms at 0.3°K., with corresponding values of dR/dT of 18.4, 113 and 902 ohms/degree.

2. Electrical Circuits—Timing.—The circuits used throughout the research were of standard design used in calorimetry,[9] except that the heater current and voltage were measured directly by a Type B Rubicon potentiometer with maximum range of 1.6 volts. A stopwatch checked against a jeweler's electric timer was used in all cases to measure time.

3. Cryostat and Magnet.—The calorimeters described above were suspended in a 2-liter Pyrex glass dewar about 38 in. long and 3 in. i.d. The upper end of the dewar was terminated in a copper-glass seal which was soldered to a stationary brass lid bearing connection valves to the gas holder and the Kinney vacuum pump.

A solenoid magnet placed with its axis coincident with the axis of the calorimeter was used to obtain the necessary fields for magnetic cooling. This magnet was cooled by means of liquid nitrogen and was a modified version of the magnets described by Fritz and Johnston,[10] Formex-coated copper wire (B. and S. No. 21) having been used in its construction, rather than cotton insulated wire. This magnet gave a field of 200 gauss/amp. at its center. The current source of the magnet consisted of twenty-four 8 volt submarine batteries of 500 ampere hours capacity. The maximum current used was about 29 amp. and was measured with a precision ammeter equipped with a precision shunt.

Procedure

The experimental methods used in the measurement of heat capacity, adiabatic demagnetization and other cryogenic techniques followed those commonly used and described extensively in the literature; only those features specific or unique in this investigation are noted below.

1. Calibration of Resistance Thermometers.—The constantan and phosphor bronze thermometers were calibrated by direct comparison with the vapor pressures of liquid helium and solid and liquid hydrogen, read on mercury and dioctyl phthalate manometers with a Gaertner cathetometer. The vapor pressures of solid and liquid hydrogen were converted to temperatures by the equations of Scott and Brickwedde.[11] The tables prepared by the Mond Laboratory were used for the same prupose for liquid helium.[12]

In the range 4–12°K. the calorimeter was employed as a gas thermometer in order to calibrate the constantan wire. The technique was the same as used by Leiden[13] and else-

(9) G. E. Gibson and W. F. Giauque, *J. Am. Chem. Soc.*, **45**, 93 (1923).

(10) J. W. Fritz and H. L. Johnston, *Rev. Sci. Inst.*, **21**, 416 (1946).

(11) H. W. Woolley, R. B. Scott and F. G. Brickwedde, *J. Research Natl. Bur. Standards*, **41**, 379 (1948).

(12) H. Van Dijk and D. Schoenberg, *Nature*, **164**, 151 (1949).

(13) C. W. Clark Thesis, Leiden, 1935.

Fig. 1.—Calorimeter for temperatures below 1°K.

where.[14] The pressure of a constant (but undetermined) amount of helium gas was observed simultaneously with the resistance of the constantan wire as the temperature was varied from 2 to 20°K. From 2 to 4°K. and from 12 to 20.4°K. the vapor pressures of the liquid helium and hydrogen were noted at the same time. (In the range 4-12°K. the temperatures were maintained constant by proper adjustment of the current in the constantan wire). The pressure–temperature plot for the gas thermometer gave a connecting and very nearly straight line for both these regions. Thus the gas pressures in the region 4-12°K. could be converted easily to temperatures, and these were then used to fix the constantan thermometer points. Since the sensitivity of the constantan thermometer is very low below 4°K., one is not justified in merely joining independent calibration curves in the helium and hydrogen regions. In addition there is a possibility of a discontinuity in the resistance of constantan wire at 7°K.[11] However, the resistance of Driver-Harris "Advance" wire used in this research was continuous throughout the temperature range studied, in agreement with the observation of other workers on similar wire.[14]

To convert from resistance values to temperatures, large-scale graphs of R versus T were made for both thermometers. From these graphs values of R were read to within 0.001 ohm at intervals of 0.02° for the phosphor bronze thermometer and 0.1° intervals for the constantan thermometer. These values were tabulated, and the first and second differences were then smoothed so that the resulting tabulated values remained within 0.001° of the plotted curves. Thus a chart was obtained for each thermometer from which the temperature corresponding to a given resistance could be readily computed. At the same time errors in calibrating or reading from a graph were minimized by this procedure.

It was not possible with the present metal apparatus to calibrate the carbon resistance thermometer directly against the magnetic susceptibility of the ferric alum as is commonly done. Excessive heating was developed by eddy currents produced in the metal by the a.c. field of the inductance ("I" in Fig. 1) originally included in the apparatus for this purpose. To establish a temperature scale below 1°, the resistance values were converted to temperatures by extrapolating the linear log R vs. log T calibration curve of the thermometer determined above 1°K. Since the thermal and magnetic properties of ferric alum are well known,[15] the final temperature that is attained with given initial magnetic fields and temperatures can be computed accurately. A difference of only 0.03° was observed at 0.1°K. between the temperature calculated in this manner with that computed from the thermometer resistance after adiabatic demagnetization of the ferric alum with no deuterium present. The extrapolated temperatures were therefore adjusted by a correction of the following form, $\Delta T = a + bT_R$, where T_R is the temperature read from the extrapolated plot a and b are constants determined by the limits, $\Delta T = 0.03$ at $T_R = 0.1°$ and $\Delta T = 0.00$ at $T_R = 1.2°$. This procedure affects the values of the heat capacity only negligibly, since the temperature differences were always taken as $^1/_{10}$ or less the mean temperature. This correction will be uncertain at most to an estimated 0.003°, which in turn represents only a 1% error at 0.3°, the lowest temperature attained with D_2, and this is lower than the errors introduced by other factors (see below).

2. **Condensation of Gas and Preparation of Various Ortho–Para Mixtures of Deuterium.**—The gas samples were measured volumetrically before condensing by means of a thermostatted 5-liter buret. This equipment, which permits an accuracy of 0.05%, is described elsewhere.[16] For the normal deuterium runs the gas was passed from the supply cylinder through liquid air trap to buret and thence to the calorimeter. Ortho-deuterium was obtained by previously converting D_2 in the liquid state at 20.4°K. for 24 hours in an activated charcoal trap. The deuterium was

transferred to the calorimeter from the trap at 23°K. to reduce the filling time, and this procedure raised the amount of para form from 2% value of the 20.4°K. equilibrium mixture to a calculated 3%.[17]

3. **Measurement of the Heat Capacities above 1°K.**—Heat capacities were determined by the usual observation of temperature drifts before and after a heating interval. The drifts were followed every half minute for about 10–20 minutes (until linear), and the temperature rise was limited to about $^1/_{10}$ of the mean temperature by proper adjustment of the energy input. Heating intervals were kept at 60 to 120 sec. in the helium range and always less than 6 min. in the range above 4°K. Both heating current and voltage were varied at random to observe the effect of superheating on the final data.

Measurements of the heat capacity were begun after pumping out the exchange gas for 1 hour at which time sufficient thermal insulation was achieved. A slow upward temperature drift developed as the thermal insulation improved in the experiments on samples containing para-deuterium. This drift was greater than the normal heat leak and was approximately proportional to the para-D_2 content. This probably came from the slow ortho–para conversion which persists in the solid state.[18] It was not possible, because of this effect, to evacuate the exchange gas for long periods of time to obtain better thermal insulation, if heat capacity runs were to be made at temperatures lower than 1.5°K.

4. **Measurement of Heat Capacity below 1°K.**—Cooling below 1°K. was achieved by adiabatic demagnetization. The procedure employed in measuring heat capacity was the same as described above. The measurements of the heat capacity of deuterium were taken after two independent magnetic cooling cycles.

Purity of Gas

The deuterium employed in the first phase of the investigation was obtained from a high pressure storage cylinder filled with gas originally prepared from electrolysis of heavy water. Its main impurity was 1.6% HD determined by mass spectrometric analysis. For the work below 1°K. the deuterium came from a cylinder of higher purity containing only 0.6% HD (mass spectrometer analysis). The gas was used for the normal deuterium work as obtained directly from the cylinder, room temperature equilibrium being assumed for the ortho–para ratio.

Experimental Results

1. **Normal Deuterium and Ortho–Para Mixtures.**—The experimental results are given in Tables I–VI and are plotted in Figs. 2–4. The values marked "Total C_p" represent the heat capacity uncorrected for number of moles or heat capacity of the empty calorimeter and HD. The columns listed "C_p" represent the corrected results per mole which actually represent values taken under saturated vapor pressure. The two values above 12°K. were corrected for the small vaporization of gas occurring during measurements.

2. **Ortho-deuterium below 1°K.**—In order to find out whether any of the entropy due to the nuclear spin degeneracy is removed at temperatures obtained in this research, a simple experiment was performed with 97% ortho-deuterium. The apparatus employed for this purpose consisted of a small cylindrical glass cell about 3.5 in. in diameter and 4 in. long, containing 0.056 mole of ferric alum in the form of loosely packed crystals. This permitted a large deuterium to salt ratio, and any removal of the nuclear spin entropy could be detected very easily by the difference in temperatures attained between two demagnetizations carried under same initial conditions, first with the salt

(14) J. E. Ahlberg, E. R. Blanchard and W. O. Lundberg, *J. Chem. Phys.*, **5**, 639 (1937).

(15) (a) N. Kurti and F. Simon, *Proc. Roy. Soc. (London)*, **A149**, 161 (1935); (b) N. Kurti and F. Simon, *ibid.*, **A152**, 21 (1935); (c) N. Kurti and F. Simon, *Phil. Mag.*, **26**, 849 (1938); (d) A. H. Cooke, *Proc. Phys. Soc.*, **A62**, 269 (1949).

(16) (a) W. F. Giauque and H. L. Johnston, *J. Am. Chem. Soc.*, **51**, 2300 (1929); (b) H. L. Johnston, E. B. Rifkin and E. C. Kerr, *ibid.*, **72**, 3933 (1950).

(17) Unpublished data in this Laboratory on the homogeneous conversion in liquid D_2 were used in these calculations.

(18) E. Cremer and M. Polanyi, *Z. physik. Chem.*, **B21**, 459 (1933).

TABLE I
HEAT CAPACITY OF NORMAL DEUTERIUM ABOVE 1°K.

Temp., °K.	ΔT, °K.	Total C_p, cal. deg.$^{-1}$	C_p, cal. deg.$^{-1}$ mole^{-1}

Run A: no. of moles D_2, 1.2041; no. of moles HD, 0.0196

1.354	0.0485	0.3282	0.2721
1.429	.0989	.3083	.2558
1.520	.1084	.2932	.2432
1.674	.1684	.2859	.2370
1.879	.1586	.2908	.2410
1.960	.1527	.2851	.2362
2.585	.2763	.2668	.2207
3.050	.3545	.2647	.2188
3.542[a]	.6951	.2722	.2132
4.041	.5062	.2625	.2158

Run C: no. of moles D_2, 1.0641; no. of moles HD, 0.0173

9.115	0.8760	0.5000	0.457
10.002	.8644	.6625	.5906
10.858	.8232	.8315	.740
11.622	.6300	1.030	.917
12.311	.7386	1.198	1.055
13.145	.9293	1.446	1.270
14.158	.9950	1.687	1.471

Run D: no. of moles D_2, 1.0494; no. of moles HD, 0.0171

1.333	0.0974	0.2778	0.2647
1.441	.1030	.2628	.2504
1.551	.1055	.2564	.2443
1.664	.1105	.2445	.2330
1.781	.1087	.2491	.2373
2.476	.1928	.2575	.2441
2.708	.2497	.2435	.2308
2.935	.2430	.2420	.2287
3.211	.3119	.2457	.2346
3.520	.3388	.2454	.2220
3.933	.5311	.2368	.2277
4.695	1.0199	.2120	.1972
5.620	0.9870	.2194	.2023
6.578	1.0982	.2474	.2249
7.565	1.1002	.2987	.2641
8.540	0.9356	.4008	.3621
9.381	.8177	.5315	.4809
10.139	.7209	.6789	.6143
10.830	.6969	.7798	.7010
11.603	.8933	1.0094	.9120
12.499	.9027	1.1990	1.080

[a] Data taken on August 4, 1950: no. of moles D_2, 1.2448; no. of moles HD, 0.0206.

TABLE II
HEAT CAPACITY OF ORTHO-DEUTERIUM ABOVE 1°K.

Temp., °K.	ΔT, °K.	Total C_p, cal. deg.$^{-1}$	C_p, cal. deg.$^{-1}$ mole^{-1}

Run B: no. of moles D_2, 1.0859; no. of moles HD, 0.0177

1.409	0.1140	0.008781	0.00783
1.540	.2770	.008267	.00776
1.802	.2335	.01063	.00920
2.075	.2847	.01159	.00995
2.412	.2779	.01192	.01004
2.749	.3445	.01347	.01123
3.226	.5984	.01780	.01462
3.878	.7748	.02615	.02142
4.080	.5468	.03447	.02874
4.490	.584	.03765	.03079
4.930	.667	.04650	.03799
5.364	.766	.05499	.05348

6.055	1.016	.1001	.09173
6.958	.951	.1504	.1273
7.818	.972	.2164	.1842
8.781	.908	.3778	.3265
9.876	1.448	.5541	.4803
10.859	0.866	.7759	.6724
11.702	.671	.9900	.8598
12.310	.577	1.156	1.004

TABLE III
HEAT CAPACITY OF 14.5° o-PARA-DEUTERIUM ABOVE 1°K.

Temp., °K.	ΔT, °K.	Total C_p, cal. deg.$^{-1}$	C_p, cal. deg.$^{-1}$ mole^{-1}

Run E: no. of moles D_2, 0.7183; no. of moles HD, 0.0008

1.369	0.0740	0.08707	0.1205
1.470	.1136	.08562	.1184
1.603	.1510	.08182	.1132
1.751	.1549	.07869	.1084
1.888	.1836	.08081	.1128
2.088	.1848	.08042	.1110
2.457	.2161	.07735	.1063
2.628	.222	.07594	.1041
2.898	.2579	.07076	.0966
3.072	.2928	.06987	.0937
3.299	.3119	.06843	.0928
3.524	.3841	.06576	.0916
3.860	.4518	.06727	.0901
4.602	.5990	.06312	.0826
5.254	.946	.07400	.0953
6.358	1.137	.09344	.1182
7.013	1.081	.1224	.1547
7.864	0.951	.1663	.2103
8.780	1.025	.2471	.3150
9.677	0.928	.3586	.4602
10.559	.891	.4677	.6003
11.399	.8611	.5549	.7070
12.053	.7055	.7424	.9554
12.431	.7100	.8319	1.067

alone and then with deuterium present. Demagnetizations carried out at 3000 gauss and with and without $^1/_2$ mole of deuterium yielded the same final temperatures (measured with a calibrated inductance), within experimental error ($\pm 0.003°$K.). These results indicate that no nuclear spin entropy is removed down to 0.3°K.

3. Probable Errors. a. Errors between 1.3 and 13°K.—The heat capacity is computed from the data using the expression

$$C_p = (1/n)(1/J)[(E \times I \times t)/T - C_{cor}]$$

where E = voltage across heater during energy interval, I = current in amperes through heater during energy interval, t = time interval in seconds, ΔT = temperature difference in degrees, C_{cor} = heat capacity of the empty calorimeter and HD impurity, n = number of moles of deuterium, and J = factor for converting joules to calories, taken as 1 calorie (defined) = 4.8133 international joules. The quantities E and I were measured to a precision better than 0.1%; the time was measured to within 0.1 sec., so that the maximum precision error for the smallest time intervals used, 60 sec., is about 0.2%. The heat capacity of the empty calorimeter comprises at most 5%, and the error introduced by it is at most 0.3%. The heat capacity of HD was computed from the Debye equation with a θ of

Table IV
Heat Capacity of 18.5° o-Para-deuterium above 1°K.

Temp., °K.	ΔT, °K.	Total C_p, cal. deg.$^{-1}$	C_p, cal. deg.$^{-1}$ mole^{-1}
Run F: no. of moles D$_2$, 0.9108; no. of moles HD, 0.0148			
1.376	0.0968	0.1363	0.1492
1.501	.1414	.1347	.1473
1.648	.1490	.1278	.1397
1.796	.1465	.1311	.1432
1.940	.1452	.1310	.1430
2.083	.1475	.1290	.1408
2.373	.1795	.1309	.1427
2.608	.2129	.1258	.1367
2.815	.1357	.1196	.1290
3.020	.2295	.1169	.1266
3.268	.3124	.1153	.1245
3.504	.3709	.1104	.1231
3.967	.5045	.1130	.1208
4.150	.2413	.1188	.1268
5.563	.9306	.1161	.1204
6.463	.9632	.1352	.1380
7.306	.9229	.1799	.1830
8.208	.9907	.2680	.2741
9.287	1.0505	.4217	.4345
10.258	0.9874	.5491	.5641
11.254	1.0127	.7415	.7621
12.212	0.9765	.9549	.9813
13.209	1.0441	1.141	1.169

Table V
Heat Capacity of Ferric Alum below 1°K.

Temp., °K.	ΔT, °K.	Total C_p, cal. deg.$^{-1}$
No. of moles of ferric alum, 0.15; initial magnetic field 3000 gauss		
0.208	0.01260	0.0404
.233	.01452	.0351
.263	.01952	.0260
.399	.02760	.0187
.452	.02989	.0174
.514	.03940	.0162
.684	.05972	.0129
.784	.05588	.0136
.888	.06849	.0119
.048	.1408	.0115
1.259	.1736	.00928

98°; the maximum error introduced by this approximation is 0.1%. Thus C_{cor} can be in error at the most 0.3%. Below 4° this correction was negligible for all measurements except those with 97% ortho-deuterium. The uncertainty in the number of moles, n, is 0.5%. The temperature difference, ΔT, was obtained by graphical extrapolation of the temperature drifts before and after the heating interval. Thermal insulation was sufficient at all times to obtain an extrapolation precision of at least 0.2% of the temperature difference. With the exception of the temperature range between 4 and 5° the resistance thermometers were sensitive enough to permit a precision in the temperatures difference of 0.1%, as was noted in the section on apparatus. The precision in the temperature difference was therefore at worst 0.2%.[19]

(19) The small and constant heating produced by the ortho–para conversion will not affect the temperature difference, and hence the value of the heat capacity, because it is cancelled out by the extrapo-

Table VI
Heat Capacity of Normal Deuterium below 1°K.
No. of moles of D$_2$, 0.09798; no. of moles of HD, 0.0005

(a) First demagnetization from initial field of 3800 gauss

Temp., °K.	ΔT, °K.	Total C_p, cal. deg.$^{-1}$	C_p, cal. deg.$^{-1}$ mole^{-1}
0.629	0.04995	0.0244	0.106
.732	.06566	.0278	.148
.847	.06306	.0290	.169
.993	.08196	.0281	.167
1.205	.05754	.0333	.240
1.262	.06085	.0313	.222

(b) Second demagnetization from initial magnetic field of 5800 gauss

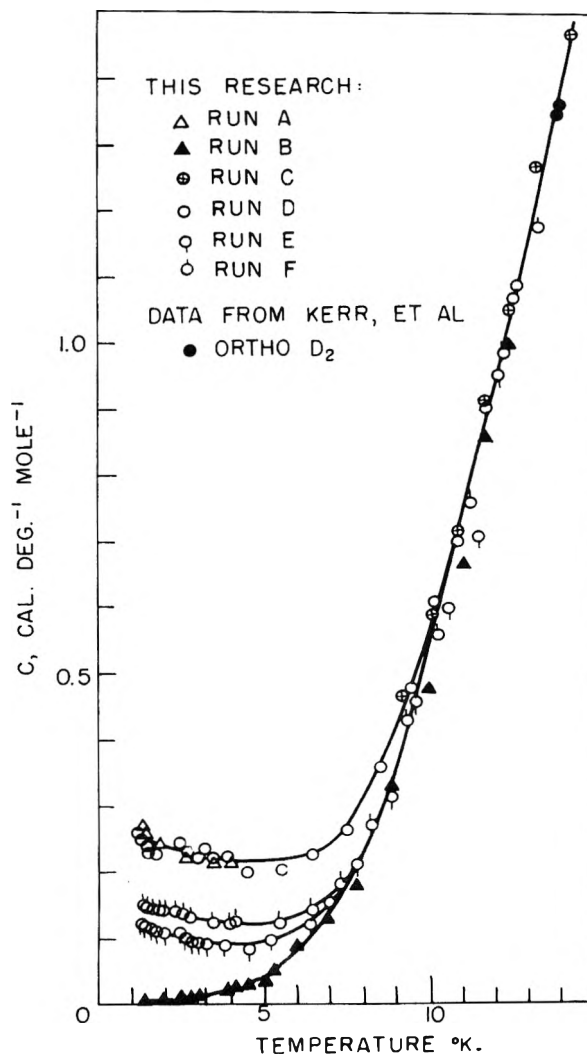| 0.331	0.03723	0.0236	0.020
.405	.03521	.0254	.068
.479	.03565	.0278	.112
.557	.04895	.0270	.118
.662	.04839	.0274	.136
.810	.06135	.0270	.146
1.238	.1109	.0290	.198
1.349	.1697	.0329	.244

Fig. 2.—Heat capacity of solid ortho-para mixtures of deuterium between 1 and 13°K.

lation. Although it will raise the value of the mean temperature, this effect was found by observation to be negligible.
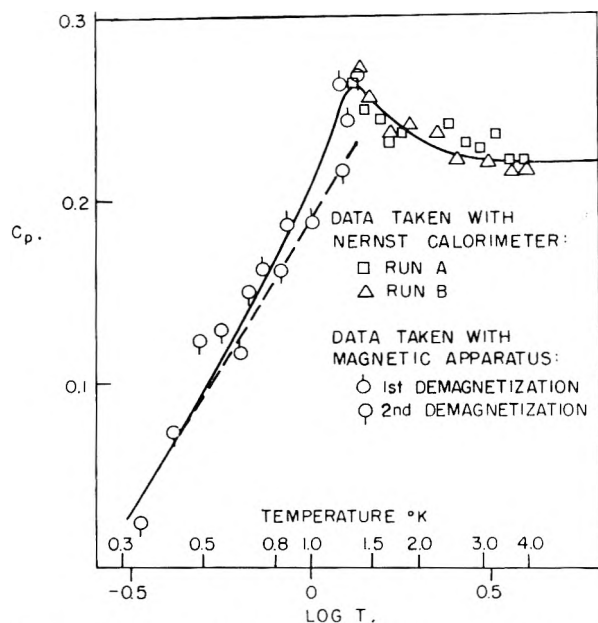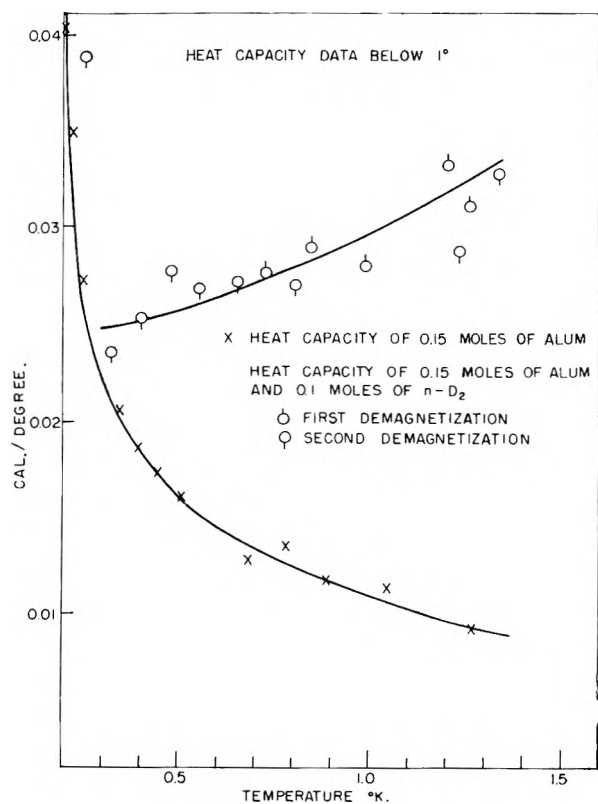
Fig. 3.—Heat capacity of normal D_2 between 0.3 and 4°K.

Fig. 4.—Total heat capacity for ferric alum and ferric alum with normal D_2.

ond, from lack of thermal equilibrium in the sample due to poor heat conductivity. Since helium gas is absorbed to some extent by solidified gases[20] it is not introduced into the D_2 sample, and superheating was possible. Lack of thermal equilibrium, however, could not be noticed from the temperature drifts nor by variation of heating voltage and was probably small. It is therefore believed that the main contributing factor to the scattering is the desorption of helium, absorbed on the outside walls of calorimeter, which occurs only during the heating interval when the local temperature at heater rises sharply. This was manifested strikingly in the region around the λ-point of helium, 2.18°K. (the heat capacity of He increases 100 times at this temperature) where the heat loss due to desorption was so great that measurements were not possible. This effect may be considered as an undetermined uncertainty in either E or ΔT.

The absolute accuracy of the smoothed curve in Fig. 2 cannot be claimed to be better than 5%, mainly due to the error in the temperature scale below 12°K. The reliability of the curve however, may be attested by the fact that it joins smoothly the data for o-D_2 obtained by Kerr, Rifkin, Johnston and Clarke using a different and more accurate type of apparatus.[21]

b. Percentage Composition of Mixtures.—The results for the heat capacity of the mixtures with intermediate compositions (originally intended to be 10 and 15%) were much higher than could be predicted from the results on the normal mixture. This discrepancy could only arise from an incomplete conversion of the ortho-deuterium used in the mixtures or to an experimental blunder in preparing the first mixture. Since experimental difficulties prevented formal analyses of the gases, a computational procedure was employed to arrive at the composition figures quoted here. The heat capacity per mole of para-deuterium was computed from the data obtained for the normal mixture at 1.3°K., where the heat capacity is due entirely to the para modification present. By means of this value the composition of the lowest mixture was calculated from its experimental heat capacity (assuming proportionality). The composition of the ortho-deuterium originally used in the preparation of the mixtures was then found, and the composition of the second mixture in turn computed from the amounts of the gases used. The heat capacity of the second mixture calculated on the basis of this composition agreed with actual experimental values to within 1% throughout the range 1.3–4°K. Although the quoted percentages are probably accurate to this figure, no quantitative claims are made for the data, and the results are reported merely to show the effect of varying ortho–para compositions on the heat capacity.

c. Errors below 1°K.—The scatter of the data below 1°K. was necessarily much greater since, in addition to the contribution of the errors discussed above, the heat capacity of the ferric alum is very great. The relation between the two is seen in

If the errors discussed above are all accumulative and of the same sign, the expected maximum precision error is 2%. The average deviation of the experimental points from the smoothed curve shown in Fig. 2 is 3%. The cause of this extra scatter can originate from two sources: first, from an additional heat exchange with the bath, resulting from the desorption, during the heat capacity measurement, or residual helium gas which apparently never was pumped out completely; and sec-

(20) W. H. Keesom and J. Schweers, Leiden Comm. 264d (1941).
(21) E. C. Kerr, E. B. Rifkin, H. L. Johnston and J. W. Clarke, J. Am. Chem. Soc., **73**, 282 (1951).

Fig. 4. The average deviation of the data from the smooth curve is 7%.

An indeterminate error of as much as 10% can exist in the data below 1° due to uncertainty of the number of moles of D_2 in the calorimeter. Although the actual number of moles condensed was known quite precisely, there was a tendency for some of the gas to collect in the capillary as the apparatus was cooled, and thus did not enter in the heat capacity measurements. In order to avoid a systematic error in the final entropy value, the curve in Fig. 3 was plotted so that the curves below and above 1° coincided. This represents an arbitrary raising of the data below 1°K. of 10%. The dotted line in Fig. 3 is the curve for the actual data obtained. The difference in entropy between the two curves is only 0.02 e.u.

Calculation of Anomalous Entropy and Heat Content

In the calculation of the entropy and heat content values associated with the heat capacity anomaly, the lattice contribution was determined in the following manner: (a) between 0.03 and 6°K. it was calculated using a Debye $\theta = 108°$ derived from the heat capacity data on 97% o-D_2 above 6°K. where no anomaly was exhibited: (b) between 6 and 10°K. the smoothed experimental values for 97% o-D_2 were taken to represent the lattice contribution. The anomalous entropy and heat content determined by graphical integration and corrected for lattice vibrations are (between 0.3 and 10°K.)

$$\Delta S = 0.60 \pm 0.04 \text{ cal. deg. mole of } n\text{-}D_2$$
$$\Delta H = 1.44 \pm 0.08 \text{ cal. mole of } n\text{-}D_2$$

The errors quoted above were based on the uncertainty figures in the data previously discussed.

Discussion

Normal deuterium in the solid state is the metastable ortho–para mixture in the molar ratio 2:1. The ortho species constitute molecules in the rotational state $J = 0$ with total molecular nuclear spins of 0 and 2 resulting from vectorial additions of the deuteron spin of 1; the para species corresponds to molecules with $J = 1$ and total nuclear spin of 1. The results of this research show that effects due to nuclear spin are absent in the temperature range studied, so that the observed anomalous heat capacity must be attributed to a phenomenon involving the "frozen-in" state $J = 1$.

Phase separation has been suggested[22] as a possible mechanism for the removal of the entropy of mixing of the ortho–para forms, and this would appear as a plausible explanation for the present results, in view of the value of ΔH obtained. Segregation normally occurs in solutions when the total free energy of the system can be reduced by formation of additional phases, and this requires a positive heat of mixing with corresponding positive deviations from Raoult's law. For hydrogen, on the contrary, the vapor pressures of ortho–para mixtures in both the solid and liquid states clearly display negative deviations from ideality.[11] A negative heat of mixing is further indicated by the value of 5.8 cal. obtained from the heats of sublimation

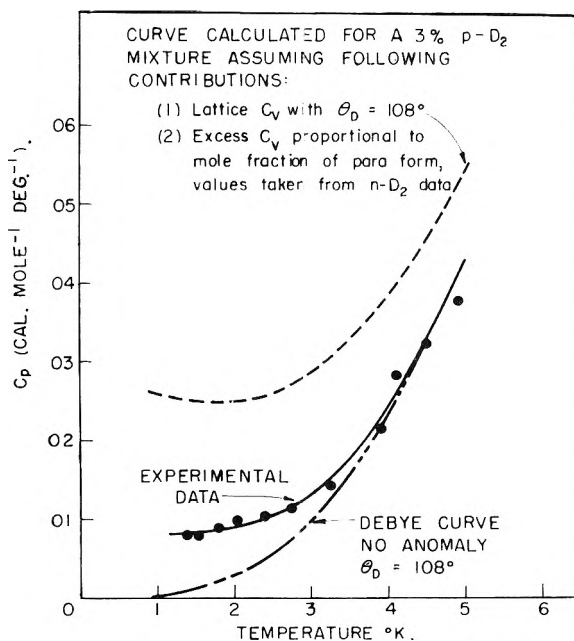(22) L. Pauling, *Phys. Rev.*, **36**, 430 (1930).

Fig. 5.—Graphical illustration of the suppression of anomaly in 3% para-D_2 sample.

for the difference between the internal energies of the 20.4°K. equilibrium and the normal solid mixtures. A corresponding (although more uncertain) difference of 1 cal. is obtained for deuterium from its vapor pressure measurements.[11] Phase separation in this temperature range therefore appears untenable. In the case of hydrogen the heat capacity measurements in the liquid helium range have shown unambiguously that the ordering was not connected with a phase separation, for while the heat effect in the latter process should reach a maximum at a mole fraction of $1/2$, the anomalous heat capacity was found to increase with the percentage of $J = 1$ species up to a value of 75%.

The only alternative mechanism which will yield values of ΔH and ΔS consistent with the experimental ones originates from the lifting of the degeneracy of the $J = 1$ rotational state by the crystalline field. Since the sublevels $m = 0$ and $m = \pm 1$ of this state correspond to dissimilar electronic probability distributions, different energies should be acquired by molecules in these sub-levels in the presence of the electric field of the lattice. This amounts to a Stark-type splitting of the $J = 1$ level into two states with one doubly degenerate and has been verified by calculations[6b,23,24] which have applied the crystalline potential as a perturbation on the rotational energy. The ordering will occur when molecules occupying the higher of these states descend into the lower at that temperature region where kT approximates the energy difference. This will be observed as an anomaly in the heat capacity, and the ΔH accompanying this effect will be a measure of the energy difference between the two states. The ΔS will be given by the entropy of rotational degeneracy $1/3 R \ln 3$, or 0.73

(23) R. B. Scott, F. G. Brickwedde, H. C. Urey and H. Wahl, *J. Chem. Phys.*, **2**, 458 (1934).

(24) K. Schaefer, *Z. physik. Chem.*, **B42**, 38 (1939).

cal./deg. for one mole of normal deuterium.[25]

By equating the experimental value of ΔH to that obtained by integration of a theoretical Schottky heat capacity curve for the Stark-type splitting discussed above, a value of 6.5 cal./mole is obtained for the energy difference in normal deuterium (an equivalent excitation temperature of $3°K.$). As will be seen later, this can be at best only an average figure, since the use of a Schottky curve is not actually justified, but it indicates that the experimental ΔH is in accord with the proposed mechanism. The experimental value of ΔS, 0.60 cal./deg./mole of n-D_2, is lower than the theoretical one by an amount which is outside experimental error. However, the data also indicate that the heat capacity is not vanishing even at $0.3°K.$, so that the difference is very probably undetected entropy below this temperature. A comparison of the results for deuterium and those for hydrogen reveals that the anomaly appears at approximately the same temperature and is similar in nature. The energy of splitting may be expected to vary inversely with the moments of inertia of the two molecules, so that a much lower temperature would therefore be predicted for the anomaly. However, a compensation is produced by the wider lattice spacing of hydrogen (which results from its larger zero-point energy), since the crystalline potential must also vary inversely with high powers of the intermolecular distance. This may be considered as additional evidence for the influence of the lattice. On the basis of these observations we believe that the anomaly observed in this research corresponds to removal of the rotational degeneracy by the crystalline field.

It was not possible to fit the data obtained in this research to either a Schottky curve derived as assumed above, or to a curve derived from three equally spaced non-degenerate levels (a Zeeman-type splitting). In the case of hydrogen even the limited early data did not yield constant values for the energy difference,[26] as required for a pure Schottky anomaly, and the recent and more extensive results of Hill have shown conclusively that this type of anomaly is not obtained in hydrogen. It is obvious that the crystalline potential must depend to some extent on the population of the sublevels $m = 0$, ± 1 and on the distribution of molecules in these levels throughout the solid, so that the anomaly should bear characteristics of a coöperative phenomenon. This was substantiated by a pronounced dilution effect in the results for 97% ortho-deuterium where the anomalous contribution of the 3% para form was considerably suppressed (see Fig. 5). Although no λ-type transition was found in this research, the results of Hill indicate that this type of transition may occur at higher concentrations of the $J = 1$ state. Further information on this question will become available from heat capacity measurements on *pure* ortho-hydrogen and para-deuterium, which can now be prepared,[27,28] and in which these dilution effects due to the presence of the $J = 0$ states would be eliminated. An investigation of this nature is now in progress in this Laboratory.

Acknowledgments.—Sincere thanks are due to Mr. Leo E. Davis and Mr. James Seiler for help in the measurements, to Mr. Lester E. Cox for aid in the design and construction of the apparatus, and to Mr. Gwynne A. Wright for the liquefaction of the large quantities of liquid helium used in this research.

(25) This value assumes that the $m = 0$ level will be the one with lowest energy: the reverse situation will yield an entropy loss of $^1/_3R(\ln 3 - \ln 2)$, or 0.27 e.u., which is not in agreement with the experimental result.

(26) R. B. Scott and F. G. Brickwedde, *J. Research Natl. Bur. Standards*, **19**, 237 (1937).

(27) Y. L. Sandler, *J. Phys. Chem.*, **58**, 58 (1954).

(28) C. M. Cunningham, D. S. Chapin and H. L. Johnston, Abstr. 120th Meeting A.C.S., September 1951, p. 19R.

CRYOSCOPIC BEHAVIOR OF WATER AND NITRIC ACID IN FUSED AMMONIUM NITRATE[1]

By A. G. Keenan

Department of Chemistry, Illinois Institute of Technology, Chicago 16, Illinois

Received January 24, 1957

H_2O and HNO_3 have been studied cryoscopically as solutes in NH_4NO_3 melts. H_2O alone, as well as mixtures of the two solutes, show ν-factors of unity based on stoichiometric mole fraction concentrations determined by analysis of the melts. A consistent set of molecular species is postulated to account for the observed ν-factor and the results related to proposed mechanisms for the thermal decomposition of NH_4NO_3.

It has been shown in a previous publication[2] that ammonium nitrate can be employed as a useful cryoscopic solvent despite its well-known thermal decomposition at higher temperatures. In the present work H_2O and HNO_3 were chosen as solutes

for cryoscopic study because of their interest in connection with proposed mechanisms for the thermal decomposition of NH_4NO_3. Only H_2O is mentioned in the prior literature.[3] The method used there was an approximate one, with an expected accuracy of ± 1°, and the lowest concentration studied was somewhat above the highest concentration in the present data.

(2) A. G. Keenan, This Journal, **60**, 1356 (1956).

(3) I. L. Millican, A. F. Joseph and T. M. Lowry, *J. Chem. Soc.*, **121**, 959 (1922).

Experimental

The freezing point apparatus and the manipulations involving the ammonium nitrate solvent have already been described.[2] Distilled water and approximately 90% nitric acid were used as solutes. The nitric acid was free of NO_2 according to the criteria given by Robertson, et al.[4] In one run 96% acid was used and this result agreed with the others. Appropriate amounts of water or nitric acid, as judged by experience, were added to the NH_4NO_3 and allowed to equilibrate in a closed flask at room temperature for about one hour. A freezing point determination was then made in the usual manner.[2]

When the cooling curves on the recorder chart indicated that crystallization of solid phase had begun (but before any appreciable amount had separated out) the melt was poured into two tared flasks. After weighing, water was added to one flask and duplicate aliquots titrated with 0.05 N NaOH using a Sargent–Malmstadt automatic differential titrator to control the titrant. The base was standardized with acid containing the same concentration of NH_4NO_3 as the solution to be analyzed. In order to determine the water content of the melt, methanol, which had been distilled from magnesium turnings through a 60-cm. vacuum-jacketed, packed column, was used as solvent for the material in the second flask. Aliquots of this solution were titrated with Karl Fischer reagent using standard procedures.[5] Again, blank determinations were used to correct for water contained in the solvent and picked up during the transfer operations. The melts were colorless at all stages, indicating the absence in the melt of NO_2 from any decomposition of the HNO_3 added. HNO_3 catalyzes the decomposition of NH_4NO_3, but the N_2O produced is insoluble in the melt.[6] Any water retained in the melt, from this source or from decomposition of HNO_3, is determined as part of the total water content by the analysis following the freezing point determination.

To study the products of decomposition of the ammonium nitrate itself, which are retained in the melt, the pure NH_4NO_3 was heated in the freezing point cell to temperatures in the range 235–250° for about one hour and the above procedures then followed.

Results and Discussion

The results are given in Table I and in Fig. 1. The line in Fig. 1 is taken from the data of the previous paper[2] and represents the freezing-point depression for a solute showing ideal cryoscopic behavior with a v-factor[7] of 1. While the scatter of the data is somewhat greater than in the previous work, due largely to less reproducibility in the analytical procedures, it is, nevertheless, quite definite that all of the systems follow the ideal depression line very closely. The data for H_2O agree with the prior literature[3] within the expected tolerance.

The ideal behavior of water as a solute is easily understood. An ammonium nitrate melt consists of the ionic species NH_4^+ and NO_3^- exclusively, contributions from the possible reaction

$$NH_4^+ + NO_3^- \rightleftharpoons NH_3 + HNO_3 \qquad (1)$$

being negligible in the liquid phase, at least for temperatures near the freezing point, as shown by the previous cryoscopic study.[2] In such a system there is no apparent reaction which the water could undergo. On the other hand, the low vapor pressure of water in the melt indicates association
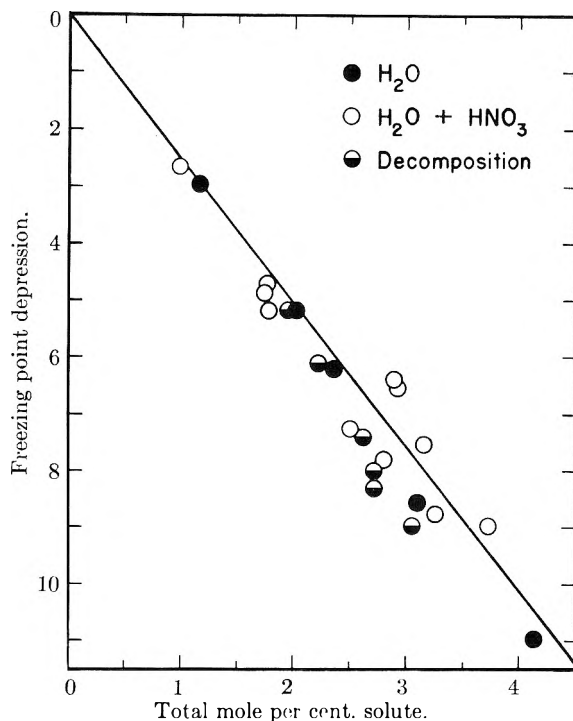
(4) G. D. Robertson, D. M. Mason and W. H. Corcoran, This Journal, **59**, 683 (1955).

(5) J. Mitchell and D. M. Smith, "Aquametry," Interscience Publishers, Inc., New York, N. Y., 1948.

(6) H. A. Bent, Doctoral Thesis, University of California, 1952.

(7) R. J Gillespie, E. D. Hughes and C. K. Ingold, J. Chem. Soc., 2473 (1950).

Fig. 1.—Observed freezing point depressions of solutions of H_2O and HNO_3 in fused NH_4NO_3. Points marked "decomposition" refer to systems where the H_2O and HNO_3 were produced by thermal decomposition of the solvent.

of some kind.[8] The evidence points to hydrogen bonding with NO_3^-, giving species of the type

$$\left[O-N \underset{O\ldots\ldots H}{\overset{O\ldots\ldots H}{<}} {\Large >} O \right]^-$$
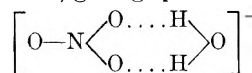
Table I

Freezing Point Depressions for Various Amounts of the Solutes Water and Nitric Acid in Fused Ammonium Nitrate[a]

Water	Concn., mole % Acid	Total	Depression $-\Delta T$, °C.
4.13		4.13	10.96
2.00		2.00	5.20
1.16		1.16	2.96
3.07		3.07	8.55
2.33		2.33	6.19
1.68	1.20	2.88	6.40
1.22	0.51	1.73	4.88
1.63	1.62	3.25	8.76
2.26	0.88	3.14	7.53
1.87	1.85	3.72	8.98
1.39	0.35	1.74	4.74
2.24	.67	2.91	6.51
2.33	.45	2.78	7.83
0.72	.26	0.98	2.65
1.00	.77	1.77	5.18
1.47	1.03	2.50	7.27
2.64	0.08	2.72	8.30
1.86	.08	1.94	5.19
2.96	.09	3.05	8.98
2.62	.09	2.71	8.00
2.55	.06	2.61	7.40
2.15	.07	2.22	6.12

[a] The data in the last six lines refer to the decomposition runs.

(8) E. Jänecke and E. Rahlfs, Z. anorg. allgem. Chem., **192**, 237 (1930).

The molecular structures are appropriate for this species, the observed ν-factor would follow in the concentration range studied, and the thermal energy (at 170°) is still an order of magnitude lower than any reasonable estimate of the H-bond energy. Furthermore, electrostatic interactions leading to non-ideal behavior of the kind usually classified under an activity coefficient would be rendered negligible by the high dielectric constant in a fused salt medium.

Nitric acid also gives a ν-factor of 1, at least when present with water in a molar concentration equal to or less than that of the water, which is the only range encountered in the data. The expected reaction (2) is definitely ruled out since it would give

$$H_2O + HNO_3 \longrightarrow H_3O^+ + NO_3^- \qquad (2)$$
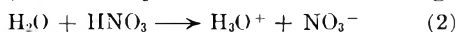
a ν-factor of zero for the nitric acid contribution to the total solute concentration (NO_3^- does not depress the freezing point, being common with the solvent anion). Reaction (2) evidently is repressed to negligible proportions by the high NO_3^- concentration in the nitrate melt used as solvent.

The autoprotolysis reaction[4] for HNO_3

$$2HNO_3 \rightleftharpoons H_2NO_3^+ + NO_3^- \qquad (3)$$
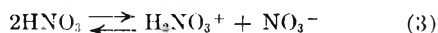
would give a ν-factor of $1/2$ and would again be repressed by the high NO_3^- concentration in the melt. Ionic self-dehydration of nitric acid (i.e., further dissociation of the $H_2NO_3^+$ in (3)) according to the reaction

$$2HNO_3 \rightleftharpoons H_2O + NO_2^+ + NO_3^- \qquad (4)$$
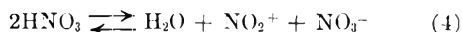
has been detected in nearly 100% HNO_3, by various techniques,[4,9,10] including Raman spectra and cryoscopy. This would give the observed ν-factor in the present systems. However, this equilibrium would also be expected to lie far to the left because of the high NO_3^- and low HNO_3 concentrations present. Because the HNO_3 persists in the

melts over long periods of time (indicating relatively low vapor pressures), whereas species such as NO_2 and N_2O do not, it seems reasonable to assume that, like the H_2O, it is tied up in a complex of some kind. Such a complex, as well as the low concentration and the repression of reaction 3, also account for the relatively greater thermal stability of the HNO_3 in the nitrate melt compared to nearly pure acid.[4,11]

Complexes of the type $(HNO_3)_nNO_3^-$ have been detected by vapor pressure and Raman spectral studies in solutions of KNO_3 in HNO_3 near room temperature.[12] Under these conditions the most probable value of n seems to be about 2. In the ammonium nitrate melts, at a higher temperature but also at a much higher nitrate ion concentration, the present cryoscopic results indicate that the value of n is one.

Finally, the products retained in the ammonium nitrate melt after partial thermal decomposition at elevated temperatures show the same cryoscopic behavior, based on stoichiometric moles of H_2O and HNO_3, as the mixtures of these constituents discussed above. Recent kinetic studies of the thermal decomposition of ammonium nitrate[6,13,14] have led to various postulated mechanisms involving reactions 1 to 3 above as important steps. None of these studies have been sufficiently detailed to allow calculation of the equilibrium concentrations of the various species. While cryoscopic experiments alone cannot determine unequivocally the species present, any mechanisms derived from kinetics must be consistent with the cryoscopic data.

The concentrated nitric acid and its analyses were supplied by Dr. George Gibson of this department.

(9) C. K. Ingold and D. J. Millen, J. Chem. Soc., 2612 (1950).

(10) R. J. Gillespie, E. D. Hughes and C. K. Ingold, ibid., 2552 (1950).

(11) C. W. Tait, J. A. Happe, R. W. Sprague and H. F. Cordes, J. Am. Chem. Soc., 78, 2670 (1956).

(12) J. Chédin and S. Fénéant, Compt. rend., 228, 242 (1949).

(13) T. M. Cawthon, Doctoral Thesis, Princeton University, 1955.

(14) B. J. Wood and H. Wise, J. Chem. Phys., 23, 693 (1955).

THERMODYNAMIC PROPERTIES OF PYRIDINE

By Kun Li

Jones & Laughlin Steel Corporation, Pittsburgh, Pennsylvania

Values of the thermodynamic properties of pyridine in the solid and liquid state up to 300°K. have been calculated from the low temperature heat capacity data. Thermodynamic functions in the ideal gaseous state have been computed by the methods of statistical mechanics at selected temperatures up to 1000°K. Combined with the available data on heat of combustion, values of heat, free energy and equilibrium constant of formation are given for the same temperatures. Other properties included are: vapor pressure, heats of vaporization and fusion, and critical constants.

Introduction

Pyridine is one of the important coal chemicals. In recent years, pyridine chemistry has received considerable attention. Numerous derivatives of pyridine have been prepared and utilized. Many more are being explored. It is apparent that the properties of pyridine are of great importance for the studies of pyridine chemistry as well as engineering calculations of industrial processes.

A thorough literature survey has been made on the thermodynamic properties of pyridine. This paper presents the values of thermodynamic properties of pyridine in the solid, liquid and ideal gaseous state in a useful and convenient form. In closing the gaps in the data reported in literature, necessary interpolation and extrapolation were made. Thermodynamic consistency was used as a criterion for analyzing the data and selecting the

best values. Thermodynamic functions in the ideal gaseous state were computed statistically on the basis of the rotational and vibrational assignments derived from infrared, Raman and microwave spectra.

Thermodynamic Properties in Solid and Liquid State.—Heat capacities at saturation pressure of the solid from 90 to 230°K. and of the liquid from 231 to 300°K. were measured by Parks, Todd and Moore.[1] The triple point was reported as 231.16° K. (−42.0°) and heat of fusion, 1977 cal./mole. The absolute error of the data was ±0.7%. When heat capacity was plotted against temperature a very sharp rise at 220°K. was noted. If a curve were drawn through this point and extended to 231.16°K., the triple point, one would have a value for the heat capacity of solid much higher than that of liquid at the same temperature. It is suspected that premelting might have taken place in the vicinity of 220°K. due to perhaps impurities in the sample. Thus a smooth curve was drawn following the trend of the points at temperatures below 220°K. and the values of heat capacity at 220, 230 and 231.16°K. were read off the curve.

In order to calculate the entropy at any temperature, extrapolation of heat capacity data to the absolute zero was necessary. The extrapolation from 90 to 20°K. was made by the method of Kelley, Parks and Huffman.[2] Below 20°K., a Debye function for six degrees of freedom with the characteristic temperature equal to 136° was used. By means of numerical integration, the heat contents, entropies and free energies were calculated. In Table I values of these thermodynamic properties are tabulated at 10° intervals from 10 to 300°K.

Vapor Pressure.—The vapor pressure of pyridine from 43 to 116° was measured by Riley and Bailey;[3] from −15 to 116° by van der Meulen and Mann;[4] from 16 to 116° by Hieber and Woerner;[5] and from 47 to 116° by Herington and Martin.[6]

The sample used by Herington and Martin[6] was of 99.85 ± 0.07 mole % purity and their measurements are believed to be more reliable than those of the others in the same range. The authors[6] correlated their data in the range of 63 to 765 mm. by means of the Antoine equation

$$\log_{10} p = 7.05811 - 1384.991/(t + 216.296) \quad (1)$$

in which p is the vapor pressure in mm. and t the temperature in °C. The boiling point at 760 mm. is calculated to be 115.256°.

No actual data were reported by van der Meulen and Mann,[4] but an Antoine equation was given to represent the data from 1 to 760 mm.

$$\log_{10} p = 6.8827 - 1281.3/(t + 205) \quad (2)$$

(1) G. S. Parks, S. S. Todd and W. A. Moore, *J. Am. Chem. Soc.*, **58**, 398 (1936).

(2) K. K. Kelley, G. S. Parks and H. M. Huffman, THIS JOURNAL, **33**, 1802 (1929).

(3) F. T. Riley and K. C. Bailey *Proc. Roy. Irish Acad.*, **38B**, 450 (1929).

(4) P. A. van der Meulen and R. F. Mann, *J. Am. Chem. Soc.*, **53**, 451 (1931).

(5) W. Hieber and A. Woerner, *Z. Elektrochem.*, **40**, 252 (1934).

(6) E. F. G. Herington and J. F. Martin, *Trans. Faraday Soc.*, **49**, 154 (1953).

TABLE I

THERMODYNAMIC PROPERTIES OF PYRIDINE IN SOLID AND LIQUID STATE

T, °K.	$-(F_{satd} - H_0^0)/T$, cal./deg. mole	$(H_{satd} - H_0^0)/T$, cal./deg. mole	$(H_{satd} - H_0^0)$, cal./mole	S_{satd}, cal./deg. mole	C_{satd}, cal./deg. mole
		Solid			
10	0.03	0.09	0.92	0.12	0.37
20	0.24	0.67	13.5	0.91	2.42
30	0.67	1.67	50.2	2.34	4.91
40	1.29	2.73	109.3	4.02	6.93
50	2.01	3.72	186.2	5.73	8.44
60	2.77	4.60	275.9	7.37	9.49
70	3.54	5.35	374.9	8.89	10.32
80	4.30	6.02	481.8	10.32	11.06
90	5.04	6.62	595.6	11.66	11.70
100	5.77	7.15	715.1	12.92	12.20
110	6.48	7.63	839.8	14.11	12.74
120	7.16	8.08	969.8	15.24	13.27
130	7.83	8.50	1106	16.33	13.87
140	8.47	8.91	1247	17.38	14.48
150	9.10	9.30	1395	18.40	15.12
160	9.71	9.69	1550	19.40	15.80
170	10.31	10.07	1712	20.38	16.56
180	10.90	10.45	1881	21.35	17.40
190	11.48	10.84	2060	22.32	18.34
200	12.04	11.25	2249	23.29	19.48
210	12.60	11.68	2452	24.28	21.04
220	13.15	12.14	2671	25.29	22.80
230	13.70	12.66	2911	26.36	25.15
231.16	13.77	12.72	2940	26.49	25.45
		Liquid			
231.16	13.77	21.27	4917	35.04	29.07
240	14.57	21.56	5175	36.13	29.39
250	15.46	21.88	5471	37.34	29.77
260	16.32	22.20	5771	38.52	30.13
270	17.17	22.50	6074	39.67	30.64
280	17.99	22.80	6384	40.79	31.21
290	18.80	23.10	6699	41.90	31.78
298.16	19.44	23.34	6960	42.78	32.24
300	19.58	23.40	7019	42.98	32.36

Maximum deviation of the calculated vapor pressure was given as 3.1%.

It is recommended that equation 1 may be used to calculate the vapor pressure from 20 to 1000 mm. With less accuracy equation 2 may be used for vapor pressures below 20 mm.

Heat of Vaporization.—Data on heat of vaporization were reported at only a few temperatures. Table II summarizes the available data.

TABLE II

t, °C.	ΔH_v, cal./mole	Ref.
0	10,180	5
0	10,210	7
20	9,710	5
114.13	8,494.1	8

The value for heat of vaporization at 25° was calculated by means of Clapeyron equation using equation 1 and Berthelot equation of state. The calculation gave $\Delta H_v = 9659$ cal./mole at 25°. The standard heat of vaporization, $\Delta H°_v$, at 25° with liquid and vapor in their respective standard state, namely, liquid at 1 atmosphere and vapor in ideal gaseous state at 1 atmosphere was found to be 9662 cal./mole. Berthelot equation of state was used for correcting the real gas to ideal gas.

(7) W. Hieber and H. Appel, *Z. anorg. allgem. Chem.*, **196**, 193 (1926).

(8) J. H. Mathews, *J. Am. Chem. Soc.*, **48**, 562 (1926).

Critical Constants.—The critical temperature was reported to be 344°[9] and the critical pressure 60.0 ± 0.5 atmosphere.[10]

Heats of Combustion and Formation.—Earlier measurements on heat of combustion were reviewed by Kharasch.[11] Recently, Cox, Challoner and Meetham[12] measured the heat of combustion in liquid state at 25° with improved accuracy. Their experimental results together with the calculations of this work are given in Table III.

<div align="center">

TABLE III

STANDARD HEATS OF COMBUSTION AND FORMATION OF PYRIDINE AT 25°

</div>

State of pyridine	$\Delta H°c$, kcal./mole	$\Delta H°f$, kcal./mole
Liquid	−665.00	+23.95
Gas	−674.66	+33.61

The standard heat of combustion refers to the reaction

$$C_5H_5N(l \text{ or } g) + 25/4 \text{ } O_2(g) \longrightarrow 5CO_2(g) + 5/2 \text{ } H_2O(l) + 1/2 \text{ } N_2(g)$$
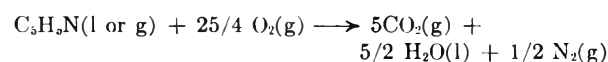
all the reactants and products being in their respective standard state, that is, liquid at 1 atmosphere and gas in the ideal gaseous state at 1 atmosphere.

From the value for heat of combustion of pyridine and the values for heat of formation of carbon dioxide[13] and water,[13] the standard heat of formation of pyridine was computed according to the reaction

$$5C(graphite) + 5/2 \text{ } H_2(g) + 1/2 \text{ } N_2(g) \rightarrow C_5H_5N(l \text{ or } g).$$

Entropy.—The entropy of pyridine in the ideal gaseous state at 1 atmosphere and 298.16°K. was calculated from S_{satd} liq at 298.16°K., heat of vaporization and Berthelot equation of state. Table IV gives a summary of these calculations.

<div align="center">

TABLE IV

ENTROPY OF PYRIDINE AT 298.16°K., CAL./DEG. MOLE

</div>

S_{satd} liq	42.784
Vaporization	32.296
Gas imperfection	0.007
Compression	−7.150
$S°$ gas, 1 atm.	68.04

Thermodynamic Properties in Ideal Gaseous State.—From studies of the microwave spectrum of pyridine in the range of 22,140 to 27,300 mc., McCulloh and Pollnow[14] determined the rotational constants for pyridine: $A = 6039.13$ mc., $B = 5804.70$ mc., $C = 2959.25$ mc.; principal moments of inertia: $I_a = 83.701$ a.m.u., Å.^{2}, $I_b = 87.081$ a.m.u., Å.^{2}, $I_c = 170.814$ a.m.u., Å.^{2}. In a similar study of microwave spectrum in the range from 20,000 to 40,000 mc., DeMore, Wilcox

(9) T. M. Lowry and A. G. Nasini, *Proc. Roy. Soc. (London)*, **A123**, 686 (1929).

(10) W. Herz and E. Neukirch, *Z. physik. Chem.*, **104**, 433 (1923).

(11) M. S. Kharasch, *J. Research Natl. Bur. Standards*, **2**, 359 (1929).

(12) J. D. Cox, A. R. Challoner and A. R. Meetham, *J. Chem. Soc.*, 265 (1954).

(13) "Selected Values of Properties of Hydrocarbons and Related Compounds," American Petroleum Institute Research Project 44, Carnegie Institute of Technology, Pittsburgh, Pennsylvania.

(14) K. E. McCulloh and G. F. Pollnow, *J. Chem. Phys.*, **22**, 681 (1954).

and Goldstein[15] also determined the rotational constants which are essentially the same as those of McCulloh and Pollnow.[14]

Based on the results of McCulloh and Pollnow[14] and an investigation of microwave spectra of monodeuteropyridines, Bak, Hansen, and Rastrup-Andersen[16] selected a model for the structure of pyridine which has the dimensions

$r(C(2)-H) = 1.085$ Å., $r(C(3)-H) = 1.080$ Å., $r(C(4)-H) = 1.075$ Å., $r(N-C(2)) = 1.340$ Å., $r(C(2)-C(3)) = 1.390$ Å., $r(C(3)-C(4)) = 1.400$ Å., $\angle C(6)NC(2) = 116° 42''$, $\angle NC(2) C(3) = 124° 00''$, $\angle C(2)C(3)C(4) = 118° 36''$, $\angle C(3) C(4)C(5) = 118° 06''$.

The symmetry number of pyridine for rotational contribution is 2.

Assignment of fundamental vibrational frequencies was first made by Kline and Turkevich[17] who also calculated the thermodynamic functions of pyridine in the ideal gaseous state from 291.15 to 1000°K. and claimed the values to be correct to within 5%. Later, Corrsin, Fax and Lord[18] in a study of infrared and Raman spectra of pyridine and pyridine-d_5 revised the earlier assignments. Product rule was used to verify the assignment. Pyridine molecule belongs to C_{2v} symmetry and has 27 fundamental frequencies which as assigned by Corrsin, Fax and Lord[18] are included in Table V.

<div align="center">

TABLE V

FUNDAMENTAL VIBRATIONAL FREQUENCIES OF PYRIDINE

</div>

Frequency no.	Species C_{2v}	Frequency, cm.$^{-1}$
1	A_1	992
2	A_1	3054
3	B_1	1218
4	B_2	675
5	B_2	942
6a, b	A_1, B_1	605, 652
7b	B_1	3054
8a, b	A_1, B_1	1580, 1572
9a	A_1	1218
10a, b	A_2, B_2	886, 749
11	B_2	703
12	A_1	1029
13	A_1	3054
14	B_1	1375
15	B_1	1148
16a, b	A_2, B_2	374, 405
17a	A_2	981
18a, b	A_1, B_1	1068, 1068
19a, b	A_1, B_1	1482, 1439
20a, b	A_1, B_1	3036, 3083

Assuming a harmonic oscillator, rigid rotator model, the rotational constants and vibrational frequencies discussed above were used for the statistical calculations of thermodynamic functions. As is usually done, the nuclear spin of hydrogen and nitrogen was neglected. The fundamental constants used were[13]: molecular weight $= 79.103$, $c = 2.997902 \times 10^{10}$ cm./sec., $h = 6.62377 \times 10^{-27}$ erg sec./molecule, $N = 6.02380$

(15) B. B. DeMore, W. S. Wilcox and J. H. Goldstein, *ibid.*, **22**, 876 (1954).

(16) B. Bak, L. Hansen and J. Rastrup-Andersen, *ibid.*, **22**, 2013 (1954).

(17) C. H. Kline and J. Turkevich, *ibid.*, **12**, 300 (1944).

(18) L. Corrsin, B. J. Fax and R. C. Lord, *ibid.*, **21**, 1170 (1953).

$\times 10^{23}$ number of molecules/mole, $k = 1.380257 \times 10^{-16}$ erg/deg molecule, $0°C. = 273.16°K.$ The calculated entropy at $298.16°K.$, 67.78 cal./deg. mole, is in satisfactory agreement with the calorimetrically determined value, 68.04 cal./deg. mole. In Table VI are tabulated the calculated values of free energy function, heat content function, heat content, entropy and heat capacity up to $1000°K.$

TABLE VI

THERMODYNAMIC PROPERTIES OF PYRIDINE IN IDEAL GASEOUS STATE

T, °K.	$-(F° - H_0°)/T$, cal./deg. mole	$(H° - H_0°)/T$, cal./deg. mole	$(H° - H_0°)$, kcal./mole	$S°$, cal./deg. mole	$C°$, cal./deg. mole
298.16	56.44	11.34	3.381	67.78	19.06
300	56.51	11.38	3.414	67.89	19.19
400	60.16	14.17	5.668	74.33	25.75
500	63.64	17.06	8.530	80.70	31.31
600	66.99	19.82	11.39	86.81	35.76
700	70.24	22.36	15.35	92.60	39.34
800	73.38	24.68	19.74	98.06	42.28
900	76.41	26.77	24.09	103.18	44.71
1000	79.33	28.67	28.37	108.00	46.74

Heat, Free Energy, Equilibrium Constant of Formation.—In conjunction with the heat of formation in Table III, and the thermodynamic functions of graphite,[13] hydrogen[13] and nitrogen,[13] values for pyridine in Table VI were used to compute the heat, free energy, and equilibrium constant of formation which are given in Table VII.

TABLE VII

HEAT, FREE ENERGY AND LOGARITHM OF EQUILIBRIUM CONSTANT OF FORMATION OF PYRIDINE

T, °K.	$\Delta H°f$, kcal./mole	$\Delta F°f$, kcal./mole	$\log_{10} K_f$
0	37.58	37.58	$-\infty$
298.16	33.61	45.52	-33.36
300	33.59	45.59	-33.21
400	32.52	49.76	-27.19
500	31.69	54.17	-23.68
600	31.06	58.73	-21.39
700	30.58	63.38	-19.79
800	30.24	68.09	-18.60
900	30.00	72.84	-17.69
1000	29.86	77.60	-16.96

COMPRESSIBILITY OF GASES. III. THE SECOND AND THIRD VIRIAL COEFFICIENTS OF MIXTURES OF HELIUM AND NITROGEN AT 30°[1]

BY GEORGE M. KRAMER AND JOHN G. MILLER

The John Harrison Laboratory of Chemistry, University of Pennsylvania, Philadelphia, Pennsylvania

Received January 29, 1957

The Burnett experiment has been used to obtain both the second and third virial coefficients of mixtures of helium and nitrogen at 30°. These mixture values have been used to compute the second virial coefficients (pure gas and interaction) as well as the third virial coefficients, C_{He}, $C_{He-He-N_2}$, $C_{He-N_2-N_2}$, and C_{N_2}.

Introduction

The compressibility factor, $Z = pv/RT$, where v is the molar volume, may be regarded as a single-valued function of the pressure, temperature and composition of any homogeneous phase and is a function of only the temperature and pressure for a pure gas or a given gas mixture. Burnett[2] has utilized this relationship to design an experiment for the determination of the compressibility of a gas from isothermal pressure measurements alone. Descriptions of the apparatus and discussions of the theory of the method have been given in earlier papers.[2-3] As an important feature of the method[3] one is able to determine the composition of a gas mixture from the same measurements which are used to determine the compressibility.

The study presented here for the helium–nitrogen system adds to the slowly increasing information concerning the behavior of binary systems and is important in that it establishes the usefulness of the Burnett experiment in determining not only the second but also the third virial coefficients of gas mixtures. To the best of our knowledge the third virial coefficients reported here are more accurate than any determined heretofore for gas mixtures, and it is hoped that such values will eventually prove useful in establishing criteria for the force constants in various intermolecular potential functions.

Treatment of Data

It has been shown[3] that the compressibility factor which may be expressed as a power series in the pressure

$$Z = 1 + Bp + Cp^2 + \ldots \quad (1)$$

may also be written in exponential form

$$Z = \exp(\alpha p - \beta p^2 + \ldots) \quad (2)$$

The latter formulation was particularly useful in treating the helium–carbon dioxide system,[3b] for it converges considerably more rapidly than the first expression. Z has been shown to be equal to $AN^r p_r$, where $A = Z_0/p_0$ is a filling constant for the apparatus, equal to the compressibility divided by

(1) Based on a dissertation to be submitted in April, 1957, by George M. Kramer in partial fulfillment of the requirements for the degree of Doctor of Philosophy. Presented at the 131st meeting of the American Chemical Society, Miami, Florida, April, 1957.

(2) E. S. Burnett, *J. Applied Mechanics, Trans. ASME*, **58**, A136 (1936).

(3) (a) W. C. Pfefferle, Jr., J. A. Goff and J. G. Miller, *J. Chem. Phys.* **23**, 509 (1955); (b) R. C. Harper, Jr., and J. G. Miller, *ibid.* **25**, in press (1957).

the pressure of the gas in the initial condition, N is an apparatus constant equal to the ratio of the combined volumes of the Burnett chambers to the volume of the first chamber, and r is an index number denoting the expansion at which the pressure is being measured. Insertion of this expression for Z in equation 2 leads to the linearized equation

$$\ln p_r = -\ln A - r \ln N + \alpha p_r + \beta p_r^2 + \ldots \quad (3)$$

The coefficients α and β may be related readily to B and C which are the temperature dependent virial coefficients by expanding equation 2 and comparing the coefficients of similar powers of p. Thus, we find

$$Z = 1 + \alpha p + \left(\frac{\alpha^2}{2} + \beta\right)p^2 + \ldots \quad (4)$$

so that

$$B = \alpha; \quad C = \frac{\alpha^2}{2} + \beta; \quad \text{etc.}$$

Equation 3 is an equation of condition containing four unknowns, A, N, α and β, and therefore four such equations are needed to permit evaluation of these terms. The initial pressure and the pressure after any expansion each contribute one such equation, and since from five to ten expansions were made in each run ample data were available to solve for the unknowns using a least-squares procedure.

Values of B found in this manner were fitted to the Lennard-Jones and Cook equation

$$B_{\text{mix}} = x_1^2 B_{11} + 2x_1 x_2 B_{12} + x_2^2 B_{22} \quad (5)$$

in which x_1 and x_2 are the mole fractions of the respective gases, B_{11} and B_{22} are the second virial coefficients of the pure gases, and B_{12} is the second virial coefficient for the helium–nitrogen interaction.

An analogous equation was used to treat the values of the third virial coefficient. This equation

$$C_{\text{mix}} = x_1^3 C_{111} + 3x_1^2 x_2 C_{112} + 3x_1 x_2^2 C_{122} + x_2^3 C_{222} \quad (6)$$

is based on the probability of the three-body interactions, the subscripts being indicative of the molecules which are involved in each term.

Experimental

The equipment for this study was the same as that used earlier[3b] and the constant temperature bath was maintained at $30.000 \pm 0.002°$.

Helium and prepurified nitrogen were obtained from the Matheson Company and analyzed by mass spectrometry. Trace quantities of hydrocarbons were the only impurities found in each tank and these gases were not further purified. "Bone dry" CO_2, also supplied by Matheson, contained a small amount of water as well as a trace of hydrocarbons and was cleaned under pressure over silica gel before being used in calibrating the piston gage. A sample of the purified gas was tested in a mass spectrometer by the Consolidated Engineering Company and was found to contain less than 0.005% of water and no hydrocarbons.

It is of interest that the manner in which a mixture is prepared enables one to calculate the mole fraction of either gas in a convenient way which eliminates the need for chemical analysis. The method consists in placing the first component, a, whose compressibility factor Z_a is known, in the first chamber and measuring its pressure p_a. The second component, b, is then added and after equilibrium has been obtained the starting pressure p_0 for the mixture is read. After the series of expansions the compressibility factor Z_0

may be deduced and the mole fraction of a determined by the relationship

$$x_a = \frac{n_a}{n_0} = \frac{p_a V_1}{Z_a RT} \frac{Z_0 RT}{p_0 V_1} = \frac{p_a Z_0}{Z_a p_0} \quad (7)$$

where n_a and n_0 are the numbers of moles of gas a and of the mixture present at the start and V_1 is the volume of the first chamber.

In a similar way, the composition of mixtures containing more than two gases can be determined along with the compressibility factor. In general, n components would require $n - 1$ Burnett experiments to determine the mole fractions of the various components.

Results

A total of twenty-one runs, two on each of the pure gases and seventeen on binary mixtures encompassing the entire concentration range were completed. All runs were made at 30° over a pressure range similar to that of the sample data given in Table I.

Table I

CORRECTED ABSOLUTE PRESSURES, p_r (IN ATM.), OF HELIUM, NITROGEN AND TWO MIXTURES AT 30°

r	He	N_2	Mixture A (p_{N_2} = 20.5375)	Mixture B (p_{N_2} = 82.0881)
0	129.9369	121.1686	103.3743	91.0569
1	87.2984	81.8946	69.4299	61.6752
2	59.0073	55.7969	46.9242	41.9708
3	40.0447	38.1463	31.8426	28.6240
4	27.2489	26.1063	21.6683	19.5416
5	18.5780	17.8749	14.7729	13.3472
6	12.6829	12.2379	10.0838	9.1192
7	8.6654	8.3792	6.8900	6.2306
8	5.9240	5.7357	4.7090	
9	4.0515	3.9268	3.2206	
10	2.7716	2.6873		

In Table II are listed the experimental values of the second and third virial coefficients found by fitting the data to equation 3. The observed variation of B_{mix}, with composition is illustrated in Fig. 1, which contains the least-squares curve

Table II

THE OBSERVED SECOND AND THIRD VIRIAL COEFFICIENTS OF MIXTURES OF HELIUM AND NITROGEN AT 30°

Mole fraction N_2	$B_{\text{mix}} \times 10^4$ (atm.$^{-1}$)	$C_{\text{mix}} \times 10^8$ (atm.$^{-2}$)
0	4.736	−5.743
0	4.694	−3.651
0.0594	5.108	−0.3824
.1067	5.269	2.990
.1594	5.436	7.196
.2111	5.743	6.075
.2628	5.777	10.35
.3215	5.838	27.24
.4040	5.624	33.59
.4716	5.408	39.27
.5231	5.038	54.52
.5826	4.605	68.33
.6315	3.965	88.19
.6779	3.534	102.8
.7284	3.062	113.2
.7848	2.569	132.8
.8720	1.268	164.3
.9152	0.2016	185.1
.9473	−0.1098	187.0
1	−1.590	234.8
1	−1.746	241.5

according to the Lennard-Jones and Cook equation. Table III gives the values of the coefficients, B_{11}, B_{12} and B_{22} determined for the least-squares curve and also the average values determined separately for the end-points.

TABLE III

The Least-Squares Second Virial Coefficients of the Lennard-Jones and Cook Equation and the Average Values of the End-Points (in atm.$^{-1}$) at 30°

	Lennard-Jones and Cook	Av. values of end-points
B_{He}	4.631×10^{-4}	4.715×10^{-4}
B_{He-N_2}	8.779×10^{-4}	
B_{N_2}	-1.416×10^{-4}	-1.668×10^{-4}

The observed third virial coefficients of the mixtures are plotted in Fig. 2. Table IV gives the least-squares values for the end-points and the interaction terms, compared with the average values determined separately for the pure gases.

TABLE IV

The Least-Squares Third Virial Coefficients of the Equation, $C_{mix} = x_1^3 C_{111} + 3x_1^2 x_2 C_{112} + 3x_1 x_2^2 C_{122} + x_2^3 C_{222}$, and the Average Values of the Pure Gas End-Points (in atm.$^{-2}$) at 30°

	Least-squares third virial coefficients	Av. values of end-points
C_{He}	-4.519×10^{-8}	-4.697×10^{-8}
$C_{He-He-N_2}$	12.10×10^{-8}	
$C_{He-N_2-N_2}$	48.08×10^{-8}	
C_{N_2}	231.0×10^{-8}	238.2×10^{-8}

Discussion of Results

Before considering the variation of the observed virial coefficients of the mixtures as a function of composition, the accuracy of the results, or the possible uses of these and similar data, it is desirable to show that the regression formula used is satisfactory. That this is so becomes apparent from a study of equation 3 with respect to the helium–nitrogen system. By rewriting equation 3 in the form

$$\ln p_r - \alpha p_r - \beta p_r^2 = -\ln A - r \ln N \quad (8)$$

we see that the terms αp_r and βp_r^2 may be considered as correction factors necessary to establish a straight line relationship between the L.H.S. of the equation and the index r. That this relationship should exist follows from the fact that both α and β would be zero for an ideal gas and the plot of $\ln p_r$ against r would be a straight line.

A non-ideal gas on the other hand would exhibit curvature in the plot of $\ln p_r$ against r, indicating the need for the correction terms. The removal of curvature in the subsequent plots of $\ln p_r - \alpha p_r$ against r and $\ln p_r - \alpha p_r - \beta p_r^2$ against r may be used as a criterion for the adequacy of equation 3.

With He, N_2 and their mixtures, very little curvature exists in the "ideal gas" plot and the application of one or two correction terms is clearly adequate to represent the data satisfactorily in the experimental pressure range. It might be expected from the magnitudes of the second and third virial coefficients of helium and nitrogen that one correction term would be sufficient to represent the former up to 100 atmospheres, while two terms
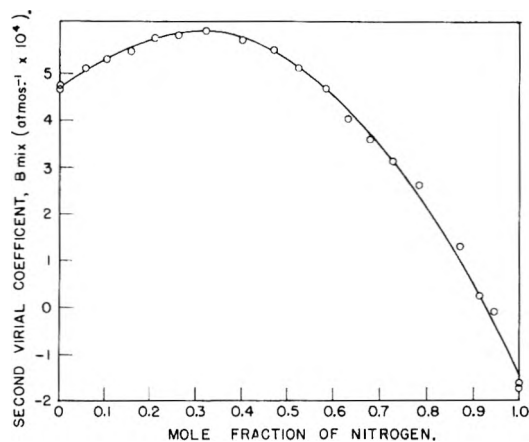
Fig. 1.—The plot of B_{mix} for helium–nitrogen mixtures at 30°. The least squares curve is drawn for the Lennard-Jones and Cook equation.
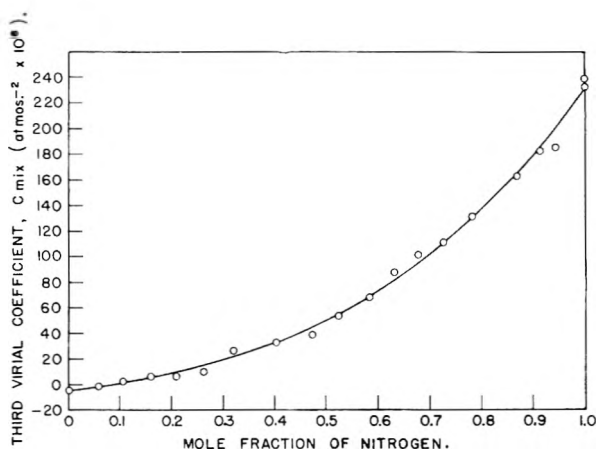

Fig. 2.—Variation of the third virial coefficient with composition for He–N_2 mixtures at 30°. The least squares curve is drawn for the equation $C_{mix} = x_{He}^3 C_{He} + 3x_{He}^2 x_{N_2} C_{He-He-N_2} + 3x_{He} x_{N_2}^2 C_{He-N_2-N_2} + x_{N_2}^3 C_{N_2}$.

might be necessary for the latter in the same range, and this is indeed the case. Figure 3 illustrates the application of this treatment to nitrogen. The drawing in the insert provides a qualitative picture of the effect of the various correction factors.

Next, it is of interest to interpret the shape of the plot of B_{mix} against composition and to consider the second virial coefficients for the various interactions. The magnitudes of the second virial coefficients may be shown to be related to the sum of two factors[4]

$$B_{xy} = b_0 - N_0 K_2$$

where b_0 is the covolume of clusters of interacting particles, x and y, N_0 is the number of molecules per mole, and K_2 is the equilibrium constant for the formation of bimolecular clusters ($K_2 = C_{xy}/C_x C_y$). The covolumes of the interacting species, He–He, He–N_2 and N_2–N_2, increase in the *order* listed which would indicate a trend in the corresponding B values in the same direction. This effect is primarily responsible for the increase in going from B_{He-He} to B_{He-N_2} but the difference

(4) K. S. Pitzer, "Quantum Chemistry," Prentice-Hall, Inc., New York, N. Y., 1954, Chapter 11.

a = ln Pr vs r
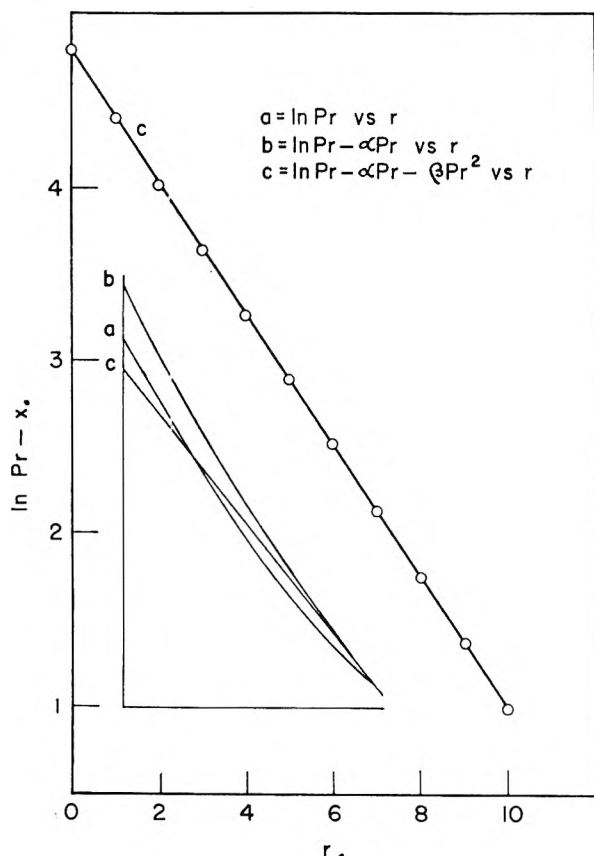b = ln Pr − αPr vs r
c = ln Pr − αPr − βPr² vs r

Fig. 3.—A test of regression formulas for Burnett data. The single curve is for nitrogen at 30°. The insert shows in schematic manner the behavior of all three plots.

in the equilibrium constants for the different interactions cannot be neglected, as evidenced by the negative value of $B_{N_2-N_2}$.

The size of the equilibrium constant is dependent not only on the separation of the molecules but also on the attractive forces which exist between the molecules. These, which are predominantly of the London dispersion type between non-polar molecules, are much stronger between two nitrogen molecules than between the other possible complexions.

The maximum in the plot of B_{mix} against composition is due to the fact that B_{12} is greater than B_{11} or B_{22} and is dominant in mixtures of balanced composition. The maximum is shifted toward the helium-rich end since B_{He} is greater than B_{N_2}. The fact that B_{12} is of maximum importance in the central region of the curve and that it is predominantly responsible for the degree of fit of the least-squares curve in this region supports the value of B_{12} listed in Table III. The probable error of an individual determination of B_{mix} from the least-squares curve is ± 0.104 × 10⁻⁴ atm.⁻¹.

In Table V the values of B_{12} found by other investigators are listed for comparison with our

value. Pfefferle[3a] used the Burnett method and his result is the least-squares best value for only three binary mixtures. The Lunbeck and Boerboom[5] value of B_{12} is a theoretical rather than an experimental value. They used empirical mixing rules to obtain the force constants for the interaction between unlike molecules.

THE INTERACTION COEFFICIENT, B_{He-N_2}, IN ATM.⁻¹

	B_{He-N_2}	$t(°C.)$
Kramer and Miller	8.78 × 10⁻⁴	30
Pfefferle, Goff and Miller[3a]	8.45 × 10⁻⁴	30
Lunbeck and Boerboom[5]	7.24 × 10⁻⁴	25
Edwards and Roseveare[6]	5.13 × 10⁻⁴	25

Edwards and Roseveare[6] used a relationship between the volume change which occurs on mixing two gases at low pressures and the Lennard-Jones and Cook equation to evaluate B_{12}. Two readings at each of two pressures were taken on a gas of a single composition, and the four results yielded the average value reported above. The source of the discrepancy between their value of B_{12} and the others is not readily apparent. It may be noted that an increase in B_{12} with temperature is to be expected since the value of the equilibrium constant, K_2, decreases with rising temperature.

Knowledge of the temperature dependence of the second virial coefficient makes it possible to evaluate the constants of any of a variety of potential functions which are customarily used to describe the interactions between molecules. While much work has been done with single component systems, accurate data concerning the behavior of mixtures is relatively scarce and quite desirable to aid in establishing the validity of mixing rules which must be used to deal with the practical problems of everyday importance.

The temperature dependence of the second virial coefficient, while sufficient to establish the values of the constants of proposed functions is not particularly useful in aiding one in the selection of a specific function. It is hoped that accurate knowledge of the temperature dependence of the third virial coefficient will provide additional aid in this selection. An investigation of the temperature dependence of these virial coefficients is underway at this Laboratory.

(5) R. J. Lunbeck and A. J. H. Boerboom, *Physica*, **17**, 76 (1951).

(6) A. E. Edwards and W. E. Roseveare, *J. Am. Chem. Soc.*, **64**, 2816 (1942).

THE SOLUBILITY AND ENTROPY OF SOLUTION OF IODINE IN OCTAMETHYLCYCLOTETRASILOXANE AND TETRAETHOXYSILANE

By Kozo Shinoda and J. H. Hildebrand

Department of Chemistry and Chemical Engineering, University of California, Berkeley, California

Iodine dissolves in octamethylcyclotetrasiloxane, $(CH_3)_8Si_4O_4$, to give a violet, "regular" solution, but in tetraethoxysilane, $(C_2H_5O)_4Si$, to give a solvated, brown solution. Its solubility, in mole fraction, conforms closely to the equations, respectively: $\log x_2 = 2.820 - 1464.3/T$ and $\log x_2 = 1.499 - 816.9/T$. The respective mole percentage and molal entropies of solution at 25° are 0.8104, 22.5 e.u., and 5.747, 12.5 e.u. The entropy of solution in $(CH_3)_8Si_4O_4$ shows no divergence from the values in other violet solutions, in spite of the unprecedented disparity in molal volume of solvent and solute, 312 and 59 cc., indicating that the entropy of solution is a function of mole fraction, not volume fraction, for quasi-spherical molecules of different size. The solubility corresponds to a solubility parameter of 8.2 instead of the value given by the energy of vaporization, 6.4. The partial molal volume, like the entropy, of iodine in the violet, siloxane solution shows no divergence from its value in neighboring solvents attributable to differences in solvent molal volumes. In the silane, however, both properties are considerably smaller, in accord with the evidence for complex formation.

The molecule of octamethylcyclotetrasiloxane, $(CH_3)_8Si_4O_4$, has an octagonal core of alternating silicon and oxygen atoms with two methyl groups attached to each silicon atom. A scale model (LaPine) shows that the methyl groups are most uniformly spaced if the four silicon atoms are twisted about half way between a square and a tetrahedral orientation, making the whole molecule quasi-spherical. The oxygen atoms are then so shielded that an iodine molecule cannot approach closely enough to form a charge-transfer complex, as shown by the pure violet of its solution. A former member of our group, D. N. Glew, found that its maximum light absorption occurs at 518 mμ. The maximum is at 517 mμ in carbon tetrachloride and at 522 mμ in n-C_7F_{16}, "f-heptane." The solution is therefore quite "regular."

The molal volume of this silicone is 312 cc. at 25°, much greater even than that of f-heptane, 225 cc., and over 5 times that of liquid iodine, 59 cc. Its iodine solution therefore affords a rare opportunity for testing the effect of disparate size upon the entropy of solution of quasi-spherical molecules.

The molecules of this silicone, furthermore, present a wide departure from a radial attractive potential and this puts a severe strain upon expressions for enthalpy of solution based upon radial fields.

We included in this study a second silicone, tetraethoxysilane, $(C_2H_5O)_4Si$, in order to emphasize, by contrast, the exceptional properties of the above compound. The oxygen atoms of this silicone are not buried by the ethyl groups, hence the iodine solution is brown in color, indicating the presence of a charge-transfer complex, with non-regular behavior. It absorption maximum is at 475 mμ, near to that for iodine in ether,[1] 462 mμ.

Materials.—The $(CH_3)_8Si_4O_4$ was pure material furnished by the General Electric Company through the kindness of R. C. Osthoff. It was vacuum distilled shortly before use in order to remove small amounts of polymer, evident from the higher viscosity of the residue.

The $(C_2H_5O)_4Si$ was obtained from Dow-Corning. It was dried, then vacuum distilled.

Results.—The solubility of iodine was determined by equilibrating in the apparatus described by Glew and Hildebrand,[2] and titrating weighed

portions of saturated solution with thiosulfate.

Our results for iodine in $(CH_3)_8Si_4O_4$ are given in Table I. The calculated values have been smoothed out by the equation: $\log x_2 = 2.820 - 1464.3/T$. This gives $100\ x_2 = 0.8104$ at 25°, and $R(d \log x_2/d \log T) = 22.5$ cal. deg.$^{-1}$.

SOLUBILITY OF I_2 IN $(CH_3)_8Si_4O_4$, MOLE PER CENT.

	20.06°	25.06°	29.96°	34.97°	39.98°
	0.667	0.816	0.973	1.176	1.388
	.672	.816	0.975	1.168	1.389
	.663	.805		1.178	1.385
	.665	.826			
Av.	0.667	0.816	0.974	1.174	1.387
Calcd.	0.670	0.813	0.975	1.170	1.392

Table II gives the corresponding figures for iodine in $(C_2H_5O)_4Si$, with $\log x_2 = 1.499 - 816.9/T$ and $R(d \log x_2/d \log T) = 12.5$ between the two higher temperatures. No measurements were made above 25° because a slow secondary reaction occurs as shown by a gradual decrease in the height of the absorption band.

SOLUBILITY OF I_2 IN $(C_2H_5O)_4Si$, MOLE PER CENT.

	11.85°	17.07°	24.99°
	4.28	4.83	5.73
	4.35	4.81	5.73
	4.33		5.76
Av.	4.32	4.82	5.74
Calcd.	4.323	4.848	5.747

The measurements are plotted in Fig. 1 in a manner similar to that used in a recent paper by Hildebrand and Glew.[3] We have omitted the point for C_7F_{16} there shown in order to show the remaining points on a larger scale. Instead of using $-\log x_2$ as abscissa, we here use $-R \ln x_2$, which represents the entropy of ideal solutions of liquid iodine. As ordinate we plot the excess of $R(\partial \ln x_2/\partial \ln T)_{satd}$ over the entropy of fusion of iodine, in cal. deg.$^{-1}$ mole^{-1}. This likewise represents the entropy of ideal solution of liquid iodine, and yields points on a 45° line starting at the origin.

(1) H. A. Benesi and J. H. Hildebrand, *J. Am. Chem. Soc.*, **71**, 2703 (1949).

(2) D. N. Glew and J. H. Hildebrand, This Journal, **60**, 616 (1956).

(3) J. H. Hildebrand and D. N. Glew, *ibid.*, **60**, 618 (1956).

Fig. 1.—Iodine solutions.

Solvent	$\left(\dfrac{\partial \ln a_2}{\partial \ln x_2}\right)_T$	$R\left(\dfrac{\partial \ln x_2}{\partial \ln T}\right)_{\text{satd}}$	$\bar{S}_2 - S_2^s$
CS_2	0.85	18.8	16.0
$CHCl_3$	.92	20.3	18.7
CCl_4	.96	21.9	21.0
$SiCl_4$	.98	23.3	22.8
$(CH_3)_8Si_4O_4$	.99	22.5	22.3

violet solutions, whereas the point for the brown solution in $(C_2H_5O)_4Si$ diverges strongly. It is near that for p-xylene. The solvation yields higher solubility and smaller entropy of solution.

The correspondence of the former solution with other violet solutions is very significant in view of the large ratio of the molal volumes of solvent and solute, 312/59. For the neighboring solvents, CCl_4 and c-C_6H_{12}, the ratios are 97/59 and 109/59, respectively. The equation

$$\bar{S}_2 - S_2^\circ = -R[\ln \phi_2 + \phi_1(1 - v_2v_1^{-1})] \quad (3)$$

for entropy of solution, (of component 2) where v's are molal volumes, yields an excess over the ideal entropy, $-R \ln x_2$, of 0.15 e.u. for the CCl_4 solution and 1.60 e.u. for the silicone solution. The plot shows no such discrepancy. The inescapable inference is that the entropy of solution of quasi-spherical molecules of different size is a function of mole fraction, not volume fraction. In a paper now in preparation on entropy of solution of gases we will present further experimental evidence in support of this conclusion. It indicates that the entropy of solution is not a function of relative size, but rather one of configuration, as envisioned in the "string of beads" model used for deriving the "Flory–Huggins" equation. The derivation by Hildebrand[6] based only upon molecular sizes, while probably valid for gas mixtures, is invalid for the more highly condensed liquid mixtures.

The second fact to which we invite attention is that the position of the point for $(CH_3)_8Si_4O_4$ is far from that indicated by the solubility parameter, 6.4, calculated by Osthoff and Grubb[7] from its energy of vaporization. This would make it nearly as poor a solvent for iodine as is f-heptane. Its position in Fig. 1, however, in relation to CCl_4, c-C_6H_{12} and $SiCl_4$, whose δ-values are 8.6, 8.2 and 7.6, respectively, corresponds to a solubility parameter practically identical with that of c-C_6H_{12}, and this we have found to accord with its behavior with two fluorocarbons, as described in the following paper.

Substituting the known values in the equation

$$\log a_2^s = \log x_2 + v_2\phi_1^2(\delta_2 - \delta_1)^2/4.575T \quad (4)$$

and solving for δ_1 gives 8.2, agreeing within the limit of error with its close neighbor, c-C_6H_{12}.

Thirdly, it is evident that the "measured" values of the entropy of solution increase more rapidly than $-R \ln x_2$ in going from the better to the poorer solvents. This is evidently related closely to increases in the partial molal volume of iodine and

The entropy of fusion of iodine at 25° is calculated from its value at the melting point and ΔC_p, the excess molal heat capacity of liquid over solid. This requires extrapolation of the heat capacity of the liquid over the interval from the melting point, 113.5°, to 25°, and the result is therefore somewhat uncertain. The data of Frederick and Hildebrand[4] that we have used heretofore, give 8.0 e.u. for the entropy of fusion at 25°. A later critical survey by Kelley[5] yields 8.2. Because the small difference is unimportant, in view of the uncertainty, we retain our original figure for the sake of consistency. Point A corresponds to the logarithm of the activity of liquid iodine, and point B the activity of iodine in an ideal solution, where it is the same as the activity of solid iodine, $a_2^s = 0.258$.

The partial molal entropy of iodine in a solution saturated with solid is

$$\bar{S}_2 - S_2^s = R(\partial \ln x_2/\partial \ln T)_{\text{satd}} (\partial \ln a_2/\partial \ln x_2) \quad (1)$$

The factor on the right, which expresses the deviation from Henry's law, is not far from unity for such dilute solutions. It may be evaluated by aid of the approximate relation

$$\ln a_2 = \ln x_2 + k\phi_1^2 \quad (2)$$

where ϕ denotes volume fraction. Using $a_2^s = 0.258$ and the measured values of x gives values for k by aid of which we obtained the values of $(\partial \ln a_2/\partial \ln x_2)_T$ shown in Table III. Multiplying the experimental values of $R(\partial \ln x_2/\partial \ln T_2)$ by these factors gives the entropy of transfer of solid iodine to saturated solution, $\bar{S}_2 - S_2^s$ in the last column. These values are indicated by stars in Fig. 1.

Discussion.—We invite attention, firstly, to the fact that the point for iodine in $(CH_3)_8Si_4O_4$ falls exactly upon the line through the points for other

(4) K. J. Frederick and J. H. Hildebrand, J. Am. Chem. Soc., 60, 1436 (1938).
(5) K. K. Kelley, U. S. Bur. Mines Bull. 476.

(6) J. H. Hildebrand, J. Chem. Phys., 15, 225 (1947).
(7) R. C. Osthoff and W. T. Grubb, J. Am. Chem. Soc., 76, 399 (1954).

the attendant entropy of expansion, pointed out by Hildebrand and Scott.[8]

In order to investigate this contribution we have determined the partial molal volume of iodine in several selected solvents including the two silicones here used. Instead of making the precise determinations of density and composition required in the usual method, we adopted a simple, direct dilatometric procedure. The dilatometer consists of a cylindrical bulb of 150-cc. capacity containing a large glass ball. It has a capillary stem with an internal diameter of 1.8 mm. This is filled at 25° with solvent extending into the lower part of the capillary. A weighed amount of iodine is sealed in a long thin glass capsule narrow enough to slip down the capillary. After the capsule is introduced it is broken and the iodine is dissolved by twirling the ball inside the bulb. After temperature is restored, the change of level in the capillary is read. From the change in volume, corrected for the volume of the glass of the capsule, the partial molal volume of the iodine is calculated.

The work is being extended to a number of solvents and will be reported later; we give here only the few results that contribute directly to interpretation of the entropy of solution of iodine in the two solvents here involved. Table IV gives results for $(C_2H_5O)_4Si$ and $(CH_3)_8Si_4O_4$ together with several others for comparison.

The contribution of expansion to the entropy of solution may be evaluated by aid of the relation $\Delta S^{Exp.} = (\bar{v}_2 - v_2^0)(\partial p/\partial T)_v$. For v_2^0 we use, as

(8) J. H. Hildebrand and R. L. Scott, *J. Chem. Phys.*, **20**, 1520 (1952).

TABLE IV

PARTIAL MOLAL VOLUMES OF IODINE, 25°

	CS_2	CCl_4	$(CH_3)_8$-Si_4O_4	n-C_7H_{16}	C_7F_{16}	$(C_2H_5O)_4$-Si
v_2, cc.	60.7	66.7	66.6	66.3	100[2]	60.5
δ_1	10.0	8.6	8.2[9]	8.1[9]	5.8	7.2[10]
$\Delta S^{Exp.}$	0.6	1.7	1.7	1.6	4.6	0.3

heretofore, 59 cc. Since we have no measured values of $\partial p/\partial T$ for the silicones we obtain approximate values from the solubility parameter as

$$(\partial p/\partial T)_v = (\partial E/\partial v)_T/T + p/T \cong (\Delta E^{vap}/v)T' = \delta_1^2/T$$

The last row in Table IV gives values of $\Delta S^{Exp.}$ so calculated. We see that the size of the $(CH_3)_8Si_4O_4$ molecule introduces no departure in either $\bar{v}_2$ or $\Delta S^{Exp.}$ from the behavior of solvents with neighboring values of δ_1 although $\Delta S^{Exp.}$ is so large as to account for much of the difference between the actual and the measured entropy of solution, as in the cases reported by Hildebrand and Scott[8] and by Reeves and Hildebrand.[11]

The fact that both the partial molal volume and the entropy of solution of iodine in the ethoxysilane is so much smaller than in the siloxane is in accord with the formation of a strong charge transfer complex.

We wish to thank Dr. R. C. Osthoff for the siloxane, Marilyn Angel for her exploratory measurements, Dr. J. E. Jolley for advice and the National Science Foundation for its support.

(9) Adjusted.
(10) Estimated from density and boiling point.
(11) L. W. Reeves and J. H. Hildebrand, THIS JOURNAL, **60**, 949 (1956).

THE LIQUID-LIQUID SOLUBILITY OF OCTAMETHYL-CYCLO-TETRASILOXANE WITH PERFLUOROMETHYLCYCLOHEXANE AND PERFLUORO-n-HEPTANE

BY J. E. JOLLEY AND J. H. HILDEBRAND

Department of Chemistry, University of California, Berkeley, Cal.

Received January 31, 1957

The liquid–liquid solubility curves of mixtures of octamethylcyclotetrasiloxane with (a) f-methylcyclohexane and (b) f-heptane have been determined. The critical temperatures are (a) 43.86° and (b) 69.97°. The mole fractions of the silicone at the curve maxima are (a) 0.38, (b) 0.44. The value of the solubility parameter of the silicone at 25° calculated from the measurements agrees well with the value 8.2 obtained from its solvent power for iodine (see preceding paper), which is far in excess of the value obtained from its energy of vaporization $(\Delta E^{vap}/v)^{1/2}$. These systems add to the mounting evidence that the solubility parameters of aliphatic hydrocarbons must be considerably increased in order to conform to regular solution theory in their interactions with molecules of other types. This calls for a critical study of intermolecular potentials.

The solubility of iodine in octamethylcyclotetrasiloxane, reported in the preceding paper, corresponds to a solubility parameter of 8.2, much larger than 6.4, the value derived by Osthoff and Grubb[1] from its energy of vaporization. The latter value would lead one to expect this substance to form nearly ideal solutions with fluorocarbons. We found, however, that it behaves like paraffin hydrocarbons in forming two liquid phases with f-heptane and f-methylcyclohexane. We have de-

termined its mutual solubility with these two fluorocarbons in order to learn whether the value 8.2 is consistent with its solvent power for substances at both extremes of the parameter range.

Materials.—The two fluorocarbons were purified by the methods described by Glew and Reeves.[2] The siloxane was from the stock described in the preceding paper.

Procedure.—To contain the mixtures, glass tubes approximately 6 mm. in diameter and 12 cm. long were sealed each at an angle of 120° to one end of a length of 1 mm. capillary tubing, the other end of which could be attached to a ground glass joint. The tubes were thoroughly washed with

(1) R. C. Osthoff and W. T. Grubb, *J. Am. Chem. Soc.*, **76**, 399 (1954).

(2) D. N. Glew and L. W. Reeves, THIS JOURNAL, **60**, 615 (1956).

chromic acid, water and methanol, and flamed out under vacuum. The pure liquids were measured in at 25° from a 1-cc. graduated pipet, separately calibrated for each component because of different retention, the siloxane wetting the glass more than the fluorocarbon. The volume fractions given below are corrected for thermal expansion but not for volume changes on mixing. The tubes were cooled in liquid nitrogen, evacuated and sealed several cm. above the bottom of the capillary. The observations were carried out in a well stirred water-bath whose rate of cooling could be adjusted to about 0.005° per minute. The thermometers used were calibrated against N.B.S. standard thermometers. The tubes were heated to one or two tenths of a degree above their consolute temperatures and allowed to cool slowly, with frequent shaking, and observed with a magnifying glass.

At volume fractions close to 0.5, mixtures are milky blue in color. This increases as the temperature falls and then disappears as the mixture suddenly changes to a heterogeneous mass of small droplets. As the volume fraction varies from the neighborhood of 0.5, the blue color diminishes and is not apparent beyond about 0.3, and the sudden appearance of tiny droplets is taken to mark the consolute temperature. The large difference in the density of the two components here used makes the separation easily observable. In all cases, the consolute temperatures were reproducible to within 0.01°, and were the same on approaching from above and from below.

The results are shown in Table I. The points fall upon smooth curves of the familiar type, hence we omit publishing a plot of them. The critical temperatures and compositions read from our plot are given at the bottom of each series. The curves are broader at the top than any so far reported. They fit the relations

$$\text{silicone and } C_7H_{14}, \; T_c - T = 58.9(x_2'' - x_2')^{3.41}$$
$$\text{silicone and } C_7H_{16}, \; T_c - T = 52.5(x_2'' - x_2')^{3.31}$$

The high exponents, in excess of the commonly used 3, express the smaller curvature. The linear relationship between $(T_c - T)^{1/s}$ and log (x_1/x_2), reported by Cox and Herington,[3] is moderately well obeyed, and therefore useful in extrapolating to lower temperatures.

TABLE I
LIQUID–LIQUID SOLUBILITY OF $(CH_3)_8Si_4O_4$
(COMPONENT 2)

With $C_6H_{11}CF_3$			With n-C_7F_{16}		
ϕ_2	x_2	t, °C.	ϕ_2	x_2	t, °C.
0.178	0.120	35.80	0.176	0.136	59.95
.290	.205	42.03	.287	.229	67.07
.399	.295	43.86	.396	.326	69.58
.495	.382	43.85	.491	.416	69.97
.598	.484	43.45	.589	.513	69.90
.703	.598	40.58	.674	.604	68.48
.817	.737	30.55	.797	.743	60.97
			.888	.852	44.78
Crit. 0.48	0.38	43.86	Crit. 0.51	0.44	69.97

We may calculate a solubility parameter, δ_2, for the silicone, by aid of the equation $4RT_c = (v_1 + v_2)(\delta_2 - \delta_1).^2$ In the solution with $C_6H_{11}CF_3$ this gives $\delta_2 - \delta_1 = 2.2$ at 43.86°. Both δ_2 and δ_1 are larger at 25° but their difference changes but little, hence if we use $\delta_1 = 6.0$, we get $\delta_2 = 8.2$. We may extrapolate values of x to 25° by using the relation of Cox and Herington, applying then the usual equation, ln $a_2 = $ ln $x_2 + v_2\phi_1^2 (\delta_2 - \delta_1)^2/RT$ to both liquid phases, with ln $a_2' = $ ln a_2'', we get

$$(\delta_2 - \delta_1)^2 = 4.575Tv_2^{-1}(\phi_1''^2 - \phi_1'^2)^{-1} \log (x_2' - x_2'')$$

(3) J. D. Cox and E. F. G. Herington, *Trans. Faraday Soc.*, **52**, 926 (1956).

This gives $\delta_2 - \delta_1 = 2.4$ and $\delta_2 = 8.4$, close to the above value.

To obtain a solubility parameter at 25° for the silicone with f-heptane involves a much wider extrapolation. It is evident, however, that our two liquid-liquid systems behave consistently, because the change from $C_6F_{11}CF_3$ to C_7F_{16} causes approximately the same rise with different second components, as shown in Table II.

TABLE II
DIFFERENCES IN LIQUID–LIQUID CRITICAL TEMPERATURES
OF C_7F_{16} AND $C_6H_{11}CF_3$ WITH OTHER LIQUIDS

	$(CH_3)_8Si_4O_4$	CCl_4	$CHCl_3$	C_6H_6
C_7F_{16}	70.0°	58.7°	78.5°	113.5°
$C_6F_{11}CF_3$	43.9°	26.8°	50.3°	85.3°
	26.1°	31.9°	28.2°	28.2°

The solubility of iodine in $(CH_3)_8Si_4O_4$ corresponds to a parameter of 8.2, as reported in the preceding paper by Shinoda and Hildebrand. We see that the solubility relations of $(CH_3)_8Si_4O_4$ with both iodine, with a very high solubility parameter, and with fluorocarbons, having very low parameters, are consistent with a parameter of about 8.2, far larger than the value of $(\Delta E^v/v)^{1/2} = 6.4$. It behaves essentially as what, peripherally, it is, a hydrocarbon, and adds one more piece of evidence to others already noted[4] of the abnormality of hydrocarbons with respect to regular solution theory. Iodine dissolves in the following solvents in conformity with their normal parameters: CCl_4, $TiCl_4$, CS_2, $CHBr_3$, $SiCl_4$, C_7F_{16}, $(C_4F_9)_3N$, f-propyl cyclic ether, but its solubilities in the following solvents can be accounted for only by adding the corrections here stated to their values of $(\Delta E^v/v)^{1/2}$: in 2,2,4-trimethylpentane, 1.0; in n-C_7H_{16}, 0.7; in 2,2-dimethylbutane, 1.1; in $(CH_3)_8Si_4O_4$, 1.8. Fluorocarbons mix with CCl_4 in accord with their normal parameters, but with hydrocarbons corrections must again be added, as follows: C_7F_{16} with 2,2,4-trimethylpentane, 1.5; with n-C_7H_{16}, 1.0; with 2,2-dimethylbutane, 1.8; C_5F_{12} with C_5H_{12}, 1.4; C_4F_{10} with c-C_5H_{10}, 1.6.

It is evident that the assumption commonly made, that molecules with peripheral hydrogen atoms have force fields similar to those with other peripheral atoms, is far from adequate, and calls for extensive critical investigation. In the case of $(CH_3)_8Si_4O_4$, the rigid core, Si_4O_4, contributes considerably to the volume but only trivially to intermolecular potential, making $(\Delta E^{vap}/v)^{1/2}$ too small to serve as an effective solubility parameter. The buried portions of the molecules of 2,2-dimethylbutane and 2,2,4-trimethylpentane may account similarly for the extra large corrections they require.

We wish to thank Dr. R. C. Osthoff and the General Electric Company for the octamethyl-

(4) (a) J. H. Hildebrand, *J. Chem. Phys.*, **18**, 1337 (1950); (b) J. A. Neff and J. B. Hickman, THIS JOURNAL, **59**, 42 (1955); (c) J. B. Hickman, *J. Am. Chem. Soc.*, **77**, 6154 (1955); (d) R. L. Scott, *Ann. Rev. Phys. Chem.*, **7**, 43 (1956); (e) E. P. McLaughlin and R. L. Scott, *J. Am. Chem. Soc.*, **76**, 5276 (1954).

tetrasiloxane, the Minnesota Mining and Manufacturing Company for the f-heptane, Dr. R. L. Scott for helpful comments, and the Atomic Energy Commission for the support of the work.

HIGH PRESSURE DISSOCIATION STUDIES OF THE URANIUM HYDROGEN SYSTEM[1]

By G. G. Libowitz[2] and Thomas R. P. Gibb, Jr.

Contribution No. 244 from the Department of Chemistry, Tufts University, Medford, Mass.

Received February 1, 1957

Pressure–composition isotherms were obtained for the uranium–hydrogen system over the temperature range 450 to 650° at pressures up to 65 atm. in a stainless steel apparatus designed for high temperature high pressure measurements. The experimentally determined plateau pressures are compared with values extrapolated from low temperature studies of Spedding and Flotow and Abraham. A value of −30.3 kcal./mole was obtained for the heat of formation of UH_3 from the dissociation pressure data.

Introduction

The pressure–temperature–composition relations in the uranium–hydrogen system have been investigated at temperatures below 430° by Spedding[3] and Flotow and Abraham.[4] These investigators found stoichiometric uranium hydride to have the formula UH_3. At temperatures above 430° the dissociation pressure of the hydride becomes greater than one atmosphere, and the usual glass-quartz apparatus can no longer be used to study this system. Mogard and Cabane[5] have measured the dissociation pressures of uranium hydride at high pressures, and Gibb, McSharry and Kruschwitz[6] have made a high pressure study of the high hydrogen composition region of this system.

It was the purpose of this investigation to study the uranium–hydrogen system at high pressures and temperatures over the whole range of hydrogen compositions from uranium metal to fully hydrided UH_3 in a stainless steel apparatus especially constructed for these investigations.

Experimental

Apparatus.—The apparatus, shown schematically in Fig. 1, consisted of a sample container, resistance furnace with temperature measurement and control systems, high pressure and pressure measuring systems, low pressure glass volume calibration system, and a hydrogen purification train. The tubing throughout the high pressure part of the apparatus was Type 316 stainless steel, $1/4$ in. o.d. and $1/8$ in. i.d. All connections were made with "Koncentrik" fittings with steel seats having Teflon ring gaskets. Valves A, B and C were Hoke Needle Valves with V point spindle. The other valves in the system are Hoke diaphragm-type packless valves.

The sample container was made from Type 316 stainless steel. The bottom was machined from flat stock and the main portion was bored and machined from solid rod. The parts were put together by atomic hydrogen welding. The cavity in the container was 7 in. by 1.5 in. diameter. The wall thickness was $1/2$ in. A lead-in tube of standard weight

(1) This research was supported by the Atomic Energy Commission. Presented at the 130th Meeting of the American Chemical Society, Atlantic City, New Jersey, September 21, 1956.

(2) Materials Research Group, Atomics International, Canoga Park, California.

(3) F. H. Spedding, A. S. Newton J. C. Warf, O. Johnson, R. W. Nottorf, I. B. Johns and A. H. Daane, *Nucleonics*, **4**, 4 (1949).

(4) H. E. Flotow and B. M. Abraham, Report AECD-3074, declassified Jan. 30, 1951.

(5) H. Mogard and G. Cabane, *Rev. met.*, **51**, 617 (1954).

(6) T. R. P. Gibb, Jr., J. J. McSharry and H. W. Kruschwitz, *J. Am. Chem. Soc.*, **74**, 6203 (1952).

$3/8$ in. stainless steel tubing with a Koncentrik fitting at the top, permitted the container to be attached to the high pressure line. By closing valve D, the bomb could be removed from the furnace without contaminating the sample.

The resistance heater consisted of two sections: the main winding and an auxiliary heater situated near the top of the furnace to eliminate thermal gradients. The main part of the furnace was a Norton Alundum core, 10 in. long and 4.5 in. in diameter wound with 16 gage Kanthal wire. The sample container rested on a steel pedestal mounted at the bottom of the furnace. The core was surrounded by firebrick at the sides and bottom, which in turn was surrounded by a galvanized iron can wrapped with asbestos. The top of the furnace was covered with a slab of $1/2$ in. transite containing openings for the sample container and thermocouples. The separately controlled auxiliary heater consisted of coiled Kanthal wire supported by three porcelain rods suspended from the bottom of the transite slab. In this way, the top of the bomb received additional heating to compensate for the heat loss due to thermal conductivity. Temperatures were measured with two calibrated Chromel-Alumel thermocouples, and controlled to ±0.5° by means of a photoelectric control circuit.

The two thermocouples were strapped to the sample container with asbestos tape, and were so situated that they measured the temperatures at the top and at the bottom of the sample when it was fully hydrided. By inserting a thermocouple inside the container under conditions similar to those used in making a run, it was found that the inside and outside temperatures differed by one to two degrees over the range studied. This difference was taken into account in setting the temperature controller.

The pressure of hydrogen over the sample was measured with a Brown Instrument Co. Recording Pressure Gauge. This was a multiple Bourdon spiral gage with three separate recording units of 0–20, 0–100 and 0–1000 p.s.i. The 0–20 and 0–100 p.s.i. units were connected to the manifold through valves which could be closed when the pressure became higher than these maximum values. During use, it was found that these pens were accurate to ±0.5% of their full scale reading.

The low pressure Pyrex glass system was separated from the high pressure portion of the apparatus by a Hoke needle valve, C. The glass system included two bulbs whose volumes were 5.535 and 12.97 liters. These were used for measuring the volumes of hydrogen gas removed from the sample during dehydriding runs. The glass system also contained a small calibrated bulb for calibrating volumes in the system and an open end mercury manometer.

Materials.—The uranium metal used was high purity Reactor grade (>99.9% U) metal furnished by the Atomic Energy Commission. A 230-gram block of metal was cleaned in 1:1 HNO_3, 0.1 N HCl, water, isopropyl alcohol and anhydrous ethyl ether in turn and transferred to the sample container under an argon atmosphere. Hydriding was carried out at about 200° and under a hydrogen pressure of 500 p.s.i. In this way uranium hydride, having the stoichiometric formula UH_3 at room temperature, could be prepared. The hydrogen was purified by passing over
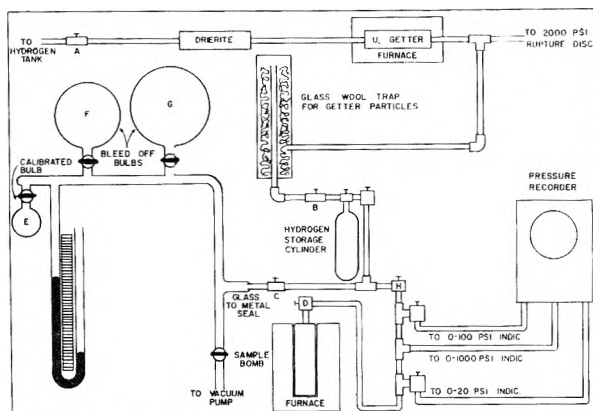
Fig. 1.—High pressure apparatus for dissociation studies.

drierite, hot uranium metal getter, and finally through a glass wool trap to remove any getter particles.

Experimental Procedure.—In a typical dehydriding run, the uranium hydride was heated to the desired temperature under a pressure of hydrogen. After the system reached equilibrium (*i.e.*, pressure did not change more than 0.5% of the full scale reading of the pen in the period of one hour), the pressure was recorded. The composition of the hydrogen in the sample was then decreased by bleeding hydrogen into the calibrated bulbs, F and G, and the pressure again recorded after it had become constant. By successive measurements in this way, pressure–composition isotherms at 50° intervals from 450 to 650° were obtained. The compositions were calculated by subtracting the S.T.P. amount of hydrogen above the sample and the amount of hydrogen bled into the glass system from the amount of hydrogen originally present in the container and the amount of hydrogen in the fully hydrided UH₃, the amount of hydrogen in each case being calculated from appropriate volumes, pressures, and temperatures. For these calculations, the non-ideality of the gas law at high pressures, as well as the hot and cold volumes of the sample container were taken into account. At least two dehydriding runs were made at each temperature.

For hydriding runs, the sample was completely dehydrided to uranium metal by evacuating at 500°. With the sample under vacuum, valve D was closed and the line between valves D and H was filled with hydrogen from the hydrogen storage cylinder at a pressure which could be read on the recorder. The sample was brought to the desired temperature, and valve D was opened to permit hydrogen to flow into the sample container. After the system reached equilibrium, the pressure was recorded, valve D was closed again, and another volume of hydrogen was added by the same procedure. From the change in pressure on opening valve D, the amount of hydrogen added and the composition was calculated. By repeating this procedure, the low composition and plateau portions of the isotherms could be obtained. At high pressures, the difference between dissociation pressure and the pressure in the manifold from D to H was too low to permit large enough increments of hydrogen to be added, so that hydriding runs were discontinued before the region of rapidly ascending pressures at high hydrogen compositions.

At temperatures above 550°, it was found that the diffusion of hydrogen through the steel was no longer negligible. The diffusion rate was measured at each temperature as a function of the pressure, and these data were used to correct the compositions for diffusion loss.

Although the temperature was controlled to within a few tenths of a degree centigrade with a photocell circuit, the uncertainty in temperature may be as high as ±2° because of slight thermal gradients in the sample. As stated above, the accuracy of a pressure measuring unit was ±0.5% of its full scale reading. Under the worst conditions, therefore (reading 100 p.s.i. on the 0–1000 p.s.i. unit), the error could be as high as ±5%, although it was usually much less. The error in plateau pressure due to uncertainty in temperature varies from ±4% for the 450° isotherm to ±2% for the 650° isotherm. In general, therefore, it can be said that the error in pressure is no higher than ±6% and usually less. Be-

cause the composition error is compounded with each removal of hydrogen, the composition at low hydrogen contents is less accurate than at high hydrogen contents. In the region of rapidly rising pressures at the high composition end of the isotherms, the precision in composition is ±0.01 H/U, so that the upper limit of the plateau can be determined to ±0.01 H/U. However, the shapes of the curves in this region can be determined more precisely since the relative error of one experimental point to the next varies from ±0.009 H/U at high pressures to ±0.001 at the plateau pressure. Notwithstanding, the lower limit of the plateau cannot be located to better than ±0.05 H/U. By shifting the low hydrogen composition portion of the isotherms so that the steeply sloping part intercepts the point of zero hydrogen composition at zero pressure, the lower limit of the plateau can be determined somewhat more precisely. This has been done for the isotherms shown. For the two hydriding runs, the error in hydrogen composition was somewhat larger. In the 500° isotherm, the error in composition at the low hydrogen composition end of the isotherms was only ±0.001 H/U. As the hydrogen composition increased in the plateau region, the error increased to ±0.03 H/U near the upper limit of the plateau. The compositions in the hydriding run at 650° were much less precise, the errors being ±0.01 H/U at the low hydrogen composition and ±0.1 H/U in the plateau region. This large error was due to the fact that the dissociation pressure was so high at this temperature, that the difference between hydriding pressure and dissociation pressure was small, thereby necessitating a large number of hydrogen additions in order to increase the hydrogen content of the sample appreciably.

Results and Discussion

The pressure–composition isotherms obtained are shown in Figs. 2 and 3. The open circles represent dehydriding runs and the black circles hydriding runs. Within experimental error, there seems to be no hysteresis between hydriding and dehydriding in this system at temperatures above 450°. Hysteresis was obtained by Spedding[3] at lower temperatures. As hydrogen is removed from the fully hydrided uranium hydride, the pressure falls rapidly until a constant pressure plateau is reached due to the dissociation of uranium hydride and the formation of two solid phases; β-uranium hydride and α-uranium metal. When almost all the hydrogen has been removed, the hydride phase disappears and the pressure again decreases sharply, indicating a single solid phase consisting of the metal containing dissolved hydrogen.

The plateau pressures obtained in this investigation are compared with the plateau pressures calculated by extrapolating the low temperature (below 430°) work of Spedding[3] and Flotow and Abraham[4] in Table I. The errors shown are the estimated maximum errors. The plateau pressures agree within experimental error with those obtained by the extrapolation of Flotow and Abraham's equation at 450 and 500°. However, at higher temperatures, it appears that the low temperature equation can no longer be used. The values obtained from the equation given by Mogard and Cabane[5] for high pressures are also shown in this table. Their values are much lower than the present values, however, (except at 650°) and are even lower than the Flotow and Abraham values at 450 and 500°. Since their work was essentially a metallographic study of UH₃, no details are given on the measurement of the pressures so that there is no indication of the accuracy of the work.

If we consider the reaction

$$U + 3/2H_2 \longrightarrow UH_3 \tag{1}$$

TABLE I

DISSOCIATION PRESSURES (ATM.) OF URANIUM HYDRIDE

Temp., °C.	Spedding	Flotow and Abraham	Mogard and Cabane	This research
450	1.51	1.50	1.33	1.44 ± 0.06
500	3.80	3.64	3.35	3.57 ± .12
550	8.5	7.8	7.5	8.4 ± .4
600	17.8	14.9	15.5	16.3 ± .5
650	33.8	26.0	29.2	29.8 ± .9

the heat of formation, ΔH, of the uranium hydride can be calculated from the integrated form of the Van't Hoff equation

$$\ln P = \frac{2\Delta H}{3RT} + \text{constant}$$

where P is the plateau pressure, T the absolute temperature and R is the gas constant. The equation for the log P vs. $1/T$ plot shown in Fig. 4 was determined to be

$$\log P_{atm} = -\frac{4410}{T} + 6.26$$

from which a heat of formation of -30.3 ± 0.1 kcal./mole was obtained, as compared to -30.8 kcal./mole from Spedding's data and -31.8 kcal./mole from the work of Flotow and Abraham. The most recent calorimetric determination by Abraham and Flotow[7] is reported as -30.35 ± 0.03 kcal./mole at room temperature. The excellent agreement between the high temperature and low temperature value indicates that ΔH remains reasonably constant with temperature.

Some recent calculations[8] indicate that the non-stoichiometry of uranium hydride is due to hydrogen vacancies in the lattice. The high composition ends of the isotherms shown in Fig. 3 can then be interpreted in the following way. As hydrogen is withdrawn from the system, vacancies are created in the lattice, and the pressure drops sharply until the saturation concentration of vacancies is reached. At this point, the lattice cannot accommodate any more vacancies, and further removal of hydrogen causes the hydride to break down, or dissociate, thus forming a two-phase region consisting of uranium metal and uranium hydride containing the maximum number of hydrogen vacancies. As the temperature increases, the number of hydrogen vacancies which the lattice can accommodate increases. If this is the case, the heat of formation calculated above is not for reaction 1, but rather for the reaction

$$(1 + x)U + \frac{3}{2} H_2 \longrightarrow U_{1+x}H_3$$
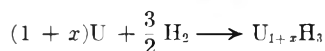
where x varies with temperature and is equal to $v/(1 - v)$, v being the fraction of vacant hydrogen sites in the lattice. However, since ΔH is constant with temperature over the range studied as shown in Fig. 4, it is obvious that the presence of vacancies does not appreciably affect the heat of formation, and the value given for ΔH is also valid for $x = 0$, or stoichiometric UH₃. The maximum value of v at each temperature is shown in Table II.

(7) B. M. Abraham and H. E. Flotow, J. Am. Chem. Soc., 77, 1446 (1955).

(8) G. G. Libowitz, submitted for publication.
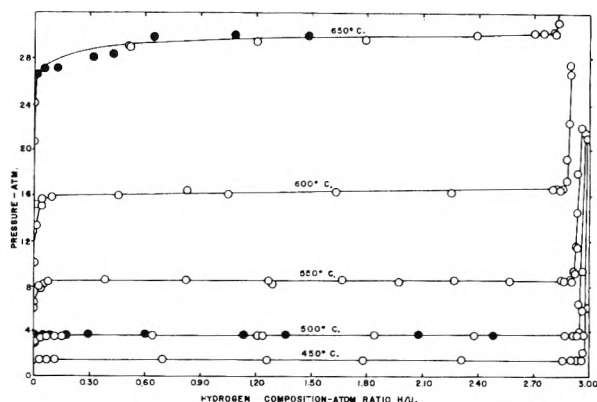
Fig. 2.—Uranium hydrogen pressure–composition isotherms: open circles represent dehydriding data; closed circles represent hydriding data.
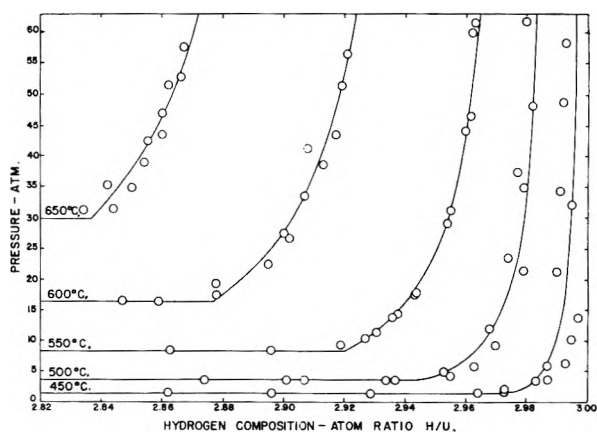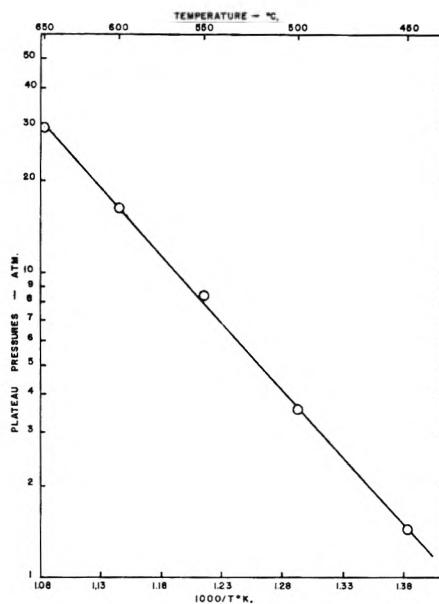

Fig. 3.

Fig. 4.—Van't Hoff isochore for uranium–hydrogen system.

TABLE II

THE SATURATION CONCENTRATION OF HYDROGEN VACANCIES IN URANIUM HYDRIDE

Temp., °C.	450	500	550	600	650
v	0.008	0.018	0.027	0.041	0.054

THE KINETICS OF REACTIONS OF SOME ALKALI HALIDES IN THE SOLID STATE[1]

By Harold F. Mason[2]

Contribution from the Chemistry Department, University of Wisconsin, Madison, Wisconsin

The rate of reaction between solid powders of certain alkali halides has been studied at about 450°. The rate was followed with X-ray measurements and found to fit the formula $1 - x = (6/\pi^2) \sum_{n=1}^{n=\infty} 1/n^2 \exp(-n^2 kt)$ which is based on the diffusion of ions into spherical particles. The reactions were KCl + NaBr and CsCl + KBr. Data of Wood were used to calculate the rate of the reaction NaI + KBr. Thermodynamic considerations are discussed. The kinetic data are explained on the hypothesis that the rate of reaction is determined by the diffusion of the cations followed by a slower diffusion of the anions.

Introduction

The equilibrium phase relations of reciprocal pairs of alkali halides have been investigated by Wood and co-workers.[3] Stable salt pairs were identified by the X-ray diffraction patterns of the crystals resulting from quenching the mixed melts and from extensive reaction in the solid state. In 57 of 60 reciprocal salt systems studied by quenching from the mixed melts complete reaction occurred and gave the stable salt pair. The stable phase pair consisted of crystals of the smaller cations coupled to the smaller anions and the larger cations coupled to the larger anions. The final product phases were nearly pure binary salts. Of the systems studied here, all showed a quenched-melt composition close to the stable salt pair. However, Wood, et al., found that the CsBr–KCl system displayed partial reversal and true equilibrium when reacting in the solid state for 36 hours at 400°.

In this work the kinetics and mechanisms of three solid–solid reaction systems of alkali halides have been studied by X-ray diffraction, NaBr–KCl, CsCl–KBr and NaI–KBr. The spacing and intensity of the X-ray lines were measured and allowance made for the formation of solid solutions. Since the phases resulting from solid-state reactions frequently contain crystal defects, thermoluminescence studies also were made.

Thermodynamics.—The thermodynamics of solid-state reactions are those for heterogeneous systems of a multiplicity of solid phases, together with any participating gaseous or liquid phases. Except for reactions involving gaseous or liquid phases, or those in which solid solution of reactants and products occurs, equilibrium is usually not possible and the reactions proceed exothermically to completion,[4] giving the stable salt pairs with smaller cation combined with smaller anion, and larger cation combined with larger anion.

For systems which are exclusively solids, equilibrium requires a free energy change of zero for reaction between phases as they actually exist. These phases may be solid solutions and thus not described by thermodynamic data for the pure phases. When true equilibrium exists in a heterogeneous system, thermodynamic equilibrium will exist *internally* within each phase as well as *externally* between the different phases. A situation could conceivably occur in which the various solid phases are not in internal equilibrium (because the crystal has many defects and is thus an "active" phase) but in which any reaction between phases as they actually exist (without changes of defect character) will be accompanied by zero change in free energy. This metastable state would be one of "external equilibrium," but might be identified experimentally as a true equilibrium. Thus thermodynamic data for pure crystalline substances should be used with reserve when predicting equilibria in solid–solid reactions; and a state of "observed equilibrium" may depart from the state of true equilibrium because of the participation of "active" phases.

The CsCl–KBr reciprocal-salt system presents an interesting example of equilibrium because of complete miscibility of reactant and product phases containing a common cation. Thus, in the reaction CsCl + KBr = CsBr + KCl, there are only two phases, a solid solution of CsCl and CsBr and a solid solution of KBr and KCl. At equilibrium only two phases exist, and, from phase-rule considerations, equilibrium should be possible under a variety of conditions.

Reaction Kinetics.—The general factors governing kinetic laws for solid–solid reactions are (1) the rates of transfer of material between phases and chemical reactions at phase boundaries, (2) the rates of diffusion of reactants, and (3) the rates of nucleation and recrystallization. The form of the over-all kinetic law will depend on the relative rates of these processes; frequently one process will be rate-controlling. The formal statement of any kinetic law will also depend upon the geometry of the reacting phases and the spatial and temporal sequence in which the various phases appear. Thus the mathematical form of the rate equation for a reaction in a mixture of powders may be different from its form for the same reaction between two parallel slabs of the reactants.[5,6] In this work we are concerned with the laws for powder systems.

Powder systems are treated here by considering

(1) Further details of this investigation are available in the Ph.D. thesis of Harold F. Mason, filed in the Library of the University of Wisconsin, Madison, Wisconsin, 1954.

(2) California Research Corporation, Richmond, California.

(3) L. J. Wood, et al., J. Am. Chem. Soc., **56**, 92 (1934); **57**, 822 (1935); **58**, 1341 (1930); **60**, 2320 (1938); **62**, 766 (1940); **66**, 1259 (1944); **74**, 727, 2355 (1952); J. Sch. Sci. and Math., **45**, 623 (1945).

(4) G. Tammann, Z. anorg. Chem., **149**, 21 (1925).

(5) W. Jost, "Diffusion in Solids, Liquids and Gases," Academic Press, Inc., New York, N. Y., 1952.

(6) B. Serin and R. T. Ellickson, J. Chem. Phys., **9**, 742 (1941).

the reaction rate to be governed by radial diffusion into spherical grains. Although these assumptions cannot be rigorously correct, the data obtained correlate with the functions derived on the assumption of spheres. Exact physical significance should not be attached to the parameters.

On the assumption that diffusion occurs into (or out of) homogeneous spherical particles of radius, a, the rate law may be derived[1,5] from Fick's first and second laws and expansion through a Fourier series

$$1 - x = \frac{6}{\pi^2} \sum_{n=1}^{\infty} \frac{1}{n^2} \exp\left(- \frac{n^2\pi^2 Dt}{a^2}\right) \qquad (1)$$

where

x = fraction of reaction or diffusion that has occurred after time t and $1 - x$ is the fraction of the reactants remaining
a = radius of spherical particles
D = diffusivity
n = integer equalling no. of term in the series expansion

The derivation implicitly assumes that diffusion will occur with an average diffusivity D through any matrix of phases (e.g., reactant and product) within the grain. This, is, of course, an approximation, and averages diffusion through crystals, along their surfaces, and through microcracks.

Values of $1 - x$ were calculated by means of a Card Programmed Calculator (IBM Model II) for various values of the exponential[7] and are plotted in Fig. 1 where x is the fraction of diffusion completed at time.

Experimental

After fusion in a platinum crucible, each pure reactant salt was poured into a cleaned platinum dish and allowed to crystallize and cool to room temperature. The solid mass was ground in a mullite mortar and sieved finer than 200 U. S. Standard. Prior to each grinding, the mortar was heated on an electric plate to prevent pickup of moisture. Sieved salts were later subjected to a microscopic count of particle size. Powders of each reactant were then weighed to obtain equimolar mixtures. The individual salts were redried at 125° and stored in a desiccator until used. Immediately prior to use the individual reactants were thoroughly mixed in a dry box.

Solid-state reactions were performed in a Lindbergh muffle furnace, with automatic temperature control. Measured temperatures were calibrated against a platinum to platinum–10% rhodium thermocouple. During all solid-solid reactions, and for at least 30 minutes before each experiment, a stream of high purity, dry nitrogen was passed through the furnace, purified by passage through a copper-copper oxide heater and a bed of Drierite.

Each series of experiments was performed with portions of the same reactant mixture. Several samples in porcelain crucibles were placed in the furnace at the same time and removed at appropriate intervals. The partially reacted mixtures were allowed to cool to room temperature in a desiccator, and then stored in a tightly sealed jar in a bed of Dry Ice until analysis. The jar contained a bed of Drierite. Particular care was taken in series B to assure rapid X-ray analysis.

Reactions were followed by X-ray diffraction, using a General Electric XRD-3 X-ray diffractometer. Intensities of diffracted X-ray beams were measured by a Geiger-Muller counter and recorded by means of a potentiometer strip recorder. Instrument errors in diffraction angle, 2θ, were corrected by calibration with standard samples. Copper Kα radiation was used throughout.

For samples of heat-treated NaBr–KCl, diffraction patterns were obtained with all of the following techniques: (1) a scanning speed of 2.0°/minute (scanning values of
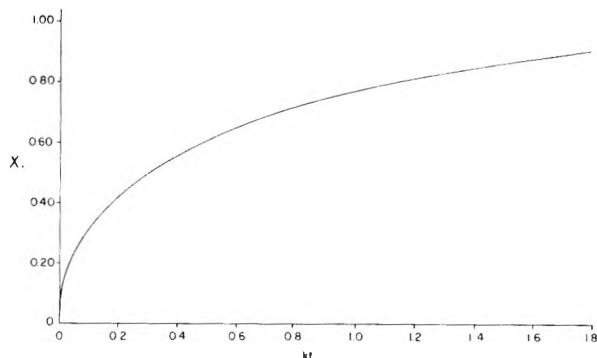

Fig. 1.—Calculations for radial diffusion into a sphere.

2θ from 20 to 80°) with thin sections of powder preparations mounted flat against a glass surface; (2) a scanning speed of 0.2°/minute with the same technique (scanning a few key patterns to detect the presence of solid solutions); and (3) a scanning speed of 0.2°/minute with powders in random orientation in thick preparations appropriate for intensity measurements (for the KCl and KBr 200 reflections). Technique (1) was used for identification of phases and measurement of unit cell dimensions. Technique (2) gave a detailed description of any solid solution formation between the KCl and KBr, and the NaCl and NaBr phases; this was required for a qualitative description of reaction mechanisms and for quantitative interpretation of intensity patterns. Technique (3) was used for the measurement of relative intensities of the KCl and KBr 200 reflections; this gave a measure of the extent of the reaction. Because they were diffuse, the NaCl and NaBr patterns were not used. Studies of the CsCl–KBr reaction system were only qualitative.

For intensity measurements by method (3) the powder was packed in an aluminum specimen holder similar to that recommended by the General Electric Company, to assure random orientation of the crystals; the depth of the packing was such that virtually complete absorption of X-rays occurred at the back face.[8] The scale deflection of the camera was calibrated against actual diffracted intensity. Diffraction patterns obtained by technique (3) above were regraphed to give a linear plot of intensity versus 2θ on the basis of this calibration curve.

In the solid state reaction, of NaBr and KCl, separate KBr and NaCl phases are formed. If these phases were each pure, relative intensity measurements of the KCl and KBr 200 reflections would determine the extent of reaction. However, some solid solution occurred between the NaCl and NaBr and between KCl and KBr, as shown by the patterns from techniques (1) and (2). On the basis of the pattern obtained by technique (2), the intensity curve from method (3) was arbitrarily subdivided into three "phases": pure KCl and KBr phases, and an intermediate solid solution, the average unit cell dimension of which was taken as an average for the measured solid solution intensities (estimated from both types of patterns taken together). Such a breakdown is shown in Fig. 2. Here the average unit cell dimension of the K(Cl,Br) solid solution corresponded to a 2θ value of 27.65.

The intensities of the three areas were determined by planimeter. The area of the composite solid–solution region was apportioned to KCl and KBr on the basis of its average unit cell dimension a and the assumption that a is a linear function of molar composition for KCl–KBr solid solutions.[3] In the above example a 2θ of 27.65 corresponds to an a of 6.447 Å. or 48.8 mole % KCl in K(Cl,Br). These apportioned areas were added to the areas for the respective pure "phases" to obtain total KCl and KBr intensities. Thus 48.8% of the K(Cl,Br) area is added to the area of the KCl "phase." The total intensities were then used to determine the extent of reaction by comparison with standard mixtures of reactants and products.

Relative intensities of the patterns of product and reactant phases were correlated with actual concentrations by

(7) Copies of these numerical solutions can be obtained by writing to this Laboratory.

(8) N. M. F. Henry, H. Lipson and W. A. Wooster, "Identification of X-Ray Diffraction Photographs," The Macmillan Co., New York, N. Y., 1951.
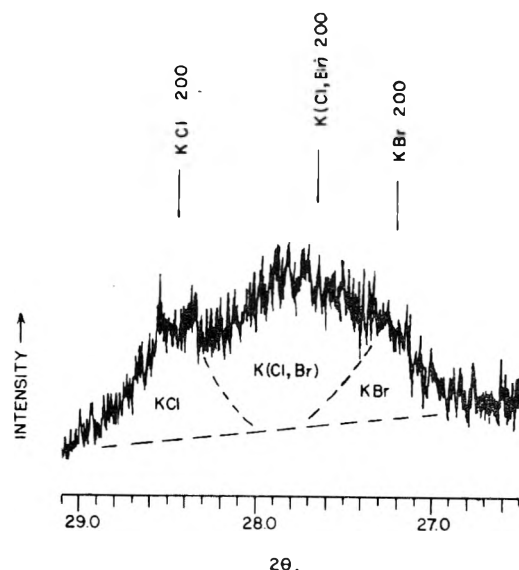
Fig. 2.—X-Ray spectrum of mixture of KCl and KBr in thick layer.

means of standard mixtures of equimolar NaBr–KCl and equimolar NaCl–KBr mixed in various proportions to simulate mixtures resulting from progressive degrees of reaction. Equivalent conversion was then correlated with the ratio of the intensities of KCl and KBr.

The thermoluminescence equipment was that developed by Rieke.[9] The apparatus consisted of a furnace and voltage-regulation circuit for heating samples at a constant rate, a light-tight box, a 1P28 photomultiplier tube, a d.c. amplifier, and a potentiometer recorder. Thirty mg. of powder covered the bottom of a small dish. The recorder kept simultaneous records of the intensity of the light incident on the photomultiplier tube and the temperature of the sample, which was heated at a uniform rate. The resulting glow curve gives peaks of higher intensity at certain temperatures.

All samples were irradiated in a cobalt-60 source, stored in Dry Ice and investigated for thermoluminescence on the same day.

Intensities were obtained by integrating the areas under peaks of the glow curve with a planimeter. The intensities were measured for composite peaks, covering the entire glow curve for a given sample from room temperature to 300°.

The Reaction KCl + NaBr.—At the reaction temperature, 450°, it is probable that all binary salt-pairs in the systems NaBr–KCl are completely miscible. High temperature X-ray diffraction was employed to study the equilibrium phase relations of the ternary system at 450 to 530°. Two phases were identified in both cases, both face-centered cubic. Unit cell dimensions calculated for the 450° pattern (heated one hour) agreed closely with values predicted for that temperature for KBr and NaCl, using data given in National Bureau of Standards Circular 539. The 530° patterns were of poor quality because of experimental difficulties; but the phases were identified as KBr and NaCl by direct comparison. Low-temperature patterns of the quenched mixed melt, the solid–solid reaction products, and the products of the quenched vapor mixture by Wood, et al.,[3] and the author,[1] confirm the conclusion that in a stoichiometric system nearly pure KBr and NaCl exist together in equilibrium at the reaction temperature, 450°. These are the stable salt-pair of the reciprocal salt system with the larger ions combined in one salt and the smaller ions combined in the other.

Phases identified by X-ray diffraction of partially reacted equimolar mixtures of NaBr and KCl are described in Table I. All reactant mixtures in any one series of kinetics experiments were portions of the same mixture of NaBr and KCl. Mixtures prepared for series A and B were prepared in a similar, standardized manner, but on different occa-

(9) J. Rieke, Ph.D. Thesis, Univ. of Wisconsin, 1954; THIS JOURNAL, **61**, 633 (1957).

sions. Since solids are highly sensitive to previous treatment, differences in the structure-sensitive properties would occur between different preparations.

TABLE I

PHASES PRESENT AFTER PARTIAL REACTION OF NaBr AND KCl IN THE SOLID STATE AT 455°

	Time, hr.	Products—cell dimension a, Å.a	Phase	No. of lines identified
Series A	5.67	5.967 ± 0.005	NaBr	3
		5.67 ± .09	NaCl	2
		6.589 ± .009	KBr	7
		6.314 ± .002	KCl	2
	14.00	5.893 ± .001	NaBr	4
		5.684 ± .012	NaCl	3
		6.585 ± .004	KBr	8
		6.303 ± .009	KCl	3
	24.25	5.974 ± .002	NaBr	2
		5.72 ± .03	NaCl	3
		6.572 ± .006	KBr	7
		6.313 ± .011	KCl	2
Series B	0.95	5.982 ± 0.006	NaBr	4
		6.59 ± .02	KBr	3
		6.29 ± .02	KCl	3
	1.90	6.003 ± .007	NaBr	3
		5.90	NaCl	1
		6.597 ± .004	KBr	2
		6.438 ± .002	K(Cl,Br)	2
		6.294 ± .018	KCl	3
	3.93	5.992 ± .001	NaBr	3
		5.73 ± .04	NaCl	2
		6.600 ± .001	KBr	3
		6.446 ± .001	K(Cl,Br)	2
		6.32	KCl	2
	5.55	5.996 ± .005	NaBr	3
		5.74 ± .03	NaCl	3
		6.609 ± .01	KBr	4
		6.47	K(Cl,Br)	1
		6.30 ± .03	KCl	3
	12.32	5.962	NaBr	2
		5.702	NaCl	1
		6.594 ± .006	KBr	5
		6.51 ± .03	K(Cl,Br)	
		6.33 ± .02	KCl	2

a The cell dimensions a for the pure phases are: NaBr, 5.977; NaCl, 5.640; KBr, 6.590; KCl, 6.297.

In both series patterns were identified for four phases: KCl, KBr, NaBr and NaCl. Diffuse patterns were observed between the KCl and KBr peaks and between the NaCl and NaBr peaks, indicating some solid solution. Except for patterns obtained after very little reaction, the intensities of the solid–solution patterns were less than those of the pure phases. There was no evidence for any perceptible solid solution of the potassium halide and sodium halide phases. Wood, et al.,[3] also identified the patterns of all four phases in their work at 400°. These workers indicated that extensive solid solution between potassium and sodium halide does not occur.

The difference in rate between series A and B is not surprising, since the reaction very probably is structure sensitive. Other evidence for structure sensitivity has been derived from electrical conductivity and self-diffusivity measurements for NaCl; these processes are structure sensitive below about 550°.[5]

The unit cell dimensions of all the pure phases except NaCl agree with the accepted values. The data for NaCl indicate that it contains some NaBr in solid solution.

On the basis of the solid solubilities of the binary salt-pairs, one would predict that the KCl and KBr phases should mix to form one solid solution, which would change

continuously in composition from pure KCl to pure KBr as the reaction progressed. Yet this is not the case. The existence of separate KCl and KBr phases in contact with the solid solutions indicates that the cations diffuse much more rapidly than do the anions. This concept is supported by electrical conductivity measurements, which are interpreted by Smekal[5] to show that at temperatures below 550°, the conductivity of NaCl is structure sensitive and is due, almost entirely, to the cations.

The solid solutions probably result from the slower, but not insignificant, diffusion of the anions. Thus diffusion of cations alone cannot give solid solutions of the type KCl–KBr, since the halide ions would still be separated on the basis of their original distribution between the NaBr and KCl phases.

Intensities of X-ray diffraction patterns from partially reacted mixtures of KCl and NaBr are summarized in Table II. The method of calculation was given in the Experimental section. Kinetic data are given in Table III and are represented in Fig. 3.

TABLE II
INTENSITIES OF DIFFRACTION REFLECTIONS (200) IN THE NaBr–KCl REACTION

Time, hr.	Pure KBr	Pure KCl	K (Cl,Br)	2θ	a	K(Cl,Br) Mole % KCl	Total intensity KBr	KCl
				Series A				
5.67	7.95	1.78	4.11	27.80	6.412	60.7	9.57	4.27
5.67	8.40	2.05	3.50	27.83	6.404	63.5	9.68	4.28
14.00	8.95	0.51	3.82	27.70	6.436	52.6	10.76	2.52
24.25	12.22	.69	5.73	27.52	6.477	38.6	15.74	2.90
				Series B				
0.95	1.51	4.13	3.16	27.80	6.413	60.4	2.76	6.04
1.90	1.11	5.38	4.20	27.67	6.442	50.5	3.19	7.50
3.93	2.71	3.73	6.34	27.65	6.447	48.8	5.95	6.82
5.55	2.00	3.30	5.54	27.55	6.470	41.0	5.27	5.57
12.32	4.14	1.16	9.88	27.50	6.481	37.2	10.34	4.84

TABLE III
FRACTION OF REACTION COMPLETED AND KINETIC DATA FOR THE NaBr + KCl REACTION

x = fraction reaction completed, as calcd. from

Time, hr.	Intensity KBr	Intensity KCl	Intensity KBr / Intensity KCl	Intensity KCl / Intensity KBr	Av. fraction completed	kt
			Series A			
5.67	0.463	0.520	0.498	0.485		
5.67	.470	.519	.499	.507	0.494	0.292
14.00	.525	.715	.651	.640	.633	.553
24.25	.855	.675	.710	.711	.738	.854
			Series B			
0.95	0.140	0.310	0.177	0.175	0.201	0.038
1.90	.161	.162	.168	.165	.164	.025
3.93	.295	.239	.280	.280	.274	.071
5.55	.268	.380	.296	.298	.311	.104
12.32	.500	.457	.488	.509	.489	.281

Fractions reacted are given as read from correlations with integrated intensities of KBr, KCl and the two ratios of these intensities (see Experimental section). These four calculations are then averaged to give the figures in the next to the last column and from these the corresponding values of kt are obtained from Fig. 1 and more accurately from tables containing numerical values calculated by eq. 2.

The data are correlated with eq. 1 rewritten as

$$1 - x = \frac{6}{\pi^2} \sum_{n=1}^{\infty} \frac{1}{n^2} \exp(-n^2 kt) \qquad (2)$$

where k is a rate constant. If the assumptions made in the derivation of this equation are obeyed rigorously, the rate constant k equals $\pi^2 D/a^2$ and the equation reduces to eq. 1. Since the physical model is only approximately realized, k is an empirical rate constant, and depends in fact on the preparation and structure of the crystals.
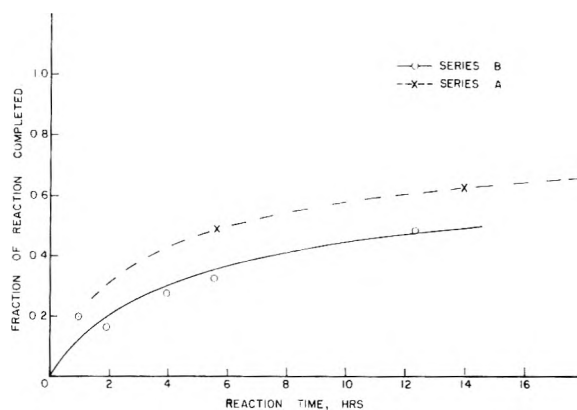

Fig. 3.—Fraction of reaction completed *versus* time for the reaction NaBr + KCl at 455°.
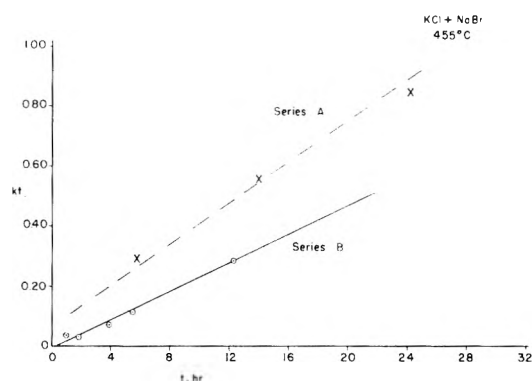

Fig. 4.—Correlation of NaBr + KCl reaction at 455°.

Values of kt were obtained from conversions measured by X-ray diffraction. These values of kt, should plot as a linear function of t if the correlation is satisfactory. Such a plot is given in Fig. 4.

These results show that eq. 2 provides a satisfactory empirical expression of the rate law for the NaBr–KCl reaction and gives k a value of 0.00232 hr.$^{-1}$ for series B (the later and more accurate series). A "diffusivity," D, calculated from eq. 1 for data from series B and for an average particle diameter of 70 μ (from microscopic particle count) was 7.9 × 10^{-13} cm.^{2} sec.$^{-1}$, compared to a value of 8.7 × 10^{-12} cm.^{2} sec.$^{-1}$ for self-diffusivity of sodium ions in NaCl calculated from ionic conductivity data given by Smekal[5] and the Nernst–Einstein equation. The agreement is surprisingly good in view of the approximate nature of our assumptions.

The Reaction CsCl + KBr.—From data of Wood and coworkers[3] the KBr–CsCl solid-state reaction appears to be unusual, because of the role played by solid solutions of CsCl–CsBr and KCl–KBr. As the reaction progressed at 480°, these solid solutions changed composition, approaching equilibrium at 79% forward reaction, starting with equimolar reactants. Wood obtained data for equilibrium studies and only the very last range of reaction was studied; rate measurements were not made and mechanisms were not discussed.

The formation of solid solutions suggested that the reaction might be followed by changes in the unit cell dimensions of the KCl–KBr and the CsCl–CsBr solid solutions. The unit cell dimension is very nearly a linear function of the molar composition (*e.g.*, CsBr in CsCl–CsBr) for both solid solutions, according to Wood, *et al.* From Wood's data the reaction appeared to progress by changes in composition of solid solutions and, accordingly, measurements of the unit cell dimensions of the solid solutions might suffice to determine the extent of reaction. This technique would obviate intensity measurements.

Cesium chloride and cesium bromide crystallize in the body-centered system, as opposed to the face-centered cubic lattice characteristic of the other alkali halides studied. Cesium chloride undergoes a polymorphic transformation

to the face-centered cubic system at $451 \pm 5°$;[10,11] cesium bromide is not reported to undergo similar transformation. The CsCl–CsBr solid solution crystallizes in the body-centered cubic system throughout the entire range of solution.

Data of Wood, *et al.*, and of this research indicate that the Cs(Cl,Br) and K(Cl,Br) phases resulting from solid reaction do not form solid solutions with each other.

Experimental results with a powder mixture, sieved between 200 and 235 U.S. mesh, are summarized in Table IV.

TABLE IV

PHASES PRESENT AFTER PARTIAL REACTION OF CsCl AND KBr IN THE SOLID STATE AT 455°

Reaction time, hr.	Products[a] a in Å.	Phase	No. lines identified	Molar % CsBr in solid soln.
5.67	4.187 ± 0.010	CsCl	3	31
	$4.274 \pm .007$	CsBr	4	72
	$6.596 \pm .008$	KBr	6	
	6.302	KCl	2	
14.00	$4.237 \pm .002$	Cs(Cl,Br)	6	66
	$6.590 \pm .010$	KBr	6	
	$6.320 \pm .004$	KCl	2	
24.25	$4.260 \pm .013$	Cs(Cl,Br)	4	79.6
	$6.565 \pm .013$	KBr	4	
	$6.307 \pm .005$	KCl	2	

Data of Wood, *et al.*, at 480°

36	4.255	Cs(Cl,Br)		76
72	4.262	Cs(Cl,Br)		78.9

[a] The cell dimensions a for the pure phases are as follows: CsCl = 4.123 Å., CsBr = 4.296 Å., KBr = 6.590 Å., KCl = 6.297 Å.

The per cent. CsBr in solid solution is calculated from the experimentally determined value of a.

The results are similar to those of NaBr–KCl except that CsCl and CsBr form a single mixed phase much more rapidly than the other salt pairs. After 5.67 hr. at 455° four phases are present—pure KCl, pure KBr and CsCl containing some CsBr in solid solution, and CsBr containing some CsCl in solid solution. After 14 hr. the KBr and KCl phases are still distinct, but the CsCl and CsBr are now mixed to give a single solid solution containing 66 mole % CsBr. After 24.25 hr., the KCl and KBr phases have mixed slightly and the cesium halide solid solution contains 79.6 mole % CsBr, close to Wood's value for equilibrium.

At the reaction temperature, 455°, pure CsCl is very close to its temperature of polymorphic transformation. A phase undergoing polymorphic transformation is highly reactive;[12] thus the reactivity of and the rate of diffusion through the CsCl phase should be greatly enhanced. This seems to be borne out by the rapid formation of the Cs(Cl,
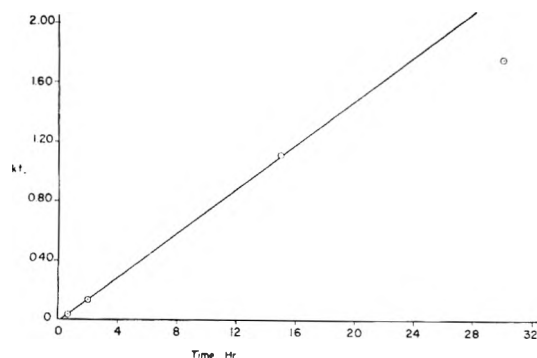
Fig. 5.—Correlation of NaI + KBr reaction at 510°.

(10) "International Critical Tables," Vol. I, Vol. IV, McGraw-Hill Book Co., Inc., New York, N. Y., 1926 and 1928, p. 352.

(11) S. Zemczwzny and F. Rambach, *Z. anorg. Chem.*, **65**, 403 (1910).

(12) J. A. Hedvall, "Reaktionsfahigkeit fester Stoffe," J. A. Barth, Leipzig, 1938.

Br) solid solution and the relatively rapid rate of the over-all reaction.

It was not possible to calculate rate constants because X-ray intensities were not measured. The products with four phases were more complicated than had been anticipated.

The Reaction NaI–KBr.—From solid solubility data given by Wood, *et al.*,[3] and by the International Critical Tables,[10] it appears likely that extensive miscibility occurs between all salt pairs except the stable pair, NaBr–KI, at temperatures above 500°.

Wood, *et al.*, report data for the conversion of NaI and KBr to the stable salt pair at 510°. Conversions were estimated from X-ray intensities of reactant and product phases. Taking their results, and calculating kt by eq. 2 above, the data of Table V are obtained.

TABLE V

KINETIC DATA FOR THE REACTION NaI + KBr BASED ON DATA OF WOOD, *et al.*

Reaction time, hr.	Fraction completed	kt
0.5	0.20	0.036
2.0	.35	0.132
15.0	.80	1.123
30.0	.90	1.750

The values of kt are plotted again t in Fig. 5. The value of k for the reaction is 0.0744 hr.$^{-1}$. The point at 90% conversion is highly uncertain since small errors in x yield relatively large errors in kt and estimates of x itself become increasingly difficult when x approaches unity.

Thermoluminescence Studies.—Product phases resulting from solid–solid reactions often are "active phases," rich in defects and possessing unusually high energy contents. Accordingly certain of their physical properties may be affected: magnetic susceptibility, adsorptive properties and catalytic activity.

One physical property of defect solids is thermoluminescence.[13–16] Thermoluminescence peaks are displayed by many irradiated alkali halides.[16] In addition, after irradiation, many of these salts display colorations and absorption bands characteristic of F-centers.

It seemed of interest to investigate any thermoluminescence effects that might be associated with solid-state reactions, and any enhanced thermoluminescence that might be due to the presence of "active phases" among the products of such reactions.

Quantitative studies were made of the integrated intensities of glow curves of the partially reacted NaBr–KCl system. Results are given in Table VI, where data are given also for the products and reactants. Areas were obtained by integrating areas under composite peaks covering the entire glow curve from room temperature to 300°. The temperature is the temperature of the maximum of the major (usually KCl) peak in the glow curve. Samples were irradiated for five hours in a cobalt-60 source, receiving approximately 25,000 roentgens. The thermoluminescent activities of the reactant and product mixtures were due almost entirely to KCl and NaCl. KCl has one sharp peak at 120°; NaCl displays thermoluminescent activity from 105 to 270°. The KCl 120°, NaCl 105° and NaBr 108° peaks are coincident and cannot be distinguished in a mixture.

In all reaction samples, only one peak could be distinguished between 105 and 130°, coincident with the KCl, NaCl and NaBr peaks in this region. No thermoluminescence was observed between 140 and 270°, the temperature range of the high-temperature NaCl peak. Temperatures at which the peaks occurred were closely reproducible.

Integrated intensities are plotted against time of reaction in Fig. 6. As the reaction time of the mixture increases, the intensity falls off from its initial value to a value somewhat above that of the product mixture, KBr + NaCl. The total change in intensities is 85% of the over-all decrease from reactants to produce, while over the same in-

(13) P. Pringsheim, "Fluorescence and Phosphorescence," Interscience Publishers, Inc., New York, N. Y., 1949.

(14) J. T. Randall and M. H. F. Wilkins, *Proc. Roy. Soc.*, (*London*) **B184**, 366, 390 (1945).

(15) F. Seitz, "The Modern Theory of Solids," 1st ed., McGraw-Hill Book Co., Inc., New York, N. Y., 1940.

(16) L. Heckelsberg and F. Daniels, THIS JOURNAL, **61**, 414 (1957).

TABLE VI

THERMOLUMINESCENCE OF PARTIALLY REACTED MIXTURES OF KCl AND NaBr

Sample	Time, hr.	Fraction reaction completed	Temp. of peaks, °C.	Thermo-luminescence intensity[d]
		Unreacted		
KCl			120	7440
KBr				
NaCl			105–270	3760
NaBr			108	460
Mixed reactants[a]			125	5550
Mixed products[b]			105–270	1480
		Partially reacted		
KCl + NaBr	0.95	0.201[c]	130	5610
	1.90	.164	120	4500
	3.93	.274	105	3060
	5.55	.324	105	1930
	12.32	.489	105	2020

[a] 50 mole % KCl + 50 mole % NaBr. [b] 50 mole % KBr + 50 mole % NaCl. [c] Fraction reacted calculated from X-ray measurements in series B. [d] Area on thermoluminescence glow curve (intensity *versus* time) in arbitrary units.

terval of reaction times, the solid phases reacted 48.9% (by X-ray diffraction). Independent studies of the thermoluminescence of solid solutions of KBr in KCl showed the presence of as little as 0.1 molar % KBr reduced the intensity of the 120° KCl peak to less than one tenth of its value for pure KCl. Thus the disproportionate decrease in thermoluminescent intensity with reaction is not surprising and may be an indication of a small amount of relatively slow anionic diffusion.

Correlation of reaction kinetics with fractional decrease in thermoluminescent activity, using eq. 2, was not successful. Because of effects of small amounts of a second species in solid solution on thermoluminescence intensity, this method does not appear to offer an attractive means for following solid–solid reactions of the alkali halides.

The effect of "active" product phases might be expected to be shown by maxima in Fig. 6. Such were not observed, with the possible exception of a questionable maximum after one hour reaction. Actually, the NaBr–KCl system is a poor test for any hypothesis of enhanced thermoluminescence resulting from "active phases." The phase giving the strongest thermoluminescence is a reactant phase, KCl; and "active phases" resulting from solid–solid reactions would be expected to be product phases. Such might be true of the reaction between CsCl and KBr, where KCl is among the products.

Glow curves of the partially reacted CsCl–KBr mixture displayed weak thermoluminescence near 100°, but it remained weak even after 24.25 hr. at 454°. No definite trends in intensity could be identified. The reaction mechanism postulated involves rapid diffusion of both potassium and bromide ions through the original CsCl phase, which is highly "active" because the reaction temperature is close to the temperature of the CsCl polymorphic transformation. Under such conditions, the creation of anything resembling a pure KCl phase is unlikely; and, indeed, the thermoluminescence data are evidence for the postulated mechanism.

In addition, unmixing of any NaCl–KCl and NaBr solid solutions probably occurred as the heated mixtures were cooled to room temperature, and these phase changes would be superimposed upon primary phase changes occurring in the course of the solid–solid reaction.

In conclusion, no evidence was found for increased thermoluminescence as a result of the formation of active phases, but these tests are not definitive.

Discussion

The X-ray patterns observed for the partially reacted NaBr–KCl system can best be explained by a relatively rapid counter-diffusion of cations, followed by a slower diffusion of anions. Predominant cationic migration is shown by the appearance
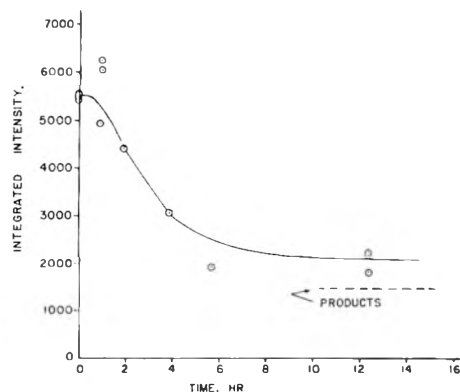
Fig. 6.—Variation of thermoluminescence intensity with extent of NaBr + KCl reaction.

of separate patterns of the product and reactant phases, while the slower anion diffusion is apparent from the simultaneous formation of Na(Cl,Br) and K(Cl,Br) solid solutions.

Consider rapid diffusion of potassium ions and a much slower diffusion of chloride ions into a NaBr grain (with counter-diffusion of sodium and bromide ions to maintain electroneutrality). In the absence of recrystallization the NaBr grain will contain a solution of sodium, bromide, potassium, and (a relatively much smaller amount of) chloride ions. The mixture will, however, recrystallize to give the stable salt pair, with excess ions going into one phase or the other. Thus NaCl and KBr phases will be formed, with excess sodium and bromide ions being distributed between the two phases. From independent studies by Daniels and Mason[1] it was found that a mixed vapor of KCl and excess NaBr crystallizes to give pure KBr and a solid solution of NaBr and NaCl (up to at least 62 molar % NaBr). No evidence was found either in this work or by Wood, *et al.*,[3] for the existence of (Na,K)Cl or (Na,K)Br solid solutions (after quenching). The proposed mechanism, then, involves the formation of KBr and Na(Cl,Br) phases by recrystallization in the NaBr grain. In similar manner, NaCl and K(Cl,Br) phases are formed in the (original KCl grain).

The total mixture, then, would contain relatively pure KBr and NaCl phases formed in the original NaBr and KCl grains, respectively, as well as solid solutions of mixed chloride and bromide of a common cation, and the unreacted reactant phases. These conclusions are consistent with the X-ray diffraction observations.

It is believed that this recrystallization occurs largely within the original reactant grains, since the crystals present after as much as 73.8% reaction, possessed the same cleaved, irregular habits and particle size distribution as the ground, unreacted reactant mixture, with no evidence of a more regular recrystallization outside the original grains.

The reaction mechanism is also consistent with the observed thermoluminescence phenomena. The total intensity of thermoluminescence of the irradiated NaBr–KCl mixture could decrease from the value for the reactant mixture as a result of (a) the removal of KCl (the most thermoluminescent

constituent) by reaction, or (b) by diffusion of bromide ions into the KCl phase. From studies of the thermoluminescence of KCl–KBr solid solutions, it is clear that the thermoluminescence intensity decreases with addition of bromide far more than would be predicted from a simple proportionality. The intensity of thermoluminescence does not decrease more rapidly than the reaction occurs (*i.e.*, than KCl is used up) until after about 30% reaction has occurred. This is interpreted to mean that the bromide ion does not precede the sodium ion into the KCl grains, and is additional evidence that the rate of diffusion of the cations is greater than that of the anions. The disproportionate reduction of intensity as the reaction progresses beyond 40% is believed to result from the presence of bromide ions in the KCl phase as a result of anionic diffusion and recrystallization of NaCl and K(Cl,Br).

A similar pattern is followed by the NaI–KBr reaction.

The CsCl–KBr reaction mechanism would be similar except that: (1) the reaction to CsBr and KCl does not proceed to completion, but to an equilibrium composition of Cs(Br,Cl) and K-(Cl,Br). Thus the CsBr phase at 455° (presumably formed by recrystallization of reactants in the KBr grain) contains 20 molar % CsCl in solid solution (compared to Wood's equilibrium value of 21 molar % at 480°). (2) A polymorphic transformation occurs in CsCl near 450°; this should greatly enhance the reactivity of the CsCl phase according to Hedvall.[12] In particular, the rates of diffusion should be increased through this "active" phase. This may explain the rapid formation of a CsCl–CsBr solid solution, since bromide ions might be able to move through the CsCl lattice with facility near the transformation point.

Acknowledgment.—The author is glad to acknowledge the help of Professor Farrington Daniels under whose direction this research was carried out, and to express appreciation to the Eastman Kodak Company for a fellowship during this work and to the Wright–Patterson Air Development Center for support during part of the work. He is indebted to Professor Sturges Bailey of the Geology Department of the University of Wisconsin for help in the determination and interpretation of the X-ray measurements, to Professor Marion Jackson of the Department of Soils for use of X-ray apparatus, to Professor John Margrave of the Department of Chemistry for advice on techniques in high-temperature chemistry, and to Mr. Fred Gruenberger of the Numerical Analysis Laboratory for assistance in the numerical solutions of eq. 2.

Summary

(1) Phases observed during the course of double decompositions of the alkali halides in the solid state consisted of all four binary salts formed by combination of two cations with two anions. This is taken to indicate a reaction mechanism based on cationic diffusion through the reactant phases, followed by recrystallization of the stable salt pair.

(2) The kinetics of the reactions of NaBr + KCl and NaI + KBr are correlated by means of the assumption of diffusion (of cations) into reactant grains and the law for symmetrical diffusion into spherical particles. A "diffusivity" term calculated for NaBr + KCl is of the order of magnitude of the structure-sensitive self-diffusivity of sodium ions in NaCl at the reaction temperature.

(3) The reaction of CsCl + KBr gives four phases in the initial stages of the reaction. The subsequent rapid formation of a CsCl–CsBr solid solution is believed to result from the enhanced reactivity of CsCl due to its polymorphic transformation near the reaction temperature, 450°.

(4) Thermoluminescence studies of the NaBr + KCl and CsCl + KBr reaction systems fail to show major effects on the glow curves resulting from the presence of highly "active" phases in the partially reacted system, although secondary effects, such as solid solution, may have masked such phenomena.

KINETICS OF SOLID STATE REACTIONS OF SILVER SULFATE WITH CALCIUM AND STRONTIUM OXIDES[1]

BY WILLIAM P. RIEMEN AND FARRINGTON DANIELS

Contribution from the Department of Chemistry, University of Wisconsin, Madison, Wisconsin

Received February 11, 1957

The rate of the reaction $Ag_2SO_4 + CaO \rightarrow Ag_2O + CaSO_4 \rightarrow 2Ag + \frac{1}{2}O_2 + CaSO_4$ has been studied in solid powders between 500 and 500°. A similar reaction with SrO has been studied between 400 and 450°. The fraction reacted is measured by loss in weight of oxygen and by amount of soluble silver remaining. The data and rate constants are in agreement with a kinetic formula. The reactions are abnormally fast at first probably due to a rapid surface reaction.

Most researches in chemical kinetics have been concerned with reactions in solution or in the gas phase. Progress in solid state physics suggests interesting studies in solid state chemistry, and several researches in this field have been carried

out in this Laboratory. Reactions of solids to give solids would be exceedingly slow except for imperfections in the crystals which act as centers for the diffusion of materials through the crystal structure. Reactions between solids are significant in geological phenomena where long periods of time have been available, and in the preparation of crystals of high purity. They are important also in catalysts

and other materials having particular impurities.

Pioneer work has been summarized by Hedvall,[2] Cohn,[3] and Rees.[4] The kinetics of the reactions between some of the alkali halide crystals around 450° has been studied in this Laboratory by Mason[5] in which the rate of the reaction was measured by the changing X-ray patterns.

The purpose of this investigation was to study a solid–solid reaction which can be followed by simple chemical means. It is not easy to find suitable reactions because further chemical changes are apt to take place during the chemical analysis which destroy the kinetic significance of the analysis. Reactions involving a loss of a product as a gas or the change in concentration of a chemical element are suitable for direct analysis. The reactions between a powder of silver sulfate and a powder of calcium oxide and strontium oxide, giving a product gas and metallic silver, were chosen for this investigation.

Theoretical.—Exchange reactions of this type proceed by diffusion through two different product layers. Several factors may be involved in the kinetic behavior, including phase boundary processes and the rates of diffusion of the reactants through each other and through the products. Jander[6] gave a mathematical treatment of diffusion assuming diffusion through a concentric shell of product on the outside of a sphere. Serrin and Ellickson[7] published a more rigorous diffusion-controlled rate equation. Mason[5] has derived this equation, and subjected it to experimental test with very good results.

The equation is

$$1 - x = \frac{6}{\pi^2} \sum_{n=1}^{\infty} \frac{1}{n^2} e^{-n^2 kt}$$

where $k = \pi^2 D/a^2$, x is the fraction of the reaction completed at time t, D is the diffusivity based on Fick's law, a is the radius of the particles, and k is the rate constant for the solid state reaction based on diffusion into a sphere. This equation has been solved by Mason[5] for numerical values of kt from 0.01 to 1.20 and the corresponding values of $1 - x$ from 0.8727 to 0.1844 with the help of an I.B.M. calculator.

In using this equation, x is determined by chemical analysis and the corresponding value of kt is obtained from the tables. Then kt is plotted against time. The resulting line should be straight if the process is diffusion controlled and the assumptions of the derivation are valid. The slope of the line gives the value of k. Straight lines have been obtained frequently in this Laboratory, even though the particles are not spherical and the diffusion law is not entirely applicable. Thus, the equation may be used as an empirical equation for powders.

(2) J. A. Hedvall, "Einfuhrung in die Festkorperchemie," F. Vieweg and Sons, Braunschweig, 1952.

(3) G. Cohn, *Chem. Revs.*, **42**, 527 (1948).

(4) A. L. G. Rees, "Chemistry of the Defect Solid State," John Wiley and Sons, New York, N. Y., 1954.

(5) H. F. Mason, Ph.D. Thesis, University of Wisconsin, 1954; THIS JOURNAL, **61**, 796 (1957).

(6) W. Jander, *Z. anorg. Chem.*, **166**, 33 (1927).

(7) B. Serrin and R. T. Ellickson, *J. Chem. Phys.*, **9**, 742 (1941).

Experimental

The reaction between silver sulfate and calcium oxide in the solid state was first studied by Hedvall[8] who applied the method of thermal analysis rather than the more convenient chemical method of gas evolution. Moreover, he gave no kinetic data which could be used to calculate a rate constant.

Solid silver sulfate reacts with solid calcium oxide in the temperature interval from 500 to 600°. Below 500° it is too slow to follow. Consequently, this research was restricted to the temperature interval of 500 to 600°. The reaction can be considered as a double decomposition reaction, as

$$Ag_2SO_4 + CaO \longrightarrow Ag_2O + CaSO_4$$
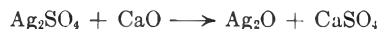
At temperatures above 300°, silver oxide is completely dissociated into elemental silver and gaseous oxygen. In these studies carried out at temperatures above 500°, the above reaction should then be written

$$2Ag_2SO_4 + 2CaO \longrightarrow 4Ag + O_2 + 2CaSO_4$$

Two means are available for following the course of this reaction. The first measures the loss in weight of the reaction mixture which occurs when oxygen is evolved. The second determines the remaining, unreacted silver sulfate.

Analytical grade materials were used throughout the research. The calcium oxide was prepared by heating calcium hydroxide at 1000° for 24 hours. This ensured that all the hydroxide was converted to the oxide. Both chemicals were heated independently at 500° for two hours to ensure complete drying. They were then ground in a mullite mortar and sieved. The fraction of the powder which passed through a 200-mesh screen and lay on a 320-mesh screen was collected and stored in a desiccator. The sieve screens were heated on a hot plate before use to remove the possibility of moisture being picked up by the powders.

At room temperature this reaction is very slow if the reactants are kept in a dry condition. Consequently a large amount of an equimolar mixture of the powdered calcium oxide and silver sulfate was prepared by weighing out the appropriate amounts of each and mixing thoroughly by passing three or four times through a sieve whose openings were several times larger than the size of the particles. These mixtures were stored in desiccators until used.

The kinetic data were obtained by the following procedure: 3.6790 g. of the reaction mixture was weighed into crucibles which had been previously dried and weighed. These crucibles were placed in a Lindberg muffle furnace controlled to ±4° for times which varied from 5 to 1000 minutes. After the reaction time had elapsed, the crucible was removed, cooled in Dry Ice to stop the reaction quickly, and reweighed. The loss of weight which represented oxygen evolution was taken as a measure of the extent of the reaction.

The procedure was repeated with another set of crucibles at the same temperature and the soluble silver sulfate which remained unreacted, was determined. The reaction mixture was treated with a dilute solution of ammonium hydroxide and filtered. Using litmus as an indicator the dissolved silver was precipitated from this filtrate with dilute hydrochloric acid, care being observed not to add too great an excess of the acid. This precipitate was allowed to digest at 80° for 1 hour. It was then filtered off into Gooch crucibles, washed and dried at 110° for 1 hour. The weight of the silver chloride was converted into silver sulfate. This value was used to obtain another measure of the extent of the reaction.

The silver analysis was not used as much as the oxygen evolution method. However, checks were made at each temperature to ascertain whether there was agreement. The comparison between the results of the two methods gave good agreement and the average difference amounted to about 5%. This difference showed no trend indicating that one method was always lower or higher than that of the other. Hence, it was concluded that the oxygen method was quite acceptable. The results of the two methods appear in Table I.

The data are summarized in Table II and presented in graphical form in Figs. 1 and 2. The rate constants for the reaction are calculated from the slopes of the curves which represent kt versus time. In Fig. 3, log k is plotted against

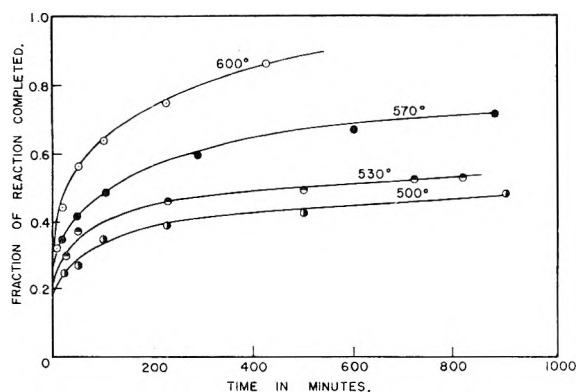(8) J. A. Hedvall, *Z. angew. Chem.*, **39**, 781 (1931).

Fig. 1.—Fraction of reaction completed *versus* time for reaction CaO + Ag$_2$SO$_4$ at temperatures 500–600°.

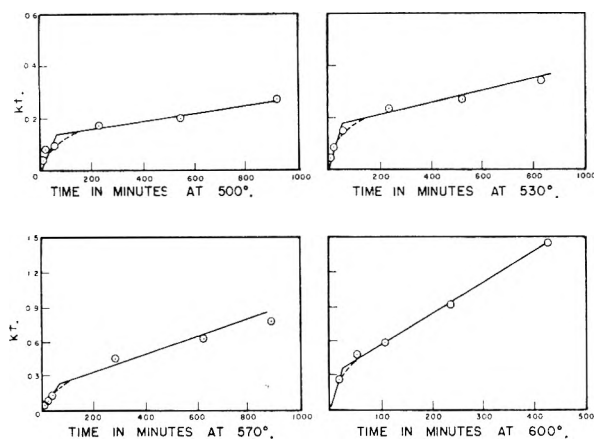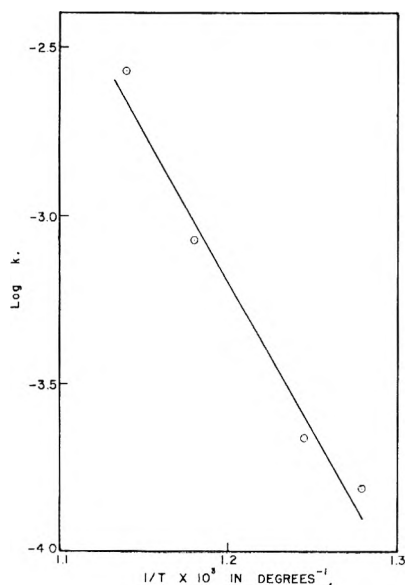Fig. 2.—Rate constant k multiplied by time *versus* time for reaction CaO + Ag$_2$SO$_4$ at temperatures 500–600°.

Fig. 3.—Log rate constant *versus* reciprocal of absolute temperature for reaction CaO + Ag$_2$SO$_4$.

the reciprocal of the absolute temperature, giving an activation energy of 41,000 cal. per mole.

The reaction between silver sulfate and strontium oxide in the solid state is similar to the reaction between silver sulfate and calcium oxide. The details of the experimental procedure were the same as those which were used in the calcium oxide and silver sulfate reaction with the exception that 4.2545 g. of a 50:50 molar mixture of the reactants was used as the react on mixture.

TABLE I
COMPARISON OF ANALYTICAL METHODS

Time, min.	Temp., °C.	Fraction of reaction completed By silver anal.	By oxygen anal.
105	500	0.32	0.37
900	500	.48	.47
285	570	.58	.61
45	600	.55	.58
225	600	.76	.73

TABLE II
KINETIC DATA FOR REACTION Ag$_2$SO$_4$ + CaO

Time, min.	Fraction reaction completed	kt	Time, min.	Fraction reaction completed	kt
	Temp., 500°			Temp., 530°	
5	0.19	0.03	5	0.23	0.05
15	.25	.06	15	.30	.09
45	.27	.07	45	.37	.15
105	.35	.13	225	.45	.23
220	.38	.17	500	.49	.28
500	.42	.20	825	.52	.34
900	.48	.27			

$k = 1.6 \times 10^{-4}$ min.$^{-1}$ $k = 2.2 \times 10^{-4}$ min.$^{-1}$

Time	Frac	kt	Time	Frac	kt
	Temp., 570°			Temp., 600°	
5	0.26	0.06	5	0.29	0.09
15	.33	.12	15	.43	.22
45	.41	.18	45	.56	.42
105	.48	.28	105	.64	.56
285	.59	.49	225	.74	.89
600	.67	.62	425	.86	1.47
885	.72	.77			

$k = 7.9 \times 10^{-4}$ min.$^{-1}$ $k = 27 \times 10^{-4}$ min.$^{-1}$

The reaction between silver sulfate and strontium oxide occurs at a measurable rate in the temperature interval of 400 to 450°. The reaction may be represented as

$$2Ag_2SO_4 + 2SrO \longrightarrow 4Ag + O_2 + 2SrSO_4$$
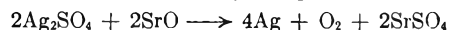
The data are summarized in Table III and presented in graphical form in Fig. 4 and 5. The rate constants k are calculated from the slopes of the lines of Fig. 5. A plot of log k against the reciprocal of the absolute temperature gives an activation energy of 14,000 cal. per mole.

TABLE III
KINETIC DATA FOR REACTION Ag$_2$SO$_4$ + SrO

	Temp. 400°			Temp., 425°			Temp. 450°	
Time, min.	Fraction reaction completed	kt	Time, min.	Fraction reaction completed	kt	Time, min.	Fraction reaction completed	kt
5	0.22	0.04	5	0.23	0.05	5	0.27	0.07
15	.28	.07	15	.29	.09	15	.33	.12
45	.34	.12	45	.36	.13	45	.35	.13
100	.42	.18	100	.40	.18	75	.41	.18
230	.48	.27	250	.45	.23	195	.45	.22
500	.52	.34	500	.57	.41	350	.57	.41
690	.58	.45	650	.60	.48	500	.68	.67
$k = 4.9 \times 10^{-4}$ min.$^{-1}$			$k = 5.6 \times 10^{-4}$ min.$^{-1}$			$k = 10 \times 10^{-4}$ min.$^{-1}$		

Discussion

It is observed that all the curves representing kt *versus* time give straight lines after the initial part of the reaction. The initial part of the reaction is also very nearly a straight line which passes through the origin. The slope of this line is greater than the slope of the straight line representing the major portion of the reaction. This behavior is ap-

parently quite general for the reactions between silver sulfate and calcium oxide or strontium oxide. The fact that the curve can be divided into two straight lines with different slopes suggests that the reaction proceeds in two stages. The later stage, after the initial stage of the reaction is complete, is controlled by diffusion into the interior of the solids. The other mechanism may be surface diffusion.[9] Presumably, the surface reaction occurs first and is a fast reaction which is completed in a short time. After the surface is covered and the surface reaction is completed, the dominant mechanism is volume diffusion. This phase of the reaction is adequately described by the spherically symmetrical diffusion rate equation given earlier. This equation does not take surface diffusion into account.

Another explanation for the deviations from the rate law for spherical diffusion which occur in the initial phase of the reaction is based on the fact that the solid state reactions are exothermic. Since the heat capacities and conductivities of solids are usually low, the powder mixture becomes heated during the reaction. The initial heat liberated will raise the reaction mixture almost immediately to a temperature higher than the furnace temperature. From this maximum temperature, the mixture gradually cools down to the furnace temperature. On this basis, the initial part of the reaction would be expected to go at a faster rate than after the mixture had cooled down. This idea was first formulated by Jander.[10] Calculations indicate that if the reaction were adiabatic there would be a sufficient rise in temperature to account for the increased rate at the beginning. However, on this hypothesis, a more gradual change to the slower rate would be expected.

Experiments indicated that surface reactions do occur rapidly in the reaction between silver sulfate and calcium oxide. Large particles of silver sulfate were placed in crucibles and completely surrounded by very small particles of calcium oxide. The large particles were about 0.5 cm. in diameter and the small particles were about 50 μ in diameter. These mixtures were heated to 625° for periods of time which varied between one and three days. A similar experiment was performed in which the large particles were calcium oxide and the small particles were silver sulfate. After each of these

(9) S. Glasstone, K. Laidler and H. Eyring, "The Theory of Rate Processes," McGraw-Hill Book Co., Inc., New York, N. Y., 1941.

(10) W. Jander, Z. anorg. Chem., 166, 33 (1927).
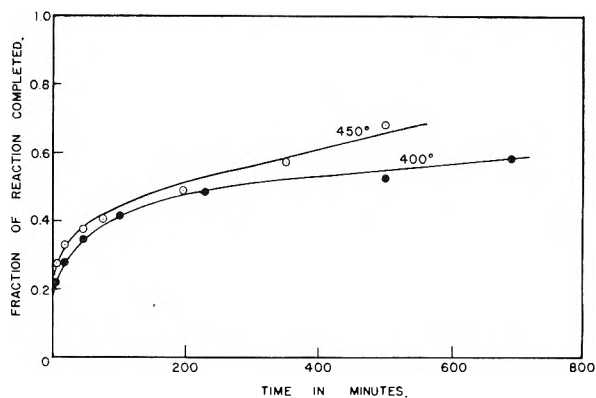
Fig. 4.—Fraction of reaction completed *versus* time for reaction SrO + Ag₂SO₄ at temperatures 400 and 450°.
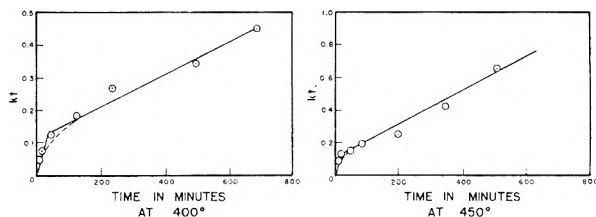
Fig. 5.—Rate constant k multiplied by time *versus* time, for reaction SrO + Ag₂SO₄ at temperatures 400 and 450°.

mixtures was heated for one day, it was removed from the furnace and a few of the large particles were taken from each crucible for visual examination. All the particles were completely covered with a grayish-black surface. The particles were then placed on a microscope slide and secured in place with Canada Balsam. They were subsequently thin-sectioned and observed under a microscope. No evidence was observed for diffusion into the interior of either calcium oxide or silver sulfate. This procedure was repeated after two days of heating and the results were the same. After three days of heating a small ring of gray silver was observed in the interior of the calcium oxide particles.

The evidence indicates that a rapid surface reaction does occur at first. However, the possibility of the heat build-up hypothesis as a partial explanation for the rate curves is not excluded.

THE DIELECTRIC CONSTANT OF SOLID PARTICLE AEROSOLS[1]

By Cullen M. Crain, Donald C. Thorn and James E. Boggs[2]

*Electrical Engineering Research Laboratory and Departments of Chemistry and Electrical Engineering,
The University of Texas, Austin 12, Texas*

The dielectric constants of aerosols consisting of polystyrene, silver iodide or iron powder suspended in dry nitrogen, or oil smoke suspended in air have been measured at a frequency of 9400 megacycles. The results are fitted well by the simple expression, equation 1, in spite of the complexity and wide diversity of the systems studied. The observed data were well fitted by this equation even in cases where magnetic as well as electric interactions would be expected.

The problem of the effective dielectric constant of a mixture of two substances of different dielectric constants has been considered by many authors[3-11] from a theoretical viewpoint. A considerable amount of simplification is necessary for the mathematical treatment to be successful, and different authors have worked with quite different models. If consideration is restricted to aerosols, where the dielectric constant of the medium is essentially unity, the size of the particles is small compared with the wave length of the measuring radiation, and interaction between suspended particles may be neglected, the results of these various investigations can all be expressed in the form

$$\Delta\epsilon = 3.0 \frac{\epsilon_1 - 1}{\epsilon_1 + 2} \frac{C}{\rho} \times 10^{-6} \qquad (1)$$

where $\Delta\epsilon$ is the difference between the dielectric constant of the suspension and that of the medium, ϵ_1 is the dielectric constant of the suspended substance, C is the mass concentration of the suspension in micrograms per cc., and ρ is the density of the suspended material. The derivations of this formula still contain a number of restrictions which are not met by aerosols and by the usual methods of measurement. The derivation of Lewin,[9] for example, assumes that the suspended particles are spheres, that no agglomeration of particles occurs, that the spheres are arranged in a cubical lattice and are stationary, and that the measurement is made with a plane-polarized electromagnetic wave.

Numerous studies have been made[12] on the dielectric constant of two phase mixtures, but these have usually been done with coarse mixtures of high concentration rather than with aerosols, in order to obtain a value of $\Delta\epsilon$ high enough to measure by the older experimental techniques. The interpretation of the results is less simple than might be anticipated for aerosols where the suspended particles are small, far apart, and essentially independent of each other.

In recent years, techniques for the measurement

of dielectric constants at microwave frequency have been developed which make possible the detection of very small differences in dielectric constant with relative ease. Dorain[13] has measured the dielectric constants of liquid drop aerosols of dioctyl phthalate and triethylene glycol di-(2-ethyl butyrate) suspended in air. His measurements show good agreement with equation 1 over the concentration range of 0 to 0.8 microgram per cc.

The problem of the dielectric constant of solid-particle aerosols would appear to be more complex than that studied by Dorain, since here the suspended particles may be far from spherical and considerable agglomeration of the particles into clusters may exist. We have studied a number of such systems to see how well experimental measurements agree with the simple theory. The aerosols chosen exhibit a wide range of particle size and shape, degree of clustering, and density, dielectric constant, conductivity and permeability of the suspended substance.

Experimental

Apparatus.—All of the measurements were made at a frequency of 9400 megacycles, using a Crain microwave refractometer.[14] In this instrument, the resonance frequency of a microwave cavity, which depends on the dielectric constant of the material within the cavity, is used to stabilize a Klystron oscillator. The resulting frequency is beat against that of a similar reference cavity and oscillator, the beat frequency being a measure of the difference in the dielectric constants of the materials in the two cavities.

For our experiments, the aerosol was passed through one cavity of the refractometer, then through a Cambridge "absolute" filter,[15] then through the other cavity of the refractometer. The filter used will remove 99.95% of particles of 0.3 μ size or larger. Thus the refractometer reading gives the difference between the dielectric constant of the suspension and that of the gas phase, or the contribution due to the suspended particles. After passing through the second cavity, the gas was passed through a wet-test gas meter to measure its volume. The weight of the suspended material in the aerosol used was determined from the increase of weight of the filter during the run. From these two measurements, the average concentration of the aerosol during the experiment could be determined. The frequency difference between the two cavities was converted to a voltage and recorded continuously, giving a plot from which the average dielectric constant difference could be calculated. The pressure drop across the filter was measured, so that if a significant pressure difference developed between the two cavities, the run could be terminated.

Aerosols.—Polystyrene spheres with an average diameter of about 3 μ were obtained from the Wright Air Development Center. Under high magnification these were seen to be nearly perfect spheres with quite a narrow range of particle size. There was very little clustering. The powder

(1) This work was supported by Air Force Contract AF 33(616)-2842.

(2) The authors would like to express their appreciation for the valuable assistance of Herbert L. Mitchell and James B. Magee.

(3) H. A. Lorentz, *Wied. Ann.*, **9**, 641 (1880).

(4) L. Lorenz, *ibid.*, **11**, 70 (1880).

(5) J. W. Rayleigh, *Phil. Mag.*, **34**, 481 (1892).

(6) K. W. Wagner, *Arch. Elektrotech.*, **2**, 371 (1914).

(7) D. A. G. Bruggeman, *Ann. Physik*, **24**, 636 (1935).

(8) R. W. Sillars, *J. Inst. Elec. Engrs. (London).* **80**, 378 (1937).

(9) L. Lewin, *ibid.*, **94**, [3], 65 (1947).

(10) H. C. Thacher, Jr., This Journal, **56**, 795 (1952).

(11) J. Fricke, *J. Appl. Phys.*, **24**, 644 (1953); This Journal, **57**, 934 (1953).

(12) C. A. P. Pearce, *Brit. J. Appl. Phys.*, **6**, 358 (1955).

(13) P. B. Dorain, "The Dielectric Properties of Aerosols," Ph.D. Dissertation, Indiana University, 1954.

(14) C. M. Crain, *Rev. Sci. Instr.*, **21**, 456 (1950); C. M. Crain and C. E. Williams, *Electronics*, **29**, 150 (1956).

(15) D. H. Northrup, *Chem. Eng. Progr.*, **49**, 513 (1953).

was placed in a flask with a conical bottom and subjected to moderate agitation with an external vibrator. A stream of carefully dried nitrogen was passed through the flask, through a settling chamber, through the refractometer cavities, and then through the wet-test meter. The aerosol density could be varied by diluting the aerosol stream with dried nitrogen, or, to some extent, by varying the flow velocity and extent of agitation.

A silver iodide aerosol was generated by heating solid silver iodide in a zirconium oxide combustion tube heated by a small tube furnace. Dried nitrogen was passed over the heated silver iodide, through a sufficient length of tubing to bring the temperature back to room temperature, through the refractometer cavities, through the wet-test meter, then through a vacuum pump. Electron micrographs of the resulting silver iodide particles showed them to have an irregular shape with a moderate degree of clustering and considerable variation in size around an average diameter of about 0.1 μ for the individual particles.

An oil smoke aerosol was generated by burning diesel oil in an inadequate supply of air, using an asbestos wick. The smoke was passed through a cold trap to remove water, and drawn through the refractometer cavities as before. Great care must be taken to remove all traces of water vapor, since it will be absorbed to some extent by the filter and it has such a high dielectric constant that small traces of it can give highly erroneous results. Electron micrographs showed this aerosol to have a strongly clustered structure, the clusters averaging about 1 micron in diameter with individual particles about 0.05 μ.

A suspension of iron particles was obtained, using "SF" carbonyl iron powder obtained from Antara Chemicals Co. These particles average 3 μ in diameter, 94% of them falling in the size range from 1.5 to 5 μ. They contain 98.2–98.8% iron, the remainder being mainly carbon and nitrogen with about 0.2% oxygen. The particles are nearly spherical and show little clustering. The powder was dispersed by the same technique used for the polystyrene. A moderate amount of iron powder was found to settle out in the first refractometer cavity, giving a gradual shift in the base line of the refractometer tracing for which a correction had to be made.

Results

The density of polystyrene is 1.032 g./cc. The refractive index at optical frequencies is 1.592, the square of which gives 2.54 for the dielectric constant. This agrees well with measurements at one megacycle, and may be taken as the value of 9400 megacycles. Using these values, equation 1 becomes $\Delta\epsilon = 0.98C \times 10^{-6}$. This line is plotted in Fig. 1, together with the measured points. The best line through the experimental points has exactly the proper slope, but an intercept of $\Delta\epsilon = -0.5 \times 10^{-6}$. This presumably corresponds to a constant error in measurement and is within the error which can be expected in the absolute value of $\Delta\epsilon$.

For silver iodide, the density is 5.67 g./cc. and the square of the optical index of refraction is 2.21. A crude measurement of the dielectric constant at 9400 megacycles gave substantial agreement with this. Substituting these values in equation 1 gives $\Delta\epsilon = 0.30C \times 10^{-6}$. This line, together with the experimental points, is shown in Fig. 2. It can be seen that the agreement is excellent.

Both polystyrene and silver iodide have low electrical conductivities, but this is not true of the particles in the oil smoke and iron suspensions. The observed change in frequency of the refractometer cavity is given by

$$\Delta f = \Delta f_e + \Delta f_m$$

where Δf_e and Δf_m are the contributions from the electric and magnetic effects considered independ-
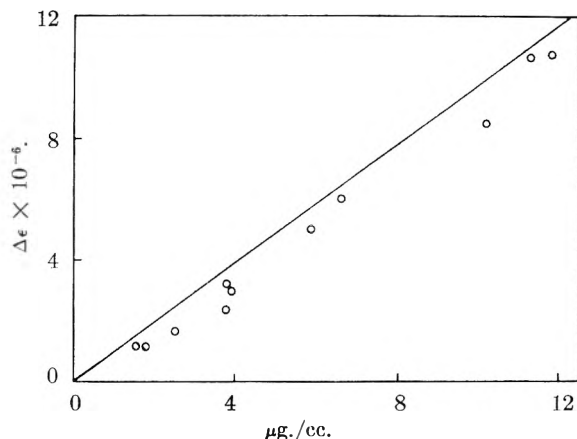

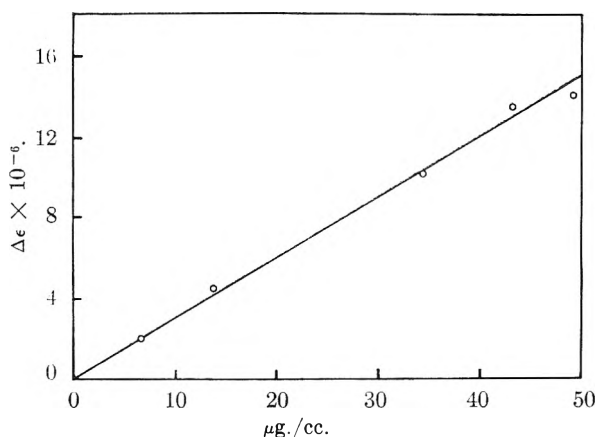Fig. 1.—Dielectric constant increment for polystyrene aerosols as a function of mass concentration.

Fig. 2.—Dielectric constant increment for silver iodide aerosols as a function of mass concentration.

ently.[16] The Δf_m term is related to the effective relative permeability, μ, in the same way that the Δf_e term is related to the dielectric constant, ϵ. For a non-magnetic non-conductor, μ is essentially 1 and Δf_m is 0. Thus the observed frequency change depends only on the electric contribution and can be interpreted in terms of the dielectric constant alone. For a substance of very high conductivity, ϵ approaches infinity and $(\epsilon - 1)/(\epsilon + 2)$ approaches 1. At the same time, the effective μ approaches 0 and $(\mu - 1)/(\mu + 2)$ approaches $-1/2$. Thus, for conducting particles, the magnetic effect should lower the observed frequency change below that predicted considering electric interaction alone. These considerations apply strictly only if one can assume that the electric field lines do not enter the conductor. At 9400 megacycles the depth of penetration is of about the same order as the diameter of the particles used, and we have not tried to make a prediction of the quantitative effect of high electrical conductivity.

Oil smoke is a rather indefinite thing chemically, but we may assume that its density is around 1.95 g./cc., an average of a number of reported values for amorphous carbon. Amorphous carbon is a moderately good conductor, so the effective dielectric constant should be high. If ϵ_1 is taken as infinity,

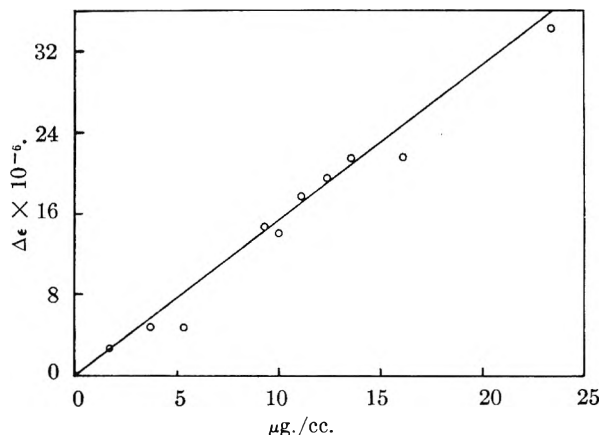(16) J. G. Linhart and T. H. B. Baker, *Brit. J. Appl. Phys.*, **6**, 100 (1955).

Fig. 3.—Dielectric constant increment for oil smoke aerosols as a function of mass concentration.
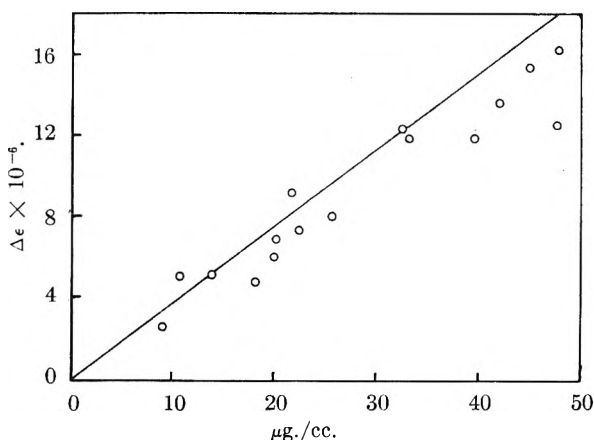

Fig. 4.—Dielectric constant increment for iron powder aerosols as a function of mass concentration.

equation 1 becomes $\Delta\epsilon = 1.54C \times 10^{-6}$. $\Delta\epsilon$ becomes rather insensitive to variations in ϵ_1 if ϵ_1 is large. Thus, a value of 50 for the dielectric constant of oil smoke would reduce the slope of the line by only about 6% from that calculated for an infinite dielectric constant. The predicted line and the observed points are compared in Fig. 3. It can be seen that the agreement is good in spite of the fact that no allowance has been made for magnetic interaction caused by the conductivity of the particles. Minor effects might not appear in our experi-

ment because of the uncertainties involved in our selection of the density and dielectric constant values.

The density of the "SF" iron particles is 7.81 g./cc. If the dielectric constant is taken as infinity, equation 1 becomes $\Delta\epsilon = 0.38C \times 10^{-6}$. Figure 4 shows this line, together with the observed points. Our measurements on iron are probably less accurate than those on the other aerosols because of the refractometer background drift caused by settling of iron particles in the first cavity. It was assumed that this drift was linear with time, but this may not be exactly true. The best line which can be drawn through the experimental points will have an intercept of $+0.6 \times 10^{-6}$ for $\Delta\epsilon$, which can reasonably be attributed to instrumental error, and a slope of 0.28. This, qualitatively, is the effect we have seen should be observed for an aerosol made up of conducting particles, but it is doubtful here whether it is beyond the limits of experimental error.

Conclusions

Equation 1, developed by different authors on the basis of various highly restrictive models, has been shown to have surprisingly wide applicability in predicting the dielectric constant of aerosols. It is to be expected that this relationship might break down at high aerosol concentrations, because of interaction between the charge distribution in closely adjacent particles. Although we have tried to produce very dense aerosols, and have measured concentrations 65 times as high as those studied by Dorain,[13] we have seen no evidence of such a deviation. While it is recognized that suspensions of materials with high electrical conductivity or permeability will have a magnetic as well as an electric interaction with electromagnetic radiation, no such effect was observed with oil smoke and only a small effect, possibly not beyond experimental error, for iron powder.

Our measurements have been made on substances with densities ranging from 1.032 to 7.81 g./cc., with dielectric constants from 2.21 to infinity, with and without high permeability, on aerosols in concentrations from 2 to 50 micrograms per cc., having particles of widely different sizes and distributions of sizes and of widely varying degrees of clustering.

NOTES

THE EFFECT OF PRESSURE ON THE SURFACE TENSIONS OF LIQUIDS

By Emil J. Slowinski, Jr., Ernest E. Gates and Charles E. Waring

Chemistry Department, University of Connecticut, Storrs, Connecticut

Received August 10, 1956

The only reported experimental measurements of the effect of pressurizing gases on the surface tensions of liquids are those of Kundt.[1] He found

that in general the surface tension of liquids decreases with increasing gas pressures. Theoretical treatments of the effect are more numerous, with Gibbs,[2] Guggenheim[3] and Rice[4] among those who have made important contributions. The effect is attributed to adsorption of the pressurizing gas

(1) A. Kundt, Ann. physik. Chem., 12, 538 (1881).

(2) J. W. Gibbs, "Collected Works," Vol. I, Yale University Press, New Haven, Conn., 1948, pp. 219–269.

(3) E. A. Guggenheim, J. Chem. Soc., 128 (1940).

(4) O. K. Rice, J. Chem. Phys., 15, 333 (1947).

on the liquid surface, but it seems no clear dependence of surface tension on actual concentration of adsorbed molecules can be derived theoretically. The difficulty is related to the necessity of quite arbitrarily defining the position of the liquid surface, usually as was done by Gibbs, before any relation between surface tension and concentration of adsorbed molecules can be stated. It thus appears that experimental measurements of dependence of surface tension on pressure would be useful, both to establish more quantitatively than could Kundt the nature of the effect and to furnish data which might aid in further developing the theoretical interpretation.

In a series of experiments we have measured the surface tensions of water and normal hexane under pressures of helium, hydrogen, nitrogen, methane, ethane and carbon dioxide. The capillary-rise technique was used and the procedures suggested by Richards[5] and Harkins[6] were followed. Experiments were carried out in a steel bomb provided with methyl methacrylate windows and having an inner diameter of about 2.5 inches and a usable length of about 6 inches. The U-tube surface-tension cell due to Richards was modified to satisfy space restrictions. The cell was of Pyrex glass, with the large tube about 38 mm. in diameter and the capillary tube made re-entrant above the level of the large meniscus and concentric with the large tube. The inner capillary diameter was about 0.4 mm. and was calibrated in accordance with Harkins' methods.

Capillary rise was measured during both increasing and decreasing gas pressure portions of a run. Calculated values of surface tension for a given system were found in general to lie on the same curve; this would imply that equilibrium conditions existed within the cell and that temperature held substantially constant during the time required for a run. Capillary rise was measured to 0.03 mm. with a cathetometer, and pressures, as measured on a Heise gage, were taken to 100 atm. where possible. All measurements were made at room temperature, about 25°.

An important feature of the surface-tension cell, necessary if one is to be able to ascertain the establishment of equilibrium, is a small capillary, made by drawing out ordinary capillary tubing, attached to the cell capillary with rubber tubing. This introduces a delay in the time for pressure equilibrium to be attained in the cell and allows one to raise or lower the small meniscus momentarily by simply increasing or decreasing gas pressure in the bomb.

Since the data do not warrant the use of equations of higher precision, calculations of surface tensions were made on the basis of the simple relation

$$\gamma = \frac{1}{2}rgh(\rho_l - \rho_g)$$

where γ is the surface tension, r is the capillary diameter, g is the acceleration of gravity, h is the capillary rise, ρ_l is density of the liquid, and ρ_g is

(5) T. W. Richards, *J. Am. Chem. Soc.*, **43**, 827 (1921).

(6) W. D. Harkins and A. Weissburger, "Physical Methods of Organic Chemistry.", Chapter IX, Interscience Publishers, Inc., New York, N. Y., 1949.

the density of the gas, all in c.g.s. units. Liquid density was taken to be that of the pure liquid corrected by a compressibility factor of 50×10^{-6}/atm. for water and 100×10^{-6}/atm. for hexane. Gas density was calculated from the van der Waals equation.

Experimental results are given in graphical form in Figs. 1 and 2, where relative surface tension, γ/γ_0, is plotted against gas pressure in atmos-
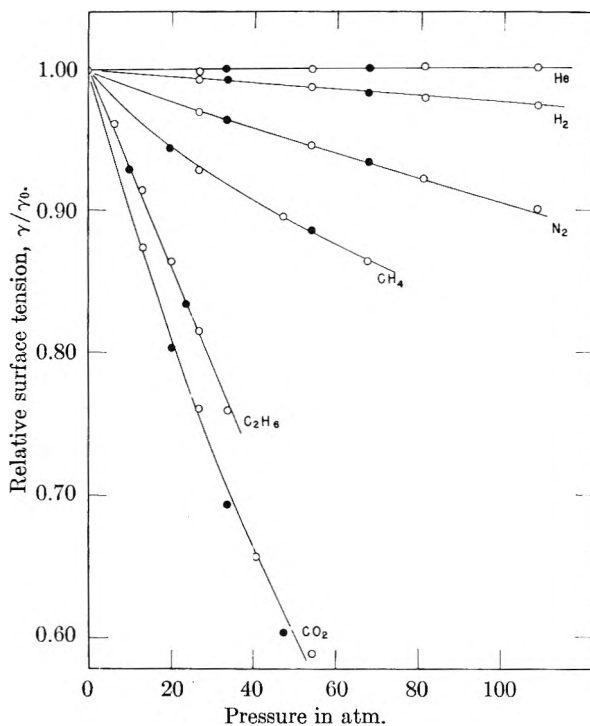

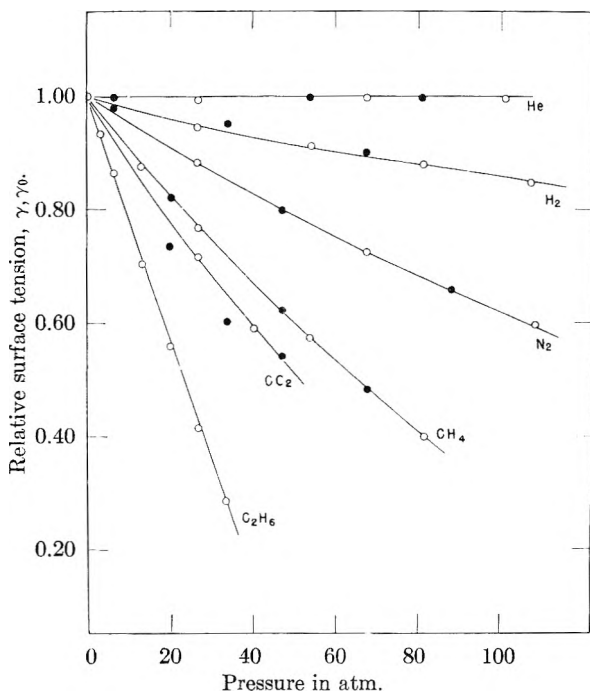Fig. 1.—The effect of gases on the surface tension of water: O, increasing pressure; ●, decreasing pressure.

Fig. 2.—The effect of gases on the surface tension of n-hexane: O, increasing pressure; ●, decreasing pressure.

pheres. It is seen that except for helium, which shows no effect, surface tensions of the two liquids decrease approximately linearly with increasing gas pressure. At a given pressure the magnitude of the effect increases with increase in critical temperature or boiling point of the pressurizing gas. The relative effect of gas pressure on surface tension is larger for hexane than for water, but if one calculates the actual change in surface tension it is found that for most of the gases a given pressure decreases the surface tension about the same number of dynes/cm. for hexane as for water. That is, $d\gamma/dP$ seems to depend mainly on the nature of the pressurizing gas and only in a minor way on the liquid.

A simple theoretical expression for the dependence of surface tension on pressure[7] is

$$\frac{d\gamma}{dP} = -\frac{\Gamma_2^{(1)}RT}{P} \qquad (1)$$

where P is the pressure of the gas (assumed to be ideal) and $\Gamma_2^{(1)}$ is taken to be the concentration of adsorbed gas in moles per unit of surface area. Since $d\gamma/dP$ is found experimentally to be essentially constant at low pressures, this means that $\Gamma_2^{(1)} = KP$, and hence concentration of adsorbed gas as defined follows what might be considered to be either a sort of Henry's law for the surface phase or the limiting form of the Langmuir adsorption equation (usually applied to solid surfaces). If under these conditions we integrate (1) we obtain as a relation consistent with our experimental results

$$\gamma - \gamma_0 = -KPRT = -\Gamma_2^{(1)}RT \qquad (2)$$

Equation 2 essentially states that a concentration of one molecule per sq. cm. for any adsorbed molecules will lower the surface tension of any liquid by an amount equal to kT dynes/cm., where k is the Boltzmann constant.

Since K in (2) appears in our work to have nearly the same value for a given gas over water and over hexane, it would seem that more precise measurements on the effect of an inert gas such as argon on the surface tensions of a group of liquids would be of interest. If K in such experiments were constant for all liquids an extension of this sort of measurement might possibly be made to include the determination of the areas of solid surfaces.

(7) For a clear derivation of this relation and a discussion of the meaning of $\Gamma_2^{(1)}$ see N. K. Adam, "The Physics and Chemistry of Surfaces," Oxford Press, 1941, pp. 107-117.

SURFACE ENTROPY AND SURFACE ORIENTATION OF POLAR LIQUIDS[1]

By ROBERT J. GOOD[2]

Contribution from the Applied Science Research Laboratory, University of Cincinnati, Cincinnati, Ohio

Received September 14, 1956

No generalizations have been made as to the surface orientation of low molecular weight liquids,

except for one isolated case. Weyl[3] has suggested that in liquid water the surface molecules all have their oxygens exposed and hydrogens all pointing inwards.

We wish to propose that the surface entropy of a liquid may be taken as a criterion of surface orientation. Orientation in the surface will lead to a lower entropy than that in the condition where the surface molecules are disordered. The question is, first, how much lower is the surface entropy of polar substances than that of non-polar substances? And second, can we set up a *simple* model which will account for the lower entropy of polar liquids, as resulting from surface orientation?

Ramsay and Shields[4] reached the conclusion empirically that there was a "normal" value (2.1) for the Eötvös constant, which is directly related to the molar surface entropy.[5-7] From various theoretical studies,[5-9] particularly that of Born and Courant, it might be expected that there should be a "normal" value for nearly spherical non-polar molecules. (The extension of this concept to non-spherical molecules cannot be made very simply, because the number of molecules "in the surface" per unit area depends on the degree of orientation as well as the ratio of length to thickness.[7]) The hypothesis of Ramsay and Shields, that the degree of association could be calculated from the ratio of the observed Eötvös constant to the "normal" value, 2.1, has of course long since been discredited;[7] but it persists in textbooks and the literature, probably because of the lack of a plausible alternative. We will show that surface orientation furnishes a much more reasonable explanation.

The molar surface entropy has been calculated for 214 organic liquids and 26 inorganic liquids of molecular structure such that they could be considered approximately spherical. The formula[9]

$$\sigma A = fV^{2/3}N^{1/3}\frac{d\gamma}{dT}$$

was used, where σ is specific surface entropy, A is molar surface area, V is molar volume, N the Avogadro number, γ the surface tension and T the absolute temperature, and f a factor[9] which depends on the "packing" or "structure" of the liquid. For hexagonal close-packed liquids, $f = 1.09$; for body-centered cubic packing, $f = 1.12$. We will employ a compromise between these two values for convenience (though recognizing that this introduces an element of uncertainty of about 2 to 3%), $f = 1.10$. $d\gamma/dT$ was calculated from data given in the recent compilation of Quayle.[10] Other data were taken from Harkins[7] and from the International Critical Tables. Density data were taken from the authors who measured the surface tensions, from the International Critical Tables, from

(3) W. A. Weyl, *J. Coll. Sci.*, **6**, 389 (1951).

(4) (a) W. Ramsay and J. Shields, *Phil. Trans.*, **A184**, 647 (1893); (b) *J. Chem. Soc.*, 1089 (1893).

(5) M. Born and R. Courant, *Phys. Z.*, **14**, 731 (1913).

(6) J. Frenkel, "Kinetic Theory of Liquids," Oxford University Press, London, 1946.

(7) W. D. Harkins, "Physical Chemistry of Surface Films," Reinhold Publ. Corp., New York, N. Y., 1952.

(8) N. K. Adam, "Physics and Chemistry of Surfaces," Oxford University Press, London, 3rd Edition, 1941.

(9) A. S. Skapski, *J. Chem. Phys.*, **16**, 386 (1948).

(10) O. R. Quayle, *Chem. Rev.*, **53**, 439 (1953).

the Chemical Rubber Handbook, and from Lange's Handbook. The values of σA and $d\gamma/dT$ are tabulated in the Appendix.[11] The frequency distribution of values of A are shown in Fig. 1, for the various compounds divided into three classes.

Figure 1a appear to have two fairly well developed peaks. Examination of the data showed that the non-hydrocarbon liquids accounted for about half of the peak to the left, and contribute nearly nothing to the peak to the right. This indicates the possibility that the non-polar non-hydrocarbon liquids are part of a different population from the hydrocarbons. However, the sample is rather small and the dispersion of the data is large; also, there is the fact that at the low temperatures employed for non-hydrocarbon liquids such as He, Ne, A, O_2, there is a larger chance for experimental error. Besides, over the range of below 100 to 293°K., there might actually be an appreciable effect of temperature on the "normal" surface entropy.

Figure 1b, for the non-hydrogen bonded polar compounds, shows some skewedness to the left; this is due (as will be discussed below) to the inclusion of the aliphatic nitriles, nitro compounds and aldehydes. When these are excluded, the distribution curve at the left is lowered to the level indicated by the dotted line; the distribution curve is then seen to be much more symmetrical.

It seems reasonable, from the overlapping of the distributions in 1a and 1b, to combine groups (a) and (b) to obtain the "normal" surface entropy. The mean for group (a) is 24.4 joules; for group (b) it is 23.8; and the lumped mean is 24.0. We can conclude that there is a "normal" range of surface entropy for non-hydrogen bonding liquids, and use the lumped mean of 24.0. Substances with surface entropy below 18 or 20 (as is evident from the graphs) can be taken as probably belonging to a separate population; and when a whole class (based on molecular structure) falls below 20, then there is a very high probability that the populations are distinct. The "normal" range corresponds to 5 to 7 cal./degree or 2.5 to 3.5 times R; the mean falls at $2.9R$ or 5.75 cal./degree.

The strongly hydrogen bonding compounds then clearly form a separate class. No significance can be attached to the mean of the strongly hydrogen bonding liquids, because there is a very strong trend toward increasing $A\sigma$ (as calculated by equation 1) with increasing molecular weight in homologous series. This trend is probably the result of the extreme orientation (to be discussed below), which leads to incipient breakdown of the relation $A \propto V^{2/3}$ (changing over toward A = constant) at lower chain lengths for hydrogen bonding compounds than for non-polar molecules. Thus the molar surface area of n-butane should be considerably larger than that of n-propyl alcohol.

This tendency to orientation of the alkyl chain can be minimized by considering the lowest members of the series, as in Table I.

(11) The appendix has been deposited as Document No. 5085 with the ADI Auxiliary Publications Project, Photo-duplication Service, Library of Congress, Washington, D. C. A copy may be secured by citing the Document number and remitting in advance $1.25 for photoprints or $1.25 for microfilm, by check or money order payable to: Chief, Photo-duplication Service, Library of Congress.
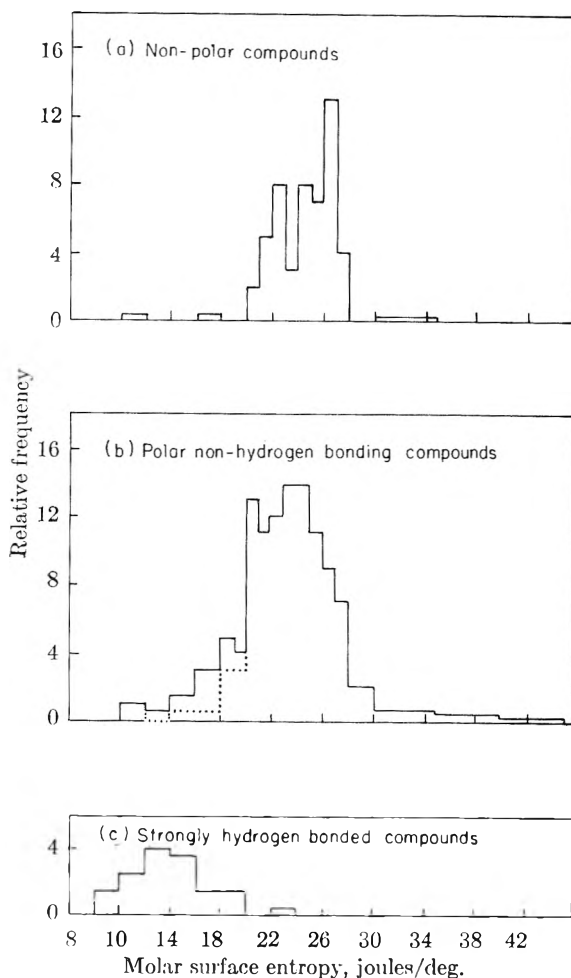

Fig. 1.

TABLE I

Substance	$-d\gamma/dT$, 20°	$A\sigma$, joules
Water	0.145	9.8
Formic acid	.108	11.3
Methanol	.096	10.0
Formamide	.084	9.1
Methyl amine	.099	10.8
Hydrogen cyanide	.125	13.5
Mean		10.8

The difference, $24.0 - 10.8 = 13.2$ joules, or 3.15 cal., may be accounted for by considering the effect of surface orientation. Energetically, the configuration of a molecule such as water or methanol in which a hydrogen sticks up out of the surface should be higher than that in which a hydrogen is directed into the liquid, by the energy of one hydrogen bond. This energy is about 4 to 7 kcal. per mole[12] for systems such as O–H—O, N–H—N, etc. The thermal energy, RT, is only about 10% of the hydrogen bond energy. Hence one would expect that thermal agitation should be too small to lead to an appreciable proportion of the hydrogens to be pointing outwards, at any time. If the surface layer is completely oriented, it would be very surprising if the second layer were not at least par-

(12) C. A. Coulson, "Valence," Oxford University Press, London, 1952.

tially oriented, and indeed if there were not still some orientation in the third layer.[13]

In the interior of a polar liquid, for every possible orientation of a given molecule there will be on the average one other molecule in exactly the opposite orientation. In the surface, for each molecule in a particular orientation, there is no molecule in the opposite orientation.[14] Hence on bringing a molecule from the interior to the surface, just half the possible orientation is lost. If the oriented surface layer is just one molecule deep, there should be a deficit of entropy, given by R times the logarithm of the ratio of the number of configurations in the surface to that in the interior.

$$\Delta S = -R \ln 2 = -5.8 \text{ joules/deg./mole} \quad (2)$$

If the completely oriented region is two molecules deep (and below that level, chaos is complete), then the deficit of entropy, when calculated with respect to a mole of molecules in a layer *one* molecule deep, should be twice the quantity. Actually there will of course be a gradation of order, from oriented outermost layer to disordered interior; but this method will give the correct order of magnitude for the number of layers, n, in which the orientation is important

$$\Delta S \simeq -nR \ln 2 \quad (3)$$

This very crude equation has the advantage that it yields qualitative information very easily.

It may be seen that the 13.2 joule deficit in entropy, for the compounds in Table I below the mean for those in Fig. 1a combined with 1b, corresponds to the value 2.3 for n. Hence the molecules in the surface layer for these strongly hydrogen bonded substances are probably completely oriented, the second layer is largely oriented, and there is at least some orientation in the third layer.

The surface entropy of water increases from 9.0 joules/deg. at 0° to 12.6 at 100°. Other liquids such as methanol and acetic acid show similar increases. (This is as opposed to almost all "normal" liquids, which have surface entropy nearly independent of temperature.) Hence the deficit of entropy, which is attributed to surface orientation, ranges from 15.0 joules at 0° down to 11.6 at 100°. This variation is now easily understood, in terms of the destruction of orientational order in the third and second layers below the surface, with increasing thermal agitation.

There are four cases where surface orientation due to hydrogen bonding might be expected, but apparently is absent. These are the tertiary alcohols (σA ranging from 19.6 to 22.2, mean = 20.8), the secondary, tertiary and aromatic amines, (σA ranging from 18.7 to 26.1), the mercaptans (σA ranging from 19.0 to 22.5, mean = 21.9), and ammonia[15] ($\sigma A = 26.9$). In the *t*-alcohols, the effect may be blamed on steric hindrance to hydrogen bonding, particularly bonding in chains of more than two molecules. A similar explanation can probably be given for the amines. It is not so clear, however, why the surface entropy of aniline

and *o*-toluidine should be so high, 23.2 and 24.2 joules/deg., respectively. Other ring compounds also have high surface entropies in contrast to the low values for aliphatic members of the series, see Table II.

TABLE II

	$-d\gamma/dT$	σA
Cyclopentanol	0.077	14.5
Cyclohexanol	.109	22.6
Phenol	.105	19.3
o-Hydroxybenzaldehyde	.133	27.4
m-Hydroxybenzaldehyde	.116	24.5 (130°)
p-Hydroxybenzaldehyde	.077	16.3 (120°)
Benzaldehyde	.114	23.0

The obvious suggestion of steric hindrance seems inadequate to explain why *both* phenol and cyclohexanol should have so much higher surface entropy than cyclopentanol. The hydroxybenzaldehydes form an interesting series. The ortho compound is internally hydrogen bonded[16] and hence should not orient. The *meta* isomer forms intermolecular hydrogen bonds, but because of its angular structure probably does not form chains very well. It should orient, and its surface entropy actually is a little lower than that of the ortho compound (though this might be an effect of temperature.) *p*-Hydroxbenzaldehyde should have a very strong tendency to form chains, and hence should exhibit orientation to a depth of two or more layers. The deficit of 11.1 joules/deg. below the *o*-isomer is in agreement with this prediction. This series, then, points to a possible explanation for the high surface entropy of substances such as phenol and aniline: as with the *t*-alcohols, the formation of hydrogen bonded *chains*, starting with a surface molecule, is somehow hindered, either sterically or in terms of availability of the necessary electronic structures in the hydrogen bonding groups.

The high surface entropy of ammonia was at first surprising. However, consideration of the "inversion vibration"[17] and of the fact that having only one electron donor site, ammonia can form only two hydrogen bonds per molecule on the average, leads to the conclusion that there should be no *net* orientation in the surface. The observed value of $A\sigma$ is well within the "normal" range.

The aliphatic nitriles form a group about which, from the low surface entropies, one would conclude that surface orientation exists. The values for σA range from 17.1 to 17.5 for three mononitriles, and down to 12.3 for dinitriles. (The aromatic nitriles have values of σA in the range of 22 joules and above, indicating that they are "normal" compounds, showing no orientation.)

The treatments of Coulson[12] and of Schneider[18] lead to the conclusion that the lone pair of electrons on the nitrile N is largely responsible for the dipole moment of 3.4 D. This means that the dipole is in a singularly exposed position. Two possibilities then exist: dipole-dipole interaction, and hydrogen bonding involving the α-methyl hydro-

(13) J. C. Henniker, *Rev. Mod. Phys.*, **21**, 322 (1949).

(14) This does not necessarily mean that all surface molecules are considered oriented *normal* to the surface.

(15) Data of γ vs. T from R. A. Stairs and M. J. Sienko, *J. Am. Chem. Soc.*, **78**, 920 (1956).

(16) L. Pauling, "The Nature of the Chemical Bond," 2nd Ed., Cornell University Press, Ithaca, N. Y., 1940.

(17) W. Gordy, W. V. Smith and R. F. Trambarulo, "Microwave Spectroscopy," John Wiley and Sons, New York, N. Y., 1953.

(18) W. G. Schneider, *J. Chem. Phys.*, **23**, 26 (1955).

gens. The former should lead to a very high inter-action energy on account of the possibility of close approach of the "exposed" dipoles on neighboring molecules to each other. The latter should also be considered very possible in view of the similarity of the "lone-pair" dipole in nitriles to that in water or ammonia.[18] In either case, the CN group should be directed away from the surface. The C–H—N bond energy of HCN is about 3 to 4 kcal.[15,19] In ali-phatic nitriles, the α-hydrogens may well be polar-ized sufficiently to take part in hydrogen bonding, just as the H is in $CHCl_3$ as shown by the complex formation of chloroform with acetone.[19] The very low surface entropy of malononitrile, 12.3 joules, tends to confirm this view, since the hydrogens on the central carbon should be more strongly polar-ized than those in mononitriles, and hence hydrogen bonding should be stronger. We have been unable to find any reference in the literature to this type of hydrogen bonding in nitriles. Hence, it may be sug-gested that independent evidence for or against such hydrogen bonding should be sought.

A similar argument may be made to explain the low surface entropy of the aliphatic nitro com-pounds (mean = 17.25), and also that of acetalde-hyde, for which σA = 16.4. Actually, for the latter compound a dimer structure has been re-ported,[12,20] with a C–H---O bond energy of 2.6 kcal. (The surface entropy of the ketones, for which this kind of hydrogen bonding is impossible, is normal—mean = 22.5.) We may conclude that the aliphatic nitriles and nitro compounds, and probably also the aliphatic aldehydes, show surface orientation, and that such orientation is very possibly the result of hydrogen bonding. Hence the elimination of these compounds from the group of Graph 1b is justified.

Conclusions

The hypothesis of surface orientation in strongly hydrogen bonded liquids appears to be well justi-fied, both energetically and as an explanation for the low surface entropy of these liquids, as com-pared to "normal" polar and non-polar liquids.

Acknowledgment.—The author wishes to thank Mr. John McAndrews for assistance in calculation of the molar entropies, and Dr. Hans Jaffe for dis-cussion of the nature of hydrogen bonds.

(19) J. H. Hildebrand and R. L. Scott, "Solubility of Non-Electro-lytes," 3rd ed., Reinhold Publ. Co., New York, N. Y., 1950.

(20) E. A. Alexander and J. D. Lambert, *Trans. Faraday Soc.*, **37**, 421 (1941).

KINETICS OF THE REACTION BETWEEN SILVER AND SULFUR IN THE SOLID STATE[1]

By William F. Riemen[2]

Contribution from the Department of Chemistry, University of Wisconsin, Madison, Wisconsin

Reactions in the solid state have been reported from this Laboratory.[3,4] The reaction between

(1) More details are available in a portion of a Ph.D. thesis by W. P. Riemen filed in the Library of the University of Wisconsin, 1955.

(2) U. S. Rubber Company, Passaic, New Jersey.

(3) H. F. Mason, Ph.D. Thesis, University of Wisconsin, 1954. This Journal, **61**, 796 (1957).
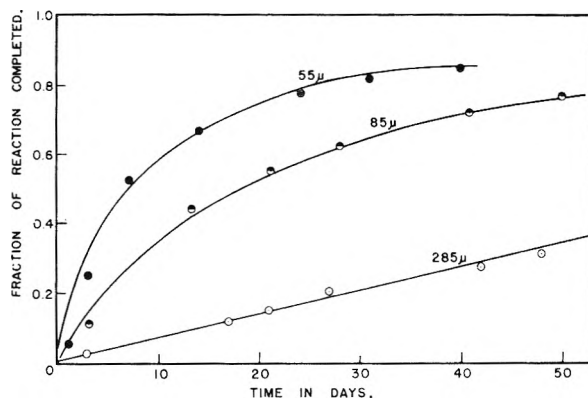

Fig. 1.—Fraction of reaction completed *versus* time, for reaction $2Ag + S \rightarrow Ag_2S$ at 25°.

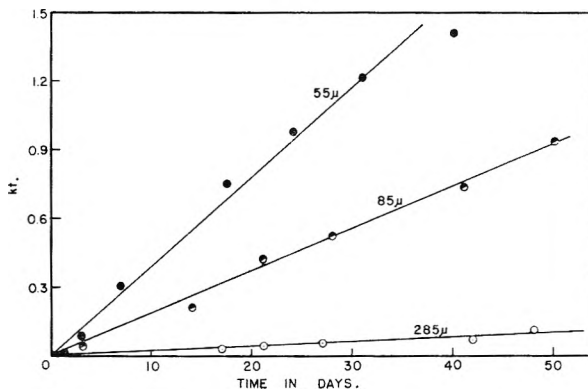Fig. 2.—Rate constant k multiplied by time *versus* time, for reaction $2Ag + S \rightarrow Ag_2S$ at 25°.
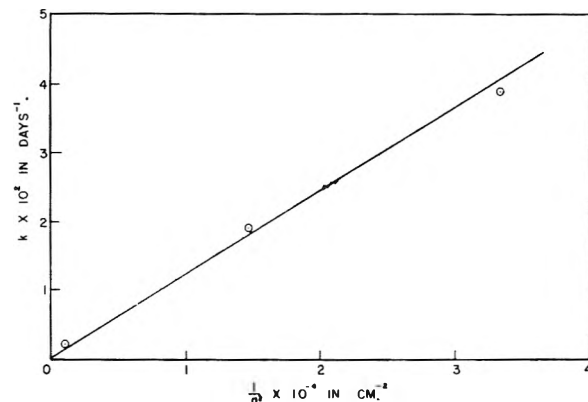

Fig. 3.—Rate constant k *versus* reciprocal of square of particle radius for reaction $2Ag + S \rightarrow Ag_2S$.

silver and sulfur is an excellent solid reaction to study because it proceeds with measurable velocity at room temperature and it can be followed readily by dissolving out the unreacted sulfur with carbon disulfide. It has been studied before.[5-8] Fur-ther research is reported here because the measure-ments fit a kinetic formula[1,3,4] and they bring out quantitatively the influence of particle size on re-action velocity.

The silver was precipitated from silver nitrate with cop-per, washed thoroughly, and dried at 200° for an hour.

(4) W. P. Riemen and F. Daniels, *ibid.*, **61**, 802 (1957).

(5) K. Fischbeck, *Z. anorg. Chem.*, **165**, 55 (1927).

(6) F. Hohn, *ibid.*, **99**, 118 (1917).

(7) J. Smith, *Bull. soc. chim.*, **7**, 706 (1940).

(8) F. Taradoire, *Bull. soc. chim. France*, **147**, 623 (1932).

The sulfur was prepared by melting flowers of sulfur, cooling and grinding the crystals in a mullite mortar. Both sulfur and silver were sieved to give uniform sizes.

2.1576 grams of silver powder was thoroughly mixed with 0.3206 g. of sulfur powder of the same size placed in weighed sintered glass-bottom crucibles at 25° for periods of time ranging from 1 to 50 days. At suitable time intervals a crucible was extracted five times with about 10 ml. of fresh carbon disulfide and the loss in weight gave the amount of sulfur still unreacted.

Experiments were also carried out in which the powders were pressed into pellets under pressure of 3 tons per sq. inch, as in the experiments of Fischbeck.[5] There was no significant difference in reaction rate between the pressed and unpressed powders and the act of compression gave no appreciable reaction. This lack of action on compression was unexpected because preliminary work on KBr and AgNO$_3$ indicated that compression under high pressures does bring about some reaction.

The data on the reaction between silver and sulfur at 25° are given in Fig. 1.

These data fit well the rate equation for solids, based on diffusion, as derived by Mason[3] and checked by him on NaBr + KCl and CsCl + KBr, and checked by Riemen and Daniels[4] on Ag$_2$SO$_4$ + CaO and SrO. The formula is

$$1 - x = 6/\pi^2 \sum_{n=1}^{\infty} \frac{1}{n^2} \exp(-n^2 kt)$$

x is the fraction of the reaction at time t, D is the diffusivity, a is the radius of particles, and k is the rate constant = $\pi^2 D/a_2$; kt is evaluated from $1 - x$ by I.B.M. calculations.[3]

Figure 2 shows the kt plot against time which permits a calculation of k. For 55 μ particles, k is 0.039 day^{-1}, for 85 μ, k is 0.019 day^{-1} and for 285 μ, k is 0.002 day^{-1}.

Figure 3 shows that the rate constant k is inversely proportional to $1/a^2$ in agreement with the formula.

The author is glad to acknowledge the help of Professor Farrington Daniels with whom this research was carried out and to acknowledge the support of the U. S. Atomic Energy Commission through Contract AT(11-1)-178.

DECOMPOSITION OF HYDROCARBONS BY SILICA–ALUMINA CATALYSTS

BY J. L. FRANKLIN AND D. E. NICHOLSON

Refining Technical and Research Divisions, Humble Oil and Refining Company, Baytown, Texas

Received October 1, 1956

The kinetics of the catalytic decomposition of eight low molecular weight hydrocarbons have been reported previously.[1] It was found that the eight hydrocarbons studied could be divided into two groups kinetically, depending on whether rates of disappearance of starting material obeyed a first-order or a 1.5-order law. Some recent studies have shown that the activation energy for cracking of 2-methylpropane remained constant, within experimental accuracy, as the specific surface of the catalyst was systematically varied from 303 to 81 sq. m. by heat and steam sintering. These data are recorded in Table I.

(1) J. L. Franklin and D. E. Nicholson, THIS JOURNAL, **60**, 59 (1956).

TABLE I

Catalyst surface area, m.²/g.	Pore vol., ml./g.	ΔE^*, kcal./mole
81	0.423	30.7
122	.477	31.5
224	.507	29.8
303	.515	30.0

The experimental procedure for making the rate measurements was described previously. On the basis of the data cited above, the average activation energy for the decomposition of 2-methylpropane on the different catalysts is 30.5 ± 0.6 kcal./mole.

An error was made in the calculation of the activation energy for disappearance of 2-methylpropane as originally presented ($\Delta E^* = 37.1$ kcal./mole) for the catalyst having specific surface of 81 sq. m. Thus the active centers on the silica-alumina catalysts of the investigation are shown to be quite similar in nature.

It may be noted that a linear relationship exists between the logarithm of the frequency factor (expressed per unit surface area) and the activation energy for decomposition of all of the hydrocarbons obeying first-order kinetics. Such a relationship has been reported before in catalysis.[2]

(2) D. A. Dowden, *Research*, **1**, 239 (1948).

NOTE ON THE CALCULATION OF THE MOLECULAR WEIGHT DISTRIBUTION OF A LINEAR AMORPHOUS POLYMER FROM ITS RELAXATION DISTRIBUTION IN THE RUBBERY REGION

BY HIROSHI FUJITA AND KAZUHIKO NINOMIYA

Physical Chemistry Laboratory, Department of Fisheries, University of Kyoto, Maizuru, Japan

Received October 5, 1956

In a recent article[1] (hereafter referred to as Paper I) a method was presented by means of which the distribution of molecular weights in a linear amorphous polymer may be predicted from relaxation spectrum data obtained over the time-scale of rubbery consistency. Stress–relaxation data on polyvinyl acetate[2] and on polystyrene[1] from this Laboratory were analyzed in terms of this method, with results in both cases which compared quite favorably with the observed data. No essential difficulty which would violate the basic assumptions of the theory was found in those applications, except for an apparent anomaly which appeared in the low molecular weight regions of the calculated molecular weight distributions. Since very extensive viscoelastic data recently have become available[3] on a sample of high molecular weight polyisobutylene distributed by the National Bureau of Standards for an international coöperative program of dynamic tests, it seemed of interest to use those data as a basis for the calculation of the molecular weight distribution, even though no experimental check of the results is possible. It was found through this calculation that

(1) H. Fujita and K. Ninomiya, *J. Polymer Sci.*, in press.
(2) K. Ninomiya and H. Fujita, *J. Colloid Sci.*, in press.
(3) A. V. Tobolsky and E. Catsiff, *ibid.*, **10**, 375 (1955).

some of the assumptions made in Paper I are no longer applicable for viscoelastic data of the type employed; some improvement must be made to make the method more generally usable. The present communication describes the results of this calculation.

Tobolsky and Catsiff[3] have presented recently in great detail their own stress–relaxation data, along with Philippoff's unpublished dynamic mechanical data, on this NBS (National Bureau of Standards) polyisobutylene sample at 25° over an extremely wide range of time-scale. The relaxation spectrum at 25°, $\Phi(\log \tau)$, derived from those data by making use of the Ferry–Williams second approximation method,[4,5] is graphically shown in Fig. 1 on a log-log plot. In the region where both transient and dynamic property data are recorded, the calculation was effected using the latter because of the greater accuracy of Φ values derived therefrom. From this relaxation spectrum the steady-flow viscosity η at 25° is calculated to be 1.8 $\times 10^{11}$ poises.

In order to calculate the molecular weight distribution from a given relaxation spectrum, it is necessary to evaluate parameters $\bar{E}$, M_c and k for the given system. We assume for $\bar{E}$, the quasi-static modulus of elasticity appearing in the initial part of the rubbery region, a value of 1.0 $\times 10^7$ dynes/cm.² from Philippoff's data for the real part of the complex dynamic modulus.[3] This same value of $\bar{E}$ was previously adopted by Ferry and colleagues,[6] who compared their extended Rouse theory of viscoelastic behavior with the data of the NBS polyisobutylene herein concerned. Tobolsky and Catsiff have provided a value 7.6 $\times 10^6$ dynes/cm.² for this quantity. This, however, seems to be a slight underestimate for the purpose of this calculation. From the viscosity data reported by Fox and Flory,[7] M_c, the critical molecular weight in the viscosity vs. molecular weight relation may be taken as 1.7 $\times 10^4$ for undiluted "solid" polyisobutylene, as proposed by Fox and Loshaek.[8] It was hoped that this value could be used successfully for the calculation concerned. However, preliminary calculation showed that this M_c value leads to a molecular weight distribution which is too narrow to be likely for an unfractionated linear polymer of very high molecular weight. Fox and Loshaek[8] have derived a relation $v_2 M_c \approx 4 \times 10^4$ for concentrated solutions of polyisobutylene from Johnson, et al.'s viscosity data[9] in xylene. Here v_2 is the volume fraction of the polymer in a given solution. Assuming that this equation may be extrapolated to the undiluted state, a value of 4 $\times 10^4$ is obtained for M_c of solid polyisobutylene. The large difference from the value of Fox and Flory may be attributed to the drastic extrapolation of the above relation to zero diluent concentration. However, it is of interest to note that any M_c
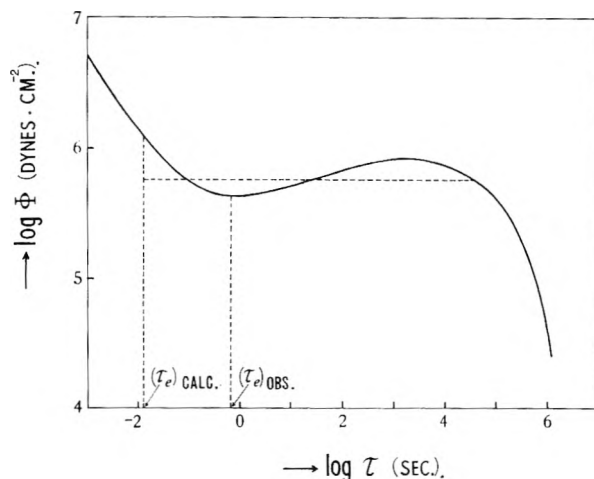

Fig. 1.—Distribution of mechanical relaxation times of the NBS sample of polyisobutylene at 25°: solid line, calculated from both Tobolsky–Catsiff's relaxation data and Philippoff's data for the imaginary part of the complex dynamic modulus; dashed horizontal line, substituted fictitious one.

value, ranging from about 1.5 $\times 10^4$ to 3.0 $\times 10^4$, may be derived from Fox–Flory's original viscosity plot (Fig. 8 of ref. 7), depending on how one draws the straight lines through the experimental points therein shown. It thus appears reasonable to regard M_c as an empirical parameter, rather than to define it rigidly as the point at which a log-log plot of the viscosity–molecular weight relation exhibits a break. It should be noted that this arbitrariness in the evaluation of M_c makes the present method only a purely empirical one, although it does not violate the mathematical framework of the theory. In what follows, M_c for solid polyisobutylene is assumed rather arbitrarily as 3.5 $\times 10^4$. The validity of this value must, of course, be checked by comparing the resulting molecular weight distribution with experimental data.

As has been shown in Paper I, k can be obtained with sufficient accuracy, provided the viscosity η at the given temperature and the z-average molecular weight of the sample are known. The value of η can be calculated from the relaxation spectrum, and has been noted above. No published value of $\bar{M}_z$ of the NBS polyisobutylene is available to us, and so we tentatively evaluate it from the reported weight-average molecular weight $\bar{M}_w$ (1.56 $\times 10^6$),[10] assuming for the molecular weight distribution in question a "most probable" shape; i.e., it is assumed that $\bar{M}_z = 1.5\bar{M}_w$. The required k value is then computed from the equation $\eta = k\bar{M}_z$ (eq. 29 in Paper I) to be 4.53 $\times 10^{-11}$.

The thin solid line in Fig. 2 shows the resulting molecular weight distribution, $\varphi(M)$. It is seen that the curve goes down to the negative side in the region of molecular weights below about 6 $\times 10^5$, a behavior in contradiction with physical reality. It is readily found by following the process of calculation described in Paper I that anomaly is associated with the positive slope of the relaxation spectrum in the corresponding region on the time-scale axis. The dashed line portion of the $\varphi(M)$ curve has been drawn arbitrarily, considering the

(4) J. D. Ferry and M. L. Williams, J. Coll. Sci., **7**, 347 (1952).

(5) M. L. Williams and J. D. Ferry, J. Polymer Sci., **11**, 169 (1953).

(6) J. D. Ferry, R. F. Landel and M. L. Williams, J. Applied Phys., **26**, 359 (1955).

(7) T. G. Fox, Jr., and P. J. Flory, THIS JOURNAL, **55**, 221 (1951).

(8) T. G. Fox and S. Loshaek, J. Applied Phys., **26**, 1080 (1955).

(9) M. F. Johnson, W. W. Evans, I. Jordan and J. D. Ferry, J. Colloid Sci., **7**, 498 (1952).

(10) R. S. Marvin, Proc. 2nd Internatl. Congress Rheology, Oxford 1953, p. 156.
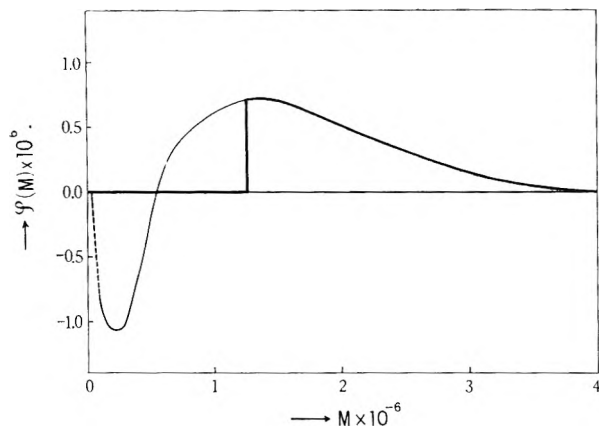
Fig. 2.—Calculated molecular weight distribution $\varphi(M)$ of the NBS sample of polyisobutylene: thin solid line, original distribution; thick solid line, modified fictitious distribution.

fact that in the corresponding region of the relaxation spectrum the effect of the transition region is apparently overlapping. This point will be discussed in detail elsewhere. The area enclosed by the $\varphi\ (M)$ curve is 0.99, indicating that the normalization condition is practically satisfied. That the calculated molecular weight distribution exhibits a negative portion doubtless implies that some of the assumptions and approximations underlying the method are either invalid or not of general applicability. By either modifying or discarding them, the method must now be improved so that it may be applicable to any relaxation spectra such as would be obtained for actual systems.

In Paper I it was assumed that the relaxation spectrum of a monodisperse fraction in the rubbery region be approximated by a "box-type" function with a lower boundary τ_e independent of molecular weight. As has been shown above, superposition of such a function, multiplied by the molecular weight distribution $\varphi\ (M)$ in the form of eq. 2 of Paper I, is not capable of representing any curve having a positive slope, without violating the physical requirement that $\varphi\ (M)$ must be positive or zero for any positive M. This fact suggests two ways for improving the method in the desired direction. One is to replace the "box" for the relaxation spectrum of a monodisperse fraction by another shape, keeping its lower boundary τ_e independent of M, and the other is to retain the box approximation in its present form but with τ_e as a parameter which depends on M. One of the present authors (K. N.) has investigated the first alternative, assuming a rectangular triangle-shaped relaxation spectrum for the monodisperse fraction, and has found that the aforementioned anomaly can be eliminated if appropriate values are assigned to the parameters involved. However, his calculation fails, for the cases of polyvinyl acetate and polystyrene, to yield as favorable results as those found in Paper I with the box approximation. The details of the calculation will be published elsewhere.[11]

In accordance with the theory described in Paper

I, the time-scale corresponding to the boundary between the transition and the rubbery region should be close to the value given by the equation

$$\tau_e = kM_c{}^{1.4}/\bar{E} \qquad (1)$$

and, as a matter of fact, it can be observed from the data of Paper I that this prediction holds with reasonable accuracy for both polyvinyl acetate and polystyrene. The τ_e calculated for the NBS polyisobutylene, using the k, M_c and $\bar{E}$ values obtained above, is 1.28×10^{-2} sec. This, however, is about one-fiftieth as large as the value estimated from the point at which the relaxation spectrum of Fig. 1 passes through a minimum. This enormous difference of the predicted from the actual value may be ascribed to a variety of reasons. One of the most probable interpretations would be in terms of the variation of τ_e with molecular weight. It is shown readily that, if the restriction that τ_e is independent of molecular weight is removed, the superposition of box functions in the form of eq. 2 of Paper I can represent relaxation spectra of any shape without introducing the anomaly that the calculated $\varphi\ (M)$ becomes negative for some values of M. The fact that the calculated τ_e from eq. 1 differs largely from the value estimated from the dip between the "wedge" and "box" spectra may also be interpreted in terms of the model of McLoughlin and Tobolsky[12] for relaxation spectra of linear amorphous polymers. According to their model, τ_e in our model should approximate the long-time boundary of the wedge spectrum associated with the glass-transition region, and may not be identified (as assumed in the present treatment) with the short-time boundary, τ_3 (in their designation), of the box spectrum associated with the rubbery region. In general, τ_e is apparently independent of molecular weight, while τ_3 increases with increasing molecular weight. For medium- and low-molecular weight polymers, the box and wedge spectra overlap. Since the latter then predominates, τ_3 becomes unrecognizable; it appears that in such cases we may identify τ_3 with τ_e with a reasonable approximation. For high enough molecular weight polymers this approximation may not be valid. It is probable that this effect is responsible for the large difference of the calculated τ_e from the actual value as found for the NBS polyisobutylene. As far as the present authors are aware, the NBS polyisobutylene is the only unfractionated polymer sample which exhibits a relaxation spectrum having a positive slope in the rubbery region; all other published relaxation spectra in the rubbery region of a variety of unfractionated linear amorphous polymers, both in solid and in concentrated solutions, have exclusively negative (or zero) slopes, increasing in absolute value with increasing relaxation time.

The thick solid line in Fig. 2 represents a fictitious molecular weight distribution obtained by subtracting from the lower molecular weight side of the positive part of the calculated $\varphi\ (M)$ curve the area equal to that of its negative portion. This molecular weight distribution is equivalent to that

(11) K. Ninomiya, J. Chem. Soc. Japan (Ind. Chem. Sect.) (to be published).

(12) J. R. McLoughlin and A. V. Tobolsky, J. Polymer Sci., 8, 543 (1952). The authors wish to thank Referee III for calling attention to this paper.

which can be obtained directly by replacing the positive slope part of the actual relaxation spectrum by a horizontal line, as shown in Fig. 1 by a dashed line, in a such a manner that the substituted relaxation spectrum yields an elastic modulus (when calculated in terms of Alfrey's approximation[1]) equal to the assumed value of $\bar{E}$ at a time-scale corresponding to τ_e calculated from eq. 1. The viscosity-average $(\bar{M}_v)$, weight-average $(\bar{M}_w)$, and z-average $(\bar{M}_z)$ molecular weights calculated from this fictitious distribution are 1.51 $\times$ 10^6, 1.73 $\times$ 10^6, and 2.18 $\times$ 10^6, respectively.[13] The first two may be compared with the experimental values, $\bar{M}_v = 1.35 \times 10^6$ and $\bar{M}_w = 1.56 \times 10^6$. The rather reasonable agreement suggests that the over-all spread and the shape in the higher molecular weight portion of the calculated molecular weight distribution are not very far from the truth.

(13) In the calculation of $\bar{M}_v$, α in the equation $[\eta] \propto M^\alpha$ was assumed as 0.64 from eq. 1 of ref. 7.

X-RAY DIFFRACTION STUDY OF THE POLYVINYL ALCOHOL–IODINE SYSTEM

By Masao Haisa and Hiroharu Itami

Contribution from the Department of Chemistry, Faculty of Science, Okayama University, Okayama, Japan

Received November 22, 1956

Numerous publications describe the formation of polyiodine chains in the hydrophilic organic polymers.[1–3] The polyvinyl alcohol–iodine system is of great interest because of the additional information on the structure of high polymers and also because of its practical implication. At present, however, it is uncertain whether the iodine molecules can be introduced into the crystalline region or into the amorphous region. In this connection we present the results of the X-ray diffraction study on the correlation between the stretching orientation of the crystallites in the polyvinyl alcohol film and the configuration of iodine molecules absorbed in it.

Experimental

Both polyvinyl alcohol and polyvinyl alcohol–iodine systems were examined in the form of films about 0.1 cm. thick. A sample of the polyvinyl alcohol–iodine system was prepared by steeping the film of polyvinyl alcohol in a potassium iodide solution of iodine.

The X-ray beam of Ni-filtered copper radiation with a wave length of 1.54 Å. from a rotating-anode tube was passed perpendicular to the stretched direction of the film. The angle of oscillation was 20°. The diffraction pattern was registered on a flat film placed at a distance of 3.663 cm. from the specimen. Accurate values for the relative intensities and for the interplanar spacings of the reflections were estimated from the photometric densitometer curves of the corrected coherent scattering. In this calculation the assumption was made that the corrected densitometer curve in the vicinity of the diffraction maxima can be fitted to a Gaussian curve.

Results and Discussion

Unstretched Films.—The reflections given by the unstretched polyvinyl alcohol and polyvinyl alcohol–iodine films were visually poorly resolved

(1) R. E. Rundle. J. Am. Chem. Soc., 69, 1769 (1947).
(2) H. V. Dietrich and F. Cramer, Ber., 87, 806 (1954).
(3) C. D. West, J. Chem. Phys., 15, 689 (1947).

and were very similar to each other. No significant difference could be detected between different preparations of the same materials. The intensities of the independent coherent scattering on the equator for the unstretched films are shown in Fig. 1.
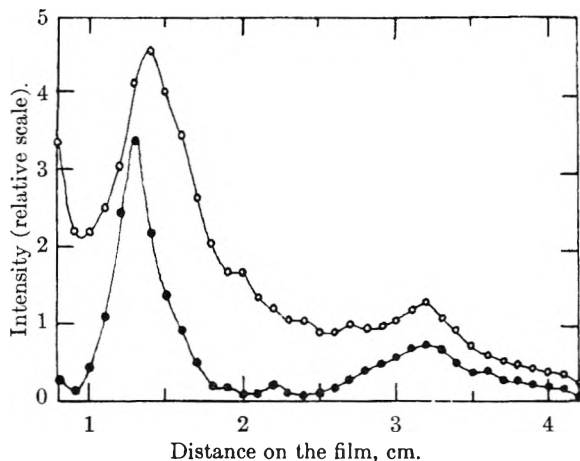

Fig. 1.—Equatorial spectra of the unstretched films of polyvinyl alcohol (-●-) and polyvinyl alcohol–iodine (-○-).

The results presented in Fig. 1 indicate that the reflections of the patterns appear alike in both position and relative intensity. Hence the absorbed iodine in the polyvinyl alcohol film did not modify the original structure of crystallites of polyvinyl alcohol and thus penetration into the interior of the crystallites seems entirely unlikely.

It is interesting, moreover, that the liquid halo corresponding approximately to the spacing of 3.5 Å. for the polyvinyl alcohol–iodine film is considerably more intense than those for the untreated polyvinyl alcohol film. The variation in the intensity of this halo seemed to accompany a change in the iodine content absorbed. Since the (111), (200) and (112) reflections due to the crystal of the orthorhombic iodine[4] could not be satisfactorily resolved owing to their marked broadening, the iodine molecules absorbed appeared to enter the amorphous regions in the form of the crystallites whose sizes average about 50 Å. at most. This interpretation supports the electron-microscopic findings, by Hess and Mahl.[5]

Stretched Films.—Excepting the characteristic reflection due to the addition of iodine, the X-ray patterns of the films with and without iodine at various degrees of stretching were much alike as in the case of the unstretched films. The agreement with the estimates of the position and intensity of the reflections from the polyvinyl alcohol reported by Mooney[6] and others[7] was satisfactory. The identity period 2.52 Å. along the stretching direction is identical with the fiber period and hence suggestive of Natta's isotactic configuration[8] of the polyvinyl alcohol chain. The abnormal reflections found out for the stretching of denatured egg al-

(4) P. M. Harris, E. Mack and F. C. Blake, J. Am. Chem. Soc., 50, 1583 (1928).
(5) K. Hess and H. Mahl, Naturwis., 41, 86 (1954).
(6) R. C. Mooney, J. Am. Chem. Soc., 63, 2828 (1941).
(7) C. W. Bunn and H. S. Peiser, Nature, 159, 161 (1947), etc.
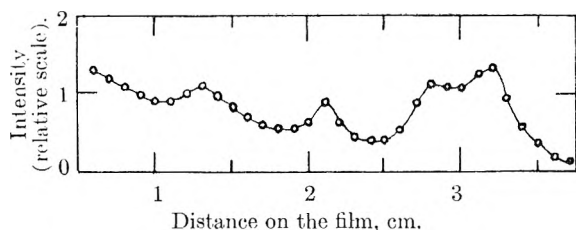(8) G. Natta and P. Corradini, J. Polymer Sci., 20, 251 (1956).

Fig. 2.—Meridional spectrum of the fourfold stretched polyvinyl alcohol–iodine film.

bumin film[9] did not occur in the case of the polyvinyl alcohol film.

At 100% elongation the preferred orientation indicated by arcing of the reflections from the crystallites of polyvinyl alcohol is conspicuous while the characteristic halo reflection caused by the polyiodine chains remains unchanged in one direction. These results would suggest that the molecular orientation does not occur but the hydrogen-bonded polyethylene sheets may be becoming parallel to the direction of elongation. Even at 300% elongation the angle of dispersion of the crystallites round the stretched direction is estimated to be about 15°.

Configuration of Iodine Absorbed.—An important feature of the patterns obtained from the stretched polyvinyl alcohol–iodine film is the appearance of a new meridional reflection corresponding to an identity period of 3.03 ± 0.03 Å. which is spread out laterally with considerable intensity. It is to be noted that the extension of the reflection must arise from the polyiodine chain predominantly, whereas the arcing of the reflections arises from the crystallites of polyvinyl alcohol predominantly. The extensiveness of the former indicates that the interplanar spacings extend from 3.03 to 2.85 Å. while the identity period in the direction of stretching remains constant. The photometric curve of the meridional spectrum of the fourfold stretched polyvinyl alcohol–iodine film is shown in Fig. 2. With the intrinsic broadening of this reflection, moreover, the approximate linear dimension of coherent region can be calculated from the Scherrer expression[10] to be more than 45 ± 10 Å. The hydrogen bonds in the polyvinyl alcohol film are expected to form a dipole field which could permit the intrusion of iodine molecules and then the formation of the polyiodine chain with average length of about 15 atoms of iodine. Under parallel conditions the absorption band of 500 mμ of iodine is shifted to 590 mμ in soluble starch,[11] and to 610 mμ in polyvinyl alcohol.[12] The results of the present work are consistent with these implications and indicate that the length of the polyiodine chain occurring in the polyvinyl alcohol film is of the same order of magnitude as that in the soluble starch.

Thus, we are presently inclined toward the view that the iodine molecules intrude into the amorphous regions between the crystallites of the poly-

vinyl alcohol and are presumed to be oriented by the dipole field to form the polyiodine chains made up of more than 15 atoms of iodine when the film is stretched.

THE CRITICAL MICELLE CONCENTRATIONS OF DECYL-, DODECYL- AND TETRADECYLAMINE HYDROCHLORIDE

By Horst W. Hoyer and Ann Greenfield

Contribution from Hunter College, New York 21, N. Y.

Received November 17, 1956

As part of an investigation into the electrophoretic mobility of the micelles of some aliphatic amine hydrochlorides and the relationship of this property to micelle structure it was necessary to determine the concentration at which the single molecules and/or ions associate into micelles. This concentration is generally called the critical micelle concentration, abbreviated CMC. We adopt the definition of Williams, Phillips and Mysels[1] for the CMC as the concentration of solute at which the concentration of micelles would become zero if their concentration were to change at the same rate as it does at a slightly higher concentration. Experimentally this means that we measure an additive property which varies linearly, or approximately linearly, with some function of the concentration of the micelles and which varies in a similar manner but with a different slope for the concentration of the unassociated solute molecules or ions. The method we chose as providing a convenient and precise means for determining the CMC is the conductivity method which depends upon the lower specific conductance of the micelles as compared to the solute ions. For our systems, and over the concentration range studied, the specific conductance was found to vary in a linear manner with the molarity of the solution for both the associated and the simple ions.

Experimental

The decyl-, dodecyl- and tetradecylamines used in these studies have already been described.[2] Solutions were prepared by dilution of a standard sample with either distilled or conductivity water depending upon the precision required. Temperature was controlled to $\pm 0.01°$ in a water thermostat. The a.c. Wheatstone bridge, constructed from a Kohlrausch 450 cm. slide wire, an oscilloscope null point detector, L & N standard resistances, a Wagner earthing circuit and a 1000 cycle oscillator, was tested against Bureau of Standards resistors. Measurements were taken at 25.0° for solutions of decyl-, dodecyl- and tetradecylamine which had been neutralized by an equivalent amount of hydrochloric acid as determined by potentiometric titration, and at 18.0 and 35.0° on similar solutions of dodecylamine. Cell constants were redetermined at each temperature. The results are summarized in Table I.

These results may be compared with those of Corrin and Harkins[3] who used a dye adsorption method which gave a value of 0.0131 mole per liter for the CMC of dodecylamine hydrochloride at 25°. Klevens[4] reports values of 0.040 for the decylamine hydrochloride at 25°, 0.013 for the dodecylamine hydrochloride at 30° and 0.0031 for the tetradecylamine salt at 40°. No results are available for the

(9) W. T. Astbury, S. Dickinson and K. Bailey, *Biochem. J.*, **29**, 2351 (1935).

(10) P. Scherrer, *Göttinger Nachrichten.*, **2**, 98 (1918).

(11) R. R. Baldwin, R. S. Bear and R. E. Rundle, *J. Am. Chem. Soc.*, **66**, 111 (1944).

(12) Y. Hoshino, *J. Electrochem. Soc. Japan*, **18**, 6 (1950).

(1) R. J. Williams, J. N. Phillips and K. J. Mysels, *Trans. Faraday Soc.*, **51**, 728 (1955).

(2) H. W. Hoyer and A. Greenfield, This Journal, **61**, 735 (1957).

(3) M. L. Corrin and W. D. Harkins, *J. Am. Chem. Soc.*, **69**, 683 (1947).

(4) H. B. Klevens, This Journal, **52**, 130 (1948).

TABLE I
CRITICAL MICELLE CONCENTRATIONS

Amine hydrochloride	Temp., °C.	CMC, moles/l.
Decyl	25.0	0.0540
Dodecyl	25.0	.0138
Tetradecyl	25.0	.0028
Dodecyl	18.0	.0145
Dodecyl	25.0	.0138
Dodecyl	35.0	.0133

temperature variations of the CMC of the aliphatic amine salts reported upon in this paper although the work of Klevens[4] and of Wright, Abbott, Sivertz and Tartar[5] shows that there is a slight increase in the CMC with rising temperatures for some alkyl sulfate, sulfonate and fatty acid salts. However, the effect of temperature upon the CMC of the alkyl sulfate is still in dispute since Flockhart and Ubbelohde[6] have reported recently that the CMC of sodium dodecyl sulfate is a minimum at 30°. Our results indicate a decrease of about 5.5% for the CMC of dodecylamine hydrochloride in the temperature range 18 to 35°.

Acknowledgment.—The authors gratefully acknowledge financial support furnished for this work by the National Science Foundation.

(5) K. A. Wright, A. D. Abbott, V. Sivertz and H. V. Tartar, *J. Am. Chem. Soc.*, **61**, 549 (1939).

(6) B. D. Flockhart and A. R. Ubbelohde, *J. Coll. Sci.*, **8**, 428 (1953).

A NEW METHOD OF DETERMINING THE ORDER OF REACTION AND THE REACTION CONSTANT FROM KINETICS DATA[1]

By Wen-hsuan Chang

Contribution from the Chemistry Department, Northwestern University, Evanston, Illinois

A new method of determining the order of reactions and the reaction constants simpler than previously proposed[2] is presented. This method permits determination of reaction order and any change of order in a chemical reaction without successive approximation. The reaction constant of any fractional order reaction can be calculated by this method as easily as for an integral order reaction. The new method proposed by Weight, et al.,[3] still involves a series of approximations.

Method of Calculating the Order of a Reaction.—If the rate expression of a chemical reaction is nth or pseudo nth order reaction, then

$$-\frac{dC}{dt} = kC^n$$

If m fraction of the reactant C_0 is consumed, then by integration

(1) The author wishes to express his sincere gratitude to Dr. Arthur A. Frost for his stimulating lectures which led to the conception of this idea and his continued guidance in completion of this work. The author is also indebted to Abbott Lab., Research Foundation Co. and Visking Co. for their financial assistance.

(2) A. A. Frost and R. G. Pearson, "Kinetics and Mechanism," John Wiley and Sons, Inc., New York, N. Y., 1953, pp. 14, 23, 40, 44. K. J. Laidler, "Chemical Kinetics," McGraw-Hill Book Co., Inc., New York, N. Y., 1950, p. 13. S. L. Fries and A. Weissberger, "Investigation of Rates and Mechanism of Reactions," Interscience Publishers, Inc., New York, N. Y., 1953, pp. 186–196.

(3) J. H. Weight, J. H. Black and J. Coull, *J. Chem. Educ.*, **33**, 542 (1956). This appeared after the present paper was submitted.
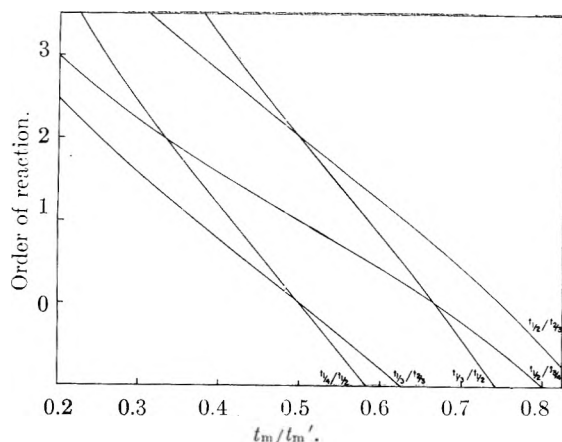
Fig. 1.—Order of reaction *vs.* t_m/t_m'.

$$\frac{1}{n-1}\left[(1-m)^{1-n} - 1\right] = kt_m C_0^{n-1} \qquad (A)$$

If m' fraction of the reactant C_0 is consumed, then by dividing two equations of type (A)

$$\frac{(1-m)^{1-n} - 1}{(1-m')^{1-n} - 1} = \frac{t_m}{t_m'} \qquad (B)$$

When $n = 1$, the equation can be derived

$$\frac{\ln\dfrac{1}{1-m}}{\ln\dfrac{1}{1-m'}} = \frac{t_m}{t_m'} \qquad (C)$$

The values of t_m/t_m' obtained from equations B and C are given in Table I.

TABLE I
VALUES OF t_m/t_m'

| Value of n	$\dfrac{t^{1/2}}{t^{2/3}}$	$\dfrac{t^{1/2}}{t^{3/4}}$	$\dfrac{t^{1/4}}{t^{1/2}}$	$\dfrac{t^{1/3}}{t^{1/2}}$	$\dfrac{t^{1/3}}{t^{2/3}}$
−1.0	0.844	0.800	0.584	0.741	0.625
−0.5	.800	.739	.542	.705	.564
0.0	.750	.667	.500	.667	.500
0.5	.693	.587	.457	.628	.435
1.0	.630	.500	.415	.585	.369
1.5	.566	.414	.374	.543	.307
2.0	.500	.333	.334	.500	.250
2.5	.436	.261	.295	.456	.199
3.0	.375	.200	.269	.417	.156
4.0	.269	.111	.196	.339	.130

From Table I, Fig. 1 can be constructed.

In order to determine the order of reaction, one plots the values of the physical or chemical property measured against the time of measurement. From the smooth curve obtained the values of t_m can be found easily by the following method. Assume λ_0 is the value of the physical or chemical property at the beginning of the reaction; λ_∞ is the value of the same property at the end of the reaction; λ_m is the value of the same property at t_m. Then

$$\lambda_m = m(\lambda_\infty - \lambda_0) + \lambda_0$$

After t_m (where m equals $\frac{1}{2}$, $\frac{1}{3}$, $\frac{1}{4}$, $\frac{2}{3}$, $\frac{3}{4}$) values are found, the values of t_m/t_m' can be calculated. The latter values will give the order of reaction from Fig. 1.

Method of Calculating the Rate Constant of a Chemical Reaction.—It can be shown that the
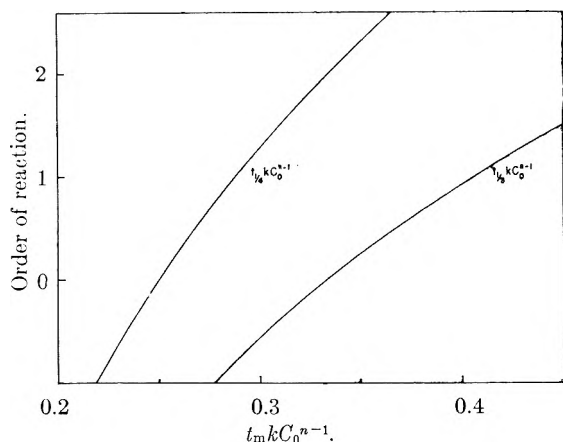
Fig. 2.—Order of reaction vs. $kt_mC_0^{n-1}$.
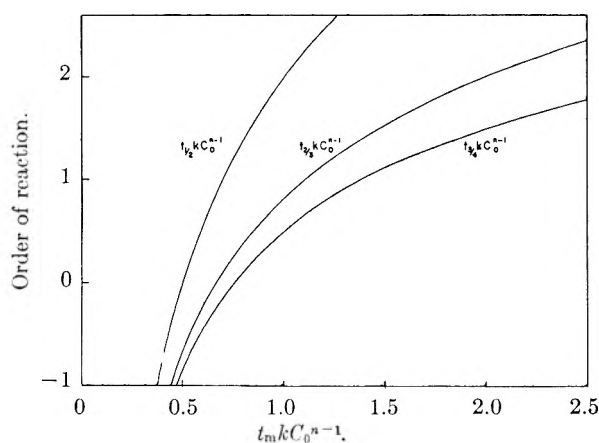
Fig. 3.—Order of reaction vs. $kt_mC_0^{n-1}$.

values of $kt_mC_0^{n-1}$ are only a function of n and m. If n is held constant, then it is a function of m only. From equation A, the equation is obtained

$$kt_mC_0^{n-1} = \frac{1}{n-1}[(1-m)^{1-n} - 1] = f(m)_n$$

For first-order reactions the following can be shown

$$kt_mC_0^{n-1} = \ln\left(\frac{1}{1-m}\right)_{n-1} = f(m)_{n-1}$$

The values of $kt_mC_0^{n-1}$ obtained are given in Table II. From Table II, Figs. 2 and 3 can be constructed.

TABLE II
VALUES OF $kt_mC_0^{n-1}$

Values of n	$kt^1/_2C_0^{n-1}$	$kt^2/_3C_0^{n-1}$	$kt^3/_4C_0^{n-1}$	$kt^1/_3C_0^{n-1}$	$kt^1/_4C_0^{n-1}$
−1.0	0.375	0.445	0.469	0.278	0.219
−0.5	.431	.539	.583	.304	.234
0.0	.500	.667	.750	.333	.250
0.5	.586	.846	1.000	.368	.268
1.0	.693	1.099	1.387	.406	.287
1.5	.828	1.464	2.000	.449	.310
2.0	1.000	2.000	3.000	.500	.334
2.5	1.219	2.797	4.667	.556	.360
3.0	1.500	4.000	7.500	.625	.389
4.0	2.333	8.667	21.000	.792	.457

From Figs. 2 and 3 the values of $t_mkC_0^{n-1}$, where m equals $1/_2$, $1/_3$, $1/_4$, $2/_3$, $3/_4$ and n equals any integral or even a fractional number between −1 and 4, can be obtained. Since the value of n can be

known from the preceding section of this paper, a simple division of $kt_mC_0^{n-1}$ by the experimental value of $t_mC_0^{n-1}$ will give the value of k.

In order to check the correctness of the result and to obtain the best value of k, t_m values obtained from a given run can be plotted against the values of $t_mkC_0^{n-1}$ obtained from Figs. 2 and 3. A good straight line should be obtained the slope of which is kC_0^{n-1}. In practice it seems that the k values obtained from the direct calculation are so consistent that the graph can be omitted.

This method has been tested in several cases and has been found useful.

THE INTEGRATED INTENSITY OF THE INFRARED O-H ABSORPTION IN PHENOLS

BY THEODORE L. BROWN

Noyes Chemical Laboratory, University of Illinois, Urbana, Illinois

Received January 14, 1957

Although frequency relationships in infrared vibrations have been studied to a considerable extent, there has only recently arisen an interest in the absolute intensities of absorption. The variations in intensity of a vibrational band which is possessed in common by a series of related molecules can in many cases be correlated with structural variations in the series. For example, the intensity of the O-H stretching band in aliphatic alcohols is determined by the inductive properties of the groups attached to the hydroxyl;[1] for the C≡N band in substituted benzonitriles it has been related to the Hammett σ-constant of the substituent.[2] In the present note the intensities of the O-H stretching band for some substituted phenols are examined to determine how this quantity is related to the nature of the substituent.

Experimental

Procedure.—The experimental procedure has been described elsewhere.[1,3] Solution concentrations in the range 0.02–0.005 molar were employed. The Perkin–Elmer model 112 spectrometer, fitted with lithium fluoride prism, was frequency calibrated by use of water vapor absorption.

Materials.—Reagent grade carbon tetrachloride was used as solvent. Mallinckrodt Analytical Reagent phenol from a newly opened bottle was used without further purification. All of the other phenols were Eastman Kodak materials. p-Methoxy, p-t-butyl and 3,5-dimethylphenol were purified by recrystallization and vacuum sublimation; the other compounds were used without further treatment.

Results

The results of the intensity measurements are shown in Table I. The first column after the compound name lists the intensity, A', in units of 1×10^4 mole^{-1} l. cm.$^{-2}$. The second column lists the half-intensity width, $\Delta\nu_{1/2}$, and the third lists the frequency of band maximum, ν_m, both in units of cm.$^{-1}$. The intensities listed are not corrected for wing absorption[4]; the relative magnitudes are con-

(1) T. L. Brown and M. T. Rogers, *J. Am. Chem. Soc.*, **79**, 577 (1957).

(2) H. W. Thompson and G. Steel, *Trans. Faraday Soc.*, **52**, 1451 (1956).

(3) T. L. Brown, J. M. Sandri and H. Hart, THIS JOURNAL, **61**, 698 (1957).

(4) D. A. Ramsay, *J. Am. Chem. Soc.*, **74**, 72 (1952).

sidered correct to within about 3%. The values of ν_m are probably correct to within about 2 cm.$^{-1}$; they are in fairly good agreement with those reported by Ingraham, et al.,[5] although in a few cases the values obtained here are somewhat lower.

TABLE I

INTEGRATED INTENSITY OF THE O–H STRETCHING BAND FOR SOME SUBSTITUTED PHENOLS

Substituent	A'^a	$\Delta\nu_{1/2}$	ν_m	σ^6	$pK_a{}^7$
m-Nitro	1.71	23	3600	0.71	8.35
m-Chloro	1.31	22	3602	.37	9.02
m-Bromo	1.29	23	3604	.39	9.11
p-Bromo	1.23	23	3607	.23	9.34
p-Chloro	1.19	22	3607	.23	9.38
None	0.99	21	3610	.00	9.95
p-Methoxy	1.06	23	3614	− .27	10.20
p-t-Butyl	1.06	21	3612	− .12	...
3,5-Dimethyl	0.95	22	3611	− .17	10.17

^{a} Units of 1×10^4 mole^{-1} l. cm.$^{-2}$.

Discussion

In the fourth and fifth columns of Table I are listed, respectively, the Hammett σ-constant for the substituent,[6] and the pK_a value for the phenol measured in water.[7] It is clear that the intensity of the O–H absorption is related to these quantities; log A' is linearly related to the pK_a values, a relationship similar to that observed by Thompson and Steel for the C≡N band of benzonitriles related to the pK_a's of the corresponding benzoic acids.[2] The slope is of the opposite sign from that which is observed for the benzonitriles, for which the intensity increases with increasing electron-release of the substituent. It has been shown that for aliphatic alcohols the intensity increases with increasing electron-withdrawal of the group attached to the hydroxyl;[1] a similar conclusion follows for phenols from the present results. The major difference between the phenols and the aliphatic alcohols, however, lies in the mode of electron-withdrawal; for the latter compounds the inductive effect alone is operative, whereas the substituents in the phenols modify the electron density in the ring through conjugative as well as inductive interactions. The O–H group itself interacts conjugatively with the ring, leading to structures of the types I and II, and this interaction is reflected in the higher values of intensity for the

phenols as compared with aliphatic alcohols. Electron-withdrawing groups, by decreasing the electron density in the ring, promote structures I and II, leading to higher intensities.

Acknowledgment–Thanks are due to Dr. H. G. Drickamer for the use of the infrared instrument.

(5) L. L. Ingraham, J. Corse, G. F. Bailey and F. Stitt, *ibid.*, **74**, 2297 (1952).

(6) H. H. Jaffe, *Chem. Revs.*, **53**, 191 (1953).

(7) E. A. Braude and F. C. Nachod, "Determination of Organic Structures by Physical Methods," Academic Press, Inc., New York, N. Y., 1955, pp. 589 and 594.

A POSSIBLE EXPLANATION OF THE PARADOX INVOLVING THE ACTIVATION ENERGIES OF THE REVERSIBLE REACTION $CH_3 + H_2 \rightleftarrows CH_4 + H$
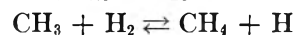
BY L. H. LONG

Department of Chemistry, The Washington Singer Lab., Univ. of Exeter Exeter, England

Various estimates lying within a wide range were formerly assigned to the activation energy of the forward process

$$CH_3 + H_2 \longrightarrow CH_4 + H \qquad (1)$$

In more recent times E_1 has been the object of careful and almost simultaneous studies by Davison and Burton[1] and by Majury and Steacie,[2] who, in using different methods, obtained very discordant results, namely > 13 and 9.7 ± 0.6 kcal., respectively. The latter investigators comment (in sufficient detail to dispense with the need of reproducing the paradoxical situation here) that their result is several kcal. too low to accord with what is known concerning the over-all heat of reaction and the activation energy of the reverse process. Other workers have also remarked on the paradox. Notwithstanding, Steacie has since[3] attempted to reconcile the disagreement in the experimental values for the activation energy of the forward process essentially in favor of his lower value. This attempt is seen to be unconvincing, however, once it is appreciated that the disagreement referred to is in essence the outcome not of experimental shortcomings but of an oversight in the theory underlying the methods.
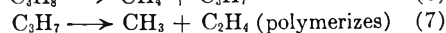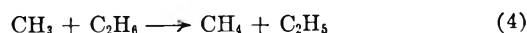
It was assumed in both experimental approaches that the only other methane-producing reaction occurring in the systems is

$$CH_3 + A \longrightarrow CH_4 + \text{products} \qquad (2)$$
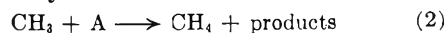
where A is a molecule of acetone (or acetaldehyde). But because of the circumstance that wherever there are methyl radicals there will inevitably be ethane on account of the rapid combination reaction

$$2CH_3 \longrightarrow C_2H_6 \qquad (3)$$
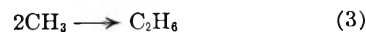
it needs to be emphasized that the ethane will itself enter into competition for methyl radicals and initiate a series of steps in a way which has recently been demonstrated for other methyl compounds[4,5]

$$CH_3 + C_2H_6 \longrightarrow CH_4 + C_2H_5 \qquad (4)$$
$$CH_3 + C_2H_5 \longrightarrow C_3H_8 \qquad (5)$$
$$CH_3 + C_3H_8 \longrightarrow CH_4 + C_3H_7 \qquad (6)$$
$$C_3H_7 \longrightarrow CH_3 + C_2H_4 \text{ (polymerizes)} \qquad (7)$$

Reactions 4 and 6 constitute additional methane-producing processes, while the former is also an ethane-consuming process, so that neglect to consider them may have far-reaching consequences. Since (4) has an activation energy of the same order

(1) S. Davison and M. Burton, *J. Am. Chem. Soc.*, **74**, 2307 (1952).

(2) T. G. Majury and E. W. R. Steacie, *Canadian J. Chem.*, **30**, 800 (1952).

(3) E. W. R. Steacie, "Atomic and Free Radical Reactions," Vol. 2, Reinhold Publ. Corp., New York, N.Y., 2nd Edition, 1954, p. 536.

(4) L. H. Long, *Trans. Faraday Soc.*, **51**, 673 (1955).

(5) L. H. Long, *J. Chem. Soc.*, 3410 (1956).

as (2), this competing mechanism cannot be excluded, and the question is the extent to which it occurs. Confirmation that it is not negligible may be seen in the observation that propane has been observed[6] in the photolysis products of acetone, even though reaction 5 will have no opportunity of building up a sizable concentration since (6) is faster than (4). Further, polymeric hydrocarbons[7,8] and unpolymerized ethylene[9] also have been observed, although a high concentration of the latter would not in any case be expected as its polymerization is photosensitized by acetone.[10,11] The effect on the cited determinations of the activation energy of reaction 1 caused by tacitly neglecting this competing mechanism is therefore worth brief consideration.

The method of Davison and Burton[1] consisted in photolyzing acetone or acetaldehyde in the presence of deuterium and of hydrogen-deuterium mixtures and studying the temperature-dependence of the CH_3D/CH_4 ratio in the products. Since the precaution was taken of subjecting the results to a logarithmic extrapolation to zero time (ethane concentration zero), it turns out that appreciable error through ignoring reaction 4 is effectively avoided.

The position is quite other with the method of Majury and Steacie,[2] which, unlike the foregoing, depends upon the rate of ethane-formation as well as that of methane-formation. These investigators studied the temperature-dependence of log $k_1/k_3^{1/2}$ when acetone was photolyzed in the presence of hydrogen, but the derivation of k_1 also involved a preliminary determination of k_2 from experiments on acetone alone (subscripts refer throughout to the numbering of reactions in the present communication). The equations assumed in the absence of hydrogen were

$$d[CH_4]/dt = R_2 = k_2[CH_3][A]$$
$$d[C_2H_6]/dt = R_3 = k_3[CH_3]^2$$

But it follows from what has already been said that they should instead be written

$$d[CH_4]/dt = R_2 + R_4 + R_6 = k_2[CH_3][A] + 2k_4[CH_3][C_2H_6]$$
$$d[C_2H_6]/dt = R_3 - R_4 = k_3[CH_3]^2 - k_4[CH_3][C_2H_6]$$

(where R_6 can be equated with R_4 because k_6 is large compared with k_4). Clearly the ethane concentration will not vary in a linear manner, and the amount remaining at the end of each run may be only a fraction of the total ethane formed. Ignoring the terms in k_4 will here exaggerate k_2, diminish k_3 and introduce appreciable error into the slope of the Arrhenius plot of log $k_2/k_3^{1/2}$. Even if satisfactory assumptions about the variation in ethane concentration could be made, it would clearly be unsound to attempt to estimate the seriousness of this error from the rate constants based on work involving precisely the same oversight regarding methane-formation that is here under discussion.

(6) L. Mandelcorn and E. W. R. Steacie, *Canadian J. Chem.*, **32**, 79 (1954).

(7) C. A. Winkler, *Trans. Faraday Soc.*, **31**, 761 (1935).

(8) H. S. Taylor and C. Rosenblum, *J. Chem. Phys.*, **6**, 119 (1938).

(9) For example, L. Mandelcorn and E. W. R. Steacie, *Canadian J. Chem.*, **32**, 331 (1954).

(10) H. S. Taylor and J. C. Jungers, *Trans. Faraday Soc.*, **33**, 1353 (1937).

(11) L. Mandelcorn and E. W. R. Steacie, *Canadian J. Chem.*, **32**, 474 (1954).

More direct evidence would be forthcoming if the ratio

$$(R_{C_2H_6} + {}^{1/2}R_{CH_4} + {}^{1/2}R_{CH_3COC_2H_5})/R_{CO}$$

were known for the system of Majury and Steacie. If their mechanism is 100% pure, this ratio will equal unity. Unfortunately the figures for $R_{CH_3COC_2H_5}$ are not given, but the experimental ratio for the rather similar system of Mandelcorn and Steacie[6] is 0.95. The deficiency of 5% corresponds to 10% decomposition by the cited competing mechanism (or some other mechanism), since the corresponding amount of methane liberated by the competing mechanism itself was unavoidably included in the said experimental ratio. Rough estimates of $R_{CH_3COC_2H_5}$ values for the runs of Majury and Steacie with acetone alone (see their Table I) can be obtained by assuming that the $R_{CH_3COC_2H_5}/R_{CH_4}$ ratios are the same in the two systems. If this is done, the ratio $(R_{C_2H_6} + {}^{1/2}R_{CH_4} + {}^{1/2}R_{CH_3COC_2H_5})/R_{CO}$ for Majury and Steacie shows for most runs a deficiency between 2 and 5 times as great as for Mandelcorn and Steacie, the deficiency being largest at the highest temperature, where the reaction turns out to be only 50–70% pure.

The effect on k_1 will be considerably more serious than that on k_2, since k_1 was derived from experiments in the presence of hydrogen (Majury and Steacie, Table II) by estimating the additional methane formed with the help of the relation

$$R_1 = R_{total \, methane} - R_2$$

where $R_1 = k_1[CH_3][H_2]$. R_1 amounted to as little as $\sim 20\%$ of R_2 in some runs, so that the error would be serious even if the purity of the pyrolysis mechanism were as high as 90%. R_1, as the difference between two much larger quantities, is hence very much more sensitive to systematic errors than R_2; it is moreover to be noted that R_2 in the above equation for determining R_1 should in reality be replaced by the complex quantity $(R_2 + 2R_4)$, in which the relative magnitude of R_4 changes in the presence of hydrogen on account of the effect of the additional competition for methyl radicals on the ethane concentration. It follows that the ethane not formed by reaction 1 cannot be simply calculated. The result of this method will therefore be a spurious slope to the Arrhenius plot for log $k_1/k_3^{1/2}$ and a misleading value for the activation energy of reaction 1 derived from it.

Clearly, were it not for such a complicating factor, the two methods[1,2] would yield the same value for E_1. Consideration of the additional factor examined here thus reveals the need for a reassessment of the evidence in favor of the higher value of >13 kcal., and this at the same time would remove the paradox involving the activation energy of the reverse process.

ON THE LOW RATES OF EQUILIBRATION IN DIALYSIS EXPERIMENTS WITH IONIC SURFACE-ACTIVE AGENTS

BY LAWRENCE M. KUSHNER AND REBECCA A. PARKER

National Bureau of Standards, Washington, D. C.

In opposition to the conclusions of Yang and

Foster[1] and Harrap and O'Donnell,[2] Klevens and Carr[3] have shown recently that in equilibrium dialysis experiments with pure ionic surface-active agents, equal concentrations of surfactant on both sides of the membrane are achieved if sufficient time is allowed for equilibrium to be attained. However, the time required to reach equilibrium increases in all cases as the surfactant concentration is increased and as the membrane pore size is decreased. They conclude that the average pore size of the membrane relative to the micelle size and to that of the individual surfactant ions is an important factor. Klevens and Carr do not discuss this further and one assumes that the sieve action of the membrane is of primary importance in determining the rate of equilibration.

The purpose of this paper is to call attention to another factor which may be of importance in explaining the long times required to reach equilibrium in dialysis experiments with ionic surface-active agents.

Sollner[4] and co-workers have shown that the ion-selectivity of membranes is due to the existence of an electric charge on the membranes, this charge being due to the ionization of appropriate groups which may occur in the structure of the membrane. In those instances in which the membrane contains no ionizing groups, it may become charged by selective adsorption of ions from solution, although one would expect such an occurrence to be unlikely in aqueous solutions of inorganic electrolytes. In the case of a solution of an ionic surfactant, however, one must expect strong adsorption of the surface-active ion at the membrane/solution interface. Such a process would cause the membrane to assume the charge of the surface-active ion, thereby increasing the activation energy for the diffusion of non-absorbed surface-active ions or their micelles across the membrane.

Below the critical micelle concentration, an increase in the concentration of surfactant would increase the adsorption on the membrane and increase its selectivity. Hence the rate of diffusion would decrease. Above the critical micelle concentration adsorption is maximal, but because of the formation of large, highly charged micelles, the rate of diffusion would continue to decrease. Further, at any particular concentration, decreasing the membrane pore size should decrease the rate of equilibration.

Since it is possible to determine the degree of ion-selectivity of membranes by electromotive force measurements in appropriate concentration cells, this has been done with a number of cells containing an ionic surface-active agent and, for comparison, a number of cells containing a non-surface-active electrolyte.

Experimental

Materials.—The surfactant was dodecyltrimethylammonium chloride obtained from Armour & Company. It was crystallized a number of times from ethyl alcohol by the addition of ether and by cooling. In earlier light scat-

tering work, the material behaved as if no ionic or non-polar impurities were present. Its critical micelle concentration, determined by light scattering, was 0.570 g./dl.

The membrane was Nojax cellulose casing obtained from the Visking Corporation.

Concentration Potentials.—If, by adsorption of the positive dodecyltrimethylammonium ion, the membrane were behaving as an ideal ion-selective membrane (i.e., permitting only the chloride ions to diffuse through), then the electromotive force of the cell

SCE/surfactant (C_1)/membrane/surfactant (C_2)/SCE (I)

would be the same as the electromotive force of the cell

SCE/surfactant (C_1)/AgCl,
Ag, AgCl/surfactant (C_2)/SCE (II)

SCE refers to a saturated calomel electrode. The concentrations of surface-active agent on each side of the membrane are C_1 and C_2.

Measurements of the electromotive force of cells of types I and II at various values of C_1 and C_2 have been made. For the sake of comparison, measurements on cells of the types

SCE/KCl (C_1)/membrane/KCl (C_2)/SCE

and

SCE/KCl (C_1)/AgCl, Ag, AgCl/KCl (C_2)/SCE

have been made. All measurements were made at room temperature. The results, corrected to 25°, are given in Tables I and II. In each of the tables E_{mem} is the electromotive force of the cell with the membrane. E_{max} is the electromotive force of the corresponding cell with a AgCl, Ag, AgCl bridge between the two solutions.

TABLE I

CONCENTRATION POTENTIALS FOR CELLS WITH
DODECYLTRIMETHYLAMMONIUM CHLORIDE

C_1, g./dl.	C_2, g./dl.	E_{mem}, mv.	E_{max}, mv.	E_{mem}/E_{max}
1.264	0.835	−4.24	−4.92	0.86
1.264	.570	−8.11	−9.76	.83
0.835	.570	−3.87	−4.87	.80
.647	.570	−1.42	−1.75	.81
.602	.570	−0.58	−0.76	.76
.570	.514	−1.57	−2.44	.64
.570	.395	−4.85	−9.27	.52
.570	.255	−10.88	−18.5	.59
.570	.133	−16.9	−34.4	.49
.324	.194	−5.93	−11.4	.52
.324	.129	−10.08	−20.8	.48
.194	.129	−5.08	−9.57	.53

TABLE II

CONCENTRATION POTENTIALS FOR CELLS WITH KCl

C_1, g./l.	C_2, g./l.	E_{mem}, mv.	E_{max}, mv.
1.610	1.450	+0.24	−2.62
1.610	1.127	+0.70	−8.92
1.610	0.724	+2.07	−19.8
1.610	.400	+3.33	−34.2
1.610	.008	+11.21	−111.4

Discussion

The data are represented graphically in Fig. 1 and show strikingly the marked ion-selectivity of the membrane when placed between two surfactant solutions. In A, cf Fig. 1, both of the solutions involved in each measurement were at or above the critical micelle concentration. In B, each of the solutions concerned was at or below the critical micelle concentration. In A, the value of E_{mem} was consistently 75 to 85% of E_{max}. In B, E_{mem} was generally about 50% of E_{max}. These data are in agreement with the anticipated higher

(1) J. T. Yang and J. G. Foster, This Journal, **57**, 628 (1953).

(2) B. S. Harrap and I. J. O'Donnell, ibid., **58**, 1097 (1954).

(3) H. B. Klevens and C. W. Carr, ibid., **60**, 1245 (1956).

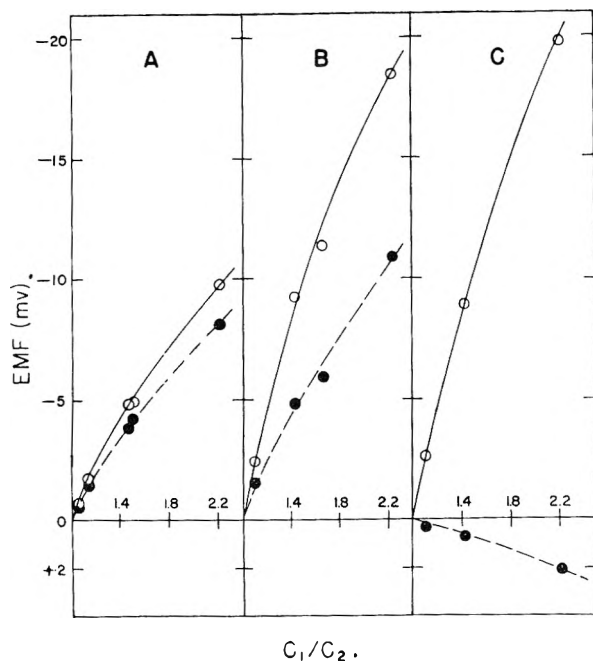(4) For an excellent review of this work see K. Sollner, J. Electrochem. Soc., **97**, 139C (1950).

Fig. 1.—A, the dependence of E_{max} (———) and E_{mem}(— —) on C_1/C_2 for dodecyltrimethylammonium chloride when each of the concentrations is at or above the critical micelle concentration; B, the dependence of E_{max} (———) and E_{mem} (— — —) on C_1/C_2 for dodecyltrimethylammonium chloride when each of the concentrations is at or below the critical micelle concentration; C, the dependence of E_{max} (———) and E_{mem} (— — —) on C_1/C_2 for potassium chloride.

selectivity of the membrane when an appreciable quantity of the surfactant is in micellar form. This is because (1) adsorption of the dodecyltrimethylammonium ion is maximal and (2) it is much more difficult for the micelles, because of their large size and high positive charge, to migrate through the membrane than it is for unassociated surface-active ions.

The data given in Table II and shown in C of Fig. 1 show that the membrane itself has little or no ion-selective character when placed between solutions of KCl. The electromotive force observed is opposite in sign to that expected if the membrane were inherently more permeable to negative ions than positive ions. The positive values observed for E_{mem} may indicate that the membrane has a slight electronegative character due to the presence of a few acid groups in its structure, although included in E_{mem} is the sum of all of the liquid junction potentials in the cell.

In the light of the above results it appears that a cellophane membrane, as used in equilibrium dialysis experiments with ionic surfactants, can become ion-selective in such a manner as to tend to prevent the passage of surface-active ions or their micelles through the membrane. Presumably this is due to the adsorption of the surface-active ions on the membrane. The precise size of the effect depends on the ratio of the concentrations of the surfactant solutions and on the absolute magnitude of the concentrations. The effect is more important when micelles are present in the system. It appears, therefore, that any explanation for the low rates of equilibration in dialysis experiments with

ionic surface-active agents should not neglect the induction of ion-selective properties in the membranes by adsorption of the surface-active ions.

AN ACTIVE SPECIES FORMED IN THE ELECTRICAL DECOMPOSITION OF DIMETHYLAMINE[1]

By Francis Owen Rice and Chester Grelecki

Contribution from the Chemistry Department, Catholic University of America, Washington, D. C.

The decomposition of dimethylamine has been studied thermally[2] and photolytically[3] and the results of these experiments indicate that the main reaction is different in the two cases. Carter, et al.,[2] have reported a kinetic study of the methylamines; their analytical results indicate that in an unpacked bulb, the products of the thermal decomposition of dimethylamine consist mainly of methane and a non-volatile residue having the empirical formula C_2H_5N corresponding to methylmethyleneimine ($CH_3N=CH_2$).

The results of the photolysis of dimethylamine have been reported by Bamford.[3] The actual experimental results showed that the main products of the photolysis of gaseous dimethylamine were hydrogen and a polymer which analyzed $(C_2H_5N)_n$.

In our present experiments, dimethylamine was decomposed in the field of a high frequency oscillator and the products were condensed as a green solid at $-196°$. This material slowly changes to a white solid when allowed to stand at liquid nitrogen temperatures for extended periods and this color change is accompanied by the evolution of hydrogen containing small amounts of methane. We tried to prepare the green material by quickly cooling the products of the thermal decomposition of dimethylamine[4] but were not successful. We were unsuccessful in attempts to prepare the green solid by the photochemical decomposition of dimethylamine.

Experimental

Anhydrous dimethylamine vapor was passed through the field of a high frequency oscillator. With the pressure of the dimethylamine between 10^{-1} and 10^{-2} mm. a glow discharge resulted when the point of a commercial type Tesla coil was placed on the tube. The vapors leaving the field were quickly condensed onto a surface cooled with liquid nitrogen. The condensate thus formed was a green solid at $-196°$. The permanent gases formed during the initial phase of the reaction were removed from the system by means of a high speed mercury diffusion pump and then analyzed on a mass spectrometer.

Anal. Found: H_2, 94.5, 95.0; CH_4, 4.5, 3.8; N_2, 1.0, 1.2.

The green deposit slowly turned white even at $-196°$; when allowed to warm up at the rate of about 5° per minute, a sharp transition occurred when the temperature reached about 173°. At this point the deposit turned white rather suddenly, there was some blistering and a permanent gas was evolved. The composition of the permanent gas was: H_2, 82.4, 81.5; CH_4, 16.3, 17.6; N_2, 1.1, 0.7.

Half-life Determinations.—In our early experiments it was observed that the end of the Tesla coil had to be near

(1) This work was supported in part by the Atomic Energy Commission, Contract Number AT-(40-1)-1305.

(2) A. G. Carter, P. A. Bosanquet, C. G. Silcocks, N. Travers and A. F. Shilshire, J. Chem. Soc., 495 (1939).

(3) C. H. Bamford, ibid., 17 (1939).

(4) See F. O. Rice and C. Grelecki, J. Am. Chem. Soc., 79, 2679 (1957).

the cold surface otherwise no green material was produced. In order to determine the half-life of the active species, a series of experiments were performed in which the distance of the coil from the cold finger was systematically varied and the time for the initial appearance of the green compound was noted. This time was taken to be inversely proportional to the concentration of the active species. We also measured, for various distances of the coil from the finger, the amount of permanent gas liberated during the transition of the green material and assumed that this is directly proportional to the concentration of radicals stabilized.

In these experiments the cross sectional area of the tube was 0.785 cm.² The pressure drop along the tube was 0.035 mm. per cm. and the average pressure at the reaction site was 0.07 mm. Since 5.42×10^{-2} mole of dimethylamine was passed through the tube in 15 minutes the average flow rate was 200 m./sec.

TABLE I

D is the distance of the coil from the cold finger. t is the time taken for the radicals to flow from the point of origin to the liquid N_2 cooled surface and is calculated by dividing the distance by the flow rate. p is the pressure of permanent gas formed after the transition of the green material. t_m is the time required for a visible green deposit to form.

D, cm.	$t \times 10^4$, sec.	p, mm.	t_m, sec.
1.5	0.75	0.70	30
2	1.00	.20	90
3	1.50	.07	240
4	2.0	.03	480

The first-order rate constant was obtained by plotting log p vs. Δt and also from the plot $1/t_m$ vs. Δt. The rate constant was the same (1.87×10^4 sec.$^{-1}$) regardless of which method was used to follow the reaction. The half-life of the green material in the vapor phase is therefore 3.7×10^{-5} sec. This is an extremely short life compared to the half-lives of other radicals which have been reported. It is smaller, by a factor of about 25, than the half-life[5] of NH and the hydrocarbon radicals[6,7] CH_3 and CH_2, and by a factor of about 250, than the half-life of the hydrazino radical.[8]

The Activation Energy of the Reaction.—When the green solid was allowed to stand for extended periods at $-196°$ it became appreciably lighter in color. Since evolution of hydrogen accompanied this reaction, the increase in pressure could be used to measure the rate of the reaction at the temperature of boiling nitrogen and boiling oxygen. The temperature of the coolant was measured to $\pm 0.2°$ with a low temperature thermometer calibrated by the National Bureau of Standards. Care was taken to ensure that the concentration of the green compound was the same at the beginning of each reaction, so that the initial rates could be compared by means of the Arrhenius equation to yield an energy of activation for the reaction.

The initial rate of appearance of permanent gas at $-195.3°$ was 1.42×10^{-3} mm. per min. and at $-183.3°$ it was 4.6×10^{-3} mm. per min. which gives an activation energy of 1.3 kcal. This result is probably accurate to within a few tenths of a kilocalorie since an error of $1°$ in the measure of the temperature difference results only in an error of 0.1 kcal. in the activation energy.

Discussion

We have not been able to determine the composition of the green material, but its extremely short life time and its reactivity at very low temperatures strongly suggest that it is a free radical stabilized in the condensed phase. We were not able to detect any trace of tetramethylhydrazine despite the fact that we examined the mass spectrum of the products very carefully. At the present time we think that our results are best explained by

(5) F. O. Rice and M. J. Freamo, *J. Am. Chem. Soc.*, **73**, 5529 (1951).

(6) F. O. Rice and W. R. Johnston, *ibid.*, **56**, 214 (1934).

(7) F. O. Rice and A. S. Glasebrook, *ibid.*, **55**, 4329 (1933).

(8) F. O. Rice and F. Scherber, *ibid.*, **77**, 291 (1955).

assuming that one of the six hydrogen atoms attached to carbon is knocked off in the electric field and the resulting radical CH_3NHCH_2 is stabilized on the cold finger.

THE REACTION OF ACID GASES WITH PYREX GLASS[1]

By James E. Boggs, Lynda L. Ryan and Laurel L. Peek

Department of Chemistry, The University of Texas, Austin 12, Texas

In an attempt to understand the mechanism of certain halogen isotope exchange reactions, Boggs and Mosher[2] have recently studied the chemical reaction between Pyrex #7220 glass wool and HCl gas. They found an extensive, diffusion-controlled reaction forming NaCl on the glass surface, proceeding at a measurable rate in the temperature range between 295 and 385°. It is the purpose of the present study to attempt to discover what other gases react in a similar manner, to determine the mechanism of the reaction, and to relate the reaction with Pyrex glass to the effect of the wall in halogen isotope exchange reactions.

Experimental

Hydrogen bromide was prepared by distillation from an acetic acid solution purchased from Eastman Kodak Co. The other gases used were purchased in cylinders from The Matheson Co. All gases were purified by fractional distillation in a vacuum system. The apparatus and experimental methods in this study were similar to those reported earlier.[2,3]

Results and Discussion

Hydrogen bromide was found to react with Pyrex #7220 glass wool in a manner very similar to that previously reported[2] for HCl. Electron microscope photographs of the glass surface after reaction showed the development of considerable thicknesses of loosely-adhering crystalline material, which when studied by electron diffraction techniques proved to be NaBr.

The specific reaction rate constants were determined by the method of Boggs and Mosher,[2] using an average of 48 experimental points at each temperature, these being taken from several separate runs using different quantities of glass wool. The shape of the curves and the reproducibility of the individual observations were similar to the earlier work. At an HBr pressure of 50 mm., the rate constant, k, has a value of 3.7×10^{-19} (moles cm.$^{-2}$)^2 sec.$^{-1}$ at 300°, 12×10^{-19} at 350° and 32×10^{-19} at 400°. An Arrhenius-type plot of these values, shown in Fig. 1, gives an activation energy for the reaction of 17 kcal./mole. Figure 1 also shows the results obtained by Boggs and Mosher[2] for the reaction of HCl with glass wool at a pressure of 500 mm. The two curves are nearly the same, the difference being barely more than the limits of experimental error. Under similar conditions, the gases H_2S, SO_2 and CH_3Cl did not react with Pyrex #7220 glass wool at a measurable rate.

(2) J. E. Boggs and H. P. Mosher, *J. Am. Chem. Soc.*, **78**, 3901 (1956).

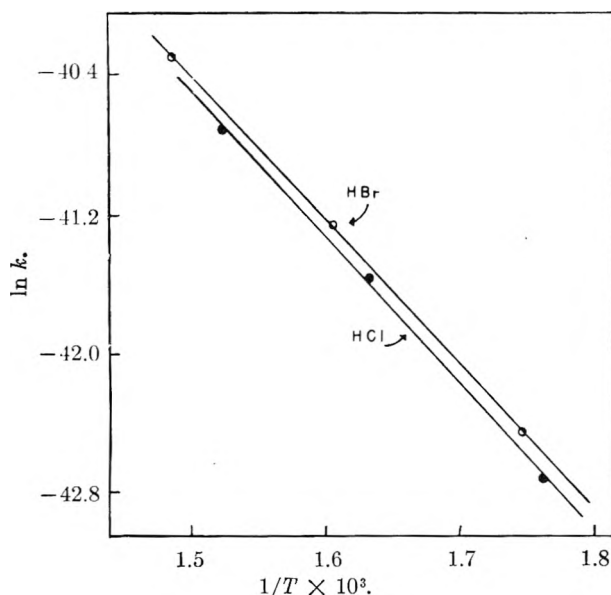(3) J. E. Boggs and L. O. Brockway, *ibid.*, **77**, 3444 (1955).

Fig. 1.—Arrhenius plot for the reaction of Pyrex #7220 glass wool with HCl or HBr.

Attempts to measure the rate of the reaction of HBr at 450° led to irreproducible results. For any one run, the kinetic results followed the same rate law as at lower temperatures, but in different runs the rate constant varied from 15×10^{-19} to 35×10^{-19}.

Unlike the reaction of HCl with glass, the rate of the reaction of HBr with glass was unaffected by the pressure of the hydrogen halide in the gas phase. Variations of HBr pressure from 30 to 430 mm. caused no measurable difference in the rate of the reaction.

We propose that the reaction of HCl or HBr with glass occurs in the following manner. Even at 400° there is a thin film of adsorbed water held tenaciously on the glass surface. The gas dissolves in this film, forming H_3O^+ ions and halide ions. Protons from the H_3O^+ ions then diffuse into the glass, Na^+ ions diffusing outward at the same rate to maintain electrical neutrality, this ionic counter-diffusion being the rate-determining step in the over-all process. At 450°, the water film is no longer maintained intact, and the rate falls off, the exact value of the rate constant being determined by the extent to which the water has been removed from the surface.

With sufficient H_3O^+ ions in the surface solution, the rate of the counter-diffusion of Na^+ ions and H^+ ions may be limited by the rate of Na^+ diffusion. Thus above a certain pressure limit, the rate would be independent of gas pressure. At lower pressures of HCl in the gas phase, the surface concentration of H_3O^+ would be decreased, so that the diffusion of H^+ takes over as the rate-determining step, leading to a slower reaction. It would be difficult to predict the relative solubilities of HCl and HBr in a surface film of moisture at these temperatures, but in bulk solutions at lower temperatures the solubility, on a molar basis, of HBr is greater than that of HCl and decreases less with temperature. Thus it might be that over the pressure range studied with HBr, there is always suf-

ficient H_3O^+ ion in solution so that the over-all rate is controlled by Na^+ ion diffusion.

Boggs and Mosher[2] studied the effect of HCl pressure only at a temperature of 385°, which was the highest temperature used in their measurements. On the basis of the above reasoning, one can predict that at a lower temperature where the solubility of HCl would be greater, there might always be sufficient H_3O^+ ion in the surface layer so that the Na^+ ion diffusion would be rate-controlling and the over-all rate would be found to be independent of HCl pressure. We have made such measurements at 295°, varying the HCl pressure between 75 and 430 mm. Within experimental error, the rate of the reaction was found to be independent of pressure under these conditions. The fact that the HCl curve in Fig. 1 falls very slightly below that for HBr may indicate that even at 500 mm. pressure of HCl, the H_3O^+ ion concentration on the surface is not sufficiently high to allow complete control by the Na^+ ion diffusion (evidence for which is also found in Fig. 3 in the paper by Boggs and Mosher[2]).

H_2S and SO_2 form weak acids when they dissolve in water, giving very low H_3O^+ ion concentrations. The rate, being controlled by these very low concentrations, would be too slow to measure. CH_3Cl might be expected to react by hydrolyzing in the surface film of water to form HCl, which would then behave as HCl alone does. Apparently this does not happen, possibly because the hydrolysis reaction removes the surface water before an adequate H_3O^+ ion concentration can be established.

Several semi-quantitative isotope exchange experiments were performed in an attempt to correlate the reaction between the hydrogen halides and glass with published studies on halogen isotope exchange reactions. Three reaction tubes of the type used by Boggs and Brockway[3] were filled with HCl containing 39.7% Cl^{37} (the normal abundance is 24.5% Cl^{37}). The tubes were then heated at 300° for 4 hours to allow the HCl to react with the glass wall. After this time, they were evacuated, filled with CH_3Cl containing the normal isotopic ratio, resealed, and heated for 2 hours. The results, summarized in Table I, show that exchange of Cl between HCl and CH_3Cl can occur through the intermediate formation of NaCl on the wall.

TABLE I

ISOTOPE EXCHANGE BETWEEN NaCl FORMED ON THE REACTOR WALL AND CH_3Cl

Pressure CH_3Cl, mm.	Temp., °C.	Cl^{37} in CH_3Cl, %
150	200	24.5
485	300	25.9
485	450	31.4

Boggs and Brockway[3] found that they could obtain reproducible exchange rates between HCl and CH_3Cl only if the reaction tubes were evacuated and heated at 450–500° for 4 hours before use. Otherwise much more rapid exchange was observed. Since the exchange rates reported in this study are higher than those reported by Boggs and Brockway in baked tubes, it appears probable that exchange through NaCl formation was responsible

for the higher rates in unbaked tubes. The extensive heating served to remove adsorbed water from the glass surface, so that any exchange would have to proceed by a different mechanism. The irreproducibility of the measurements in unbaked tubes could have been caused by variations in the surface area of NaCl exposed on the surface (see Fig. 1 of Boggs and Mosher[2]).

It is to be expected, of course, that HCl and HBr will react with glasses of different composition to quite different extents, dependent mainly on the sodium content of the glass. The alkali content of the Pyrex #7220 glass used in these studies is higher than that of the Pyrex #7740 commonly used in the construction of laboratory apparatus. Pyrex #7740, however, contains 3.6% Na, and from the results of the isotope exchange experiments it appears that it reacts in a similar manner.

KINETIC EFFECTS IN DETERMINING HEATS OF REACTION BY DIFFERENTIAL THERMAL ANALYSIS

By HANS J. BORCHARDT

General Engineering Laboratory, General Electric Company, Schenectady, New York

The dynamic gas method of differential thermal analysis as developed by Stone[1] recently has been used to measure the heat of reaction of the magnesite dissociation.[2]

$$MgCO_3 \rightleftarrows MgO + CO_2 \qquad (1)$$
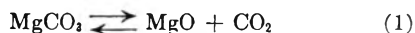
Differential thermographs for this decomposition were obtained in atmospheres ranging from 0.001 to 3320 mm. of CO_2. Increasing CO_2 pressures displaced the peak to higher temperatures. The ln of the pressure was plotted against the reciprocal of the reaction temperature[3] according to the equation

$$\ln P_{dta} = -\frac{\Delta H}{RT} + C' \qquad (2)$$

where P_{dta} is the pressure of CO_2, T the reaction temperature in °K., ΔH the heat of reaction, R the gas constant, and C' a constant. The slope of this plot being $-\Delta H/R$ gives the desired heat of reaction.

This use of a Clausius–Clapeyron type equation makes the implicit assumption that the reaction temperature can be treated as the equilibrium decomposition temperature at the particular partial pressure of CO_2 employed. The purpose of the present discussion is to examine the validity of this assumption.

We first inquire as to the significance of the reaction temperature. *This is the temperature at which the rate of reaction, hence the rate of heat absorption, is sufficiently rapid to establish a temperature differential which the instrument is just able to detect.* This minimum detectable rate of heat absorption (rate of reaction) is a property of the apparatus

and material ($MgCO_3$) only, hence is the same for all the differential thermographs, regardless of the CO_2 pressure.[4] The constraint must therefore be imposed that the rate of reaction is the same at all the reaction temperatures. In order to obtain an expression for the rate of reaction, we assume the rate equation

$$r = k_f f(MgCO_3) - k_r P_{dta} g(MgO) \qquad (3)$$

Here r is the net rate of reaction, k_f and k_r the rate constants for the forward and reverse reactions, respectively, and P_{dta} the pressure of CO_2; $f(MgCO_3)$ and $g(MgO)$ are functions, respectively, of the activities of $MgCO_3$ and MgO. By defining r as a constant, equation 3 is restricted to those sets of temperatures (including the reaction temperatures) where the rate of reaction is the same. Dividing equation 3 by $k_r g(MgO)$ gives

$$P_{dta} = \frac{k_f f(MgCO_3)}{k_r g(MgO)} - \frac{r}{k_r g(MgO)} \qquad (4)$$

The term k_f/k_r is by definition the equilibrium constant which for this reaction is equal to the equilibrium partial pressure of CO_2 (P_{eq}). Since P_{eq} is truly given by the Clausius–Clapeyron equation, $P_{eq} = \exp(-\Delta H/RT + C)$, equation 4 becomes

$$P_{dta} = \frac{f(MgCO_3)}{g(MgO)} e^{-\Delta H/RT + C} - \frac{r}{k_r g(MgO)} \qquad (5)$$

Substituting for k_r with the Arrhenius equation, $k = S \exp -E/RT$, gives

$$P_{dta} = \frac{f(MgCO_3)}{g(MgO)} e^{-\Delta H/RT + C} - \frac{r}{S g(MgO)} e^{E_r/RT} \qquad (6)$$

where S is for all practical purposes a constant and E_r the activation energy for the reverse reaction. Equation 6 relates the reaction temperature to the pressure in the DTA sample holder without the assumption made in equation 2 that equilibrium conditions exist.

The behavior predicted by equation 6 can best be seen by the substitution of data. ΔH is taken as 10.1 kcal./mole, the value given by Stone.[2] C is evaluated by taking $P_{eq} = 1$ atmosphere at 410° as reported by Cremer and Gatt.[5] The activation energy for the forward reaction has been observed to be 35.6 kcal./mole.[6] This gives E_r as $35.6 - 10.1 = 25.5$ kcal./mole. The functions $f(MgCO_3)$ and $g(MgO)$ are, in the absence of data, taken as unity. The constant r/S is evaluated by taking $P_{dta} = 0.001$ mm. at 350° as reported by Stone.[2]

With these data, equation 6 is plotted as a continuous curve in Fig. 1. The circles represent the data reported by Stone.[2] The broken line was used by Stone to calculate ΔH. Relatively good agreement is obtained. It should be noted however that the agreement between the theoretical curve and Stone's data with regard to the limiting slope and the temperature at which P_{dta} approaches

(1) R. L. Stone, *J. Am. Ceram. Soc.*, **35**, 76 (1952).

(2) R. L. Stone, *ibid.*, **37**, 46 (1954).

(3) The term "reaction temperature" is used to designate the temperature at which the peak is first observed to appear.

(4) This assumes that the instrument itself does not undergo any significant changes in the temperature range under consideration. A formal justification for this interpretation of the reaction temperature can be derived from the kinetic equations described by H. J. Borchardt and F. Daniels, *J. Am. Chem. Soc.*, **79**, 41 (1957).

(5) E. Cremer and F. Gatt, *Radex Rundschau*, **4**, 144 (1949); *Ceram. Abstr.*, 56d (1950).

(6) H. T. S. Britton, S. J. Gregg and C. W. Winsor, *Trans. Faraday Soc.*, **48**, 63 (1952).
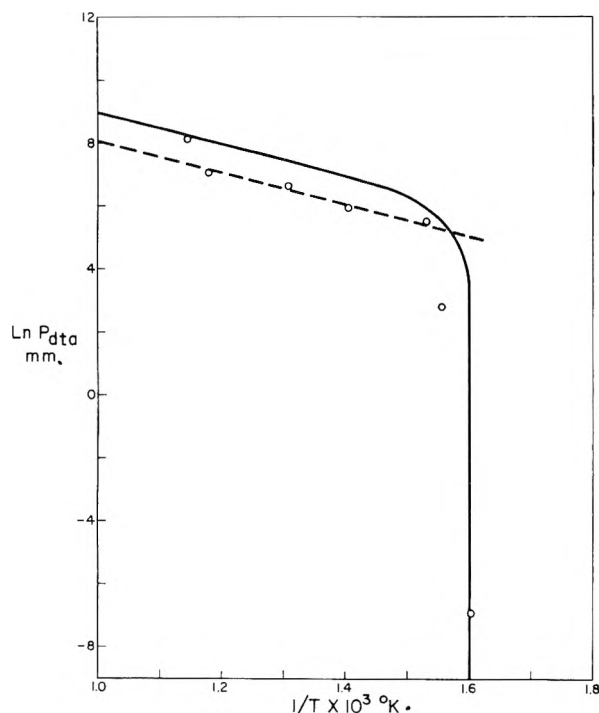
Fig. 1.—The solid curve is plotted according to equation 6. The circles represent the data reported by Stone.[2]

zero is due solely to the use of Stone's data in evaluating the constants of equation 6 (ΔH and r/S).

Due to the inverse exponential appearance of temperature in the terms on the right-hand side of equation 6, the second term will become negligible at elevated temperatures and equation 6 reduces to

$$P_{\text{dta}} = \frac{f(\text{MgCO}_3)}{g(\text{MgO})}\, e^{-\Delta H/RT + C} \tag{7}$$

The temperature at which equation 7 becomes applicable depends very much upon the sensitivity of the apparatus. The constant r is essentially a sensitivity parameter, diminishing as the sensitivity increases. With the present data, equation 7 becomes applicable above 394° ($1/T$ less than 1.5×10^{-3}).

Three conditions can be realized with equation 7; where the ratio $f(\text{MCO}_3)/g(\text{MgO})$ is (1) unity, (2) a constant other than one, (3) a variable. If the ratio is unity, the system is at equilibrium and equation 7 reduces to the Clausius–Clapeyron equation. If the ratio changes slowly so that its ln is essentially a constant, equation 2 is applicable but the constant C' is not the same as in the Clausius–Clapeyron equation. This appears to be the case with Stone's measurements. It is seen in Fig. 1 that the high temperature data points fall systematically below the theoretical curve in which the functions are assumed to be unity.

If the ratio of the functions is a variable, the plot of ln P versus $1/T$ will be non-linear at the temperatures where equation 7 applies.

It may therefore be concluded that if the plot of ln P_{dta} versus $1/T$ is linear at elevated temperatures, the slope of this line is $-\Delta H/R$. These data cannot however be taken as equilibrium data.

SEMIEMPIRICAL POTENTIAL ENERGY FUNCTIONS. II. GENERAL DIATOMIC MOLECULES[1]

BY PAUL SHIH KAN CHEN, MURRAY GELLER AND ARTHUR A. FROST

Department of Chemistry, Northwestern University, Evanston, Illinois

Received January 19, 1957

In paper I[2] of this series there was presented the following potential energy function V for the H_2 and H_2^+ molecules as a function of the internuclear distance R.

$$V = e^{-aR}\left(\frac{e^2}{R} - b\right) \tag{1}$$

The parameters a and b were determined from known spectroscopic constants such as D_e, the dissociation energy from the minimum R_e, the equilibrium internuclear distance k_e, the force constant, etc. The form of V was chosen to satisfy the following theoretical criteria: (a) the purely electronic energy ($V - e^2/R$) must remain finite as R approaches zero and must vary as $-e^2/R$ when R is large, and (b), V must be capable of going through a minimum.

For general diatomic molecules the simplest generalization of equation 1 is

$$V = e^{-aR}\left(\frac{c}{R} - b\right) \tag{2}$$

where the new parameter c might be expected to have the form

$$c = Z_1 Z_2 e^2$$

or, in atomic units

$$c = Z_1 Z_2 \tag{3}$$

where Z_1 and Z_2 are some kind of effective nuclear charges of the two atoms.

The purpose of this paper is to test this function against known spectroscopic data.

Determination of the Parameters.—Whereas the two parameters of equation 1 required a graphical solution, equation 2 permits direct algebraic evaluation of the three parameters, a, b and c from the spectroscopic constants, D_e, R_e and k_e as

$$\left.\begin{array}{l}
a = p/R_e \\[4pt]
b = D_e(1 + p)\exp(p) \\[4pt]
c = D_e R_e p \exp(p) \\[4pt]
\text{where } p = \left(1 + \dfrac{k_e R_e^2}{D_e}\right)^{1/2} - 1
\end{array}\right\} \tag{4}$$

Table I shows the spectroscopic constants and the resulting values of the parameters for the ground states of a set of hydrides and homonuclear molecules. These molecules include all of those in Herz-

(2) A. A. Frost and B. Musulin, J. Chem. Phys., 22, 1017 (1954).

berg's[3] tables for which accurate values of all three experimental constants were known.

TABLE I
HYDRIDES AND HOMONUCLEAR DIATOMIC MOLECULES
(All quantities are expressed in atomic units)

Molecule: Hydrides	k_e	R_e	D_e	a	b	c
CH	0.2881	2.116	0.1342	1.067	4.178	6.126
OH	.5006	1.833	.1683	1.263	5.652	7.235
HCl	.332	2.407	.1697	1.044	7.349	12.653
KH	.0361	4.24	.0684	0.5280	2.077	6.088
ZnH	.0971	3.013	.0349	1.369	11.056	26.812
HBr	.264	2.670	.1440	1.030	8.454	16.554
CdH	.0774	3.33	.0281	1.386	15.960	43.685
HI	.2018	3.033	.1176	1.021	10.657	24.434
HgH	.0732	3.29	.0169	1.799	43.543	122.555
Homonuclear						
H_2	0.368	1.40	0.1743	0.9049	1.402	1.0972
Li_2	0.0164	5.05	.0386	0.4832	1.524	5.459
N_2	1.4756	2.067	.3640	1.587	41.413	65.601
O_2	0.756	2.280	.1904	1.602	34.143	61.111
Na_2	.01103	5.82	.0272	0.4878	1.785	7.682
P_2	.357	3.58	.1867	1.131	54.143	155.45
Cl_2	.2113	3.76	.0923	1.270	63.257	196.67
K_2	.00632	7.41	.01912	0.4556	2.448	13.994
Br_2	.1576	4.32	.0732	1.254	105.81	385.86
I_2	.1107	5.04	.0572	1.207	177.47	768.17

Test of the Function. Having determined the parameters it would be desirable to make predictions of properties other than those used in determining the parameters. Third and fourth derivatives at the potential energy minima have been calculated and compared with those obtained from the spectroscopic constants α_e and $\omega_e X_e$. Although the calculated values are the right order of magnitude (often within 20%) the results are no better than obtainable in the same way with the Morse function or with the more recent Lippincott[4] function, or with the reduced potential energy function.[5] Therefore these calculations will be omitted here.

More interesting is the test of the parameter c as a product of effective nuclear charges (eq. 3). For hydrides, since the H atom would presumably have $Z = 1$, $C = Z_e$, the effective charge of the other

TABLE II
EFFECTIVE ATOMIC NUMBERS RELATED TO THE PARAMETER c

Element	Hydride c	Homonuclear $c^{1/2}$	Effective Atomic No. Z_e	Effective Atomic No. Z_s	Ratio Z_e/Z_s
H		1.04	1.04	1.00	1.04
Li		2.33	2.33	1.30	1.80
C	6.12		6.12	3.25	1.88
N		8.09	8.09	3.90	2.07
O	7.23	7.81	7.52	4.55	1.66
Na		2.77	2.77	2.20	1.26
P		12.47	12.47	4.80	2.60
Cl	12.65	14.02	13.34	6.10	2.19
K	6.08	3.74	4.91	2.20	2.24
Zn	26.81		26.81	4.35	6.16
Br	16.55	19.64	18.10	7.60	2.38
Cd	43.69		43.69	4.35	10.1
I	24.43	27.72	26.08	7.60	3.44
Hg	122.6		122.6	4.35	28.1

(3) G. Herzberg, "Spectra of Diatomic Molecules," 2nd Edition, D. Van Nostrand Co., Inc., New York, N. Y., 1950.

(4) E. R. Lippincott, *J. Chem. Phys.*, **21**, 2070 (1953); E. R. Lippincott and R. Schroeder, *ibid.*, **23**, 1131 (1955).

(5) A. A. Frost and B. Musulin, *J. Am. Chem. Soc.*, **76**, 2045 (1954).

atom. In the case of homonuclear molecules $C = Z_e^2$.

Table II lists for the hydrides and homonuclear molecules of Table I, c and $c^{1/2}$, respectively. For five elements both values are available and are generally comparable except for K. The fourth column lists as Z_e either c or $c^{1/2}$, or the average where both are available. Inspection reveals that these values for effective charge show a periodicity and lie in general between the core charge as a lower limit and the atomic number as an upper limit. A more quantitative comparison is shown in the last two columns in which are given Z_s and Z_e/Z_s where Z_s is the effective charge acting on the valence electrons as calculated by Slater's rules. With the exception of Zn, Cd and Hg the ratio Z_e/Z_s shows a general trend as the atomic number increases.

Discussion

Although the generalized semi-empirical equation 2 is not as well-founded on theoretical principles as is equation 1, which is restricted to hydrogen, the present results show that the interpretation of the parameter c as a product of effective nuclear charges has some semblance of truth. It is particularly gratifying that the pairs of Z_e values for O, Cl, Br and I agree so well.

Of course no such simple potential energy function as equation 2 would be expected to be universally valid. In particular ionic states would require special treatment and can be handled by an extension of the methods of Paper I. Furthermore, since Pitzer[6] has found that London forces may contribute considerably to bond energies equation 2 should probably be modified to give an inverse sixth power law at large distances.

(6) K. S. Pitzer, *J. Chem. Phys.*, **23**, 1735 (1955).

THE HEAT OF FORMATION OF SILANE

By E. O. BRIMM AND HARRIE M. HUMPHREYS

Contribution from the Research Laboratory of Linde Air Products Company, a Division of Union Carbide and Carbon Corporation, Tonawanda, New York

The heat of formation of silane gas from crystalline silicon and hydrogen at 25° and one atmosphere pressure was measured by a direct calorimetric method. The value obtained was +7.8 kcal./mole with an average deviation of ±3.5 kcal./mole.

The values for the heat of formation of silane given in the literature[1-3] vary from −8.7 to −14.8 kcal./mole. In addition, these values are not consistent with certain other observed properties of silane.[4,5] The present investigation was undertaken in order to provide an additional, independent determination of the quantity and, if possible, to reconcile the existing inconsistencies.

(1) H. Von Wartenberg, *Z. anorg. allgem. Chem.*, **79**, 71 (1913).

(2) F. R. Bichowsky and F. D. Rossini, "The Thermochemistry of Chemical Substances," Reinhold Publ. Corp., New York, N. Y., 1936, p. 253.

(3) U. S. National Bureau of Standards Circ. No. 500, "Selected Values of Chemical Thermodynamic Properties," Washington, 1952.

(4) T. R. Hogness, T. L. Wilson and W. C. Johnson, *J. Am. Chem. Soc.*, **58**, 108 (1936).

(5) J. C. Brantley and T. Smist, unpublished data.

Previous determinations of the heat of formation have been based on indirect measurement, either the heat of combustion of silane or the temperature coefficient of the equilibrium constant for the reaction

$$Si(s) + 2H_2(g) \rightleftharpoons SiH_4(g) \qquad (1)$$
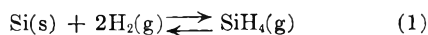
The first method depends upon the heat of formation of hydrated silica, which is not accurately known.[6] The second depends upon the establishment of a true equilibrium, and the existence of such an equilibrium is questionable.[2] Also, the values obtained for the heat of formation of silane, namely, -8.7, -13.7^2 and $-14.8^{3,6}$ kcal./mole are not consistent with the following observed properties of this compound. Hogness, Wilson and Johnson (ref. 4) allowed finely divided silicon and hydrogen to remain in contact for several days at temperatures up to 480° and a total pressure of one atmosphere. No pressure drop was observed; no silane could be detected. Measurements made in this Laboratory[5] show that, when silane and excess hydrogen are mixed at 425° and a pressure of 100 atmospheres, complete decomposition of the silane takes place. However, if the values for the heat of formation listed above are combined with the free energy functions (obtained from heat capacity or spectrographic measurements) for silicon, hydrogen and silane,[7-9] calculated values of the equilibrium constant for reaction 1 require large equilibrium mole percentages of silane under the conditions used by Hogness, Wilson and Johnson or by Brantley and Smist. In view of these contradictory results, a direct determination of the heat of formation of silane seemed necessary.

The heat of formation was measured by a standard calorimetric procedure,[10] purified silane being decomposed to crystalline silicon and hydrogen at 680°. The calorimeter was designed to operate at 550° but a temperature of 680° proved necessary to ensure complete decomposition of the silane. At 680° there was considerable thermal lag in the calorimeter system. Also the ratio of electrical energy to silane decomposition energy was 60:1 in contrast to 35:1 at 550°. These facts probably account for the large average deviation in the measurements. The value obtained, based on five calibration runs and four runs in which silane was decomposed, was $+7.8 \pm 3.5$ kcal./mole. The heat of formation is positive in contrast to the negative values reported previously. Because of the limited data and large average deviation in the calorimetric experiments, the sign of the heat of formation was checked by another method.

A 1-inch quartz tube was fitted with gas inlet and outlet tubes, a gas flow meter in the inlet side, and a thermocouple in the center of the quartz tube about 3 cm. downstream from the inlet tube. This assembly was placed in a tube

furnace and heated to 600°. The system was flushed with hydrogen and was then allowed to come to temperature equilibrium with no gas flowing through the system. Hydrogen was then allowed to flow through the system and the thermocouple registered a large temperature drop (about 10°). The thermocouple returned to its original equilibrium value when the hydrogen flow was stopped. Next, silane was allowed to flow at the same rate, and the thermocouple registered an increase in temperature (about 2°). The system returned to equilibrium when the silane flow was stopped. This procedure was repeated several times with the same results. The temperature of the furnace was then set at 320° and the same experiments performed. At this temperature, which is well below the temperature at which silane decomposes rapidly, a flow of either silane or hydrogen resulted in a decrease in the temperature of the thermocouple (about 4° for silane, 10° for hydrogen). The temperature increase observed during the silane flow at 600° must then result from the exothermic decomposition of this gas.[11]

Calculated values of the equilibrium constant for reaction (1) based on $\Delta Hf° = +7.8$ kcal./mole and the data from references 7, 8 and 9 are: $K_p = 1.9 \times 10^{-10}$ at 25° and $K_p = 1.4 \times 10^{-7}$ at 450°. The amount of silane present at equilibrium at 450° is therefore extremely small, about 1.4×10^{-5} mole % in the gas phase at one atmosphere pressure and about 1.4×10^{-3} mole % at a pressure at 100 atmospheres. This explains the failure of Hogness, Wilson and Johnson to form silane and the essentially complete decomposition of silane under the conditions employed by Brantley and Smist. The stability of silane at room temperature must be attributed to a very slow rate of decomposition rather than to a favorable equilibrium.

(11) Mr. E. G. Caswell of this Laboratory carried out these confirming experiments.

THE METHYL IMINO RADICAL[1]

By Francis Owen Rice and Chester J. Grelecki

The Catholic University of America, Washington, D. C.

The thermal decomposition of methyl azide has been studied[2] and found to be a homogeneous, unimolecular reaction. Leermakers[3] reported the results of a study of the reaction in a static system at temperatures between 200-240° and pressures from 0.078 to 46.6 cm., and suggested that the methylimino radical forms, and then undergoes a rearrangement to methyleneimine. Our experiments were designed to stabilize the methylimino radical or other active species by freezing the products of the thermal decomposition in a high speed flow system.[4]

(1) This work was supported in part by the United States Atomic Energy Commission, contract No. AT-(40-1)-1305.

(2) H. C. Ramsperger, J. Am. Chem. Soc., 51, 2134 (1929).

(3) J. A. Leermakers, ibid., 55, 3098 (1933).

(4) For a description of the technique see F. O. Rice and M. Freamo, ibid., 73, 5529 (1951).

(6) T. L. Cottrell "The Strength of Chemical Bonds," Academic Press Inc., New York, N. Y., 1954, p. 241.

(7) Calculated from data given by K. K. Kelley, Bur. Mines Bull., 371 (1934).

(8) N.B.S.-N.A.C.A. Tables of Thermal Properties of Gases, Tables 7.10 and 7.11.

(9) (a) C. Cerny and E. Erdos, Chem. Listy, 47, 1742 (1953); (b) A. P. Altschuler, J. Chem. Phys., 23, 361 (1955).

(10) See, for example, W. H. Johnson, R. G. Miller and E. J. Prosen. N.B.S. Report No. 2257, January 15, 1953.

Experimental

Methyl azide was prepared by allowing dimethyl sulfate to react drop by drop with an alkaline solution of sodium azide heated on a steam-bath. The evolved gases were passed over anhydrous calcium chloride and collected at $-78°$. The crude material was distilled through a Vigreux type column and fractions of the distillate were analyzed on the mass spectrometer as the distillation proceeded. The main impurity was found to be the lower boiling dimethyl ether which was removed by a careful fractionation. The pure methyl azide obtained in this manner boiled between 20 and 21°, and was stable indefinitely when stored in the dark at $-80°$. The mass spectrum of the methyl azide was obtained before each experiment and did not vary from day to day.

Methyl azide was allowed to expand into an evacuated reservoir of known volume, fitted with a manometer. In a typical experiment about 10^{-2} mole of methyl azide was passed through a quartz tube heated to about 900°. The rate of flow was adjusted by means of a suitable capillary so that the pressure at the inlet end of the furnace was about 0.1 mm. The products of the reaction which were condensable at $-196°$ were frozen out onto a surface cooled with liquid nitrogen, located about 2.5 cm. from the exit end of the furnace. The non-condensable gases which were formed at this stage of the reaction were removed from the reaction chamber by means of a high speed pumping system, and were passed into a gas measuring buret. Use was then made of the mass spectrometer as an analytical tool for the determination of the composition of these gaseous products.

Anal. N_2, 76.5, 80.0; H_2, 22.6, 18.5; CH_4, 0.9, 1.4.

The other products condensed on the cold finger at $-196°$ in the form of a clear colorless glass. When the liquid nitrogen was removed from the finger, the deposit almost immediately underwent a rapid transition to a white opaque solid. The change was quite vigorous and was accompanied by a slight "ping" with small pieces of the deposit being shot off the tube. No hydrogen or other gas was produced during this phase of the reaction. This transition was not observed in a blank experiment where all conditions were the same except that the furnace was not heated.

When the deposit was finally warmed to room temperature, the pressure in the system increased and a thick sirup remained on the glass surface. The vapor phase was analyzed on the mass spectrometer and found to consist practically entirely of ammonia and hydrogen cyanide. *Anal.* NH_3, 55%; HCN, 45%. Under our conditions ammonium cyanide is completely dissociated. Table I gives the amounts of the gaseous products formed per mole of methyl azide used.

TABLE I

ANALYSIS OF GASES (MOLES) FORMED DURING THE THERMAL DECOMPOSITION OF METHYL AZIDE

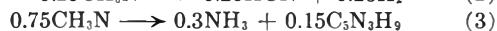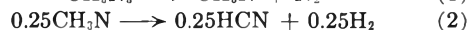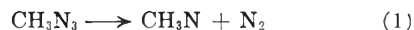|	Expt. 1	Expt. 2
Methyl azide used	1.00	1.00
Nitrogen	0.98	0.96
Hydrogen	0.23	0.28
Methane	trace	trace
Ammonia	0.27	0.29
Hydrogen cyanide	0.22	0.23

Under the conditions of the experiment essentially all of the methyl azide was decomposed. Each mole of methyl azide which decomposed yielded on the average 1.25 moles of permanent gas, of which one mole was nitrogen and $1/4$ mole was hydrogen. For each mole of methyl azide consumed there was also produced $1/2$ mole of products, which condensed at $-196°$ but were gases at room temperature. This result may be slightly low due to the solubility of some of the gases in the condensed phase at room temperature. These gases consisted of about 0.28 mole of ammonia and 0.23 mole of hydrogen cyanide for each mole of methyl azide decomposed.

The only other product was the polymeric material whose empirical formula could be calculated by difference since the quantities of all other products were known. This calculation gave an empirical formula of $C_5N_3H_9$. The calculated analysis of $C_5N_3H_9$ is: C, 54.1; N, 37.8; H, 8.1. The actual analysis for the material gave: C, 55.12, 55.27; N, 35.19, 35.04; H, 9.48, 9.64. Extensive attempts to sublime this material in order to obtain a crystalline product failed. It did not sublime in a vacuum when heated to 100°. When heated *in vacuo* for extended periods at temperatures near 150°, it turned brown but only minute amounts of a tan sirup appeared on the condenser. Leermakers identified both ammonium azide and hexamethylenetetramine in the white crystalline solid which formed during the thermal decomposition of methyl azide in a static system. The polymeric material formed in our experiments did not contain ammonium azide or hexamethylenetetramine in any detectable quantity since these would certainly sublime from the condensate during the extensive attempts to sublime it.

Discussion

A mechanism which is consistent with the results of the analysis of the product is

$$CH_3N_3 \longrightarrow CH_3N + N_2 \qquad (1)$$
$$0.25CH_3N \longrightarrow 0.25HCN + 0.25H_2 \qquad (2)$$
$$0.75CH_3N \longrightarrow 0.3NH_3 + 0.15C_5N_3H_9 \qquad (3)$$

The $C_5N_3H_9$ represents the empirical formula of the material required to complete the mass balance.

Reaction 1 involves the formation of the methylimino radical (CH_3N) by the elimination of a mole of nitrogen. The radical can decay at least in part, according to (2). This reaction takes place exclusively during the initial stage of the reaction and does not occur in the solid at $-190°$. This reaction probably only goes with an appreciable rate at the elevated temperature in the furnace, since neither hydrogen nor hydrogen cyanide is found in products of the thermal decomposition at 200–240°. If some of the methylimino radicals are stabilized on the cold finger at $-190°$, then (3) is the reaction which occurs at liquid air temperatures and is accompanied by the physical transition.

It is possible that the methylimino radical is not stabilized but rather rearranges to methyleneimine, either in the vapor phase or on contact with the cold surface. Then $CH_2=NH$ is the active species stabilized and this polymerizes on slight warming. This polymerization may be initiated by some isolated methylimino radicals that are trapped in the deposit.

COMMUNICATION TO THE EDITOR

STABILITY OF SULFONATED CROSS-LINKED ION EXCHANGE RESIN IN HYDROGEN PEROXIDE

Sir:

The sulfonated copolymers of styrene divinylbenzene have become important as solid acid catalysts in epoxidation, esterification and inversion. The literature is rather limited on the stability of these cation exchange resins under various conditions. Soldano[1] showed the loss of active groups on prolonged heating of the hydrogen form of the cation exchanger at 200°. He also observed that the swelling of the resin from the dry to the wet form decreased with the heating of the resin in the hydrogen form, indicating that there was a loss in active groups rather than a change in the crosslinking of the resin since reduction in crosslinking would increase the degree of swelling.

Tests in our laboratory on resins in the sodium form indicate no change in capacity upon heating to 150° in vessels under pressure, but the resins undergo crosslink degradation when the sodium exchangers are heated in the presence of hydrogen peroxide.

In catalytic work on epoxidation of various unsaturated oils, we have also observed that the degree of crosslink degradation of the hydrogen form exchanger in the presence of strong peroxide solutions (10–50%) is increased considerably by the presence of trace amounts of iron in the resin. Such amounts of iron are usually found in commercial exchangers. Copper is next to iron in its activity for crosslink degradation. Nickel and zinc on the other hand show no catalytic effect in the decrosslinking of the hydrogen cation exchange resin in the presence of hydrogen peroxide. This would indicate that the decrosslinking of the resins

(1) B. A. Soldano, *J. Phys. Chem.*, 60, 456 (1954).

is catalyzed by those cations which bring about the decomposition of hydrogen peroxide.[2]

The breakdown of the crosslinking in the resin is shown by changes in the physical character of the resin. The resin swells so that the increase in volume of the exchanger after heating it for three hours in 50% hydrogen peroxide can be used as a measure of the degree of cross-link degradation. If the crosslink degradation is high, the resin goes into solution so that the loss in weight is another indicator of the degradation. Similarly, the degree of water retention by the exchanger can be another guide of crosslink degradation since the amount of water retained by the ion-exchange resin is a measure of the degree of crosslinking.

If the iron concentration is high enough, the whole resin goes into solution. No loss was found in active groups of the decrosslinked resin when the determination was made on weight basis. Temperature, peroxide concentration and quantity of iron affect the degree of degradation. Table I shows the effect of iron on the degree of degradation.

TABLE I

STABILITY OF PERMUTIT Q (SULFONATED CROSSLINKED POLYSTYRENE) IN 50% HYDROGEN PEROXIDE (60° C.)

Iron added, mg. per liter of wet resin	Volume increase of resin, %	Weight decrease of resin, %
0	3	0.07
100	17	6
500	190	23
700	—	60
800	—	100

RESEARCH LABORATORY
THE PERMUTIT COMPANY   WILLIAM WOOD
BIRMINGHAM, NEW JERSEY

(2) W. C. Schumb, C. N. Satterfield and R. L. Wentworth, "Hydrogen Peroxide," A.C.S. Monograph 128, Reinhold. Publ. Corp., New York N. Y., 1955.

ANNOUNCING

New Rates for Single Copies of Current Issues and Back Numbers, *Effective January 1, 1956*

PUBLICATIONS OF THE AMERICAN CHEMICAL SOCIETY

Journal	Current Year Rate	Back Year Rate	Foreign Postage	Canadian Postage
ANALYTICAL CHEMISTRY				
Vols. 1-4, each issue	.....	$2.00	$0.15	$0.05
Vols. 5-8, each issue	.....	1.25	0.15	0.05
Vols. 9-27, each issue	.....	1.50	0.15	0.05
Vol. 28 et seq., each issue	$1.50¹	2.00¹	0.15	0.05
(1) April issue appears in two parts; sold as unit for $2.00 current year or $2.50 back year.				
CHEMICAL AND ENGINEERING NEWS				
Vols. 1-24, each issue	.....	0.25	0.10	.....
Vol. 25 et seq., each issue	0.40	0.50	0.10	.....
INDUSTRIAL AND ENGINEERING CHEMISTRY	1.50²	2.00²	0.25	0.10
(2) March and September issues in two parts; each sold as a unit for $2.50 current year or $3.00 back year.				
JOURNAL OF AGRICULTURAL AND FOOD CHEMISTRY	1.00	1.50	0.15	0.05
JOURNAL OF THE AMERICAN CHEMICAL SOCIETY				
Vols. 1-31 (Order volumes prior to 32 from Walter J. Johnson, 125 E. 23rd St., New York 10, N. Y.)				
Vols. 32-77, each issue	.....	1.75	0.15	0.05
Vol. 78 et seq., each issue	1.50	1.75	0.15	0.05
THE JOURNAL OF PHYSICAL CHEMISTRY				
Vols. 1-55 (Order volumes prior to 56 from Walter J. Johnson, 125 E. 23rd St., New York 10, N. Y.)				
Vol. 56 et seq., each issue	1.35	1.75	0.15	0.05
THE JOURNAL OF ORGANIC CHEMISTRY				
Vols. 1-16 (Walter J. Johnson)–Vols. 17-19 (Williams & Wilkins Co., Baltimore 2, Md.)				
Vol. 20 et seq., each issue	2.50	3.00	0.15	0.05
CHEMICAL ABSTRACTS				
Vols. 1-10 (Order volumes prior to 10 from Walter J. Johnson, 125 E. 23rd St., New York 10, N. Y.)				
Vols. 11-30				
Numbers 1-22, each issue	.....	1.25	0.15	0.05
Numbers 23 and 24, each	.....	3.00	0.45	0.15
Vols. 31-49				
Numbers 1-22, each issue	.....	2.25	0.15	0.05
Number 23 (Author Index)**	.....	12.00	0.30	0.10
Number 24 (Subject Index)**	.....	24.00	0.60	0.20

THE CHEMICAL ABSTRACTS SERVICE (formerly known as CHEMICAL ABSTRACTS)
Vol. 50 et seq. Single issues commencing with Volume 50 are sold in accordance with prices listed here until January 1 of the second year following the close of the volume year, after which they will be sold at back issue prices also shown here.

	Members Personal-Use	Colleges & Universities	All Others			
Numbers 1-22, each	$ 2.00	$ 3.00	$15.00	2.50	0.15	0.05
Author & Patent Index*	5.00	15.00	20.00	15.00	0.30	0.10
Subject & Formula Index*	10.00	35.00	40.00	30.00	0.60	0.20

* Patent Index will be bound with either Subject or Author Index as determined by production schedules.
** A special rate of 50% of these amounts applies to orders from ACS members for personal use.

Rates for Volumes of Back Numbers

Journal	Rate	Foreign Postage	Canadian Postage
ANALYTICAL CHEMISTRY (formerly Analytical Edition)			
Volumes 1-8	$ 7.50	$0.75	$0.25
Volumes 9-27	15.00	0.75	0.25
Volume 28 et seq.	20.00	0.75	0.25
CHEMICAL AND ENGINEERING NEWS			
Volumes 1-24	5.00	2.25	0.75
Volume 25 et seq.	20.00	2.25	0.75
INDUSTRIAL AND ENGINEERING CHEMISTRY			
Volume 1 et seq.	20.00	2.25	0.75
JOURNAL OF AGRICULTURAL AND FOOD CHEMISTRY			
Volume 1 et seq.	15.00	1.50	0.50
JOURNAL OF THE AMERICAN CHEMICAL SOCIETY			
Volumes 1-31 (Order volumes prior to 32 from Walter J. Johnson, 125 E. 23rd St., New York 10, N. Y.)			
Volumes 32-77	20.00	1.50	0.50
Volume 78 et seq.	35.00	1.50	0.50
THE JOURNAL OF PHYSICAL CHEMISTRY			
Volumes 1-55 (Order volumes prior to 56 from Walter J. Johnson, 125 E. 23rd St., New York 10, N. Y.)			
Volumes 56-59	15.00	1.20	0.40
Volume 60 et seq.	18.00	1.20	0.40
THE JOURNAL OF ORGANIC CHEMISTRY			
Vols. 1-16 (Walter J. Johnson)–Vols. 17-19 (Williams & Wilkins Co., Baltimore 2, Md.			
Volume 20 et seq.	30.00	1.50	0.50
CHEMICAL ABSTRACTS			
Volumes 1-10 (Order volumes prior to 11 from Walter J. Johnson, 125 E. 23rd St., New York 10, N. Y.)			
Volumes 11-30	25.00	2.40	0.80
Volumes 31-49	65.00	2.40	0.80

THE CHEMICAL ABSTRACTS SERVICE (formerly CHEMICAL ABSTRACTS). Back volumes commencing with Volume 50 are sold in accordance with prices listed here after January 1 of the second year following the close of the volume year.

Volume 50 et seq.	80.00	3.00	1.00

AMERICAN CHEMICAL SOCIETY
BACK ISSUE DEPARTMENT

1155 SIXTEENTH STREET, N.W.   WASHINGTON 6, D.C.